List of Contributors

David J. Craik, *Centre for Drug Design and Development, The University of Queensland, Brisbane, QLD 4072, Australia*

Shangwu Ding, *Department of Chemistry, University of British Columbia, 2036 Main Mall, Vancouver, B.C., Canada V6T 1Z1*

Antonín Lyčka, *Research Institute for Organic Syntheses, CZ-532 18 Pardubice-Rybitví, Czech Republic*

Charles A. McDowell, *Department of Chemistry, University of British Columbia, 2036 Main Mall, Vancouver, B.C., Canada V6T 1Z1*

Martin J. Scanlon, *Centre for Drug Design and Development, The University of Queensland, Brisbane, QLD 4072, Australia*

Chaohui Ye, *Laboratory of Magnetic Resonance and Atomic and Molecular Physics, Wuhan Institute of Physics and Mathematics, The Chinese Academy of Sciences, PO Box 71010, Wuhan 430071, China*

Preface

The protean nature of NMR is amply demonstrated by the contributions to this volume of *Annual Reports on NMR Spectroscopy*. Like many of its predecessors Volume 42 consists of timely reports from somewhat disparate area of molecular science. Multinuclear NMR Studies of Azo Dyes and their Metal Complexes are covered by A. Lycka. Following this is an account of Recent Progress in Solid State NMR by C. Ye, S. Ding and C. A. McDowell, while the third contribution is from D. J. Craik and M. J. Scanlon and covers Pharmaceutical Applications of NMR.

My gratitude is due to all of these reporters for their timely and interesting reports. It also a pleasure for me to record my thanks to the production staff at Academic Press (London) for their keen support and cooperation in the presentation of this series of reports.

University of Surrey
Guildford, Surrey
England

G. A. WEBB
November 1999

Multinuclear NMR of Azo Dyes and Their Metal Complexes

ANTONÍN LYČKA

Research Institute for Organic Syntheses CZ-532 18 Pardubice-Rybitví, Czech Republic

1. INTRODUCTION

Section 2 of this review covers the literature dealing with NMR spectra of azo dyes measured in solution since the publication of last review[1] in 1993 and focuses on azo compounds. Hydrazo compounds have been included either when prepared by diazonium salt coupling reactions or when they are important for azo–hydrazone tautomerism description. The ^{13}C and ^{15}N CP/MAS NMR spectra are discussed in Section 3. Azo–hydrazone tautomerism, a property that is indivisibly linked to azo dyes, is the topic of Section 4. NMR spectra of metal complexes of azo dyes are reviewed in Section 5.

2. NMR SPECTRA OF AZO DYES IN SOLUTION

2.1. ^{1}H NMR spectra

Azobenzene exists in the thermodynamically much more stable *trans* form (**1**), while the *cis* isomer (**2**) must usually be prepared by irradiation of **1** and then separated chromatographically. The ^{1}H NMR spectra of compounds **1** and **2** in

ANNUAL REPORTS ON NMR SPECTROSCOPY
VOLUME 42 ISBN 0-12-505342-8

several solvents[2–4] are collected in Table 1. In solution state, there is free rotation around the C1–N bond (fast on the NMR time scale) and, thus, the proton chemical shifts of H2/H6 and H3/H5 pairs are equivalent.

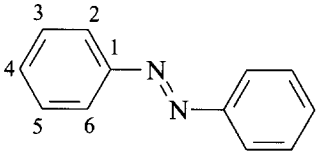

[1]

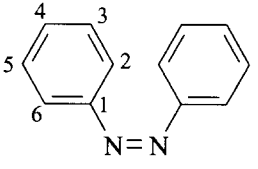

[2]

Some 4-substituted *cis*-azobenzene derivatives are stable in aqueous solution.[4] An ultrafast photoisomerization of 4-(4′-aminophenylazo)benzoic acid[5] was studied and ^{1}H NMR spectra of products were published.

^{1}H NMR spectra are often used by synthetic chemists to characterize azo dyes. Sets of proton chemical shifts and, in some cases, also selected coupling constants are published surprisingly frequently without any signal assignment or with only partial assignment.

^{1}H chemical shifts were measured of dyes prepared by diazonium salt coupling with 2,2′,4,4′-tetrahydroxybenzophenone (mono and bisazo compounds),[6] 3-amino-5-nitro[2,1]benzisothiazole,[7] basic dyes derived from 3-(acetoacetamido)- pyridine,[8] 5-sulfonylpiperidino- and morpholino-8-hydroxyquinoline,[9] 5,6-dichloro- and 6,7-dichloro-2-aminobenzothiazoles,[10] H-acid,[11] 1-butyl-3-cyano-6-hydroxy-5-methyl-2(1*H*)pyridone,[12] ethyl-2-hydroxyazulenecarboxylate,[13] GM1 synthon,[14] 3-cyano-2(1*H*)-pyridinethiones,[15] 2-amino-6-(2-chloroethoxy) benzothiazole and 2-amino-4-(2-hydroxyethoxy)-benzothiazole,[16] 2-aminothiophenes,[17] 3-amino-4-methoxyacetanilide,[18] 1(4)-substituted pyrazol-5-one[19] and barbituric acid.[20] Lists of proton chemical shifts were published for analogues of Disperse Red 167,[21] products of coupling

Table 1. ^{1}H chemical shifts (ppm) in compounds **1** and **2** in several solvents

Compound	Solvent	H-2	H-3	H-4	Ref.
1	Acetone-d_6[a]	7.9	7.6	7.6	2
1	DMSO-d_6	7.905	7.599	7.617	3
		7.921	7.648	7.603	4
1	$CDCl_3$	7.922	7.521	7.471	3
2	Acetone-d_6[a]	6.85	7.25	7.15	2
2	DMSO-d_6	6.855	7.326	7.207	4

[a] Values read from published ^{1}H NMR spectrum.

reaction of diazonium salts derived from 2-amino-6-nitrobenzothiazole and from 2-aminobenzothiazole with dialkylanilines,[22] 2,6-diaminobenzothiazole,[23] in heterocyclic Hansa Yellow analogues,[24] Azoxine S (8-hydroxyquinoline-5-sulfonic acid) azo dyes,[25] 4-26 bis-3,3′(*p*-tolylazo)-2,2′-dihydroxydinaphthalene and bis-3,3′-(*p*-anisylazo)-2,2′-dihydroxydinaphthalene,[27] C.I. Disperse Orange 29,[28] C.I. Disperse Yellow 23,[29] azo pyridone dyes,[30] chromone azo dyes,[31] 6-(perfluoroalkyl)benzothiazolylazo dyes,[32] model reactive dyes containing the vinylsulfonyl group,[33] substituted 2-thiazolylazoanilines,[34] 5-((4-heptyloxyphenyl)azo)-salicylaldimine[35] and disperse dyes containing a built-in oxalanilide stabilizer.[36]

Complete assignment of proton chemical shifts in reaction products of model vinyl sulfonyl reactive dyes with methyl-α-D-glucoside[37–39] was published. In ref. 39, two basic types, **3** and **4**, were separated and ^{1}H NMR spectra were measured at 600 MHz and analysed.

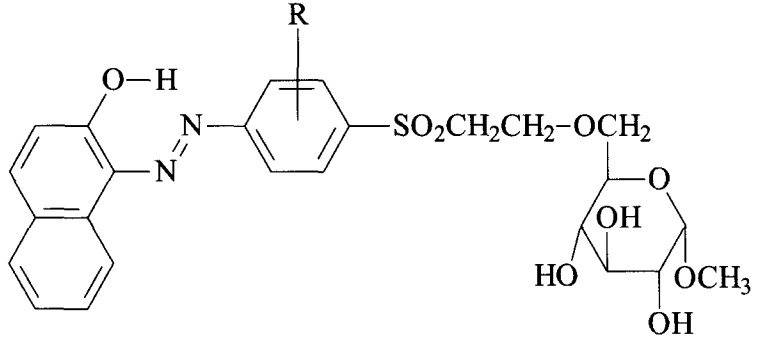

[3]

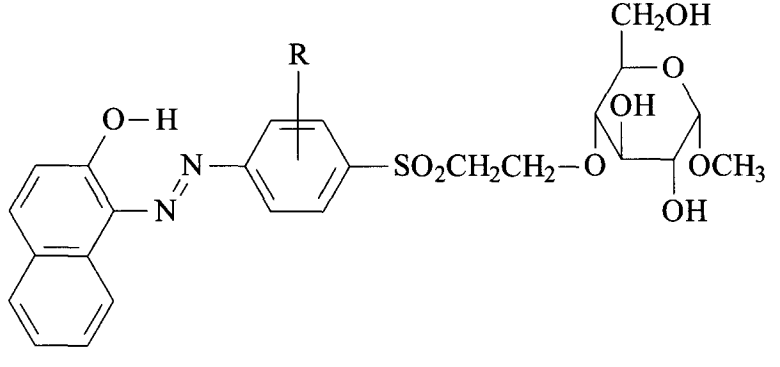

[4]

A series of 25 disperse dyes **5–7** obtained by diazotization of nitroanilines and heterocyclic amines and coupling with dialkylanilines was prepared[40] and their ^1H chemical shifts are given in Table 2.

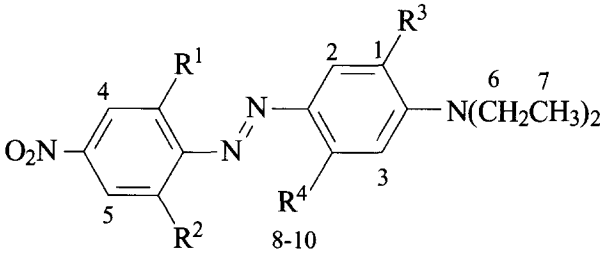

[5]

Compound	R^1	R^2	R^3	R^4
5a	H	H	H	$NHCOCH_3$
5b	Br	CN	H	$NHCOCH_3$
5c	Br	CN	H	$NHCOCH_2CH_3$
5d	Br	CN	H	CH_3
5e	Br	NO_2	H	$NHCOCH_3$
5f	Br	NO_2	OCH_3	$NHCOCH_3$
5g	Br	NO_2	H	$NHCOCH_2CH_3$
5h	Br	NO_2	H	CH_3
5i	CN	CN	H	$NHCOCH_3$
5j	CN	CN	H	$NHCOCH_2CH_3$
5k	CN	CN	H	CH_3
5l	CN	NO_2	H	$NHCOCH_3$
5m	CN	NO_2	OCH_3	$NHCOCH_3$
5n	CN	NO_2	H	$NHCOCH_2CH_3$
5o	CN	NO_2	H	CH_3

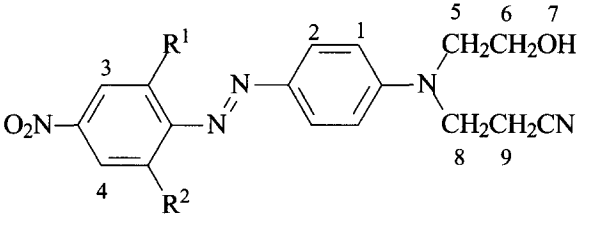

[6]

Compound	R^1	R^2
6a	Br	CN
6b	Br	NO_2
6c	CN	CN
6d	CN	NO_2

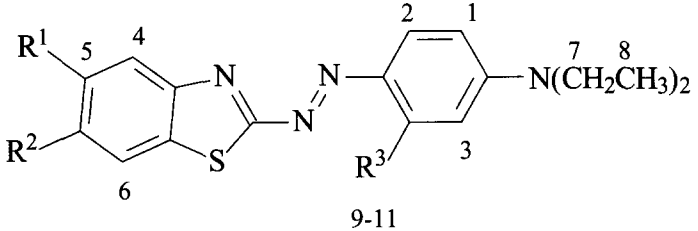

9-11

[7]

Table 2. ^1H chemical shifts (ppm) in compounds **5–7**

Compound	H1	H2	H3	H4	H5	H6	H7	H8	H9	H10	H11
5a	6.52	8.51	7.77	7.81	8.34	3.52	1.30	8.51	2.29		
5b	6.53	8.01	8.17	8.49	8.67	3.57	1.32	9.40	2.32		
5c	6.55	8.02	8.21	8.49	8.68	3.58	1.33	9.37	2.61	1.24	
5d	6.56	7.99	6.60	8.52	8.67	3.52	1.28	2.76			
5e	6.51	7.90	8.17	8.32	8.65	3.55	1.30	9.40	2.30		
5f[a]	–	7.27	8.15	8.28	8.64	3.64	1.32	9.38	2.30		
5g	6.55	8.03	8.19	8.34	8.65	3.55	1.31	9.37	2.57	1.26	
5h	6.58	7.93	6.51	8.40	8.65	3.50	1.27	2.48			
5i	6.59	8.16	8.22	8.66	8.66	3.63	1.33	9.36	2.33		
5j	6.58	8.15	8.25	8.64	8.64	3.63	1.36	9.32	2.62	1.23	
5k	6.64	8.14	6.59	8.68	8.68	3.57	1.32	2.75			
5l	6.54	7.93	8.17	8.56	8.64	3.60	1.34	9.18	2.33		
5m[b]	–	7.29	8.25	8.55	8.61	3.76	1.35	9.22	2.35		
5n	6.58	7.83	8.12	8.48	8.55	3.54	1.23	9.19	2.54	0.82	
5o	6.60	7.98	6.55	8.58	8.67	3.55	1.30	2.60			
6a	6.83	8.06	8.55	8.72	3.94	3.78	4.06	3.83	2.80		
6b	6.80	7.91	8.58	8.72	3.94	3.76	4.07	3.83	2.79		
6c	6.84	8.14	8.76	8.76	3.98	3.65	4.06	3.83	2.84		
6d	6.76	7.26	8.52	8.58	4.05	3.65	4.07	3.90	2.37		
7a[c]	6.50	7.05	8.10	7.27	7.28	7.92	3.53	1.29	9.25	2.33	
7b[d]	6.50	7.04	7.93	7.27	7.28	7.92	3.53	1.29	9.26	2.59	1.35
7c[e]	6.60	7.05	7.99	7.94	6.55	7.28	3.49	1.27	9.26	2.68	
7d	6.58	7.52	7.86	8.22	–	8.58	3.59	1.32	9.26	2.32	
7e	6.56	7.28	8.04	8.09	8.31	8.71	3.59	1.34		2.63	1.26
7f	6.58	6.63	8.03	8.07	8.31	8.71	3.54	1.30	2.68		

[a–e] $\delta(OCH_3)$ = 3.86[a], 3.86[b], 3.89[c], 3.89[d], 3.90[e].

Compound	R^1	R^2	R^3
7a	H	OCH_3	$NHCOCH_3$
7b	H	OCH_3	$NHCOCH_2CH_3$
7c	H	OCH_3	CH_3
7d	Cl	Cl	$NHCOCH_3$
7e	H	NO_2	$NHCOCH_2CH_3$
7f	H	NO_2	CH_3

The ^1H chemical shifts were assigned in C.I. Disperse Yellow 211,[41] in sodium 1-(2-,1-(3- and 1-(4-trifluoromethylphenylazo)-2-hydroxy-5-benzenesulfonate,[42] in some *o,o'*-dihydroxyazo dyes containing the sulfo group[43] and 1(4)-substituted pyrazol-5-one azoderivatives **8**.[44]

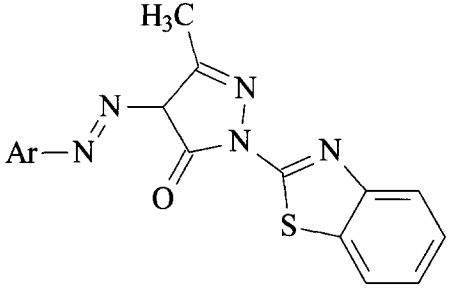

[8]

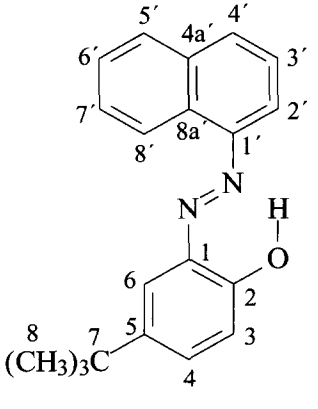

[9]

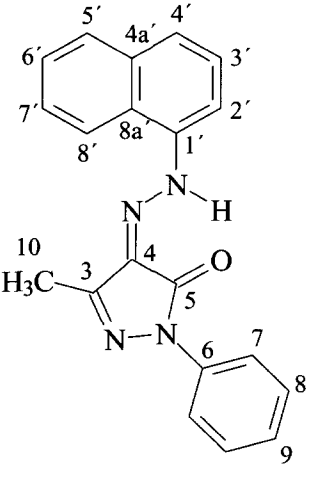

[10]

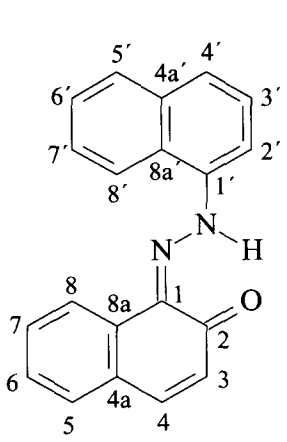

[11]

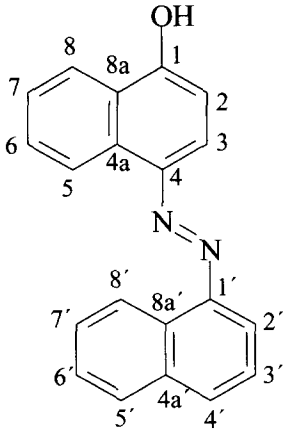

[12]

2.2. ^{1}H and ^{13}C NMR spectra

From the author's experience, a combination of one-dimensional (1D) and two-dimensional[45–48] (2D) ^{1}H and ^{13}C NMR spectra is very useful in assignment of proton and carbon resonances. With only unambiguous assignment of all signals, definitive conclusions can be made on various problems.

Figures 1–6 show selected 2D NMR spectra of compound **11**. The H,H-COSY spectrum (Fig. 1) reveals proton–proton connectivity mainly via $^{3}J(^{1}H, ^{1}H)$; in the long-range H,H-COSY spectrum (Fig. 1) (in naphthalene this spectrum is very similar to TOCSY), it is possible to observe connectivity of protons due to very small coupling constants, in many cases even due to those not resolved in a standard 1D proton spectrum. Many nondiagonal signals in **11** are observable both in NOESY and COSY spectra (Fig. 2), but the mechanism of their creation is completely different (dipolar cross-correlation of nuclei in close spatial proximity versus indirect spin–spin interaction). In our case, the through-space correlations of protons H4 ($\delta = 7.74$ ppm) and H5 ($\delta = 7.61$) and protons H4′($\delta = 7.81$) and H5′ ($\delta = 7.91$) are visible only in the NOESY spectrum. Gradient-selected HMQC spectrum (Fig. 3) was used to correlate protons and appropriate carbons via $^{1}J(^{13}C, ^{1}H)$ and the HMBC spectrum (Fig. 4) via $^{n}J(^{13}C, ^{1}H)$ coupling constants. In the case of complex spectra, gradient-selected HMQC-RELAY (Fig. 5) and gradient-selected HMQC-TOCSY (Fig. 6) can be applied. Starting from the HMQC cross-peak, one can find in the same row in F1 additional signal(s), which are are caused by a RELAY transfer (showing —CH—CH— arrangement) or by a TOCSY transfer (showing —CH—CH—CH ... arrangement). The sequence of protons in ^{1}H NMR spectra in Figs 1–6 is as follows: H8, H8′, H2′, H5′, H4′,

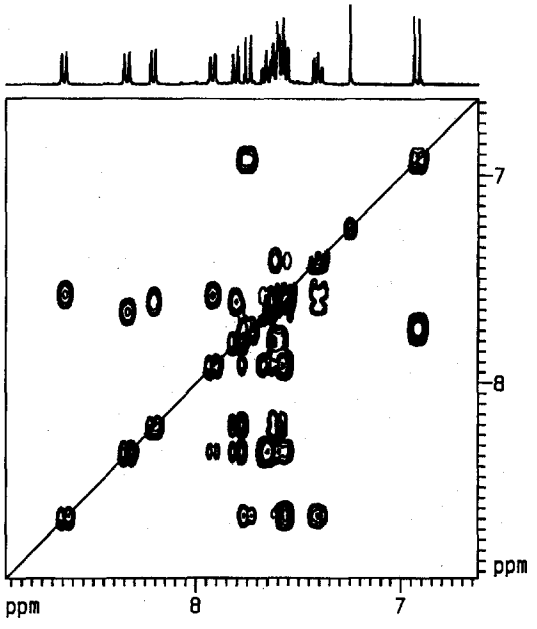

Fig. 1. H,H-COSY (upper left part) and H,H-COSYLR (bottom right part) spectra of compound **11** in $CDCl_3$.

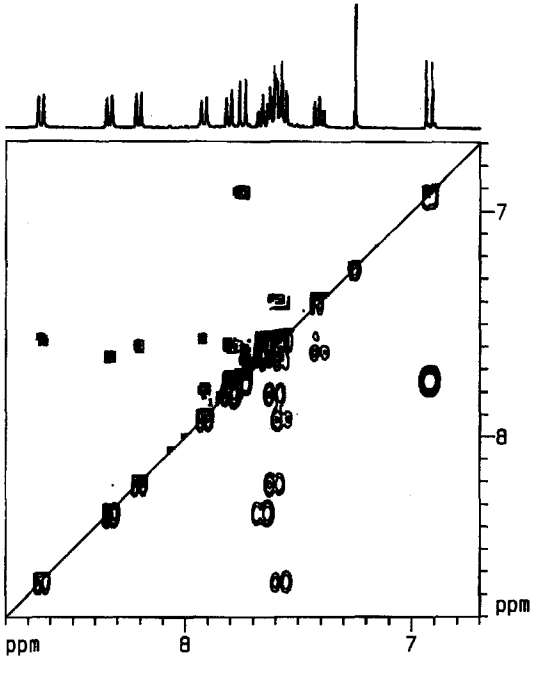

Fig. 2. NOESY (upper left part) and H,H-COSY (bottom right part) spectra of compound **11** in $CDCl_3$.

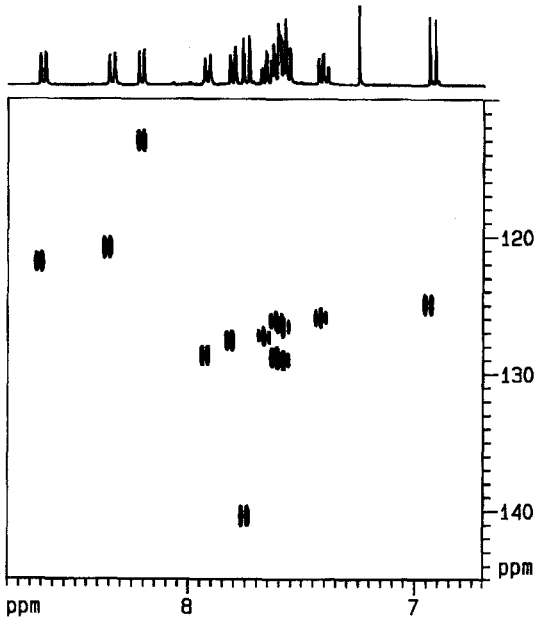

Fig. 3. Gradient-selected HMQC spectrum of compound **11** in $CDCl_3$.

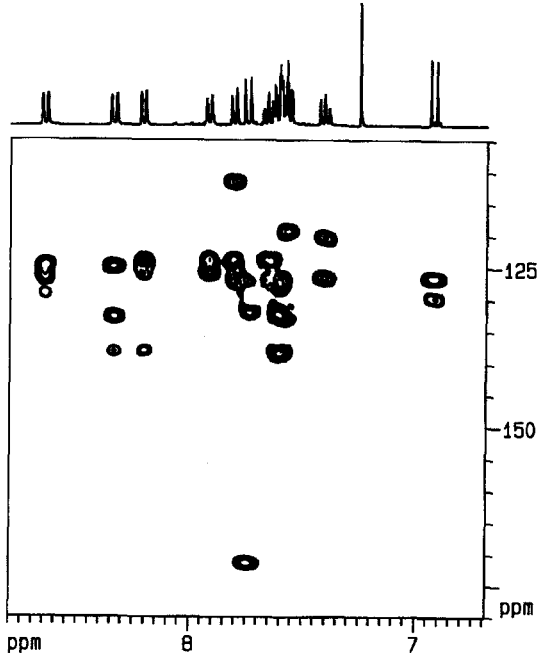

Fig. 4. Gradient-selected HMBC spectrum of compound **11** in $CDCl_3$.

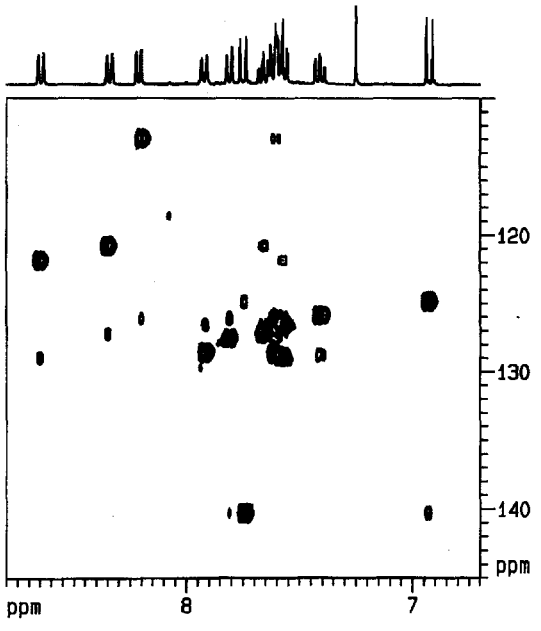

Fig. 5. Gradient-selected HMQC-RELAY spectrum of compound **11** in $CDCl_3$.

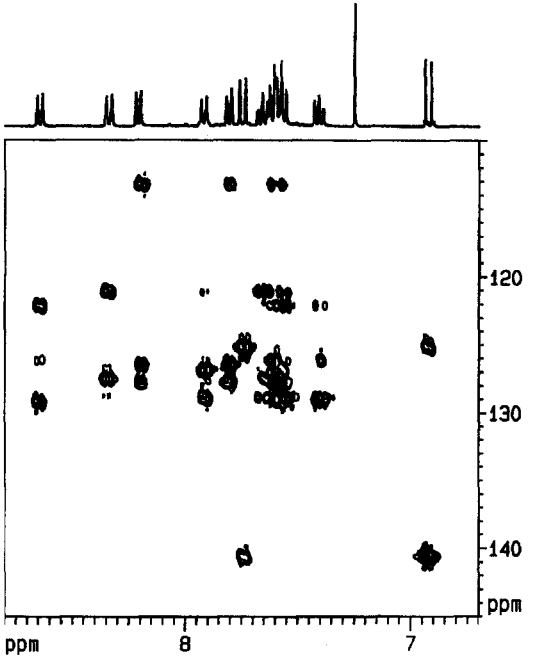

Fig. 6. Gradient-selected HMQC-TOCSY spectrum of compound **11** in $CDCl_3$.

Table 3. ^{1}H chemical shifts (ppm) in compounds **9–11** in deuteriochloroform and **12** in hexadeuteriodimethyl sulfoxide

Hydrogen atom no.	Compound			
	9	**10**	**11**	**12**
1	–	–	–	–[d]
2	–[a]	–	–[c]	7.16
3	7.06	–	6.92	8.18
4	7.46	–	7.74	–
5	–	–	7.61	9.06
6	8.05	–	7.41	7.79
7	–	7.99	7.57	7.65
8	1.41	7.48	8.64	8.33
9	–	7.22	–	–
10	–	2.38	–	–
1′	–	–[b]	–	–
2′	7.93	7.69	8.21	8.01
3′	7.58	7.52	7.60	7.74
4′	7.93	7.91	7.81	8.12
5′	7.97	7.87	7.91	8.11
6′	7.58	7.53	7.57	7.71
7′	7.63	7.61	7.66	7.77
8′	8.49	8.05	8.33	9.01

[a] δ(OH) = 13.08. [b] δ(NH) = 14.49. [c] δ(OH/NH) = 17.24. [d] δ(OH) = 11.34.

H4, H7′, (H5 and H3′), (H7′ and H6′), H6, CHCl3, and H3. ^{1}H and ^{13}C NMR chemical shifts[49] for compounds **9–12** are given in Tables 3 and 4.

An analogous approach has been used in assigning ^{1}H and ^{13}C NMR chemical shifts in anthracenedione phenylhydrazones,[50] 1,3-bis(phenylazo)-2-naphthol and its precursors.[51] Azo and hydrazone compounds **13** derived from Fischer base (1,3,3-trimethyl-2-methylidene-2,3-dihydroindole) were studied by two groups.[52,53]

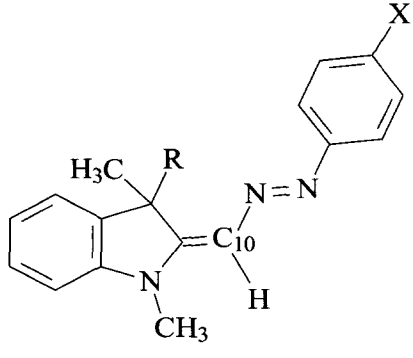

[13]

Table 4. ^{13}C chemical shifts (ppm) in compounds **9–11** in deuteriochloroform and **12** in hexadeuteriodimethyl sulfoxide

Carbon atom no.	Compound			
	9	**10**	**11**	**12**
1	137.73	–	131.28	158.07
2	150.38	–	172.91	108.72
3	117.65	148.52	124.97	114.63
4	131.13	129.86	140.46	140.55
4a	–	–	128.12	132.96
5	143.06	158.05	128.71	122.78
6	129.77	137.98	125.91	127.97
7	34.17	118.78	129.99	125.59
8	31.39	128.97	121.83	122.57
8a	–	–	133.52	124.55
9	–	125.29	–	–
10	–	11.83	–	–
1′	146.35	136.01	139.96	147.67
2′	113.21	111.29	112.93	111.86
3′	126.76	126.01	126.15	126.64
4′	129.37	125.89	127.51	130.56
4a′	134.26	134.04	134.17	134.12
5′	131.29	128.81	128.64	128.13
6′	126.69	126.58	126.56	126.08
7′	127.51	127.08	127.24	127.01
8′	122.18	119.37	120.75	123.13
8a′	129.47	123.12	125.25	130.66

Both Buss and Eggers[52] (for R = C_3H_7) and we[53] (for R = CH_3) have observed the existence of two conformations existing in dynamic equilibrium, the major component having *E,E* arrangement of substituents on noncyclic double bonds. Buss and Eggers[52] proposed *Z* arrangement on the C=C bond in the minor component while we found that $^2J(^{15}N, C10)$ is about 4.3 Hz, which lies beyond the expected range for planar molecules, and this value corresponds to the arrangement in which the plane of the five-membered ring and the plane determined by the =C(10)H—N— group and azo bond are roughly perpendicular on average.

Mustroph and Bach[54] proposed, without having any NMR results, that the reaction of diazonium salts with 1-phenyl-3-methyl-4-(α-acet-ethylidene)-pyrazol-5-one gave compounds **14**. Detailed analysis of 2D ^1H and ^{13}C NMR spectra revealed[55] that the reaction gives rise the compound **15**, possibly owing to nucleophilic attack of nitrogen to carbonyl group. The empirical formulae of compounds **14** and **15** are the same and, therefore, the reaction products cannot be differentiated using elemental analysis data or the *m/z* value in the mass spectrum.

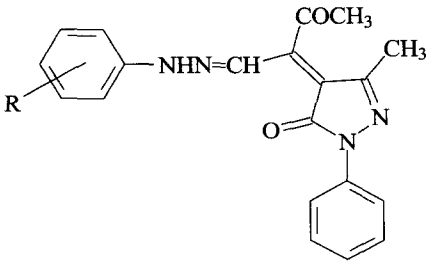

[14]

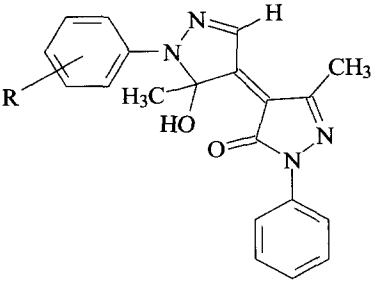

[15]

Coplanarity in 2,6-dimethylazobenzenes[56] and its effect on the efficiency of transmission of electronic effects from one ring to the other was studied by Byrne and Happer using ^{13}C chemical shifts. The methyl groups have a substantial effect on the planarity of the system, but, surprisingly, a loss of planarity has relatively little effect on the efficiency of transmission of both polar and resonance effects between the two rings. ^{1}H and ^{13}C NMR studies of substituent effects on the molecular planarity was performed by Koleva *et al.*[57] Jirman[58] was interested in ^{1}H and ^{13}C NMR spectra (Tables 5 and 6) of 2,2′-disubstituted azobenzenes (**16**) and 2,2′-azopyridine (**17**) suitable for preparation of metallized azo dyes.

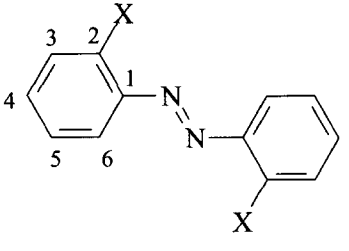

[16]

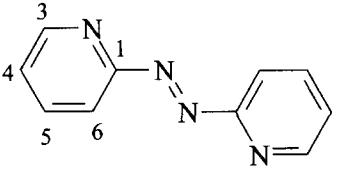

[17]

Compound	X
16a	OH
16b	NH2
16c	$NHCOCH_3$
16d	COOH

Table 5. ^{1}H chemical shifts (ppm) in compounds **16** and **17**

Compound	H3	H4	H5	H6	X[a]
16a[b]	7.04	7.35	7.03	7.70	12.21
16a[c]	7.13	7.42	7.04	7.89	11.6
16b[b]	6.76	7.17	6.78	7.67	5.48
16b[c]	6.87	7.15	6.63	7.90	6.42
16c[b]	8.66	7.50	7.16	7.63	[d]
16c[c]	8.27	7.57	7.28	7.96	[e]
16d[c]	7.91	7.61	7.69	7.55	6.22
17[b]	8.73	7.42	7.88	7.92	–
17[c]	8.78	7.65	8.11	7.80	–

[a] The protons in X group. [b] In deuteriochloroform. [c] In hexadeuteriodimethyl sulfoxide. [d] δ(NH) = 9.36, $\delta(CH_2)$ = 2.29. [e] δ(NH) = 10.13, $\delta(CH_3)$ = 2.25.

Table 6. ^{13}C chemical shifts (ppm) in compounds **16** and **17**

Compound	C1	C2	C3	C4	C5	C6
16a[a]	135.21	152.99	118.63	133.19	120.25	131.20
16a[b]	137.77	154.11	118.14	133.29	119.89	123.63
16b[a]	137.76	143.13	117.03	131.35	117.65	124.21
16b[b]	136.74	145.31	115.69	131.28	116.60	121.91
16c[a,c]	[d]	137.43	120.55	133.45	123.45	116.54
16c[b,e]	141.59	137.35	122.67	132.42	123.98	117.29
16d[b,f]	151.99	130.91	130.19	131.17	132.61	118.42
17[a]	162.61	–	149.51	126.00	138.40	115.16
17[b]	162.62	–	149.65	126.63	139.23	113.99

[a] In deuteriochloroform. [b] In hexadeuteriodimethyl sulfoxide. [c] $\delta(CH_3)$ = 25.31; the signal of the CONH carbon atom was not observed due to low solubility of the substance. [d] The signal was not observed because of low solubility of the substance. [e] δ(CONH) = 169.00, $\delta(CH_3)$ = 24.32. [f] δ(COOH) = 168.71.

^{13}C chemical shifts in diethyl and dibutyl [α-(4-benzeneazoanilino)-*N*-2-hydroxybenzyl]phosphonate were studied by Tušek-Božič *et al.*[59] Hallas and Towns[60] prepared 2-thienylazo dyes **18** and similar derivatives.[61] Their ^{13}C chemical shifts are given in Table 7.

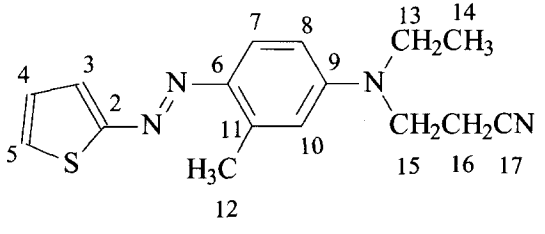

[18]

Compound	Substituent position		
	3	4	5
18a	CN	*a*	*a*
18b	$COOCH_3$	*a*	*a*
18c	$COOC_2H_5$	*a*	*a*
18d	$COOC_2H_5$	*b*	*b*
18e	CN	CH_3	CN

a—$CH_2CH_2CH_2$—, *b*—$CH_2CH_2CH_2CH_2$—

Selected ^{13}C chemical shifts in azines derived from 4-acetyl-3-methyl-1-phenyl-5-pyrazolones,[62] methylol groups in formaldehyde-fast bisazo dyes[63] and pyridyl-substituted azobenzenes[64] are available. The ^{13}C chemical shifts in 16 substituted azobenzenes were published by Savarino *et al.*[65] (however, most of them are mentioned in ref. 1) and some additional data can be found in ref. 66 by Fedorov *et al.*

The ^{1}H and ^{13}C NMR spectra of azo compounds incorporated into monomers and polymers have been measured.[67–73] Chiral methacrylic polymers containing azobenzene chromophore,[67,68] epoxy-based polymers functionalized with tricyanivinylphenylazo chromophores,[69] 4-vinylazobenzene and homo- and copolymers,[70] microstructure of *trans*-4-acrylooyloxyazobenzene/methyl methacrylate copolymers,[71] optically active poly[(*S*)-4-(2-methacryloyloxypropanoyloxy)azobenzene][72] and polyetherurethane pendant with azo dye by *N*-substitution[73] have been studied.

Deuterium isotope effect on ^{13}C NMR spectra has been studied in selectively deuterated azobenzene,[74] in dyes containing amino and acetamido groups[75] and on ^{19}F NMR spectra.[76]

2.3. ^{15}N NMR spectra

Nitrogen NMR spectra of azo, azoxy and hydrazo compounds have been reviewed by J. Mason.[77]

Most published ^{15}N chemical shifts have been measured using ^{15}N-labelled compounds; alternatively, a long-term accumulation of ^{15}N NMR spectra at the natural abundance level of the ^{15}N nucleus had to be used. ^{1}H inverse-detected NMR spectra of ^{15}N-labelled and nonlabelled 1-phenylazo-2-naphthol were measured to test the applicability of this method and to determine the concentrations of dye necessary to obtaining NMR signals.[78]

The ^{15}N chemical shifts in several anthracenedione phenylhydrazones,[50] in 1,3-bis(phenylazo)-2-naphthol and its precursors,[51] and compounds **9**–**12**,[49], **13**,[53] **15**[55] were measured.

Table 7. ^{13}C chemical shifts (ppm) in compounds **18**

Compound	C2	C3	C4	C5	C6	C7	C8	C9	C10	C11	C12	C13	C14	C15	C16	C17	Others
18a	170.46	104.50	*a*	*a*	*a*	117.64	110.31	149.50	112.56	141.70	18.07	45.78	12.56	46.31	16.29	119.16	*b*
18b	164.28	*c*	*c*	*c*	143.73	117.88	110.80	149.35	113.24	142.06	18.66	46.28	13.17	46.96	16.82	118.35	*d*
18c	163.20	*e*	*e*	*e*	142.18	117.26	110.17	148.68	112.62	141.44	18.05	45.67	12.56	46.34	16.21	118.91	*f*
18d	159.90	*g*	*g*	*g*	142.03	117.88	110.05	148.63	112.59	141.27	18.15	45.61	12.53	46.28	16.21	118.58	*h*
18e	171.19	*i*	*j*	*i*	145.44	117.35	110.87	j	112.68	141.99	18.40	46.19	12.76	46.335	16.53	120.71	*k*

[a] 145.88, 142.78, 142.37. [b] (CN) 114.63, ((—CH_2)$_3$—) 30.22, 27.97, 27.56. [c] 148.66, 124.71. [d] (CO_2CH_3) 167.05, (CO_2CH_3) 52.26, ((—CH_2)$_3$—) 30.55, 28.06. [e] 147.08, 124.54. [f] ($CO_2CH_2CH_3$) 166.29, 60.47, 14.34, ((—CH_2)$_3$—) 29.90, 27.45. [g] 137.27, 135.66, 129.36. [h] ($CO_2CH_2CH_3$) 164.13, 60.68, 14.46, ((—CH2)$_4$—) 25.70, 25.23, 22.81, 22.34. [i] 108.24, 103.71. [j] 151.86, 149.88. [k] (CN) 113.35, 113.06, (CH_3) 15.6.

Omura *et al.*[79] reported $\delta(^{15}N)$ chemical shifts in compounds **19** (Table 8).

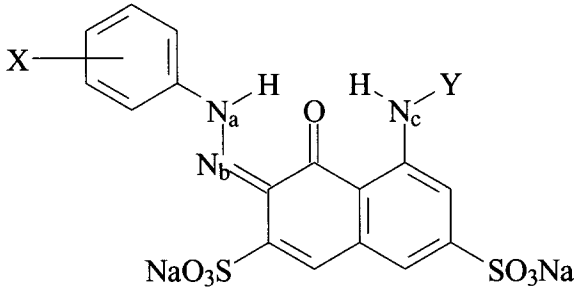

[19]

Compound	X	Y
19a	*o*-SO_3Na	R
19b	*m*-SO_3Na	R
19c	*p*-SO_3Na	R
19d	*o*-SO_3Na	H
19e	H	H

R =

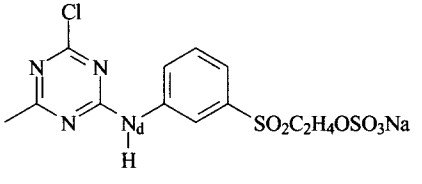

Table 8. ^{15}N chemical shifts (ppm) in compounds **19** in dimethyl sulfoxide

Compound	N_a	N_b	N_c[a]	N_d[a]
19a	−191.1	0.2	−262.5	−266.1
19b	−188.9	3.5	−262.6	−265.8
19c	−189.2	3.8	−262.6	−265.6
19d	−203.8	14.1	−302.0	
19e	−200.6	−7.6		

[a] The assignment may be interchanged.

Omura[80] reported $\delta(^{15}N)$ chemical shifts in twice coupled H-acid (**20**), where nitrogen chemical shifts of the arylazo group in the ortho position to the amino group are typical of the azo form ($\delta(^{15}N_a{=}) = 140.3$, $\delta(^{15}N_b) = 81.8$ ppm) while those of the arylazo group situated in the ortho position to the original hydroxy group exist almost completely in hydrazone form ($\delta(^{15}N_c{=}) = -196.2$, $\delta(^{15}N_d) = 2.5$ ppm) in one model compound. The ^{15}N chemical shift assignment of $^{15}N_a$ and $^{15}N_b$ should probably be interchanged because we have found that nitrogen forming a hydrogen bond is shifted upfield.[1]

This conclusion is supported by Stefaniak[81] with ^{15}N chemical shifts in compounds **21** again existing in the azo forms. The ^{15}N chemical shifts measured are extremely useful in characterization of azo–hydrazone equilibrium and they are discussed in Section 4.

2.4. NMR spectra of other nuclei

Suzuki *et al.*[82] have performed ^{2}H NMR study of the self-assembly of an azo dye–cyclomaltooctaose (γ-cyclodextrin) complex.

Neutral phosphorus(V) compound containing divalent tridentate azo ligands were studied by Cavell and coworkers.[83] The ^{31}P and ^{19}F chemical shifts and $J(^{31}P, ^{19}F)$ coupling constants are collected in Tables 9 and 10 for (2,2′-azophenoxy)trifluorophosphorus (**22**), *trans*-(2,2′-azophenoxy)(trifluoromethyl)difluorophosphorus (**23**) and *cis*-(2,2′-azophenoxy)(trifluoromethyl) difluorophosphorus (**24**).

The ^{31}P, ^{13}C and ^{1}H NMR spectra were published[84] for 6-(diphenylphosphanyl)-1-phenylazonaphthalen-2-ol (**25a**), 6-(diphenylphosphinoyl)-1-phenylazonaphthalen-2-ol (**25b**) and 6-(diphenylphosphinothionyl)-1-phenylazonaphthalen-2-ol (**25c**) (Table 11).

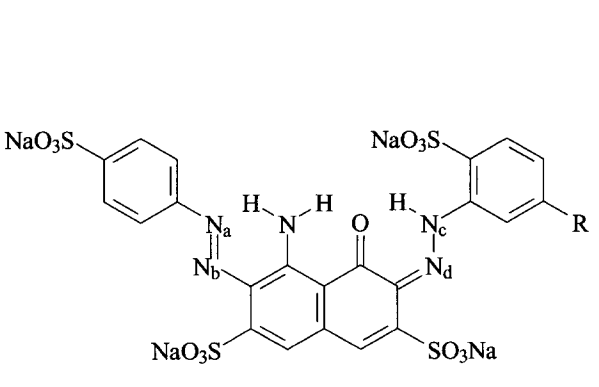

[20]

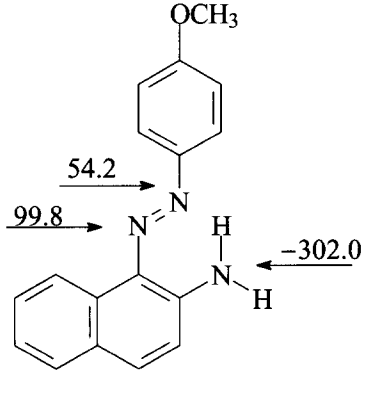

[21]

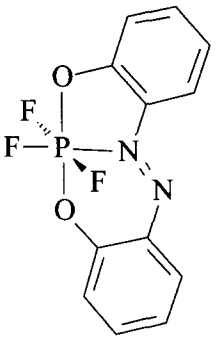

[22]

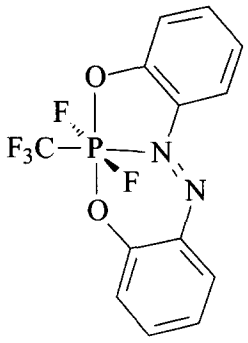

[23]

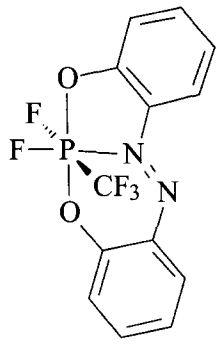

[24]

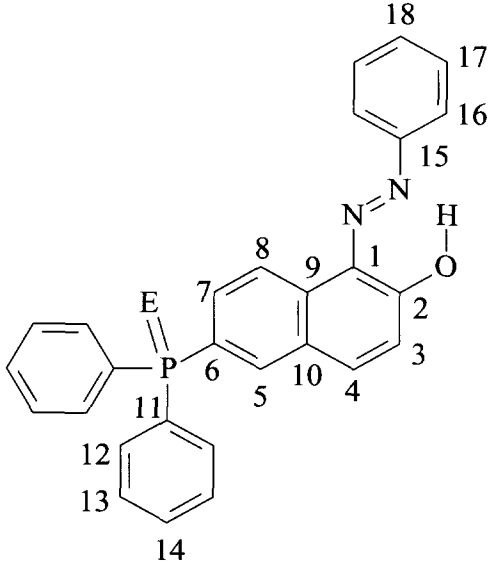

[25]

Compound	E
25a	None
25b	O
25c	S

Table 9. ^{31}P and ^{19}F chemical shifts (ppm)[a] in compounds **22–24**

Compound	^{31}P	$^{19}F(CF_3)_{ax}$	$^{19}(F(CF_3)_{rad}$	$^{19}(F(PF_3)_{ax}$	$^{19}F(PF)_{rad}$
22	−143.6			−51.2	−80.0
23	−148.9		−68.9	−62.1	
24	−146.0	−69.3		−57.7	−82.3

[a] Positive values indicate resonance to high field; standards: 85% H_3PO_4, $CFCl_3$.

Table 10. $J(^{31}P, ^{19}F)$ and $J(^{19}F, ^{19}F)$ coupling constants (Hz) in compounds **22–24**

	$^1J_{PF}$		$^2J_{PF}$		$^3J_{FF}$	$^3J_{FF}$		Solvent
Compound	ax	rad	ax	rad		*cis*	*trans*	
22	842	770			47			CD_3CN
23	894			134		10		CD_3CN
24	833	853	128		56	12	4	CD_3CN

Table 11. ^{31}P and ^{13}C chemical shifts (ppm) in compounds **25a–c** and $^nJ(^{31}P, ^{13}C)$ coupling constants (Hz) values in parentheses)

	25a	**25b**	**25c**
$\delta(^{31}P)$	−5.2	30.1	43.6
$\delta(^{13}C)$			
C1	129.9	129.4	129.4
C2	169.5	170.1	170.2
C3	124.9	125.4	125.3
C4	139.7	139.3	139.4
C5	134.3 (22.4)	133.6 (9.9)	133.7 (11.6)
C6	128.6 (9.5)	128.6 (106.0)	129.8
C7	133.5 (17.8)	130.7 (9.9)	130.8 (10.5)
C8	121.8 (6.2)	121.9 (6.8)	121.8 (11.6)
C9	127.7	127.5	127.3
C10	133.8	135.8	135.5
C11	137.0 (10.5)	132.3 (108.3)	133.4
C12	133.7 (16.7)	132.1 (9.9)	132.2 (10.5)
C13	128.5 (7.3)	128.6 (12.2)	128.6 (12.6)
C14	128.8	132.1 (2.3)	131.6
C15	144.9	145.0	145.0
C16	118.7	119.2	119.1
C17	129.7	129.6	129.6
C18		128.4	128.3

3. SOLID-STATE NMR OF AZO DYES

In contrast to the large number of NMR spectra of azo dyes measured in solution, relatively little attention has been paid to high-resolution solid-state NMR studies of these compounds. A review article on this subject[85] has been published.

In the solution state, there is a free rotation around the C(1)—N (fast on the NMR time scale) and, thus, average chemical shifts are observed for C2 and C6 and likewise for C3 and C5 in azobenzene as well as in 4,4′-disubstituted *trans*-azobenzenes. In the solid state, locked planar *trans* configurations are detected, resulting in nonequivalence of C2/C6 and C3/C5 signal pairs. Chippendale *et al.*[86] reported in 1981 the ^{13}C solid-state NMR spectra of azobenzene and symmetrically 4,4′-disubstituted *trans*-azobenzenes (**26**). ^{13}C chemical shifts are given in Table 12.

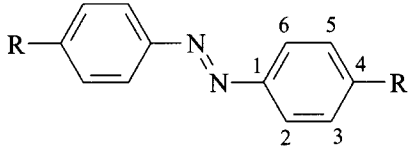

[26]

Typical differences in the C2/C6 chemical shifts were found to be 13–18 ppm and in the C3/C5 shifts they are about 1–3 ppm in the solid state. Using 2,2′-dimethylazobenzene as a model compound, it was shown that C6 absorbs at higher field than C2 in *trans*-azobenzene (δ(C2) = δ(C6) = 122.9 ppm in solution, δ(C2) = 130.7, δ(C6) = 117.9 ppm in the solid state). The ^{13}C CP/MAS NMR spectrum of Disperse Orange 25 was recorded and proposed peak assignments were made.[2]

Maciejewska *et al.*[87] have published ^{13}C CP/MAS NMR spectra of nine 4′-substituted-4-dimethylamino-*trans*-azobenzenes **27** (Table 13). The nonequivalence of C2/C6 and of C2′/C6′ was observed and the difference in ^{13}C chemical shifts was 14.0–22.0 ppm for C2/C6 and 12.2–22.5 for C2′/C6′. The ^{13}C CP/MAS NMR spectra of the compound with 4′-CHO substituent were measured in the temperature range 298–373 K but the spectra did not exhibit any substantial changes except for a small high-frequency shift of all resonances. These results confirm the lack of ring dynamics in the above-mentioned temperature range.

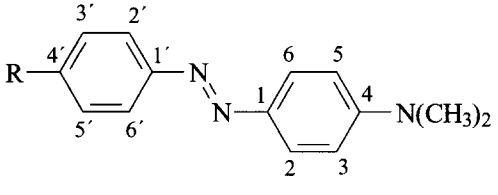

[27]

Table 12. ^{13}C chemical shifts (ppm) for the 4,4′-*trans*-R—C_6H_4N=NC_6H_4—R (**26**) in the solid state and in solution (values in parentheses)

R	C1	C2	C3	C4	C5	C6	Mean of C2 and C6	C=O	CH_3
H	152.5	130.7	130.7	130.7	130.7	117.9	124.3		
	(152.7)	(122.9)	(129.1)	(130.9)	(129.1)	(122.9)	(122.9)		
OH	148.0	132.6	115.1	162.7	115.1	115.1	123.9		
	(145.2)	(123.9)	(115.7)	(159.8)	(115.7)	(123.9)	(123.9)		
COCl	154.3	130.2[a]	130.2[a]	132.4[a]	130.2[a]	114.4	122.3	173.3	
	(154.3)	(122.5)	(130.3)	(133.3)	(130.3)	(122.5)	(122.5)	(166.3)	
CO_2H	153.5	130.0[a]	132.6[a]	132.6[a]	130.0[a]	114.0	122.0	172.9	[b]
	(154.2)	(122.1)	(130.1)	(133.3)	(130.1)	(122.1)	(122.1)	(166.1)	
$NHCOCH_2$	147	132.3	119.5[a]	140.8	118.2[a]	115.6	124.0	169.5	23.6
	(147.7)	(122.9)	(119.2)	(141.6)	(119.2)	(122.9)	(122.9)	(168.4)	(23.7)
CH_2	149.8	[a]	131.0[a]	139.8	128.9[a]	[b]			(19.8)
	(150.1)	(121.9)	(129.4)	(140.7)	(129.4)	(121.9)	(121.9)		(20.4)

[a] These assignments are interchangeable.
[b] Broad unresolved signals.

Table 13. ^{13}C chemical shifts (ppm) for 4′-substituted 4-dimethylamino- *trans*-azobenzenes (**27**) in the solid state and in DMSO-d_6 (values in brackets) at room temperature

R	C1′	C2′	C3′	C4′	C5′	C6′	C1	C2	C3	C4	C5	C6	$N(CH_3)_2$
$NHCH_3$	144.3	132.0	113.7	151.5	114.1	116.1	143.0	131.0	110.4	150.4	110.4	116.1	38.8
	(143.1)	(124.0)	(111.7)	(151.2)	(111.7)	(124.0)	(143.0)	(123.5)	(111.3)	(151.6)	(111.3)	(123.5)	(39.6)
NH_2	142.4	132.8	110.6	150.9	110.6	118.4	142.0	131.0	111.8	151.0	113.2	117.0	37.7
	(143.1)	(124.1)	(113.6)	(151.1)	(113.6)	(124.1)	(143.4)	(123.6)	(111.8)	(151.4)	(111.8)	(123.6)	(40.0)
OH	143.3	129.2	107.2	156.2	111.3	115.1	139.5	129.2	115.1	149.4	115.1	115.1	38.0
	(143.9)	(124.2)	(115.8)	(159.2)	(115.8)	(124.2)	(138.1)	(124.6)	(111.9)	(152.4)	(111.9)	(124.6)	(40.3)
OCH_3	146.4	130.8	113.4	161.3	115.5	118.6	143.7	132.5	109.9	150.7	111.7	118.6	38.6
	(143.6)	(123.8)	(114.1)	(160.9)	(114.1)	(123.8)	(138.1)	(124.8)	(111.8)	(152.1)	(111.8)	(124.8)	(40.5)
CH_3	149.0	127.3	128.9	136.5	129.2	114.4	141.0	131.1	109.4	149.0	111.0	114.4	37.3
	(150.2)	(122.2)	(129.6)	(136.9)	(129.6)	(122.2)	(139.6)	(124.8)	(111.6)	(150.3)	(111.6)	(124.8)	(40.3)
$NHCOCH_3$	151.2	136.7	120.9	141.0	120.9	114.2	143.0	131.0	116.7	151.2	116.7	111.2	39.0
	(148.1)	(122.7)	(119.2)	(140.7)	(119.2)	(122.7)	(142.7)	(124.5)	(111.7)	(152.3)	(111.7)	(124.5)	(39.9)
Br	149.4	128.8	131.6	–[a]	132.5	112.7	140.6	128.8	109.4	149.4	109.4	114.8	37.3
	(154.2)	(124.6)	(133.0)	(142.3)	(133.0)	(124.6)	(142.3)	(125.4)	(112.3)	(152.9)	(112.3)	(125.4)	(40.3)
CHO	156.5	135.2	125.0	142.5	126.4	113.2	142.4	135.2	111.6	153.0	111.6	113.2	39.0
	(156.1)	(125.6)	(130.8)	(142.8)	(130.8)	(125.6)	(136.0)	(122.4)	(111.7)	(153.3)	(111.7)	(122.4	(39.9)
NO_2	154.0	128.1	121.4	142.5	122.8	114.8	142.5	133.4	107.9	150.5	109.2	114.8	37.2
	(156.8)	(122.6)	(126.0)	(147.4)	(126.0)	(122.6)	(143.7)	(124.6)	(111.4)	(153.3)	(111.4)	(124.6)	(40.3)

[a] C4′signal is broad and split by quadrupolar interaction with ^{79}Br, ^{81}Br.

The nonequivalence of some signals that are equivalent in solution NMR complicates the interpretation of the ^{13}C CP/MAS NMR spectra of azo dyes, even for simple compounds where the chemical shifts measured in solution and their interpretation are available. The dipolar dephasing experiment permits the selective measurement of nonprotonated carbon (i.e. with no directly bound hydrogen). We have used C_6D_5 deuterated isotopomers[88] in the analysis of the ^{13}C CP/MAS spectra of azo dyes. ^{13}C CP/MAS NMR spectra of 4-[*N*,*N*–bis(2-hydroxyethyl)amino]azobenzene (**28**), 2-hydroxy-5-*tert*-butylazobenzene (**29**) 4-(*N*,*N*-dimethylamino)azobenzene (**30**), 4-methoxyazobenzene (**31**) and 4-hydroxybenzene (**32**) were recorded.

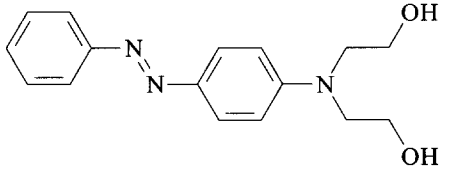

[28]

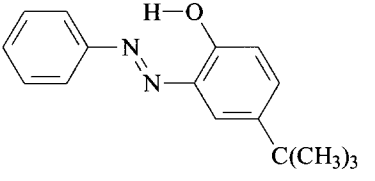

[29]

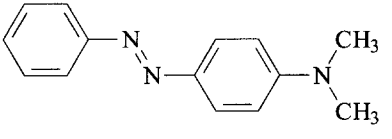

[30]

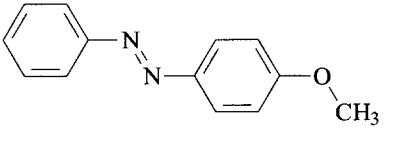

[31]

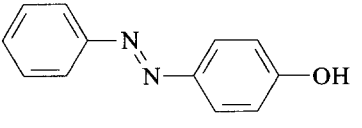

[32]

The appropriate C_6D_5 deuterated isotopomers of **28**, **29** and **32** were also studied. C—D carbons in the deuterated isopotomers behave in dipolar dephased spectra as quaternary carbons and the changes in spectral patterns of nondeuterated and pentadeuterated compounds were used for ^{13}C chemical shift assignment. The spectra of **28**, **30**, **31** and **32** were also recorded at elevated temperature. It was found, contrary to Maciejewska's results,[87] that in **28**, **30** and **32** rotation of the aromatic rings is induced at elevated temperatures.

Forber *et al.* published solution and solid-state NMR spectra of symmetrically *o*,*o'*-disubstituted azobenzenes.[89]

^{13}C CP/MAS NMR spectra of 1-(2′-nitro-4′-methylphenylazo)-2-naphthol (C. I. Pigment Red 3), 1-(2′-nitro-4′-chlorophenylazo)-2-naphthol (C. I. Pigment Red 6) and 1-(4′-nitrophenylazo)-2-naphthol (C. I. Pigment Red 1) were published.[90] The results were in agreement with diffraction data, confirming the existence of these compounds mainly as hydrazone structures in the solid phase. The effect of ($^{13}C-^{14}N$) residual coupling constants on ^{13}C CP/MAS NMR signals was discussed using two different frequencies for recording ^{13}C CP/MAS NMR spectra.

Harris *et al.*[91] used C. I. Pigment Red 57 : 1 as a model compound in testing a pulse sequence for generating ^{13}C CP/MAS NMR spectra of proton-bearing carbons only. The sequence is based on difference spectroscopy and enables the observation of peaks that are otherwise severely overlapped by others.

Olivieri *et al.*[92] have reported the ^{13}C CP/MAS NMR spectra of substituted 1-phenylazo-2-naphthol derivatives using standard and dipolar-dephased experiments and compared the structural results with solution NMR and x-ray data.

Hsieh *et al.*[93] measured 4-(3′,5′-dinitro-2′-hydroxyphenylazo)-3-hydroxy-2-naphthanilide and Fedorov[94] studied 4-(4-nitrophenylazo)-1-naphthol in the solid state. The typical feature of all of these spectra is the strong overlapping of signals in the aromatic region of the spectra, especially in the range of $\delta(^{13}C)$ from 110 to 140 ppm. It is therefore difficult to assign ^{13}C resonances in this region with certainty. On the other hand, such spectra provide important information pertaining to azo–hydrazone tautomerism. The ^{13}C CP/MAS NMR signals of C=O/C—OH are shifted downfield from the aromatic region and from the values of $\delta(^{13}C)$ of this carbon (175.8 ppm in 4-(3′,5′-dinitro-2′-hydroxyphenylazo)-3-hydroxy-2-naphthanilide and 184.7 ppm in 4-(4-nitrophenylazo)-1-naphthol)), the authors concluded that the compounds measured exist predominantly or completely in the hydrazone form.

Chromogens of different classes, viz., arylazo derivatives of resorcinol, naphthols, naphthylamines, chromotropic acid and its cyclic modification, and also some formazans, were investigated by Fedorov *et al.*[95] using ^{13}C CP/MAS NMR. Usually only negligible changes of $\delta(^{13}C)$ were found on comparing solution and solid-state spectra. Table 14 shows solution and the solid-state data for azo resorcinols in alkaline media existing in *para*-quinoidic structure **33**, not in the *ortho* one typical of some other compounds.

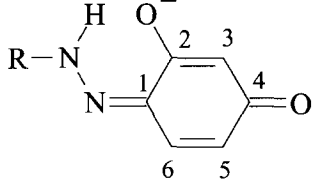

[33]

Table 14. ^{13}C chemical shifts (ppm) of arylazo derivatives **33** of resorcinol

R		Conditions	C1	C2	C3	C4	C5	C6
33	R = C_6H_5	D_2O (pH 10–0)	134.5	175.7	106.5	184.4	123.1	135.7
	p-$NO_2C_6H_4$	D_2O (pH 10–7)	137.0	177.0	106.5	186.1	126.1	135.7
	m-$SO_3NaC_6H_4$	D_2O (pH 10–6)	135.1	177.6	106.6	185.1	124.0	135.9
	Py (Na-form)	DMSO	136.5	175.2	105.0	183.5	127.8	133.4
		Solid	136.5	177.8	108.2	184.1	126.3	133.3

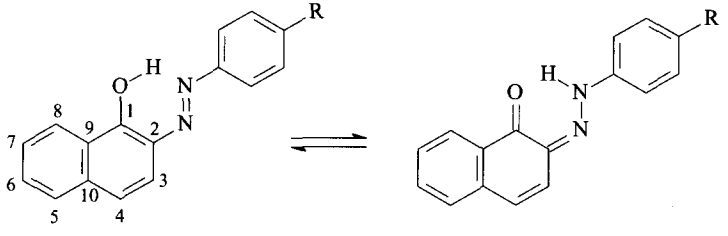

[34]

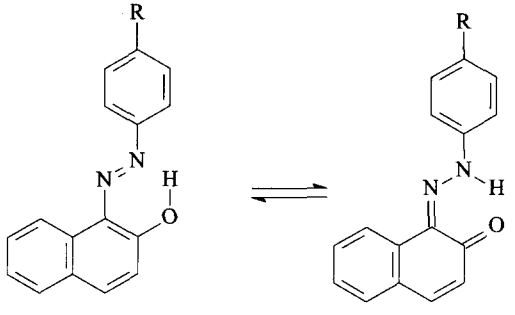

[35]

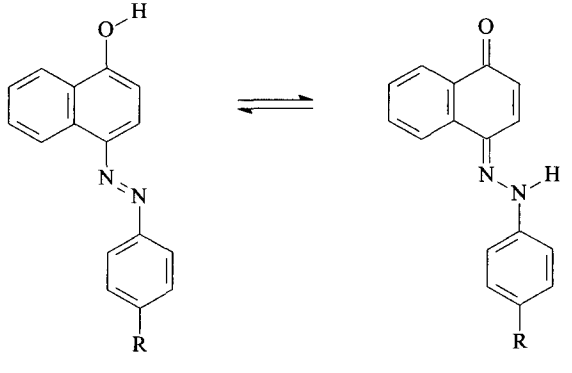

[36]

Table 15. ^{13}C chemical shifts (ppm) of compounds **34–36**

Compound	R	Conditions	C1	C2	C3	C4	C5	C6	C7	C8	C9	C10
34	*p*-CH_3	$CDCl_3$	170.9	132.4	128.2	120.3	127.4	131.5	125.9	126.3	129.7	137.4
		Solid	170.0	134.5	129.4	120.2	128.0	129.4	125.3	125.3	129.4	138.8
35	*p*-NH_2	$CDCl_3$	129.2	157.7	121.3	135.0	128.0	124.3	127.6	121.5	133.0	128.6
	p-NMe_2	CD_2Cl_2	129.4	156.1	121.0	134.0	127.4	124.1	128.1	121.7	133.3	
		Solid	128.6	154.7	121.6	131.3	128.6	123.1	128.6	123.1	132.8	128.6
	H	$CDCl_3$	129.9	171.5.	124.6	139.8	128.6	125.5	128.4	121.6	133.4	127.9
		Solid	126.1	172.7	126.1	140.0	126.1	126.1	126.1	120.5	131.9	126.1
	p-NO_2	$CDCl_3$	131.9	180.0	126.3	143.4	129.7	127.5	129.1	122.4	133.0	128.5
		Solid	128.9	179.5	126.4	144.4	129.2	129.2	129.2	123.1	[a]	128.9
36	*p*-SO_3Na	D_2O(pH 2.4)	136.0	125.8	123.3	186.4	125.3	132.9	128.1	126.6	128.9	132.1
	p-NO_2	Solid	135.4	126.0	123.0	186.4	126.0	132.0	128.3	126.0	128.5	133.2

[a] Data not available.

In Table 15, ^{13}C chemical shifts in arylazo derivatives of 2-naphthol (**34** and **35**) and 1-naphthol (**36**) are presented.

The structure of a reagent known under the commercial name 'calcion-calcichrom' has been studied[96] in solution and in the solid state using ^{13}C CP/MAS NMR. The actual structure of this reagent (**37**) differs from the earlier supposed structure.

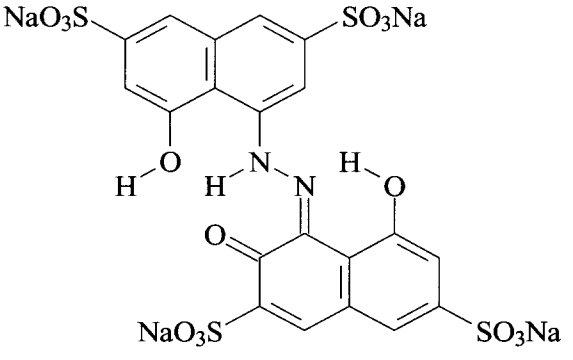

[37]

Fedorov and Rebrov[97] studied the ^{13}C CP/MAS NMR spectrum of dithiazone and compared the data obtained with those from x-ray studies.

Table 16. ^{13}C chemical shifts (ppm) of the polymorphs of compound **38**

Carbon atom no.	Polymorph A	Polymorph B	Polymorph C
1	155.7	155.3	156.0
2	130.5	130.3	131.4
6	114.9	115.0	114.9
3,5	124.2	123.0	123.8, 125.7
4	147.0	145.3	146.7
1′	130.0	131.7	134.4
2′	141.4, 135.2	141.5, 135.9	140.5
3′	99.0	100.8	106.7
4′	153.7	155.3	151.4
5′	107.5	107.6	109.0
6′	138.8, 117.9	138.7, 116.7	118.4
a	46.0	45.2	49.9, 48.2
b	33.8, 28.6	31.3, 30.5	33.7, 31.8
c	172.6	172.6, 172.1	171.4
d	51.9	51.6, 50.7	52.6, 51.9
e	26.6	27.0	24.3
f	170.0	169.7	169.8

Polycrystalline powder samples of disperse dyestuff 2′-acetamido-4′-(*N*,*N*-bis(2-methoxycarbonylethyl)amino)-4-nitroazobenzene[98] (**38**) have been investigated using solid-state and solution-state ^{13}C and ^{15}N NMR spectroscopy in an attempt to understand the effect of polymorphism. ^{13}C chemical shifts of three polymorphs A, B and C were assigned (Table 16). Assignment of the ^{13}C spectra indicates that it is possible to form an intramolecular hydrogen bond resulting in two conformations coexisting in the crystal structure of two of the polymorphs as well in solution, and differing by internal rotation of a side-chain acetamido group. This is clearly evident in the solid-state spectra at ambient temperature and in solution at sufficiently reduced temperatures (−80 °C). Each polymorph contains a varying amounts of each conformer as a result of different crystal interactions and conformer interchange can be shown to occur even in the solid state.

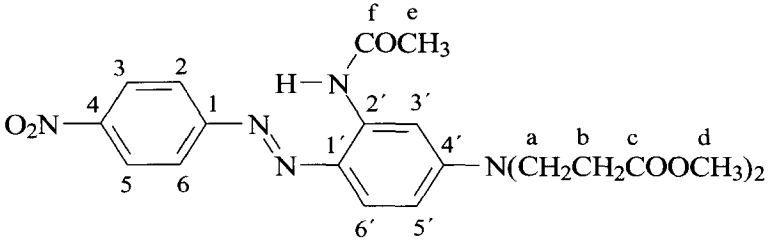

[38]

This remarkable finding is accounted for by the open nature of the crystal structures, resulting from the steric effect of substituents, as attested by packing coefficients and molecular modelling.

Maciejewska[99] has published ^{13}C CP/MAS NMR spectra of 2-methyl-4-(4-X-phenylazo)imidazoles. Proton transfer phenomena can occur in imidazoles. Depending on the nature and orientation of the substituent X it was possible to identify one tautomer for X = H, Br and NO_2 and two tautomers for X = OCH_3. Solid 2-methyl-4-(4-X-phenylazo)imidazoles form hydrogen-bonded chains with N—H···N bonds and C—H···O or C—H···N interactions.

Chippendale *et al.*[100] studied ^{13}C and ^{15}N CP/MAS NMR of free acids and sodium salts of a series of sulfonated azobenzene dyestuffs (**39**). In solution the spectra of both free acid and salts are characteristic of *trans*-azobenzene structures, as are the spectra of the solid samples of the salts. The spectra of the solid free acids are markedly different from those of the corresponding solid sodium salts (Tables 17 and 18) and exist as azonium tautomers (three resonance structures are shown for **39f**). Solid-state structures of this type are probably stabilized by the formation of intermolecular bonds.

Table 17. Solid-state ^{13}C NMR chemical shifts (ppm) for sodium salts of sulfonic acid **39**

Compound	C1	C2	C3	C4	C5	C6	C1′	C2′	C3′	C4′	C5′	C6′	Other
39a[a]	158.4	130.7	127.8[b]	146.0[c]	126.4[b]	116.4	144.2[c]	135.1	116.4[d]	158.7	112.9[d]	119.9	–
39c[e]	152.2	–	–	143.69	–	–	143.6	143.6	–	159.6	–	–	19.3
39e[f]	150.6	133.1	126.5	~142	126.5	116.2	~133	~159	103.6	~159	109.4	~129	–

[a] Assignments for carbon atom with attached protons are tentative.
[b,c,d] Interchangeable pairs of assignments.
[e] Spectrum very broad and peaks from carbon atoms with attached protons poorly resolved.
[f] Poorly resolved spectrum.

Table 18. Solid-state ^{13}C NMR chemical shifts (ppm) for the free sulfonic acids **39**

Compound	C1	C4	C1′	C2′	C4′	Methyl	Other aromatic carbon atoms
39b	141.3	146.3	140.1	–	172.2	–	118.9, 120.2, 121.2, 124.0, 126.5, 129.7
39[a]	141.4	146.4	139.7	–	172.2	–	118.9, 120.1, 121.1, 123.8, 126.3, 129.6
39d	143.1	145.6	139.3	159.1	173.0	18.5	117.0, 120.6, 124.8, 127.5, 128.8
39d[a]	143.3	145.6	138.6	158.8	173.3	18.3	117.0, 120.5, 124.0, 125.6, 127.6, 128.9
39f[a]	142.7	144.2	128.5	167.6	174.7	–	106.0, 116.1, 119.8, 123.0, 126.6, 128.5
39g	142.6	144.1	136.2	–	160.0	43.3, 41.1	115.5, 117.1, 119.7, 124.3, 125.3, 129.9

[a] From the $^{15}N_b$-labelled compound.

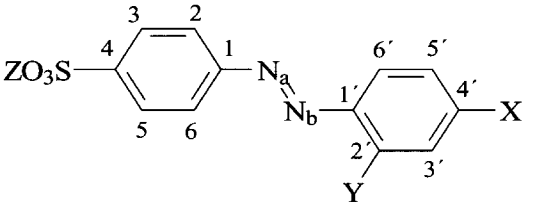

[39]

Substituent	**39a**	**39b**	**39c**	**39d**	**39e**	**39f**	**39g**
X	OH	OH	OH	OH	OH	OH	$N(CH_3)_2$
Y	H	H	CH_3	CH_3	OH	OH	H
Z	Na	H	Na	H	Na	H	H

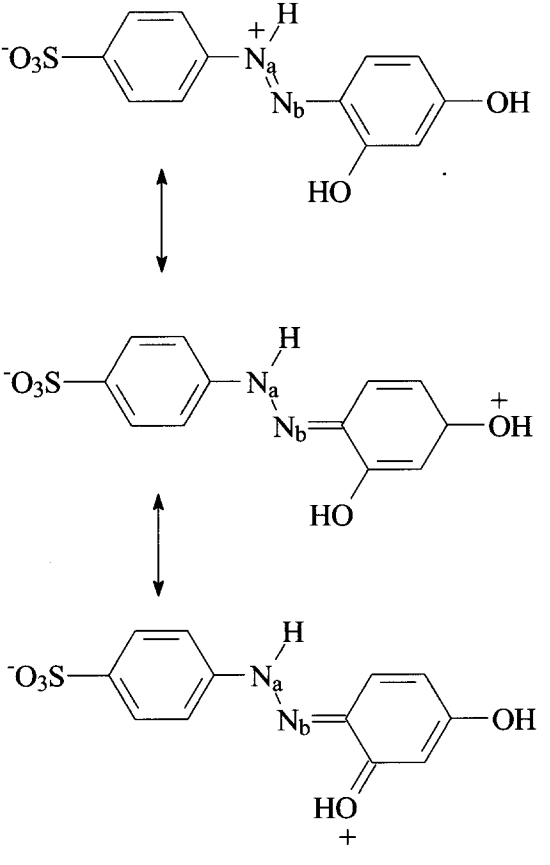

[39f]

The ^{13}C and ^{19}F CP/MAS NMR spectra[101] of two fluorinated pigments and the data were compared with their unfluorinated analogues. Law *et al.*[102] measured ^{13}C CP/MAS NMR spectra of some 'bisazo' pigments prepared by coupling starting diamino compounds with 2-hydroxy-3-naphthalanilide. Studies of the temperature and substituent effects on the ^{13}C CP/MAS NMR spectra indicate that the keto-hydrazone structure is stable and is unaffected by electronic and steric effects exerted by the substituents in the coupler moieties. The dominance of the hydrazone tautomers is attributable to both intra- and intermolecular hydrogen bondings.

Wasylishen *et al.*[103] recorded the dipolar ^{15}N NMR spectrum of a static powder sample using high-power decoupling and cross-polarization, and also the ^{15}N CP/MAS NMR spectrum of (^{15}N)-enriched *trans*-azobenzene. The shielding anisotropy for the two crystallographically nonequivalent molecules of *trans*-azobenzene is 925 and 880 ppm. The isotropic shielding constants for the two nonequivalent molecules are same within experimental error ($w_{uz} < 20$Hz). Principal components and orientation of the ^{15}N chemical shift tensor have been reported. Several years later, ^{15}N NMR spectrum of thermally unstable ^{15}N double-labelled *cis*-azobenzene[104] was studied at the same laboratory. Analysis of the ^{15}N NMR spectrum of a static sample yielded three principal components of the nitrogen chemical shift tensor: $\delta_{11} = 1006$ ppm, $\delta_{22} = 469$ ppm and $\delta_{33} = 112$ ppm. A comparison of observed and calculated NMR lineshapes indicated that the most shielded component, δ_{33}, is perpendicular to the C—N=N—C plane, while the least shielded component, δ_{11}, is in the C—N=N—C plane and oriented at approximately 15° with respect to the —N=N— internuclear vector. The observation of a doublet in the ^{15}N MAS spectrum of an 'equivalent' spin pair in ^{15}N doubly-labelled *cis*-azobenzene is due to an effect of spinning rate (changes in both intensity and lineshape of isotropic ^{15}N NMR signal) and should not be interpreted erroneously as arising from crystallographic nonequivalence. Extensions of the Hamiltonian theory and the Floquet theory indicate that as the MAS spinning frequency becomes much larger than the chemical shift anisotropy, the ^{15}N NMR lineshape will collapse into a singlet. The nitrogen chemical shift tensor in *cis*-azobenzene was compared with shifts in *trans*-azobenzene (Table 19) and compounds containing the X—N=C fragment. The difference observed between the isotropic ^{15}N chemical shifts for solid *cis*- and *trans*-azobenzene (~18 ppm) is practically the

Table 19. Experimental and theoretical ^{15}N chemical shift parameters (ppm) for *cis*- and *trans*-azobenzene (value of α^{CS} is 90°)

Compound	δ_{11}	δ_{22}	δ_{33}	δ_{150}	β^{CS}, deg	γ^{CS}, deg
cis-Azobenzene	1006	469	112	528.8	90	15
trans-Azobenzene (I)	1034	391	109	511.0	83	37
trans-Azobenzene (II)	1005	400	125	510.0	78	46

same as determined for these two isomers in $CDCl_3$ (17.5 ppm). This observation suggest that the structural and conformational integrity of both isomers of azobenzene are maintained in $CDCl_3$ solution.

The ^{15}N CP/MAS NMR spectra of ^{15}N doubly-labelled (N_a from (^{15}N) aniline, N_b from $Na^{15}NO_2$), 3-methyl-1-phenylpyrazole-4,5-dione 4-phenylhydrazone (**40**), 1-phenylazo-2-naphthol (**35**, R = H), 2-hydroxy-5-*tert*-butylazobenzene (**29**) and 4-hydroxyazobenzene (**32**) have been recorded and the temperature dependence of $\delta(^{15}N)$ (Table 20) was followed[105]. For compound **35** (R = H), representing a mixture of the azo and hydrazone forms, the hydrazone content was calculated from the ^{15}N chemical shifts of both nitrogen atoms at various temperatures (Table 21). The dependence of ln K (K = [hydrazone form]/[azo

Table 20. Temperature dependence of $\delta(^{15}N)$ (ppm) for compounds **40**, **32**, **29** and **35** in the solid state

Compound	Temperature (K)	$\delta(^{15}N_a)^a$	$\delta(^{15}N_b)$
40	305	−222.9	−37.0
	358	−222.8	−36.9
32	305	94.2[b], 57.2[b]	102.9[b], 69.0[b]
29	306	53.8	114.4
	323	54.1	114.4
35 (R = H)	194	−185.9[b], −190.2[b]	−15.9[b], −20.3[b]
	203	−183.9[b], −188.6[b]	−14.6[b], −19.1[b]
	243	−172.9[b], −178.2[b]	−8.5[b], −13.0[b]
	305	−156.4[b], −144.0[b]	−0.2[b], −3.7[b]
	358	−144.0[b], −149.7[b]	7.0[b], 3.6[b]

[a] Signal of $C_6H_5N(H)$. [b] Two signals observed.

Table 21. Temperature dependence of the hydrazone content and the equilibrium constant K (= [hydrazone form]/[azo form]) for **35** (R = H) in the solid state

Temperature (K)	Hydrazone (%)[a]	K^a	Hydrazone (%)[b]	K^b
358	71.6[c]	2.52	71.0[c]	2.45
	73.6[d]	2.79	73.2[d]	2.73
305	76.1[c]	3.18	75.7[c]	3.12
	78.1[d]	3.57	78.1[d]	3.57
243	82.0[c]	4.56	81.3[c]	4.35
	83.8[d]	5.21	84.2[d]	5.33
203	86.0[c]	6.14	85.3[c]	5.80
	87.7[d]	6.13	88.2[d]	7.47
194	86.7[c]	6.52	86.1[c]	6.19
	88.3[d]	7.55	89.0[d]	8.09

[a] Calculated from $\delta(N_a)$, signal of $C_6H_5N(H)$.
[b] Calculated from $\delta(N_b)$.
[c] High-frequency signal (see Table 20).
[d] Low-frequency signal.

Table 22. Thermodynamic data for the azo–hydrazo tautomerism of **35** (R = H) in $CDCl_3$ solution and in the solid state calculated from $-\Delta G/RT = \ln K = \Delta H/RT + \Delta S/R$ (K = [hydrazone form]/[azo form])

Nitrogen	K	ΔG^a (kJ mol^{-1})	ΔH (kJ mol^{-1})	ΔS (kJ mol^{-1})	N^b	r^e
N_a[d]	2.11[e]	−1.92[e]	(−6.23 ± 0.10	(−13.88 ± 0.35)	6	0.9995
N_b[d]	2.19[e]	−2.02[e]	(−6.37 ± 0.10)	(−14.00 ± 0.34)	6	0.9995
N_a[f,g]	3.18[h]	−2.93[h]	(−3.35 ± 0.12)	(−1.47 ± 0.48)	5	0.9982
N_a[f,i]	3.57[h]	−3.23[h]	(−3.52 ± 0.13)	(−1.06 ± 0.26)	5	0.9980
N_b[f,g]	3.12[h]	−2.89[h]	(−3.23 ± 0.12)	(−1.33 ± 0.49)	5	0.9980
N_b[f,i]	3.57[h]	−3.23[h]	(−3.81 ± 0.12)	(−2.04 ± 0.50)	5	0.9985

[a] Calculated from $\Delta G = -RT \ln K$.
[b] Number of temperature measurements.
[c] Correlation coefficient.
[d] $CDCl_3$ solution; data from ref. 106.
[e] 310 K.
[f] Solid state.
[g] Calculated from high-frequency signals (see Table 24).
[h] 305 K.
[i] Calculated from low-frequency signals.

form]) is shown in Table 22. Some hydrazone content was found in **32** in the solid state, in contrast to the measurements in solution.

The ^{15}N CP/MAS NMR spectra of compounds **41–43** have also been recorded.[107] The results indicated that compounds **41** and **42** exist practically completely in the hydrazone form. For compound **43**, evidence for an equilibrium mixture of azo and hydrazone forms was found. In this case, two ^{15}N chemical shifts were detected in the ^{15}N CP/MAS NMR spectrum. A possible explanation for this is the existence of two molecules in the unit cell that differ in their hydrazone content as a result of different orientations of the ester methyl group.

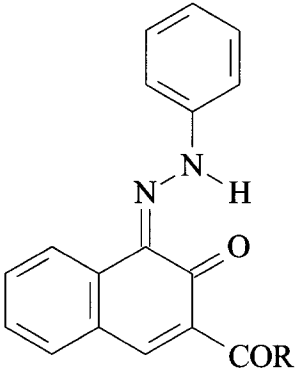

[41] R = H; **[42]** R = NHC_6H_5; **[43]** R = OCH_3

Harris *et al.*[108] investigated the ^{15}N CP/MAS NMR spectra of selectively ^{15}N-enriched C.I. Pigment Red 57 : 1 (the monohydrated calcium salt of 1-(2-sulfo-4-methylphenylazo)-2-hydroxynaphthalene)-3-carboxylic acid). ^{15}N chemical shifts provided direct evidence for the existence of the keto/hydrazone structure. ^{15}N CP/MAS NMR spectra of three ^{15}N-enriched isotopomers of polymorph 2′-acetamido-4′-(*N*,*N*-bis(2-methoxycarbonylethyl)amino)-4-nitroazobenzene[109] (**38**) were studied by Harris's group and assignment was established by rotational resonance (Table 23). The shielding tensor components were determined, and the angles of change between their orientation were established by a two-dimensional exchange experiment. Exchange rates were measured both by selective polarization inversion and by bandshape analysis. Thermodynamic parameters for the barrier are reported.[109]

4. AZO–HYDRAZONE TAUTOMERISM

Azo–hydrazone tautomerism is a property that is indivisibly linked to azo dyes. NMR techniques used for its characterization were described in the previous review.[1] Since its publication, data on several model compounds have been measured.

Although 2-hydroxy-5-*tert*-butylazobenzene (**29**) exists as a true azo compound, annelation of the benzene ring results in 1,2-naphthoquinone 1-phenylhydrazone (**35**, R = H) and 1,2-naphthoquinone 2-phenylhydrazone (**34**, R = H) being in a prevailing tautomeric form in compounds derived from 1-naphthol and 2-naphthol. 4-Hydroxyazobenzene (**32**) and 1-hydroxy-4-phenylazonaphthalene (**36**, R = H) exist in DMSO as true azo compounds. Next step in annelation of the benzene ring in the passive component led to anthracene derivatives. These compounds exist almost completely in hydrazone tautomeric forms (>95%) irrespective of the fact they were formally derived from 1-hydroxyanthraquinone or 2-hydroxyanthraquinone.[50] ^{15}N chemical shifts show nicely the dramatic changes for compounds **32**, **36**, (R = H) and 1,4-anthraquinone phenylhydrazone (**44**).

Table 23. ^{15}N chemical shift assignment for polymorphs B and C of **38** (natural abundance samples). Chemical shifts are in ppm relative to the signal for nitromethane

	$\delta^{15}N$ (solid)		$\delta^{15}N$ (solution)	
Nitrogen	Polymorph B	Polymorph C	DMSO-d_6	$CDCl_3$
N_2		59.3	62.3	
N_5		104.7	111.3	
NO_2	−14.3	−12.4	−11.9	−13.2
$NHCOCH_3$	−249.5	−254.8	−254.7	−253.9
$N(CH_2CH_2COOCH_3)_2$	−291	−298.0	−294.4	−294.7

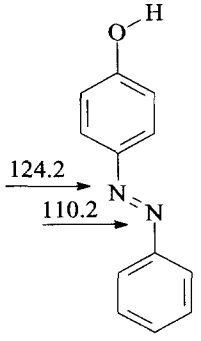

[32]

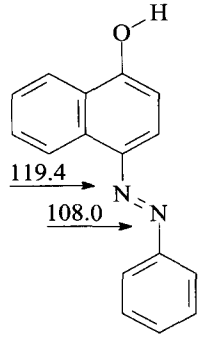

[36]

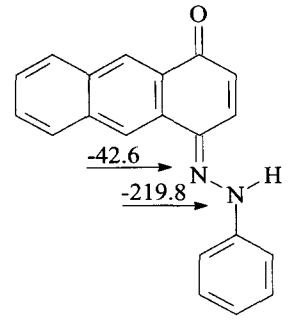

[44]

Annelation of the benzene ring in active components was also studied.[49] In contrast to annelation of the benzene ring in passive components, this effect has practically negligible influence on azo–hydrazone equilibrium, comparing the results for 1,2-naphthoquinone 1-(1-naphthyl)hydrazone (**11**) versus 1,2-naphthoquinone 1-phenylhydrazone (the increase in hydrazone content in the former compound was in the range 1–2.7% calculated from $\delta(^{15}N_a)$ (nitrogen originating from naphthylamine) and $\delta(^{15}N_b)$, and 1.2–1.6% using $J(^{15}N_a, H)$ and 1-hydroxy-4-(1-naphthyl)azonaphthalene versus 1-hydroxy-4-phenylazonaphthalene, respectively.

It was found[51] on the basis of ^{15}N chemical shifts that compound **45** is predominant while its precursor **46** exists completely in hydrazone form in position 1. Remarkable differences in $\delta(^{15}N)$ between azo and hydrazone forms in position 3 can be seen.

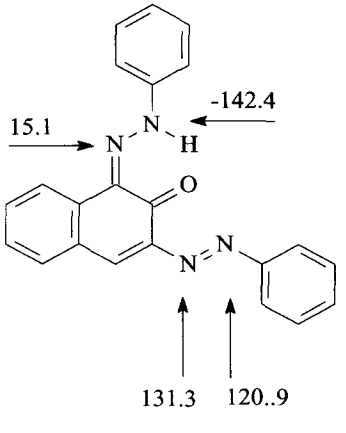

[45]

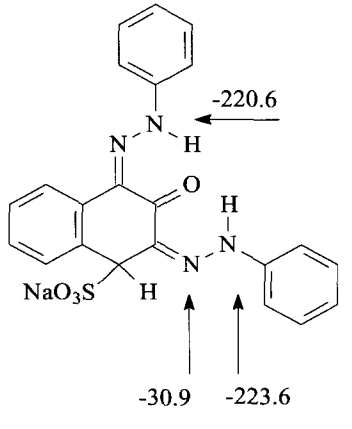

[46]

The values of $\delta(^{15}N)$ lead to the conclusion that aminoazo dyes, prepared by diazonium salt coupling reactions with aminobenzenes, aminonaphthalenes and aminoanthracenes as passive components, exist completely (in contrast to analogous compounds containing hydroxy groups) in appropriate azo forms over a wide temperature range.[1] A nice example was shown by Omura,[79] who reported $\delta(^{15}N)$ chemical shifts in twice coupled H-acid, where nitrogen chemical shifts of the arylazo group in the *ortho* position to the amino group are typical of the azo form ($\delta(^{15}N_a=)$ = 140.3, $\delta(^{15}N_b)$ = 81.8 ppm), while those of the arylazo group situated in the *ortho* position to the original hydroxyl group exist almost completely in the hydrazone form ($\delta(^{15}N_c=)$ = −196.2, $\delta(^{15}N_d)$ = 2.5 ppm) in one model compound (**20**).

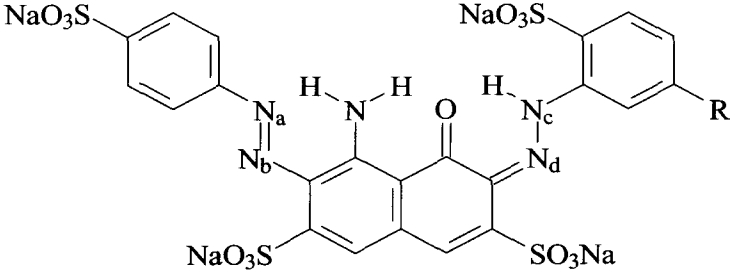

[20]

We have succeeded in showing the existence of azo–hydrazone tautomerism due to an interaction with nitrogen atom in special amino derivatives: compounds prepared by diazonium salt coupling reactions with enaminones (**47**).[110] In both ^1H and ^{13}C NMR spectra, 4-(4-Y-phenylimino)-3-(4-X-phenylhydrazonopentan-2-one **48** give only one set of data. In 4-(4-methoxyphenylimino)-3-phenylhydrazonopentan-2-one the corresponding values are $\delta(^{15}N_aH)$ = −186.2 ppm, $^1J(^{15}N_a, ^1H)$ = 83.2 Hz, $\delta(^{15}N_b=)$ − 6.4 ppm. If we consider the values of $\delta(^{15}N_aH)$ and $\delta(^{15}N_b=)$ of pentane-2,3,4-trione 3-phenylhydrazone to be limiting values for the hydrazone form with a very close structure, and if we take the chemical shifts $\delta(^{15}N_aH)$ = 69.4, $\delta(^{15}N_b=)$ = 126.9 in 2-hydroxy-5-*tert*-butylazobenzene[11] for the limiting values of corresponding nitrogen atoms in the pure azo form, then according to ref. 1 it is possible to calculate the proportion of hydrazone form in the tautomeric mixture to be 93.6% and 87.4% calculated from $\delta(^{15}N_a)$ and from $^1J(^{15}N, ^1H)$, respectively. These conclusions concerning the composition of the tautomeric mixture of the compound studied are also supported by the value $^1J(^{15}N_c, ^1H)$ = 7.6 Hz found for the nitrogen atom of the 4-methoxyphenylimino group. The ^{15}N chemical shift of nitrogen atom of the 4-methoxyphenylimino group is −80.6 ppm, which corresponds to a change by ~200 ppm as compared with the starting enaminone.

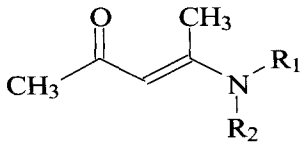

[47]

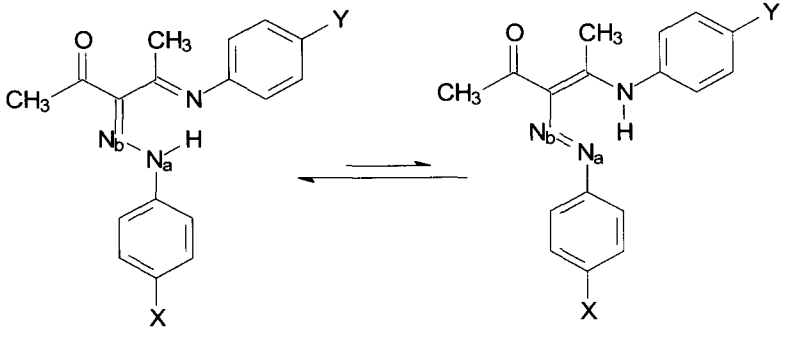

[48]

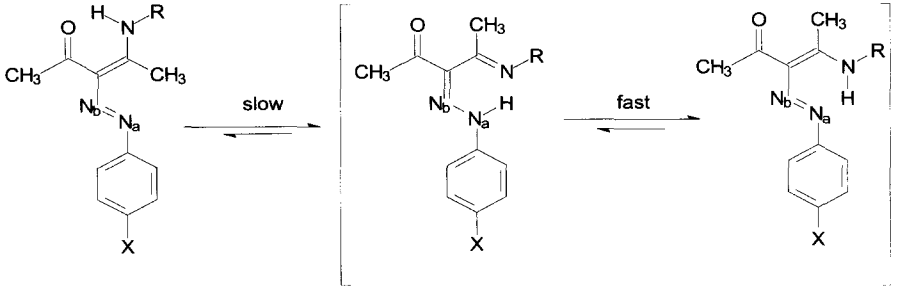

[49]

The behaviour of compounds **49** where R = H and CH_3 from is even more complicated. For example, 4-methylamino-3-(4-X-phenylazo)pent-3-ene-2-one (**49**) contains two isomers. The tautomeric form of both isomers was confirmed with the help of 2D ^1H-^{15}N GHMQC spectra. The minor isomer is very similar to the tautomeric form of azo-enamine ($^1J(^{15}N, ^1H)$ = 89.6 Hz); the major isomer possesses a somewhat stronger character of hydrazono-ketimine form ($^1J(^{15}N, ^1H)$ = 74.5 Hz; about 80% azo and 20% hydrazone). These conclusions are confirmed by the values of $\delta(^{15}NH_2)$: in the minor isomer it is $\delta(^{15}N)$ = −269.0 ppm (i.e. almost the same as in the starting enaminone with

$\delta(^{15}NH_2) = -276.4$ ppm), whereas in the major tautomer it is considerably higher ($\delta(^{15}NH_2) = -228.9$) and closer to $\delta(^{15}NH=)$ of the imino group. 4-Dimethylaminopent-3-ene-2-one undergo a subsequent diazonium salt coupling reaction to give compound **50**.[111]

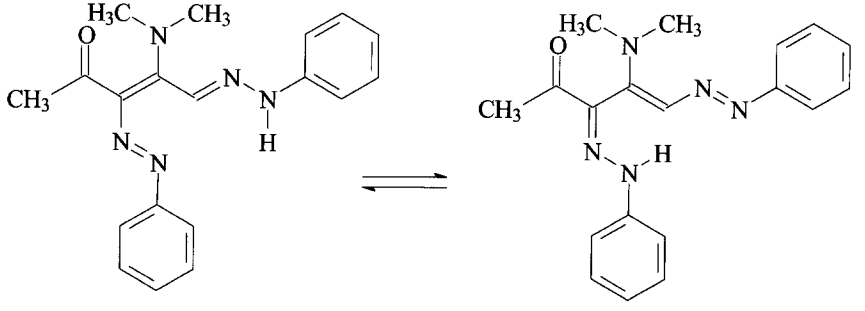

[50]

Kurasawa *et al.*[112,113] published two papers on ^1H and ^{13}C NMR of 3-(arylhydrazono)methyl-2-oxo-1,2-dihydroquinoxalines (**51**), describing the existence of hydrazone imine-diazenylenamine tautomerism.

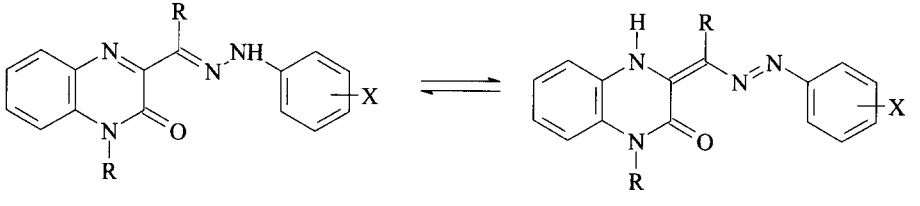

[51]

According to the author of this review, the more probable interpretation is that Kurasawa *et al.* succeeded in studying *E/Z* isomerism on the C(R)=NNH double bond than azo–hydrazone tautomerism because ^{13}C chemical shifts of ipso carbons of $=NNHC_6H_4X/-N=NC_6H_4X$ groups are about 144 ppm in both 'tautomers'. This value is typical of $=NNHC_6H_5$ arrangement, while ^{13}C chemical shift of ipso carbons in $-N=N-C_6H_5$ group would have to be about 152 ppm.[1]

Mazzola *et al.*[114] studied azo–hydrazone tautomerism and acid–base equilibria of FD&C Yellow 6 (**52**). The compound exists as a hydrazone below pH 9 and as an azo anion species at pH 14. A dynamic NMR effect was observed at pH ~12 (corresponding to pK_a according to potentiometric titration), where the midpoint of the azo–hydrazone equilibrium occurs. The observed NMR line broadening is due to slow proton transfer between

hydrazone NH and water. The conclusions are based on ^{1}H, ^{13}C, ^{15}N and $J(^{15}H, ^{13}C)$ experimental values.

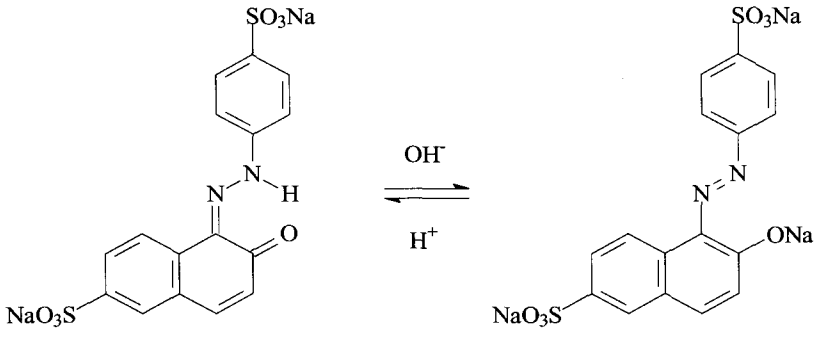

[52]

Szántay[115] and co-workers focused on a different approach to solve an analogous problem to Mazzola. They studied azo–hydrazone tautomerism in two reactive dyes (**53, 54**) using homonuclear and heteronuclear NOE measurements by measuring the spectra in DMSO as a solvent so as to observe signals of exchangeable protons. The hydrazone form is the strongly predominant tautomer over a wide range of pH values.

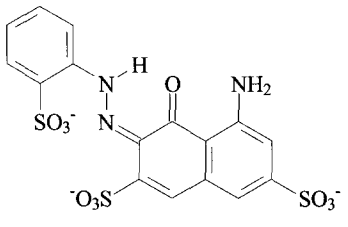

[53]

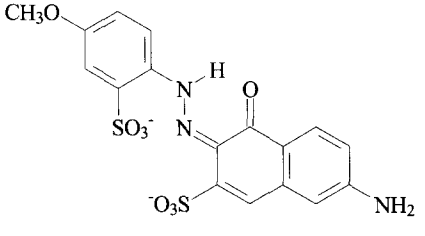

[54]

^{13}C chemical shifts of C—OH/C=O groups were used with the aim of determining azo–hydrazone tautomeric equilibrium in derivatives of squaric acid and in hydrazones of *ortho*-hydroxy aldehydes.[116]

Azo–hydrazone tautomerism of pentafulvene derivatives was studied by a Spanish group.[117,118] Compounds **55** exist as hydrazones forming hydrogen bonds to a carbonyl group. Compounds **56** containing $CH(OCH_3)_2$ group exist in *E* and *Z* hydrazone isomers. $^{1}J(^{15}N, H)$ coupling constants of NH group in ^{15}N-enriched compounds were in the range 94.5–96.5 Hz.

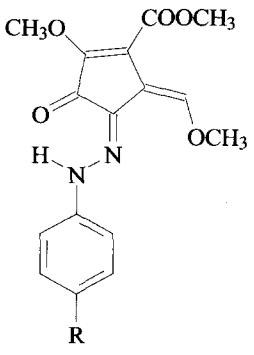

[55]

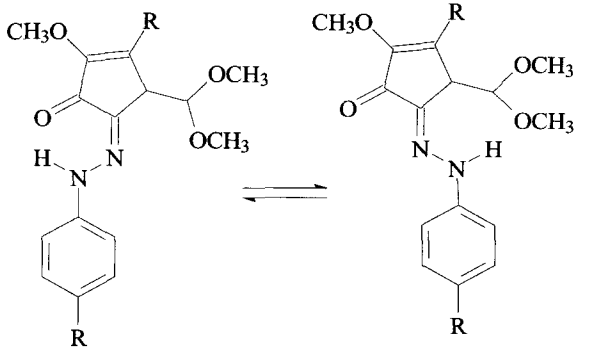

[56]

5. METAL COMPLEXES OF AZO DYES

Metal–dye complexes play a very important role in dyestuff technology and find applications in many other fields, e.g. in analytical chemistry.[119–123] Except for copper phthalocyanine, metal–azo compound complexes are the most important and the most widely used as dyes and pigments. Typical precursors are shown in Scheme 1.

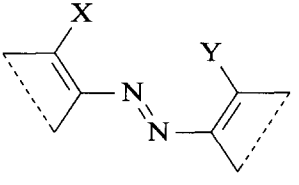

X	Y	X	Y
OH	H	OH	COOH
NH_2	H	OH	NH_2
OH	OH	OH	OCH_2COOH

Scheme 1

The metals commonly used are chromium, cobalt, copper and nickel.[119–123] More stringent governmental regulations tend to limit their use owing to the toxicological and ecological drawbacks of these colorants. There are tendencies now to substitute the above-mentioned metals by less toxic ones such as by aluminium[124] and to prepare environmentally safer dyes.

Single crystal x-ray structure determination would be an ideal tool in determining the structure of these compounds. The practical problem is that it is very difficult to grow single crystals of the metal–dye complexes and the number of structures known is thus very limited. Of the other physical methods used for the study of metal–dye complexes, NMR spectroscopy is a powerful technique. The main problems to be solved are as follows.[125]

(a) the existence of metal–dye complexes in either the azo (A) or hydrazone (B) forms in the sense of the following formulae:

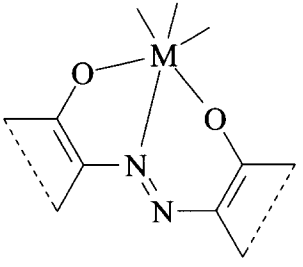

A

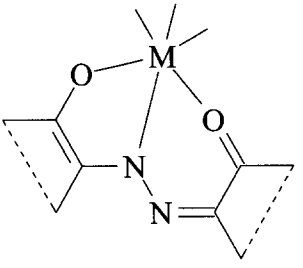

B

(b) *E*/*Z* isomerism

(c) N_a/N_b isomerism of the type shown for the azo group (and analogously for the hydrazone forms):

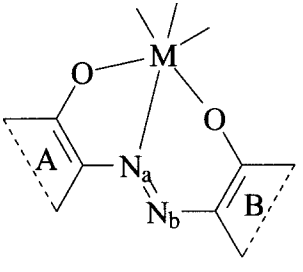

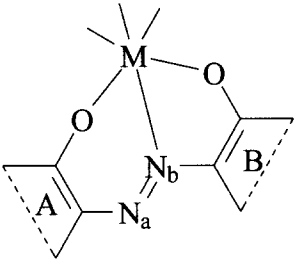

(d) The *fac* and *mer* arrangement of ligands.[119–123]

Proton NMR spectroscopy is usually used for a confirmation of the uniformity of a sample and provides a basic piece of information on a symmetry of complexes. Steiner and Schetty[126] used ^{1}H NMR spectra to show the existence of all three possible isomers (N_a, N_a,; N_a, N_b; N_b, N_b). Protons are situated on the periphery of the molecules and can hardly provide detailed information on the coordination sphere of the metal atom. NMR spectra of nuclei directly involved in coordination – nitrogen and, when possible, also the metal – are much more suitable for this purpose.

^{15}N NMR spectroscopy is a very sensitive method for the determination of coordination position of nitrogens from $-N_a=N_b-$ bonds. Pregosin and Steiner[127] have observed large *upfield* coordination chemical shifts for ^{15}N in platinum complexes **57** (−179.6 ppm) and **58** (−63.8 ppm) in which the starting ^{15}N mono-labelled substituted 2.2′-dihydroxyazobenzene exists in the azo form.

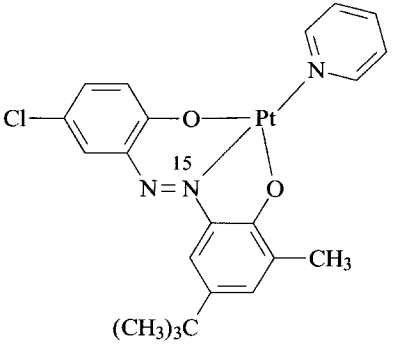

[57]

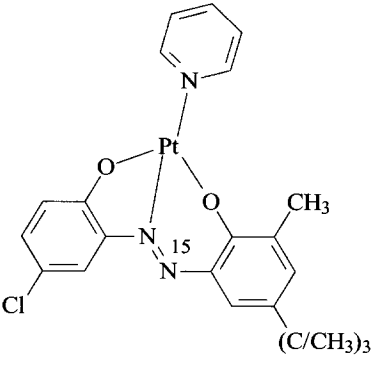

[58]

We studied so-called 2:1 cobalt(III) complexes **59** of azo dye precursors existing almost completely in their hydrazone forms.[125] In contrast to Pregosin and Steiner's results,[127] we found large *downfield* 'coordination' chemical shifts for N_a (97.2 ppm) and N_b (53.5 ppm) in **59** (X = Cl). Our results can be explained in the following way. The changes are due to a combination of two effects: the coordination, and the formal change of the hydrazone tautomeric form to the azo form. If we add the $\delta(^{15}N)$ difference observed by Pregosin and Steiner and those that we obtained, we obtain values of 276.8 (N_a) and 117.3 ppm (N_b). These data are in reasonable agreement, from the viewpoint of ^{15}N NMR, with the ^{15}N chemical shifts in the model azo and hydrazone dyes having intramolecular hydrogen bonds[106] (274 ppm for N_a and 143 ppm for N_b). This implies that metal–azo dye complexes from precursors that are either in the azo or hydrazone forms exist in their azo forms in the sense of formula **59**. ^1H, ^{13}C and ^{15}N chemical shifts are given in Table 24.

The 2:1 aluminium(III) complexes of azo dyes **60**, **61** and **62**, as environmentally safer (less toxic) dyes, have the advantage that, in addition to ^{15}N NMR spectra, ^{27}Al NMR spectral behaviour can also be studied in solution and in the solid state[128] from the viewpoint of coordination at the aluminium atom.

The aluminium atom in 2:1 complexes **60**–**62** was expected to be four-coordinated.[124] This proposal is based on a common structural presentation of simple aluminium compounds. In the case of **60**, **61** and **62**, the increase in coordination number might also be due to intramolecular bonding to one nitrogen of $-N=N-$ or $-NHN=$ bonds, respectively, per ligand.

Table 24. ^{1}H, ^{13}C and ^{15}N chemical shifts and $^{n}J(^{15}N_b, ^{13}C)$ coupling constants (Hz) of compounds **59a–c** (**a**: R = H, **b**: R = Cl, **c**: R = NO_2) in hexadeuteriodimethyl sulphoxide

	59a			**59b**			**59c**[a]	
H/C no.	$\delta(^{1}H)$	$\delta(^{13}C)$	$^{n}J(^{15}N_b, ^{13}C)$	$\delta(^{1}H)$	$\delta(^{13}C)$	$^{n}J(^{15}N_b, ^{13}C)$	$\delta(^{1}H)$	$\delta(^{13}C)$
1	2.82	26.3		2.82	26.2		2.90	26.5
2		195.8	11.8		196.1	13.1		197.1
3		119.1	1.6		119.0	3.5		119.6
4		154.9			154.4	1.0		154.4
5		137.5			136.9			136.8
6	7.04	119.8		7.03	119.6		7.07	120.2
7	7.11	128.7		7.14	128.5		7.17	128.2
8	6.98	123.8		7.02	123.9		7.04	124.1
1′		141.7	6.1		147.3	6.4		146.8
2′		167.7	2.3		165.9	1.8		173.7
3′	6.63	117.5		6.63	117.7		6.79	117.0
4′	6.92	127.9		6.93	126.7		7.94	124.1
5′	6.67	114.2			117.8			136.6
6′	8.23	114.9	3.0	6.13	113.8	3.2	9.04	110.6
N_b		47.9[a]			46.3[a,b]			
N_c	13.07	−249.1[a,c]		13.02	−247.8[a,d]		13.04	

[a] $\delta(^{15}N)$, [b] $^{1}J(^{15}N_a{}^{15}N_b)$ = 10.3 Hz, doubly labelled compound; $\delta(^{15}N_a)$ = −113.7.
[c] $^{1}J(^{15}NH)$ = 86.7 Hz, [d] $^{1}J(^{15}NH)$ = 87.9 Hz.

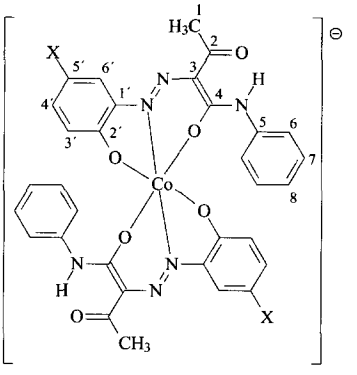

[59]

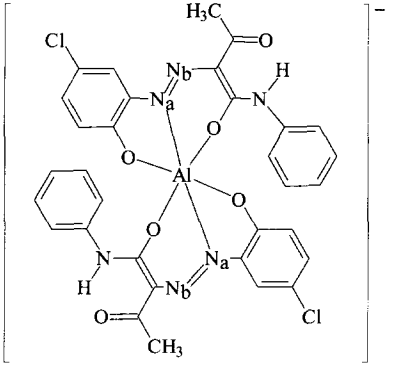

[60]

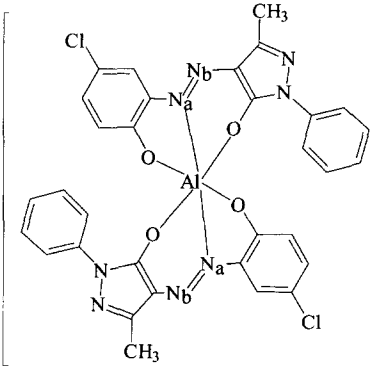

[61]

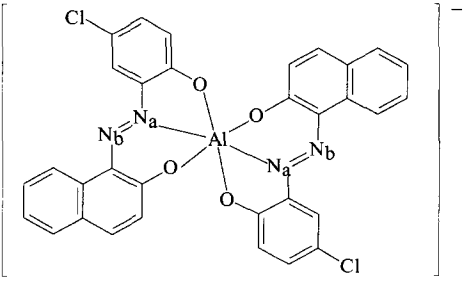

[62]

^{27}Al NMR spectroscopy is as powerful a tool for coordination number studies of aluminium[129–132] as is ^{15}N NMR for the same purpose in nitrogen-containing molecules. The ^{27}Al chemical shifts in compounds **60–62** were found to be in a very narrow range from 12.8 to 14.8 ppm. They give evidence for the aluminium central atom being six-coordinated. The differences in ^{27}Al chemical shifts measured in DMSO solution and in the solid state are less than 10 ppm (the values of ^{27}Al MAS spectra being shifted upfield, i.e. in the direction of 'stronger' sixfold coordination). Therefore, we can exclude the coordination to DMSO and, thus, coordination via nitrogen is necessary. Very similar ^{15}N chemical shifts to those observed in compounds **59** were measured in compounds **60–62** both in solution and in the solid state, giving evidence of N_a coordination.[125] ^{1}H, ^{13}C, ^{15}N and ^{27}Al chemical shifts are given in Tables 25–27.

$^{2}J(^{15}N, ^{13}C)$ coupling constants are known to show stereospecific behaviour.[133] Carbon atoms in position *cis* to the nitrogen lone pair give $^{2}J(^{15}N, ^{13}C)$

Table 25. ^{1}H, ^{13}C, ^{15}N and ^{27}Al NMR chemical shifts (ppm) in compound **60** and the appropriate precursor **60a** in DMSO-d_6 and $^{n}J(^{15}N_b, ^{13}C)$ in **60**

	60a[a]		**60**[b]		
Atom no.	$\delta(^{1}H)$	$\delta(^{13}C)$	$\delta(^{1}H)$	$\delta(^{13}C)$	$^{n}J(^{15}N_b, ^{13}C)$
1	2.55	25.5	2.62	25.96	1.7
2	–	198.5	–	197.33	12.0
3	–	127.0	–	122.86	1.3
4	–	161.7	–	159.46	
NH	11.27	–	12.53	−251.2[c]	
5	–	136.8	–	136.48	
6	7.64	120.3	7.22	120.95	
7	7.40	128.7	7.14	128.92	
8	7.18	124.3	7.08	124.97	
1′	–	130.8	–	140.77	6.3
2′	10.60	144.9	–	157.97	2.7
3′	6.99	117.0	6.49	117.77	
4′	7.21	124.4	6.95	127.11	
5′	–	123.9	–	118.47	
6′	7.54	113.8	7.45	112.52	3.6
N_a	14.29	−210.8[c]	–	−103.2[c,d]	
N_b	–	−7.4[c]	–	46.8[c,d]	
				46.8[c,d]	
N_b(solid)	–	–	–	54.5[c,e]	
				49.6[c,e]	
Al	–	–	–	12.8[f]	
Al (solid)	–	–	–	6.6–8.6[f]	

[a] Data taken from ref. 171. [b] Prepared in DMF. [c] $\delta(^{15}N)$. [d] Measured at the natural abundance level of ^{15}N. [e] ^{15}N-labelled compound. [f] $\delta(^{27}Al)$.

Table 26. ^{1}H, ^{13}C, ^{15}N and ^{27}Al NMR chemical shifts (ppm) in compound **61** and the appropriate precursor **61a** in DMSO-d_6 and $^{n}J(^{15}N_b, ^{13}C)$ in **61**

	61a		**61a**[a]		
Atom no.	$\delta(^{1}H)$	$\delta(^{13}C)$	$\delta(^{1}H)$	$\delta(^{13}C)$	$^{n}J(^{15}N_b, ^{13}C)$
3	–	148.95	–	148.44	8.1
4	–	128.81	–	124.56	2.6
5	–	156.96	–	150.82	
6	–	137.69	–	137.97	
7	7.93	117.48	7.61	119.13	
8	7.47	128.71	7.33	128.99	
9	7.25	124.70	7.16	125.41	
10	2.33	11.31	2.47	11.73	
1′	–	130.03	–	139.37	5.3
2′	10.83	144.89	–	158.99	2.9
3′	7.01	117.06	6.52	118.98	
4′	7.10	125.14	7.05	129.57	
5′	–	123.94	–	118.85	
6′	7.58	113.66	7.57	113.45	3.8
N_a	13.43	–	–	–	
N_b	–	−26.0[b,c]	–	37.7[b,c]	
N_b(solid)		–		38.3[b,c,d]	
Al	–	–	–	14.8[e]	
Al(solid)	–	–	–	6.6[e]	

[a] Prepared in DMF. [b] $\delta(^{15}N)$. [c] ^{15}N-labelled compound. [d] Broad signal. [e] $\delta(^{27}Al)$.

coupling constants of about 8–13 Hz in planar model compounds, while carbon atoms in position '*trans*' to the nitrogen lone pair have the $^{2}J(^{15}N, ^{13}C)$ coupling constants close to zero. In ligands of **61** and **62**, there is only one oxygen atom in the pyrazolone or naphthol parts of the molecules capable of complexing aluminium. The respective parts in the complexes are rigid and $^{2}J(^{15}N_b, ^{13}C)$ coupling constants can be used as an additional and independent proof of N_a versus N_b isomerism. In ligand **60**, there are two oxygens ($CH_3C(=O)-$ and $-CONH-$) in the acetoacetanilide part of the molecule capable of complexing aluminium. The complexation of metals via the $CH_3C(=O)-$ oxygen is presented in the literature.[1–6] According to ^{15}N chemical shifts, similar to those in compounds **61** and **62**, compound **60** is the N_a isomer. $^{2}J(^{15}N_b, ^{13}C)$ is 12.0 Hz for C2 and <1 Hz for for C4 giving evidence that, analogously to the cobalt compounds **59**, the aluminium is bound to oxygen originating from the amide group in compound **60** and not to the oxygen from $COCH_3$ group as usually reported.[6]

The ^{1}H and ^{13}C of 1 : 1 square-planar nickel(II), palladium(II) and platinum(II) complexes **63** of some *o*,*o*′-dihydroxyazoarenes were studied by Abilagaard *et al.*[134] Pyridine or tributylamine were used to increase the

Table 27. ^{1}H, ^{13}C, ^{15}N and ^{27}Al NMR chemical shifts (ppm) in compound **62** and the appropriate precursor **62a** in DMSO-d_6 and $^{n}J(^{15}N_b, ^{13}C)$ in **62**

	62a		**62**[a]		
Atom no.	$\delta(^{1}H)$	$\delta(^{13}C)$	$\delta(^{1}H)$	$\delta(^{13}C)$	$^{n}J(^{15}N_b, ^{13}C)$
1	–	130.18	–	130.45	
2	–	174.97	–	158.27	
3	6.80	125.54	6.73	125.52	
4	7.91	141.20	7.81	137.29	
4a	–	127.81	–	126.50	
5	7.73	129.04	7.78	128.22	
6	7.45	126.35	7.39	123.47	
7	7.61	129.37	7.65	128.12	
8	8.50	121.68	8.75	120.76	
8a	–	132.79	–	134.08	8.2
1′	–	132.21	–	140.44	4.9
2′	10.97	147.01	–	160.64	2.8
3′	7.05	117.59	6.52	119.63	
4′	7.21	126.85	7.14	131.15	
5′	–	124.35	–	118.98	
6′	7.91	115.04	7.84	114.33	3.8
N_a	16.22	−156.9[b]	–	–	
N_b	–	−1.5[b]	–	50.8[b,c]	
N_b(solid)	–	–	–	54.0[b,c]	
Al	–	–	–	13.3[d]	
Al (solid)	–	–		6.3–9.4[d]	

[a] Prepared in DMF. [b] $\delta(^{15}N)$. [c] ^{15}N-labelled compound. [d] $\delta(^{27}Al)$.

coordination number of metals to 4. The ^{1}H and ^{13}C chemical shifts in compounds **63** prepared form symmetrical precursor are listed in Table 28 to show the differences in chemical shifts for nonequivalent benzene nuclei in complexes.

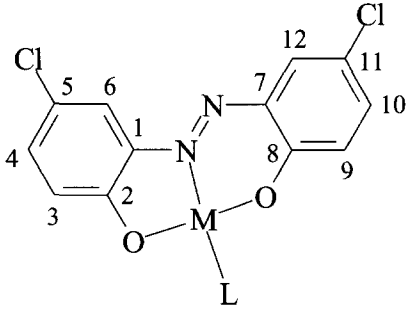

[63]

Table 28. ^{1}H and ^{13}C chemical shifts (ppm) for 5,5′-dichloro-2,2′-dihydroxyazobenzene (DCDHAB) and compounds **63a** (M = Ni, L = pyridine), **63a**, **63b** (M = Pd, L = pyridine), **63c** (M = Pt, L = pyridine), and **63d** (M = Pt, L = tributylamine)

	DCDHAB[a]		**63a**[b]		**63b**[b]		**63c**[b]		**63d**[c]	
Atom no.	^{1}H	^{13}C	^{1}H	^{13}C	^{1}H	^{13}C	^{1}H	^{13}C	^{1}H	^{13}C
1		139.0		146.9		147.0		147.0		146.7
2	11.02	154.5		164.5		166.9		167.2		167.7
3	7.10	119.9	6.79	117.9	6.99	119.4	7.18	118.3	7.09	118.3
4	7.43	132.9	7.14	129.4	7.21	131.6	7.27	130.8	7.24	130.4
5		123.9		121.5		121.5		121.9		121.1
6	7.97	119.2	8.03	116.6	8.08	117.2	8.29	118.4	8.26	116.7
7				140.5		140.6		141.8		141.6
8				149.2		150.1		148.6		148.3
9			7.02	121.9	7.23	122.1	7.30	122.9	7.16	123.1
10			7.22	132.6	7.33	134.0	7.50	132.3	7.45	131.6
11				122.2		121.6		122.9		122.1
12			7.85	131.7	7.96	132.3	8.17	131.3	8.12	131.0
1′[e]	8.62[d]	149.9	8.69	149.8	8.96	149.3	9.19	149.8	3.13	56.6
2′	7.28	123.7	7.47	124.5	7.56	125.2	7.62	125.4	1.18	26.7
3′	7.68	135.9	7.88	138.8	7.96	139.2	8.02	139.3	1.34	20.5
4′									0.94	13.9

[a] 0.1 mol L^{-1} in DMSO-d_6 at 310 K. [b] Saturated in $CDCl_3$ at 300 K. [c] 0.1 mol L^{-1} in $CDCl_3$ at 300 K. [d] 0.1 mol L^{-1} py in $CDCl_3$ at 300 K. [e] The primes refer to the chemical shifts from pyridine and tributylamine.

The compounds mentioned above are basically metal salts of organic acids, the coordination number of the metal being increased by the coordination with one nitrogen atom of the —N=N— bond. However, some azobenzenes and azonaphthalenes are capable of forming organometallic compounds by so-called cyclometallation reactions using transition metals (ref. 135 and references therein). The great potential of cyclometallation products consists in reactions with numerous reagents that provides synthetic chemists with a method of preparing molecules that are difficult to obtain by conventional preparations. Cyclopalladation[135] has been used very often. Changes in ^{15}N chemical shifts of selectively labelled phenylazonaphthalene precursors[136] were used with the aim of determining the coordinating nitrogen of the $—N_a=N_b—$ pair. A 151 ppm upfield coordination shift was obtained for nitrogen N_a in compound **64** (existing as a dimer) and a 195.8 ppm upfield coordination for nitrogen N_a in compound **65**, while ~49.9 ppm upfield shift was found for nitrogen N_b in the same compound. Two selectively ^{15}N-labelled cyclopalladated compounds had to be prepared, purified and measured.

We modified the labelling procedure by preparing only one ^{15}N doubly-labelled compound[137] with different degrees of enrichment of N_a and N_b (95 vs. 15–20% of ^{15}N, respectively). The ^{15}N NMR spectra were measured in cyclopalldated *m*toluidine analogues.[138]

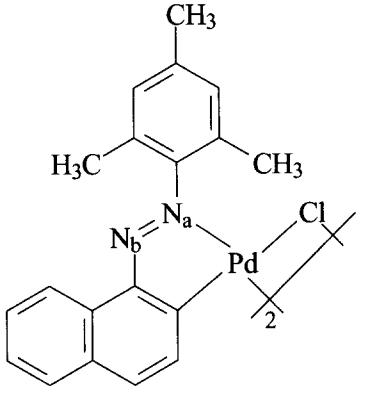

[64]

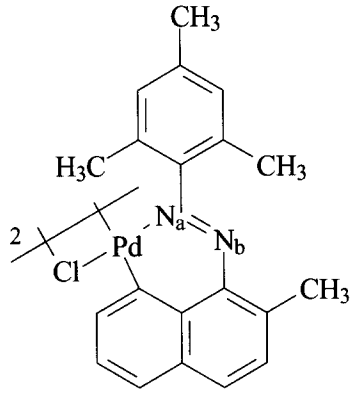

[65]

^{1}H and ^{13}C chemical shifts are very useful in determining the position of cyclometallation on aromatic rings in cases where several possible positions exist, e.g. in **66** and similar arylazonaphthalenes,[139–142] as well as in the characterization of reaction products (ref. 135 and references therein).

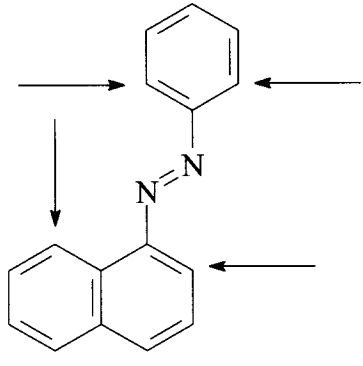

[66]

^{1}H chemical shifts have been published for palladium complexes of dialkyl a-anilinobenzylphosphonates,[143] cyclopalladated substituted azo- and azoxybenzenes,[144] phosphorus-containing palladacycles derived from 2-oxopropionaldehyde phenylhydrazones,[145] 2-oxopropionaldehyde, benzoylformaldehyde and butane-2,3-dione phenylhydrazones,[146] substituted azobenzenes with monoaryliminophosphorane ligands[147] (in last three papers ^{31}P chemical shifts were also reported), substituted azobenzenes with N,O-chelators,[148] complexes in which palladium is coordinated to one nitrogen of the azo bond and nitrogen from imidazole[149,150] and complexes in which platinum is coordinated to one nitrogen of the azo bond and sulfur from a thiother or sulfinyl group.[151]

Azo compound derivatives have been used quite frequently as ligands coordinating a wide variety of metals. These compounds can hardly be used as dyestuffs, but their NMR spectra contribute to our knowledge about them. Many of these compounds can be used as reagents in analytical chemistry.[152–154] ^1H chemical shifts have been published, for example, for nickel complexes of arylazopyrazolyl ligands,[155] ruthenium complexes[156–158] (*trans*, *cis*-$Ru(CNS)_2$(2-arylazopyridine),[156] three configurational isomers[157] of [(2,2′-bipyridine)Ru(2,2′-azobispyridine)] and *cis-trans-cis*-$Ru^{II}[NC_5H_4N{=}NC_6H_4(R)]_2$ where R = H, *o*-CH_3/Cl, *m*-CH_3/Cl and *p*-CH_3/Cl[158]). ^1H and ^{13}C chemical shifts have been reported in cobalt complexes[159,160] ([Co^{III}-*o*-$SC_6H_4N{=}NC_5H_4N)_2]ClO_4$,[159] $Co^{II}[o\text{-}OC_5H_3(R)N{=}NC_5H_4N)_2]ClO_4$ where R = H, *o*-CH_3/Cl, *m*-CH_3/Cl and *p*-CH_3/Cl,[160] ^1H and ^{13}C chemical shifts in Zn(II) complexes of 2-(2-thiazolylazo)-1,3-dicarbonyls have been reported.[161] ^1H and ^{13}C chemical shifts in mercury, silver, and gold complexes of 4, 4′-disubstituted azobenzenes can be found in ref. 162. ^1H NMR spectra of tungstenoxodidodecanoylbenzene-diazenylcalix[4]arene and its pyridine complex were published by Harvey *et al.*[163] and evidence for host–guest chemistry was demonstrated by ^1H NMR spectroscopy. Chisholm *et al.*[164] studied the reactions of $W_2(H)(OR)_7$, $W_2(OR)_6(py)_2$ and $W_4(OCH_2{}^cC_4H_7)_{12}$ with azobenzene using ^1H and ^{13}C NMR spectroscopy. Very extensive sets of proton chemical shifts in diaromatic azo derivatives of tungsten and molybdenum were published by Coe *et al.*[165] Chelation of some bisazophenyl-β-diketones with lanthanide metal ions was studied by Moustafa and co-workers[166] using ^1H NMR. Sinha *et al.*[167] published proton chemical shifts in aryazopyridine-mercury(II) coordination and organometallic compounds **67** and **68**.

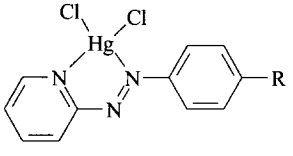

[67]

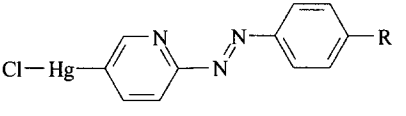

[68]

Suitably substituted azo compounds can form organometallic complexes or compounds without any participation of azo group nitrogens. 2,2′-Azopyridine reacts with diorganotin(IV) compounds[168] to form complexes via pyridine nitrogens as clear from ^1H and ^{13}C NMR spectra. Willem *et al.*[169] studied ^{119}Sn and ^{13}C NMR spectra both in solution and in the solid state of compounds **69** (R = CH_3, C_2H_5, 1-C_4H_9, C_6H_5 and C_6H_{11}) in which the tin atom is coordinated by two oxygen atoms of the carboxylic group.

We observed the same behaviour also for dibutyltin(IV) compounds derived from azo dyes existing partially or completely in the hydrazone forms.[170]

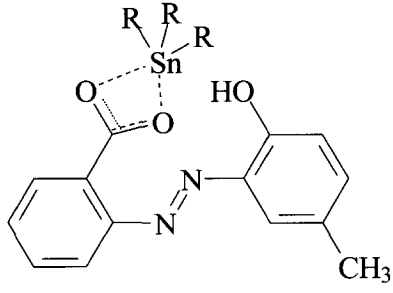

[69]

REFERENCES

1. A. Lyčka, *Annu. Rep. NMR Spectrosc.*, 1993, **26**, 247.
2. L. S. Lever, M. S. Bradley and C. S. Johnson, *J. Magn. Reson.*, 1986, **68**, 335.
3. H. S. El Khadem, M. A. Shalaby, B. Coxon and A. J. Fatiadi, *J. Chem. Soc., Perkin Trans.*, 1992, **1**, 1511.
4. E. J. Chambers and I. S. Haworth, *J. Chem. Soc., Chem. Commun.*, 1994, 1631.
5. J. Wachtfeitl, T. Nägele, B. Puell, *et al.*, *J. Photochem. Photobiol. Chem.*, 1997, **105**, 283.
6. K. F. Shuhaibar, *Dyes Pigm.*, 1992, **18**, 125.
7. J. Sokolowska-Gajda, *Dyes Pigm.*, 1992, **18**, 103.
8. M. M. Girges, *Dyes Pigm.*, 1992, **19**, 21.
9. A. A. A. Hafez and I. M. A. Award, *Dyes Pigm.*, 1992, **20**, 197.
10. A. T. Peters, E. Tsatsaroni, Ma Xisai, *Dyes Pigm.*, 1992, **20**, 41.
11. K. Bredereck and C. Schumacher, *Dyes Pigm.*, 1993, **21**, 23.
12. N. Ertan and F. Eyduran, *Dyes Pigm.*, 1995, **27**, 313.
13. K. Takagi, A. Mizuno, H. Iwamoto, S. Kawashima, S. Nishida and T. Hashikawa, *Dyes Pigm.*, 1994, **26**, 51.
14. G. J. Mohr, T. Werner and O. S. Wolfbeis, *Dyes Pigm.*, 1994, **24**, 223.
15. Yuh Wen Ho and Ing Jing Wang, *Dyes Pigm.*, 1995, **29**, 117.
16. T. G. Deligeorgiev and D. Simov, *Dyes Pigm.*, 1998, **38**, 115.
17. G. Hallas and Jae-Hong Choi, *Dyes Pigm.*, 1999, **40**, 99.
18. Kong Hyun Sunwoo, Dong Chan Kim, Kye Jung Shin, Kyung Ho Yoo, Dong Jin Kim and Sang Woo Park, *Dyes Pigm.*, 1999, **41**, 19.
19. A. Emandi, I. Serban and R. Bandula, *Dyes Pigm.*, 1999, **41**, 63.
20. R. Chandra and N. N. Ghosh, *Thermochim. Acta.*, 1991, **189**, 83.
21. H. S. Freeman and J. C. Posey, Jr, *Dyes Pigm.*, 1992, **20**, 147.
22. Jolanta Sokolowska-Gajda and Harold S. Freeman. *Dyes Pigm.*, 1992, **20**, 137.
23. D. Désilets and G. K. Hamer, *Dyes Pigm.*, 1993, **22**, 183.
24. M. A. Hanna, *Dyes Pigm.*, 1993, **21**, 113.
25. A. L. El-Ansary, W. F. El-Hawary, Y. M. Issa and A. F. Ahmed. *Asian J. Chem.*, 1996, **8**, 757.
26. E. H. El-Mossalamy and A. S. Amin, *Monatshefte für Chemie*, 1997, **128**, 23.
27. B. B. Mahapatra, R. R. Mishra, P. Roy and D. Panda, *Asian J. Chem.*, 1997, **9**, 175.
28. H. S. Freeman, S. A. McIntosh and P. Singh, *Dyes Pigm.*, 1997, **35**, 11.
29. H. S. Freeman, S. A. McIntosh and P. Singh, *Dyes Pigm.*, 1997, **35**, 149.
30. N. Ertan and P. Gürkan, *Dyes Pigm.*, 1997, **33**, 137.
31. Y. M. Issa, A. E. El-Ansary, O. E. Sheriff and M. M. El-Ajily, *Asian J. Chem.*, 1997, **9**, 301.

32. M. Matsui, Y. Marui, M. Kushida, *et al.*, *Dyes Pigm.*, 1998, **38**, 57.
33. Yao Sheng and Zhu Zhenghua, *Dyes Pigm.*, 1998, **38**, 137.
34. M. Matsui, M. Kushida, K. Funabiki, *et al.*, *Dyes Pigm.*, 1998, **37**, 283.
35. A. A. Khandar and Z. Rezvani, *Polyhedron*, 1999, **18**, 129.
36. H. S. Freeman, M. A. Mason and J. Lye, *Dyes Pigm.*, 1999, **42**, 53.
37. Zhu Zheng-Hua and Ji Cheng-Zhong, *Dyes Pigm.*, 1992, **19**, 265.
38. Zhu Zheng-Hua and Yiaodong Zhang, *Dyes Pigm.*, 1993, **21**, 173.
39. Zhu Zheng-Hua and Zhu Wei-Ping, *Dyes Pigm.*, 1994, **24**, 281.
40. Y. C. Chao and S. S. Chen, *Dyes Pigm.*, 1994, **24**, 205.
41. J. Přikryl, L. Burget, A. Halama, J. Královský and J. Akrman, *Dyes Pigm.*, 1994, **26**, 107.
42. K. Hamada, M. Uchida, M. Mitsuishi, M. Ohira and K. Mesada, *Dyes Pigm.*, 1996, **31**, 195.
43. M. Dakiky and I. Němcova, *Dyes Pigm.*, 1999, **40**, 141.
44. M. Dakiky, K. Kanan and M. Khamis, *Dyes Pigm.*, 1999, **41**, 199.
45. R. R. Ernst, G. Bodenhausen and A. Wokaun, *Principles of Nuclear Magnetic Resonance in One and Two Dimensions*, Clarendon Press, Oxford, 1987.
46. W. Hull, in *Two-Dimensional NMR Spectroscopy. Application for Chemists and Biochemists* (ed. W. R. Croasmun and R. M. K. Carlson) 2nd edn, Chapter 2, VCH, New York, 1994.
47. S. Braun, H.-O. Kalinowski and S. Berger, *150 and More Basic NMR Experiments*, VCH, Weinheim, 1998.
48. A. Lyčka and J. Jirman, in *Colour Chemistry* (ed. A. T. Peters and H. S. Freeman), Chapter 10, Elsevier Applied Science, London, 1991.
49. A. Lyčka, *Dyes Pigm.*, 1999, **43**, 27.
50. A. Lyčka, J. Jirman and H. Mustroph, *Dyes Pigm.*, 1995, **28**, 207.
51. Vrba Z. and A. Lyčka, *Dyes Pigm.*, 1996, **32**, 7.
52. V. Buss and L. Eggers, *Tetrahedron Asymmetry*, 1997, **8**, 1531.
53. A. Lyčka, J. Jirman and A. Koloničný, *Coll. Czech. Chem. Commun.*, 1998, **63**, 1012.
54. H. Mustroph and G. Bach, *Z. Chem.*, 1985, **25**, 25.
55. A. Lyčka and H. Mustroph, *Dyes Pigm.*, 1996, **34**, 101.
56. C. J. Byrne, and D. A. R. Happer, *Aust. J. Chem.*, 1993, **46**, 887.
57. V. Koleva, T. Dudev and I. Wawer, *J. Mol. Struct.*, **412**, 1997, 153.
58. J. Jirman, *Coll. Czech. Chem. Commun.*, 1991, **56**, 2160.
59. M. Čurič, Lj., Tušek-Božič and D. Vikič-Topič, *Magn. Reson. Chem.*, 1995, **33**, 27.
60. G. Hallas and A. D. Towns, *Dyes Pigm.*, 1996, **32**, 135.
61. G. Hallas and A. D. Towns, *Dyes Pigm.*, 1997, **33**, 319.
62. I. Timtcheva, A. Pentchev, St. Metsov, Sn. Bakalova, V. Koleva and P. Nikolov, *Dyes Pigm.*, 1995, **28**, 131.
63. T. Omura, *Dyes Pigm.*, 1994, **24**, 125.
64. G. Viscardi, P. Savarino, P. Quagliotto, G. Alberti and A. Loi, *Dyes Pigm.*, 1992, **19**, 291.
65. P. Savarino, G. Viscardi, E. Barni, E. Montoneri and P. Quagliotto, *Dyes Pigm.*, 1992, **20**, 1.
66. L. A. Fedorov, P. Savarino, V. I. Dostovalova, G. Viscardi, P. Carpinano and E. Barni, *Zh. Strukt. Khim.*, 1992, **33**, 91.
67. A. Altomare, F. Ciardelli, M. S. Ghiloni, R. Solaro and N. Tirelli, *Macromol. Chem. Phys.*, 1997, **198**, 1739.
68. A. Altomare, F. Ciardelli, M. S. Ghiloni and R. Solaro, *Gaz. Chim. Ital.*, 1997, **127**, 143.
69. Xiaogong Wang, Jeng-I Chen, S. Marturunkakul, L. Li, J. Kumar and S. K. Tripathy, *Chem. Mater.*, 1997, **9**, 45.
70. L. Angiolini, F. Ciardelli, N. Tirelli and R. Solaro, *Macromolecules*, 1997, **30**, 1298.
71. A. S. Brara and M. Thiyagarajan, *Polymer*, 1998, **39**, 5923.
72. L. Angiolini, D. Caretti, L. Giorgini, *et al.*, *Polymer*, 1998, **39**, 6621.
73. Xudong Jia and Xuehai Yu, *J. Appl. Polym. Sci.*, 1996, **62**, 1979.
74. D. Vikič-Topič, P. Novak, V. Smrečki and Z. Meič, *J. Mol. Struct.*, 1997, **410–411**, 5.
75. Hansen P. E., A. Koloničný A. and A. Lyčka, *Magn. Reson. Chem.*, 1992, **30**, 786.

76. P. E. Hansen, S. Bolvig, A. Buvari-Barcza and A. Lyčka, *Acta Chem. Scand.*, 1997, **51**, 881.
77. J. Mason, in *The Chemistry of the Hydrazo, Azo and Azoxy Compounds* (ed. S. Patai), Vol. 2, Wiley, Chichester, 1997.
78. A. Lyčka and J. Pelnař, *Dyes Pigm.*, 1994, **25**, 79.
79. T. Omura, Y. Kayane and Y. Tezuka, *Dyes Pigm.*, 1992, **20**, 227.
80. T. Omura *Dyes Pigm.*, 1994, **24**, 125.
81. L. Stefaniak, *Polish J. Chem.*, 1999, **73**, 173.
82. M. Suzuku, M. Tsutsui and H. Ohmori, *Carbohydr. Res.*, 1994, **261**, 223.
83. C. Y. Wong, R. McDonald and R. G. Cavell, *Inorg. Chem.*, 1996, **35**, 325.
84. M. J. Alder, W. I. Cross, K. R. Flower and R. G. Pritchard, *J. Chem. Soc., Dalton Trans.*, 1999, 2563.
85. A. Lyčka, J. Jirman and J. Straka, *Analytical Chemistry of Synthetic Colorants* (ed. A. T. Peters and H. S. Freeman), Chapter 2, Blackie Academic & Professional, London, 1995.
86. A. M. Chippendale, A. Mathias, R. K. Harris, K. J. Packer and B. J. Say, *J. Chem. Soc., Perkin Trans.*, 1981, **2**, 1031.
87. D. Maciejewska, V. Koleva and I. Wawer, *Polish J. Chem.*, 1998, **72**, 2531.
88. J. Straka, B. Schneider, A. Lyčka and J. Jirman, *Magn. Reson. Chem.*, 1991, **29**, 500.
89. C. L. Forber, E. C. Kelusky, N. J. Bunce and M. C. Zerner, *J. Am. Chem. Soc.*, 1985, **107**, 5884.
90. R. K. Harris, P. Jonsen, K. J. Packer and C. D. Campbell, *Magn. Reson. Chem.*, 1986, **24**, 977.
91. R. K. Harris, P. Jonsen and K. J. Packer, *Magn. Reson. Chem.*, 1984, **22**, 269.
92. A. C. Olivieri, R. B. Wilson, I. C. Paul and D. Y. Curtin, *J. Am. Chem. Soc.*, 1989, **111**, 5525.
93. B. R. Hsieh, D. Desilets and P. M. Kazmeier, *Dyes Pigm.*, 1990, **14**, 165.
94. L. A. Fedorov, *Izv. Acad. Nauk SSSR, Ser. Khim.*, 1991, 2302.
95. L. A. Fedorov, A. I. Rebrov and Shen Liafang, *Dyes Pigm.*, 1992, **18**, 207.
96. L. A. Fedorov, *Izv. Acad. Nauk SSSR, Ser. Khim.*, 1991, 2775.
97. L. A. Fedorov and A. I. Rebrov, *Izv. Acad. Nauk SSSR, Ser. Khim.*, 1992, 113.
98. G. McGeorge, R. K. Harris, A. M. Chippendale and J. F. Bullock, *J. Chem. Soc., Perkin Trans.*, 1996, **2**, 1733.
99. D. Maciejewska, *J. Mol. Struct.*, 1999, **478**, 121.
100. A. M. Chippendale, G. McGeorge, R. K. Harris and C. M. Brennan, *Magn. Reson. Chem.*, 1999, **37**, 232.
101. G. Chisholm, B. Hay, K. D. M. Harris, S. J. Kitchin and K. M. Morgan, *Dyes Pigm.*, 1999, **42**, 159.
102. K.-Y. Law, S. Kaplan, R. Crandall and I. W. Tarnawskyj, *Chem. Mater.*, 1993, **5**, 557.
103. R. E. Wasylishen, W. P. Power, G. H. Penner and R. D. Curtin, *Can. J. Chem.*, 1989, **67**, 1219.
104. R. D. Curtis, J. W. Hilborn, G. Wu, M. D. Lumsden, R. E. Wasylishen and. J. A. Pincock, *J. Phys. Chem.*, 1993, **97**, 1856.
105. A. Lyčka, J. Jirman, B. Schneider and J. Straka, *Magn. Reson. Chem.*, 1988, **26**, 507.
106. N. Lyčka, D. Šnobl, V. Macháček and M. Večeřa, *Org. Magn. Reson.*, 1981, **17**, 16.
107. A. Lyčka, J. Jirman, M. Nečas, J. Straka and B. Schneider, *Col. Czech. Chem. Commun.*, 1990, **55**, 193.
108. R. K. Harris, P. Jonsen, K. J. Packer and C. D. Campbell, *Magn. Reson Chem.*, 1986, **24**, 977.
109. G. McGeorge, R. K. Harris, A. S. Batsamov, *et al.*, *J. Phys. Chem.*, 1998, **102**, 3505.
110. V. Macháček, A. Lyčka, P. Šimůnek and T. Weidlich, *Magn. Reson. Chem.*, 2000, **38**, 293.
111. V. Macháček, A. Lyčka and P. Šimůnek to be published.
112. Y. Kurasawa, A. Takano, K. Kato, A. Takada, H. S. Kim and Y. Okamoto, *J. Heterocyclic Chem.*, 1996, **33**, 421.
113. Y. Kurasawa, A. Takano, K. Kato, H. S. Kim and Y. Okamoto, *J. Heterocyclic Chem.*, 1997, **34**, 305.
114. E. F. Mazzola, S. A. Turujman, S. J. Bell, *et al.*, *Tetrahedron*, 1996, **52**, 5691.

115. C. Szántay Jr, Z. Csepregi, P. Aranyosi, I. Rusznák, L. Töke, and A. Vig, *Magn. Reson. Chem.*, 1997, **35**, 306.
116. G. N. Ledesma, G. A. Ibanes, G. M. Escandar and A. J. C. Olivieri, *J. Mol. Struct.*, 1997, **415**, 115.
117. P. Victory, A. Alvarez-Larena, X. Batllori, *et al.*, *An. Quim.*, 1992, **88**, 499.
118. P. Victory, A. Alvarez-Larena, X. Batllori, J. I. Borrell, J. Sanchez-Monge, J. F. Piniella and J. P. Rose, *J. Chem. Res. Synop. (S)*, 1993, 478.
119. R. Price, in *The Chemistry of Synthetic Dyes* (ed. K. Venkataraman), Vol. III, Chapter VII, Academic Press, New York, 1970.
120. H. Baumann, in *Ullmanns Encyclopaedie der Technischen Chemie*, Vol. 16, Verlag Chemie, Weinheim, 1978.
121. F. Beffa and G. Back, *Rev. Prog. Color Relat. Top.*, 1984, **14**, 33.
122. H. Zollinger, *Color Chemistry. Syntheses, Properties and Application of Organic Dyes and Pigments*, Verlag Chemie, Weinheim, 1987.
123. K.-H. Schündehüte, in *Meth. Organ. Chem. (Houben-Weyl)*, 1965, **10**(3), 434.
124. B. L. Kaul and D. Pflieger, GB Patent 2 259 305 A, 1993.
125. A. Lyčka, J. Jirman and A. Cee, *Magn. Reson. Chem.*, 1990, **28**, 408.
126. G. Schetty and E. Steiner, *Helv. Chim. Acta*, 1974, **57**, 2149.
127. P. S. Pregosin and E. Steiner, *Helv. Chim. Acta*, 1976, **59**, 376.
128. A. Lyčka, P. Rys and P. Skrabal, *Magn. Reson. Chem.*, 1998, **36**, 279.
129. O. Kříž, B. Čásensky, A. Lyčka, J. Fusek and S. Heřmánek, *J. Magn. Reson.*, 1984, **60**, 375.
130. J. W. Akitt, in *Multinuclear NMR* (ed. J. Mason), Chapter 9, Plenum Press, New York, 1987.
131. J. W. Akitt, *Progr. NMR Spectrosc.*, 1989, **21**, 1.
132. *Coord. Chem. Rev.* (ed. A. B. P. Lever) Vol. 149, pp. 1–400, 1996.
133. M. Witanowski, L. Stefaniak and G. A. Webb, *Annu. Rep. NMR Spectrosc.*, 1986, **18**, 195.
134. J. Abilgaard, P. E. Hansen, J. Josephsen and A. Lyčka, *Inorg. Chem.*, 1994, **33**, 5271.
135. A. J. Klaus, in *Modern Colorants: Synthesis and Structure* (ed. A. T. Peters and H. S. Freeman), Chapter 1, Blackie Academic, London, 1995.
136. K. Gehrig, M. Hugentobler, A. J. Klaus and P. Rys, *Inorg. Chem.*, 1982, **21** 2493.
137. Tušek-Božič Lj., M. Čurič, D. Vikič-Topič and A. Lyčka, *Coll. Czech. Chem. Commun.*, 1997, **62**, 1888.
138. W. Mossi, A. J. Klaus and P. Rys, *Helv. Chim. Acta*, 1992, **75**, 2531.
139. A. J. Klaus and P. Rys, *Helv. Chim. Acta*, 1981, **64**, 1452.
140. M. Hugentobler, A. J. Klaus, H. Mettler, P. Rys and G. Wehrle, *Helv. Chim. Acta*, 1982, **65**, 1202.
141. K. Gehrig, A. J. Klaus and P. Rys, *Helv. Chim. Acta*, 1983, **66**, 2603.
142. M. Hugentobler, A. J. Klaus, P. Ruppen and P. Rys, *Helv. Chim. Acta*, 1984, **67**, 113.
143. M. Čurič, Lj. Tušek-Božič, D. Vikič-Topič, *et al.*, *J. Inorg. Biochem.*, 1996, **63**, 125.
144. M. Ghedini, S. Morrone, F. Neve and D. Puzzi, *Gaz. Chim. Ital.*, 1996, **126**, 511.
145. J. Albert, A. Gonzlez, J. Granell, R. Moragas, C. Puerta and P. Valerga, *Organometallics*, 1997, **16**, 3775.
146. J. Albert, A. Gonzalez, J. Granell, R. Moragas, X. Solans and M. Font-Bardia, *J. Chem. Soc., Dalton Trans.*, 1998, 1781.
147. J. Vicente, A. Arcas, D. Bautista and M. C. Ramirez de Arellano, *Organometallics*, 1998, **17**, 4544.
148. K. Bag, T. K. Misra and C. Sinha, *Polyhedron*, 1998, **17**, 4109.
149. D. Das and C. Sinha, *Transition Met. Chem.*, 1998, **23**, 309.
150. D. Das and C. Sinha, *Indian J. Chem.*, 1998, **37A**, 531.
151. C. Sinha, *Polyhedron*, 1993, **12**, 2363.
152. L. A. Fedorov, *NMR Spectroscopy of Metal Organic Compounds* (in Russian), Nauka, Moscow, 1984.

153. L. A. Fedorov, *NMR Spectroscopy of Organic and Analytical Reagents and their Complexes with Metal Ions* (in Russian), Nauka, Moscow, 1987.
154. S. Oszwaldowski and M. Jarosz, *Chem. Anal. (Warsaw)*, 1997, **42**, 739.
155. A. la Cour, M. Findejsen, K. Hansen, *et al.*, *J. Chem. Soc., Dalton Trans.*, 1997, 2045.
156. M. Kakoti, S. Chaudhury, A. K. Deb and S. Goswami, *Polyhedron*, 1993, **12**, 7.
157. M. Heilmann, F. Baumann, W. Kaim and J. Fiedler, *J. Chem. Soc., Faraday Trans.*, 1996, **92**, 4227.
158. P. Munshi, R. Samanta and G. K. Lahiri, *Polyhedron*, 1998, **17**, 1913.
159. B. K. Santra and G. K. Lahiri, J. *Chem. Soc., Dalton Trans.*, 1997, 188.
160. A. Bhararth, B. K. Santra, P. Munshi and G. K. Lahiri, *J. Chem. Soc., Dalton Trans.*, 1998, 2643.
161. K. Krishnankutty and D. K. Babu, *J. Indian. Chem. Soc.*, 1996, **73**, 379.
162. K. Vicente, M. D. Bermúdes, F. J. Carrión and G. Martnez-Nicolás, *J. Organometal Chem.*, 1994, **480**, 103.
163. P. D. Harvey, J. Gagnon, R. Provencher, Bing Xu and T. M. Swager, *Can. J. Chem.*, 1996, **74**, 2279.
164. J. T. Barry, M. H. Chisholm, K. Folting, J. C. Huffman and W. E. Streib, *Polyhedron*, 1996, **16**, 2113.
165. B. J. Coe, J.-D. Foulon, T. A. Hamor, *et al.*, *J. Chem. Soc., Dalton Trans.*, 1994, 3427.
166. M. M. Moustafa, A. S. Amin and R. M. Issa, *Monatshefte für Chemie*, 1997, **128**, 423.
167. K. Bag, N. K. De, B. R. De and C. Sinha, *Proc. Indian Acad. Sci.*, 1997, **109**, 159.
168. F. Caruso, M. Giomini, A. M. Giuliani and E. Rivarola, *J. Organomet. Chem.*, 1996, **506**, 67.
169. R. Willem, I. Verbruggen, M. Gielen, *et al.*, *Organometallics*, 1998, **17**, 5758.
170. A. Lyčka, unpublished results.
171. J. Jirman and A. Lyčka, *Dyes Pigm.*, 1987, **8**, 55.

1. INTRODUCTION

The purpose of this article is to review the progress of solid-state nuclear magnetic resonance over the last 4 years (ca. May 1995–May 1999) and is written as a sequel to our previous review.[1] As in that review, the emphasis will be placed on the methodological developments. Nevertheless, the applications of the technical advances, particularly those that are significant to chemistry, biochemistry, biology and materials science, will also be mentioned.

In general, the overall trend of solid-state NMR, spectroscopy and imaging alike is still dependent on improvements in resolution and sensitivity. Higher magnetic fields, more intense decoupling power, higher spinning rates, more robust pulse sequences and novel designs of RF coils remain the routes pursued in achieving better solid-state NMR spectra. For instance, NMR spectrometers operating up to 800 MHz and equipped with solid-state accessories have been in use in a few laboratories, while a 1 GHz spectrometer with resistive magnet has been tested.[2]

RF field strength in solid-state NMR has been reported as high as 300 kHz, and this was believed to be particularly powerful for quadrupolar spin systems.[3] On the other hand, the magic angle spinning (MAS) rate with 1–2.5 mm i.d. rotors has reached 30–35 kHz in several laboratories.[4–10] Pulsed gradient field strength up to 12 000 $G\,cm^{-1}$ was generated by Zhang and Cory,[11,12] who observed spin diffusion in a strongly coupled homogeneous spin system for the first time.

These advances, mainly in hardware, along with developments of pulse sequences, have tremendous potential in virtually every aspect of solid-state NMR and nuclear magnetic resonance imaging. Each will be covered in the following sections.

We begin with the theoretical and computational progress in solid-state NMR, which includes calculations of the lineshapes and dynamic processes based on density matrix theory or computations of the interaction parameters based on quantum (statistical) mechanics.

Apart from MAS, another popular method for obtaining high-resolution NMR spectra is the efficient decoupling of dipolar interactions in solid samples. Section 3 is devoted to progresses in this area, which has witnessed renewed interests in the past few years.

Although more powerful hardware is almost always considered as an answer to achieving better solid-state NMR spectra, new problems can emerge with the improvement of the existing techniques. Most conspicuously, while MAS with very high spinning rate serves well in obtaining high-resolution NMR spectra

for solids, it may either eliminate crucial information that is desirable in structural determinations and dynamic analyses or invalidate certain mechanisms, resulting in less efficient spin dynamics processes such as cross-polarization and spin diffusion. This was clearly shown in the past few years when much work was devoted to recovering the dipolar and chemical shift tensors that had been averaged by MAS. Section 4 summarizes recently proposed recoupling schemes.

The most direct result of higher resolution and higher sensitivity brought about by the advances mentioned, as well as those reviewed in previous article,[1] is perhaps the blossoming of correlation spectroscopy in solid-state NMR. Indeed, many recoupling schemes were motivated by implementing certain types of correlation spectroscopy. Various types of correlation spectroscopy are reviewed in Section 5.

Section 6 reviews developments in cross-polarization and spin diffusion/exchange. This section is closely related to Section 4 because of the interplay between these spin dynamics processes and the recoupling schemes at high-speed spinning, which now is almost invariably used for high resolution. Actually, many recoupling techniques were motivated by effecting cross-polarization and spin diffusion under fast MAS.

Because of the close connection between spectroscopy and imaging, improvements in resolution and sensitivity in solid-state NMR spectroscopy may bring parallel progress in imaging. However, the effort invested in solid NMR imaging has been much less visible recently than that at the beginning of the 1990s. The main achievements are summarized in Section 7.

Section 8 mentions some of the 'less active' fields in solid-state NMR. However, as can be judged by the reader, at least some of these studies represent new directions in solid-state NMR.

2. THEORY AND COMPUTATION

Floquet theory is increasingly frequently used in solid-state NMR, ranging from the calculation of lineshapes, dynamics and analysis of physical processes to designing pulse sequences with prescribed functions. It has recently been extended to the calculation of proton systems[13] undergoing cross-polarization (CP) and spin diffusion (SD) involving both spin-$\frac{1}{2}$,[13] ^{2}H exchange dynamics[14] and half-integer quadrupolar spin systems.[15] Perturbation expansion based on Floquet theory is usually employed for the case of off-rotational resonance.[16] Nevertheless, with application of a proper rotation transform before performing expansion, rotational resonance lineshape can also be calculated.[17] For spin-$\frac{1}{2}$ pair systems, Kundla *et al.*[18] indicated that the lineshape can be analytically calculated, and they also reported results that could be compared with those based on Floquet theory or exact multistep calculation.

It was shown that the three methods – multistep method, perturbation expansion and diagonalization of the Floquet matrix – are numerically equivalent[19] in treating the time evolution of spin systems, though not equally efficient for the different cases. By treating the sample spinning in terms of an angular momentum operator, a physical interpretation of the Floquet description of MAS experiments in solids was presented by Boender *et al.*[20] The sample rotation was treated as a continuous 'irradiation' on the spin system by the 'phonons' from the RF field; accordingly, the Floquet Hamiltonian consisted of the spin–phonon interaction.

Floquet theory was also combined with the multistep method to develop an efficient scheme called COMPUTE[21] and more recently was extended to γ-averaged COMPUTE.[22–25] The COMPUTE scheme, which fully employs the periodicity of the Hamiltonian of a spinning spin system, significantly reduces the computing time so that the resolution of a solid NMR spectrum is not compromised even when the spectral width is very broad. This is extremely important when dealing with, for example, a spectrum with very strong sidebands where each sideband has complicated structure and requires high resolution for parameter elucidation.[21] The γ-averaged COMPUTE[22–25] further reduces CPU time by integrating γ analytically, which also usually increases accuracy because of the feature of the γ average. Comparison of γ-averaged COMPUTE, COMPUTE and the direct multistep method is shown in Fig. 1. Much greater saving in time by γ-averaged COMPUTE than by the other two methods is clearly seen.

A simple method for calculating the evolution of many-spin systems was proposed[26] that can be used to treat short-time behaviour (e.g. spin diffusion). A 10-proton system was studied and the result was compared with those by the exact treatment.

A general treatment of spin $\frac{1}{2}$ coupled with quadrupolar spins was given using density matrix theory.[27] This formulation enables one to calculate, on the same theoretical basis, the lineshapes of the systems with different ratios of the quadrupolar interaction to the Zeeman interaction. Additionally, it includes the spinning sidebands very naturally.

The origin of the SPEDA (Single Pulse Excitation with Delayed Acquisition) spectrum was analysed from a fundamental point of view based on long-time tail theory.[28] The macroscopic memory effect can be attributed to the correlation diffusion in the wave vector space. The nuclear spin magnetization decays at a rate much slower than exponential, depending on the dimension of the spin network embedded in the space. This explanation sheds new light on the phenomenon and hints at potential applications of this method in determining the dimension of the spin network at the mesoscopic level (1–10 nm). Because SPEDA offers high resolution in the simplest way, it may also find interesting applications in structural determination of biomolecules and imaging in the solids.

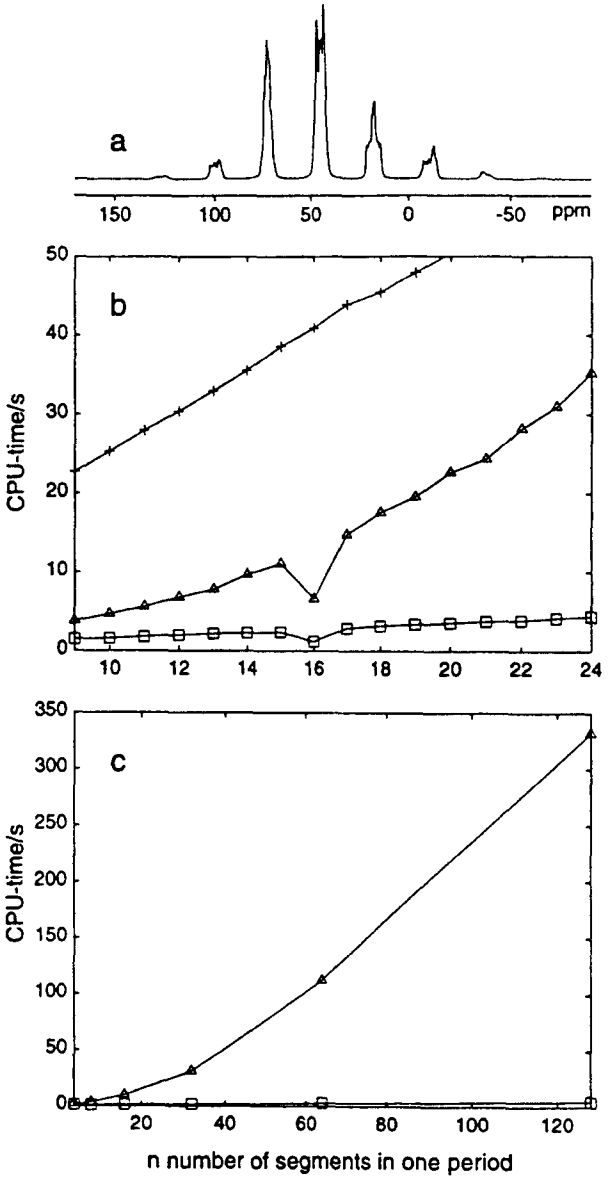

Fig. 1. (a) Simulation of a ^{31}P MAS NMR spectrum of $NiP_2C_{32}H_{36}O_2$ corresponding to a static field of 7.1 T and a spinning speed of 1111 Hz. The simulation used $n = 16\gamma_{CR}$ angles and rotor divisions, and 256 pairs of $(\alpha_{CR}, \beta_{CR})$ crystallite angles. The simulation required only 1.2 CPUs using the γ-COMPUTE algorithm, while 9.7 and 47.3 CPUs were needed for COMPUTE and the direct method, respectively. (b) The total number of CPUs used for calculating the spectrum in (a) as a function of number n for the direct method (crosses), COMPUTE (triangles), and γ-COMPUTE (squares). (c) The same as in (b) but using only Fourier numbers. (Reproduced from Hohwy *et al.*[24] with permission.)

A systematic investigation of the application of Lie algebra to NMR was presented.[29] The symmetry properties of the nuclear spin systems were naturally included in selection of the sets of the basis operators. With this theoretical framework, the existing sets of basis operators used for various specific purposes can be treated in a unified manner and their respective advantages and disadvantages can be evaluated. A number of ^{2}H MAS spectra calculated on the basis of that theoretical framework are shown in Fig. 2. The

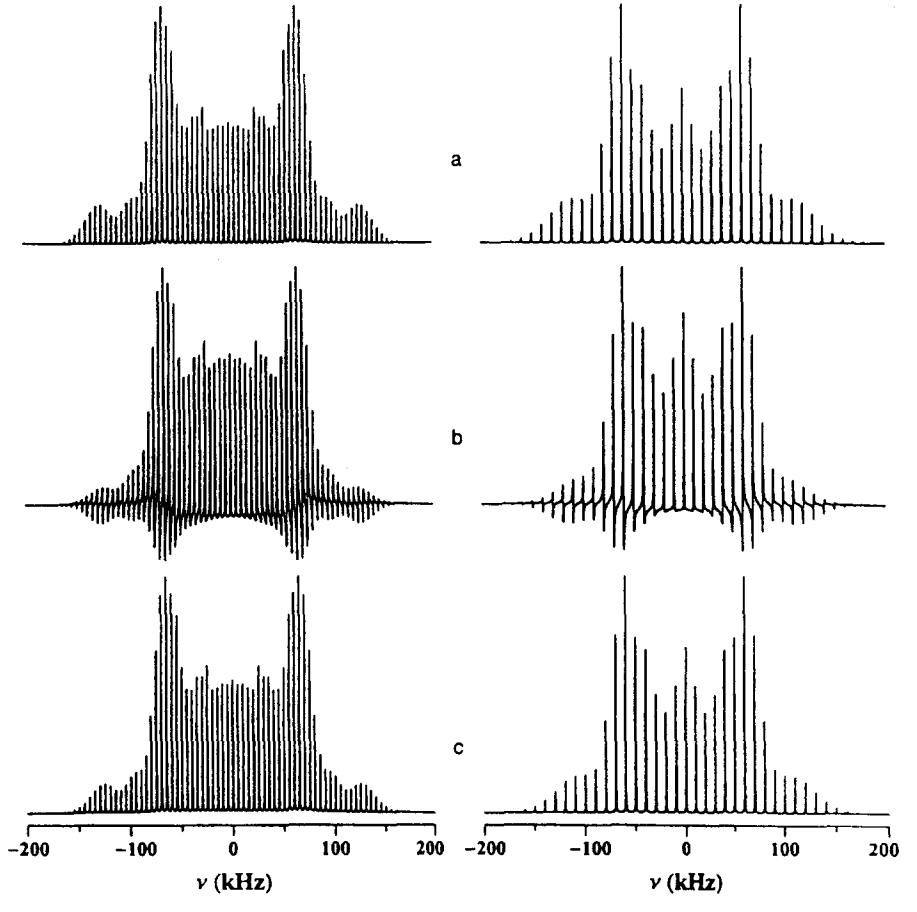

Fig. 2. Theoretical ^{2}H MAS NMR spectra calculated with quadrupolar coupling constant $C_Q = 200$ kHz, asymmetry parameter $\eta_Q = 0.10$, rotation frequency $\nu_r = 5.0$ kHz (left) and $\nu_r = 10.0$ kHz (right). The spectra represent (a) ideal RF irradiation conditions with RF field strength $\nu_{RF} = 100$ kHz and optimum pulse length $\tau_p^* = 2.25$ μs, and (b,c) nonideal RF irradiation conditions with $\nu_{RF} = 25$ kHz and $\tau_p^* = 4.25$ μs. The phase distortion effects are illustrated in (b), while (c) demonstrates the result of performing a first-order phase correction. (Adapted from Kristensen *et al.*[29] with permission.)

nonideal pulse irradiation case can be treated naturally and the phase distortion is effectively corrected.

With the advances in experimental solid-state NMR and computational resources (both software and computing power), it is now possible to use both the experimental and computational results (sometimes in a complementary way) to study biologically important macromolecules such as proteins. The quantum-chemical computation (particularly by density functional theory) of NMR parameters in solids has found important application in protein structure determination.[30–36] Tesche and Haeberlen[37] calculated the proton chemical shift tensor of the methyl groups in dimethyl terephthalate and found the theoretical results were in good agreement with the multiple pulse experiment.

So far, most of the quantum-chemical computations of solid compounds have assumed a free molecular model; that is the intermolecular effects are initially not considered. Although these second-order effects are minor in many cases and do not cause much disagreement with solid-state NMR measurements, they might become significant and should not be neglected. Recently a series of publications has addressed this problem, based on a supercell technique.[38–41] The appealing feature of this new method is that it can deal not only with free molecules but also with crystals, amorphous materials or materials with defects.

There have been a few interesting fundamental papers on ergodicity.[42–45] The distinction was emphasized between true equilibrium and quasi-equilibrium phenomena, which now are frequently observed in NMR. An isolated finite system should not be expected to become ergodic. Two other fundamentally interesting processes that have been demonstrated with solid-state NMR are dephasing caused by randomization of geometric phase,[46,47] and the possibility of the chaotic behaviour of spin systems.[48,49]

An analytical solution for the DANTE pulse sequence was found by Canet *et al.*[50] that might be useful for designing new selective pulse sequences. Goldman *et al.*[51] analysed the NMR frequency shift induced by sample spinning. For spin-$\frac{1}{2}$ systems in solids, it was shown that the intensities of the two MAS-induced RF fields are only about one-thousandth of the real RF field, hence causing no problems in most experiments. However, it becomes important in NQR experiments, for example in the appearance of geometric phase.[52]

Two new powder average approaches were proposed, named REPULSION[53] and SHREWED (spheric harmonic reduction or elimination by a weighted distribution).[54] Both techniques need only a few hundred orientations for (α, β) (instead of thousands or more for previous approaches) to obtain highly precise lineshapes of powdered (or oriented) samples. REPULSION focuses on finding the optimal set of orientations by iteratively determining an equilibrium state (minimal energy state) of a group of particles on a spherical surface under the repulsive Coulomb-like potential. SHREWED, however, may be more efficient because it focuses on reducing the error. More

interestingly, a powder (or ordered) spectrum can be improved with SHREWED by optimizing the weights without increasing the number of orientations.

A novel spectral processing approach based on information theory and the matrix pencil method was proposed by Lin *et al.*[55] that enhances sensitivity and restores the baseline and phase properties, and hence is particularly useful, for example, for delayed acquisition experiments such as SPEDA spectra.

3. DECOUPLING

3.1. Homonuclear decoupling

Interesting progress in spin decoupling, both homonuclear or heteronuclear, has been made in the past few years. For static and low-spinning-speed MAS experiments, WAHUHA, MREV-8 and BR-24 remain the widely used pulse sequences in homonuclear decoupling. Prigl and Haeberlen[56] summarized the latest development of these multiple-pulse sequences in static solids, including the spectrometer requirements, apparatus design and experimental setup as well as theoretical calculations with a five-spin system. They identified, by experimental results and numerical simulations, that the major contribution to the residual linewidth is the finite pulse width. They also offered suggestions on how to minimize the effects of the sources that cannot easily be addressed in multipulse experiments, such as sample shape and, in the case of single-crystal experiments, the crystal orientation in the sample holder.

The performance of several pulse sequences for line narrowing including MREV and WUHUHA under far off-resonance conditions was investigated by Chang *et al.*[57,58] Remarkably, it was found that these sequences remain effective even with large offsets. Cho[59] showed how to design appropriate phase cycling to avoid artefacts in multiple pulse experiments. By combining high-speed MAS and rotor synchronization, Larsen *et al.*[60–62] extended the CPMG (Carr-Purcell-Meiboom-Gill) pulse sequence to odd-half-integer quadrupolar spin systems. It was found that QCPMG (controlled CPMG) can be one order of magnitude more sensitive than quadrupolar echo MAS experiments. Assisted by numerical simulation, the QCPMG MAS experiments can be used to determine the quadrupolar as well as chemical shift tensors.[62]

Usually a homonuclear decoupling pulse sequence does not simultaneously decouple heteronuclear dipolar interactions, albeit in many cases the heteronuclear dipolar couplings need to be retained. With a significantly modified magic-sandwich sequence, Schmidt-Rohr proposed a pulse sequence that can eliminate both, at least up to first order.[63] This sequence is particularly useful for enriched ^{13}C pairs and can be readily combined with 2D experiments. It would be interesting to investigate whether such a sequence or similar ones can work for other nuclei particularly large-γ species.

For high-speed MAS experiments where the spinning period is close to the multiple pulse cycle, interference between the sample spinning and RF pulsing occurs and the aforementioned sequences might become ineffective unless extra care is taken. Hafner and Spiess[64,65] proposed that, using windowless or semi-window sequences and synchronization between pulsing and rotation, those sequences remain effective and MAS can actually play an important role in the averaging of residual dipolar interactions and helping eliminate high-order terms so that the resolution can be further improved by MAS. Demco *et al.*[66] showed that the synchronization must be set carefully: only certain ratios of the the cycle time of the pulse sequence to the spinning period can be used in order to achieve the sample spinning enhanced decoupling. For example, for the experiment with one magic-sandwich pulse, the ratio should be 1/3.

Using time-dependent perturbation theory and taking full account of the symmetry and commutation relations for the high-order dipolar Hamiltonians, Hohwy *et al.*[67–69] gave a systematic analysis of homonuclear decoupling under sample rotation and proposed a novel approach to the design of multiple-pulse experiments. Based on the theoretical analysis, they proposed a pulse sequence that can average dipolar interaction up to the fifth order. One example of these pulse sequences is shown at the top of Fig. 3. This sequence is sufficiently powerful that it is possible to obtain precise measurement of proton chemical shift anisotropies, as shown in Fig. 3.

Spin decoupling schemes in spin space, i.e. the Lee-Goldburg (LG) scheme,[70] or frequency-switched LG (FS-LG)[71,72] have also been used widely in solid-state NMR, particularly in multidimensional experiments[73–81] where MAS is not used or the evolution time is not allowed to be long enough for MAS to be effective. To implement LG or FS-LG in fast spinning experiments, several schemes have been designed[82,83] using the RF offset switch and rotor synchronized pulsing. These extended synchronization experiments are particularly important to recoupling experiments where heteronuclear coupling is to be restored as much as possible while the homonuclear dipolar coupling is suppressed to the maximum extent.

3.2. Heteronuclear decoupling

For heteronuclear decoupling, the TPPM (Two Pulse Phase Modulation) sequence[84] is now widely employed in solid-state NMR. It was extended to PMFM and FMPM by Gan and Ernst,[85] who also found that the phase inversion in TPPM brings about a secondary averaging that further reduces the heteronuclear coupling. Eden and Levitt[86] revisited the problem of heteronuclear decoupling based on the symmetry consideration of the Hamiltonian. Based on the property of the lower orders of the interaction Hamiltonians, a general theorem on the pulse sequence was conjectured that allows one to predict which terms are eliminated and which are symmetry-allowed without

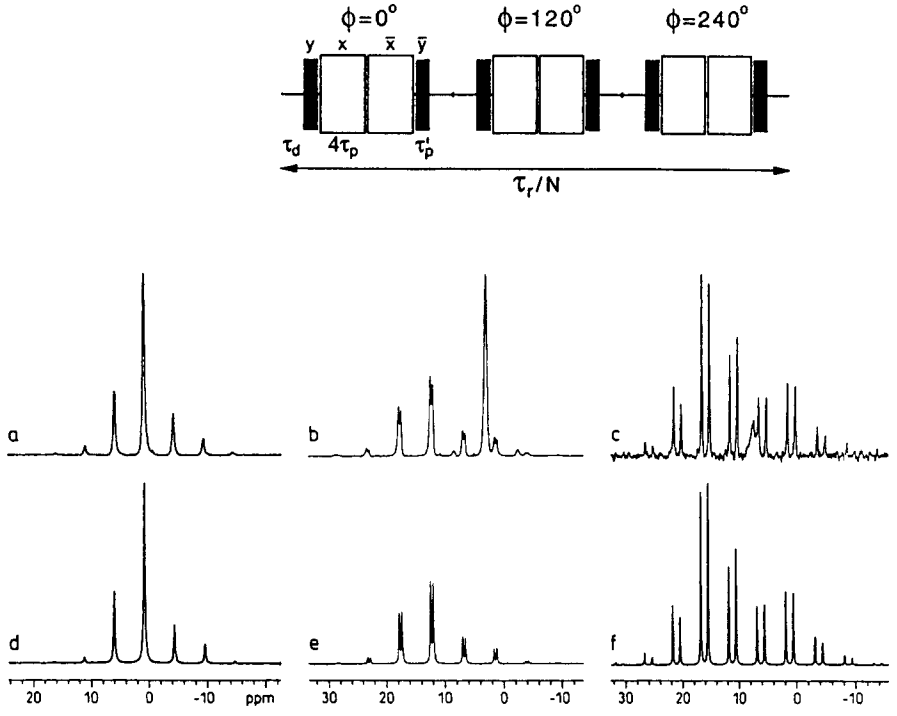

Fig. 3. *Top*: MSHOT-3 homonuclear decoupling sequence. The effective amplitudes of the bracketing ($(\pi/2)_{\pm x}$ (filled bars) and $(2\pi)_{\pm x}$ (open bars)) pulses are different (corresponding to effective 90° pulses of duration τ_p' and τ_p, respectively) to mimic the effect of finite pulse rise times; $\tau_d = 2\tau_p - \tau_p'/4$ and ϕ represent respectively the bracketing delay and overall phase (in addition to the quadrature phases $y, x, -x, -y$) of the three magic sandwich elements constituting the MSHOT-3 sequence. A small delay is inserted between adjacent RF pulses to allow accurate quadrature phase cycling. The pulse sequence is rotor synchronized to an integral number N (larger than 3) of MSHOT-3 cycles within the rotor period $\tau_r = 2\pi/\omega_r$ and one complex data point is sampled prior to each MSHOT-3 cycle. *Bottom*: ^{1}H CRAMPS (400 MHz) spectra of (a) $Ca(OH)_2$ ($\omega_r = 710$ Hz, $N = 15$), (b) malonic acid ($\omega_r = 751$ Hz, $N = 14$) and (c) $KHSO_4$ ($\omega_r = 697$ Hz, $N = 15$). (d)–(f) are simulations of (a)–(c), respectively. (Adapted from Hohwy *et al.*[69] with permission.)

any detailed calculations. They offered the following general recommendations for obtaining good heteronuclear decoupling. (i) The heteronuclear dipolar Hamiltonian should be suppressed to the first order. (ii) The second order of the heteronuclear dipolar Hamiltonian consists of the commutation terms of the homonuclear dipolar Hamiltonian and the heteronuclear dipolar Hamiltonian should be minimized. (iii) The homonuclear dipolar Hamiltonian should be retained.

The new decoupling pulse sequences CN_n^ν as shown in Fig. 4 were found to be competitive with TPPM. Furthermore, as can be seen from Fig. 5, they

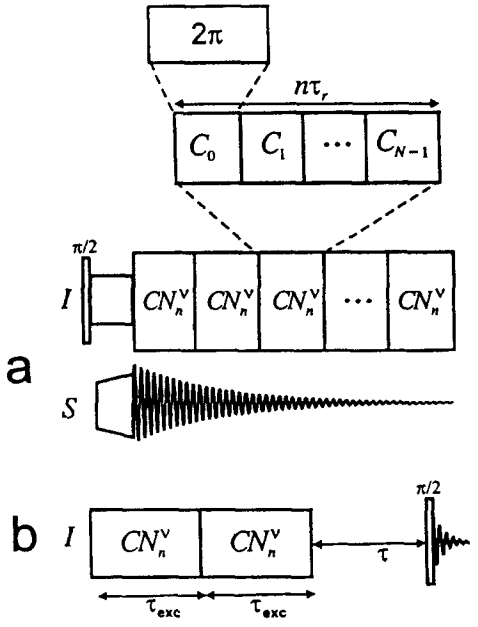

Fig. 4. (a) RF pulse scheme for acquiring a cross-polarized S-spin spectrum while irradiating the I spins with a periodic decoupling sequence CN_N^ν. C_q is shown here as a 2π pulse, with phase $\phi_q = 2\pi\nu q/N$ and duration $\tau_C = n\tau_r/N$. (b) Pulse sequence for observing 2Q filtered ^{1}H spectra. A repeating CN_n^ν sequence of total duration τ_{exc} is used for transfer of longitudinal magnetization into 2QC. The 2QCs are reconverted into longitudinal magnetization by another period τ_{exc} of CN_n^ν irradiation. After a delay τ, transverse magnetization is created by a strong $\pi/2$ pulse. Standard phase cycling is used to select NMR signals passing through $\pm 2QC$ between the CN_n^ν sequences, and through longitudinal magnetization before the $\pi/2$ pulse. (Reproduced from Eden and Levitt[86] with permission.)

demonstrated, both theoretically and experimentally, that properly breaking the symmetry of the pulse sequence, certain terms that involve the homonuclear dipolar Hamiltonian can be recovered and the heteronuclear decoupling can be improved. These results are in agreement with the observation by Tekeley *et al.*[87] who found that, to achieve good heteronuclear decoupling, homonuclear coupling should be retained as much as possible, as a manifest of self-decoupling phenomena. A similar demonstration of self-decoupling was given by Ernst *et al.*,[88] who observed that the linewidth of the ^{13}C spectrum (without heteronuclear decoupling) increases with the spinning speed. When the spinning speed is so high that the proton homonuclear dipolar coupling is effectively eliminated, the linewidth is largest.

VanderHart and Campbell[89] pointed out that the linewidth contributed by off-resonance irradiation can be effectively removed by TPPM (or its variants), but inhomogeneous contributions such as anisotropic bulk susceptibility,[90] which

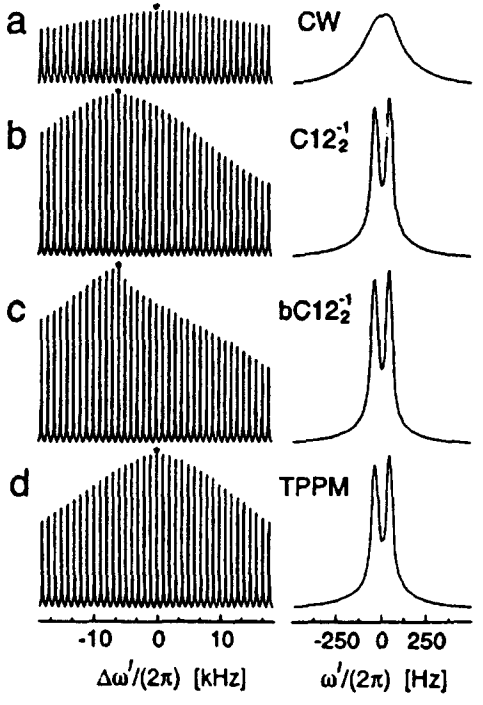

Fig. 5. ^{13}C spectra of calcium formate in a filled 4 mm zirconia rotor at a magnetic field of 9.4 T and spinning frequency of 11.7 kHz. (a) CW irradiation; (b) $C12_{\bar{2}}^{-1}$; (c) $bC12_{\bar{2}}^{-1}$; (d) TPPM. The decoupling field was $|\omega_{nut}^{I}/2\pi = 70.2$ kHz in each case, and increased to 91 kHz every twelfth cycle of the $bC12_{\bar{2}}^{-1}$ scheme. Each diagram represents an array of the proton RF frequency offset, spanning 36 kHz in steps of 1 kHz, specified relative to the centre of the proton spectrum. Expanded views of the spectra indicated by asterisks are at the right. (Reproduced from Eden and Levitt[86] with permission.)

may be much larger than that from off-resonance effect, cannot be removed. The interference between, for example, the heteronuclear dipolar and chemical shift tensors, may lead to recoupling and cause a new source of broadening that cannot be removed by TPPM, as has been shown by Ernst *et al.*[91] Moreover, slow molecular motion and MAS-assisted dipolar fluctuation may contribute to linewidth that cannot be suppressed with existing pulse schemes.[89,92].

It is worth pointing out that all of the above-mentioned decoupling schemes focus on manipulating spin-$\frac{1}{2}$ systems. It is not obvious whether they are effective or useful for decoupling schemes involving manipulation of quadrupolar spins. Fu *et al.*[93] showed that by reversing the phase of the irradiation field applied to deuterium, the heteronuclear decoupling (between proton and deuterium) can be significantly improved over CW decoupling even when a very weak irradiation field is used. They also showed that quadrupolar interactions can be refocused with properly frequency-modulated pulses.[94]

4. RECOUPLING

Restoring the interactions that are averaged out by (high-speed) MAS has been the most active research area in solid-state NMR in recent years. Novel pulse sequences for this purpose, including those can restore heteronuclear dipolar coupling, homonuclear dipolar coupling, chemical shift, etc., have been continually proposed. Some of these sequences were reviewed in the previous article,[1] hence only new developments in this direction will be summarized in the following.

4.1. Rotation echo double resonance (REDOR)

By using multiple π pulses to ensure the maximum amplitude of the refocused signal, it was found that $^{13}P-^{19}F$ REDOR can be used to measure distances in the range of 12–16 Å.[95,96] An early version of REDOR is very useful for systems with isolated spin pairs. When more spins (a cluster) are coupled to a distant spin, the homonuclear dipolar interaction within the spin clusters may cause the REDOR to decay very rapidly. A number of approaches to avoid this problem have been proposed, for example using fast MAS to suppress the intracluster dipolar interaction,[92,97] double-quantum filtering[98] because 2Q coherence is independent of dipolar coupling constant, and using multipulse sequences to decouple clusters.[99] REDOR usually offers distance information, but it was recently found that by analysing the sidebands orientational or molecular motion information might be obtained.[100,101] To cover these developments, a group of general numerical algorithms that can calculate REDOR signals of multiple-spins in the presence of molecular motion was created.[101] To enhance the REDOR signal sensitivity and/or reduce the errors caused by imperfections in the reverse 180° pulses, it was found that 4-, 8- or 16-step phase cycling[102] is sufficient in most cases and that supercycling or permutation of the phases is unnecessary.[103]

A new type of REDOR experiment (SEDOR) was proposed,[104] in which the echo amplitude is measured as a function of the spin flip angle S instead of the dephasing time as in the original REDOR. This flip angle is stepped from 0° to 180°. It is found that this θ-REDOR (SEDOR) can be used to determine how many S spins couple the observed spin I, offering an alternative way of counting spins.

Klug and Schaefer[105] extended CEDRA (Controlled-SEDRA, Simple Excitation for the Dephasing of Rotation-Echo Amplitude), which was used for heteronuclear systems, to homonuclear systems. This is named T-CEDRA. Distance can be measured but no definite information about the orientations can be obtained with T-CEDRA.

As shown by Mueller *et al.*[106–108] by so-called 'REDOR transform', i.e. the integral transform between the REDOR signal and the coupling constant

distribution, the dipolar coupling constant can be read directly from the 'spectral peaks'. This allows the determination of the coupling distribution without *a priori* assumptions.[108] This inversion problem was given by a more general analysis,[109,110] which may be equally significant to other MAS experiments.

Echo dephasing as used in REDOR has been incorporated into a series of 2D chemical shift–dipolar correlation experiments by Hong *et al.*[111,112] to apparently amplifying the coupling. In addition to the coupling constant, which gives the internuclear distance, this 2D spectrum can be used to determine the torsion angle ϕ over the full range of 360°.

It was shown that REDOR or its variants can be used when one coupling partner is a quadrupolar spin.[113,114] However, there are some limitations, such as the fact that only a fraction of the spin-$\frac{1}{2}$ nuclei are involved in the dephasing.[115] Accordingly, more specific dephasing methods have been proposed for this type of system. One is TRAPDOR (transfer of population in double resonance), which uses continuous irradiation.[116] The other is REAPDOR (rotational-echo, adiabatic passage, double resonance),[117,118] which is a more straightforward extension of REDOR.

4.2. Radiofrequency-driven recoupling (RFDR)

By applying $\pi/2$ pulses to a heteronuclear spin, RFDR can be used to recouple the heteronuclear dipolar interaction with frequency selection.[119] This opens a way to determine distances in multispin systems rather than spin-pair systems only. Both rotational and static samples can be used; the difference being that the $\pi/2$ pulses are synchronized with the sample spinning for the former and are synchronized with the RFDR pulses for the latter. RFDR was extended to homonuclear recouping by Bennett *et al.*[120] The mixing pulse sequence is the same as in the original RFDR experiment. The weak coupling can be measured, with advantages including insensitivity to RF pulse errors, applicability to systems with large chemical shift tensors and simplicity of experimental implementation and data analysis. The technique can also be used to measure multispin systems. It is found that distances up to 4.5 Å can be determined. The constant-time version (to refocus chemical shifts) which can be expressed as $CP_{90+\xi}-(RFDR)_L-90_\xi-90_0-(RFDR)_M-90_{180}-90_{90}-(RFDR)_N-ACQ$ with $L+M+N$ kept constant, was used to generate double-quantum coherence that is minimally affected by residual heteronuclear coupling and transverse relation. This method has been demonstrated to be technically undemanding and useful for the measurement of torsion angles of large molecules.[121] A pulse scheme combining TPPI and time reversal for obtaining phase-sensitive 2D RFDR homonuclear correlation spectra was proposed by Boender and Vega.[122] This method can be used to measure distances in the range of 4–6 Å, as shown with a singly-labelled sample.[123]

4.3. The CN_n^ν family

To avoid the shortcomings of early published recoupling schemes, such as the exceeding sensitivity to isotropic chemical shifts of R2, low recoupling efficiency of DRAMA and its variants, and sensitivity to RF field errors of HORROR, Lee *et al.*[124] proposed a pulse sequence named C7, as shown at the top of Fig. 4, which uses phase-shifted pulses spanning two spinning periods with phase stepping from 0 to $12\pi/7$. This sequence overcomes the aforementioned disadvantages; in particular, it offers the highest double-quantum efficiency so far, about 73%. It can also be used to excite triple-quantum coherences[125] in ^{13}C systems with an efficiency of 8%. Because of its superiority, C7 has found many applications such as elucidating dipolar coupling networks,[126] determining torsion angles ψ, ϕ in peptides,[127–129] obtaining solid-state dipolar INADEQUATE spectra,[130] and measurement of multiquantum relaxation times.[131] With a minor modification, it was found to be useful for spin counting with multiple-quantum coherence excitation up to 20 quanta.[132]

As summarized below, several C7 variants have been proposed involving permuting pulses, introducing offset and combining with MLEV. It was found that if the original basic element $C_\phi^{\bar{4}\bar{4}} = (2\pi)_\phi 2\pi)_{\phi+\pi}$ in C7 is replaced by cyclically permuted element $C_\phi^{\bar{1}\bar{4}3} = (\pi/2)_\phi(2\pi)_{\phi+\pi}(3\pi/2)_\phi$, the new sequence, termed POST-C7 (permutationally offset stabilized C7),[133] will have better tolerance towards isotropic as well as anisotropic chemical offsets and RF inhomogeneity. If the permutation is changed into $C_\phi^{\bar{1}\bar{4}3} = (\pi)_\phi(2\pi)_{\phi+\pi}(\pi)_\phi$ as in MLEV, it is found that the new version of C7, termed CMR7 (combining MLEV refocusing and C7),[134] offers almost the same high double-quantum excitation efficiency as C7 but recouples dipolar interaction over a broad band of around ± 10 kHz and has tolerance towards RF inhomogeneity as good as that of POST-C7. The usefulness of this sequence for multispin systems with large isotropic and anisotropic chemical shifts was demonstrated in ^{13}C–^{13}C correlation spectroscopy.[135] Furthermore, if the irradiation offsets are introduced to the 2π pulses in C7 in the same way as used in the LG scheme, it can be used to recouple chemical shift and heteronuclear dipolar interaction in spin systems with strong homonuclear dipolar interactions.[136] The homonuclear interaction is removed by LG pulses, while the reintroduced heteronuclear dipolar coupling and/or chemical shift anisotropy can be used to measure distances, the real chemical shift anisotropies and the relative orientation of the two tensors. Because of the RF offset, the effective field is tilted, hence the sequence is named TC_n.

4.4. Back-to-back (BABA)

A simple back-to-back (BABA) pulse sequence for generating broadband multiquantum excitation was proposed by Feike *et al.*[137] This was used to

measure dipolar couplings with double-quantum spectra,[138] triple-quantum spectra of dipolar solids at fast MAS[139] and up to 12-quantum coherence was observed at a spinning speed of 13 kHz and triple-quantum coherence at a spinning speed of 35 kHz.[140]

An extensive analysis of the MQMAS sideband pattern (for both spin-$\frac{1}{2}$ and half-integer quadrupolar systems) was given by Griedrich *et al.*[141]

4.5. Rotating/laboratory frame-driven transfer (R/L)

A pulse scheme recovering the zero-quantum Hamiltonian was proposed by Baldus and Meier.[142] It is weakly dependent on spectral parameters and a faithful measure of internuclear distances. This sequence is based on the former rotor-synchronized 'R/L-driven' polarization transfer experiments.[143,144] It uses the LG or FS-LG, which is used to decouple the high-γ spins, and combined MAS and RF irradiation of low-γ spins to decouple the heteronuclear dipolar interactions. With phase-inversion and amplitude attenuation in the rotating frame and refocusing pulses in the laboratory frame part of the pulse sequence, a zero-quantum average Hamiltonian can be obtained with optimum chemical-shift/offset independence.

4.6. Frequency-switched Lee-Goldburg (FS-LG $2\bar{m}2$)

Takegoshi and Terao[145] proposed a heteronuclear recoupling scheme based on FS-LG. The pulse sequence consists of pairs of back-to-back FS-LG pulses with given phases and frequency offsets. When the sample spinning period is equal to one or two cycle times of the pulse sequence, a zero-quantum term of the dipolar Hamiltonian is recovered, allowing this sequence to work in the spinning speed ranging from a few kilohertz to 30 kHz.

4.7. Rotational resonance (R2)

Rotational resonance has become a routine experiment and is now increasingly employed in practice. In addition to the conventional situations, its usefulness has been expanded recently. Costa *et al.*[146] found that while '$n = 1$ rotational resonance' can be used to determine the internuclear distance, the '$n = 2$ rotational resonance' contains the information for determining the relative orientation of the chemical shift and dipolar tensors.

Rotational resonance of inhomogeneously broadened systems was studied by Heller *et al.*[147] With nonlinear least-squares fitting, the distance, the inhomogeneous broadening, the zero-quantum relaxation time, and their respective errors, can be obtained. For short distances, all three parameters can

be obtained from the magnetization curves. Then the optimized zero-quantum relaxation time and inhomogeneous broadening obtained from short distances are used to determine the longer distances. It is found that zero-quantum correlation at R2 can be used to determine distances in systems such as compatible polymer blends.[148]

R2 has found several new cousins.[149–152] Takegoshi *et al.*[149] proposed an R2 experiment in the tilted rotating frame, called R2TR. The principle is actually the same as the cross-polarization experiment in a fast-rotating sample, where the Hartman–Hahn condition is altered so that the sum or the difference of the two effective fields must be a multiple of the sample spinning rate. The usual R2 experiment requires large isotropic chemical shift difference between the spin pair to be recoupled. In R2TR, because the resonance condition is fulfilled in the tilted rotating frame, the sum or the difference of the two effective fields is used to match the spinning rate. Therefore, this technique can be used for recoupling two spins with small chemical shift difference. Moreover, it is easy to switch the spin pairs to be recoupled by changing the RF irradiation. This means that multiple spin pairs, for example in a multiply labelled sample, can be selected separately and the individual distances can be determined. This is illustrated in a 2D selective homonuclear polarization transfer experiment.[150] The application of this feature was demonstrated by determining the complete structure of a uniformly labelled molecule.[151]

One problem in normal R2 experiments is that the spin dynamics at rotational resonance are influenced by zero-quantum lineshape parameters such as transverse relaxation time and chemical shift dispersion. R2 tickling (R2T),[152] where a ramped RF field is applied to induce fast passage through the resonance condition, can abate this problem. It is found that the tickling greatly reduces the dependence of the zero-quantum parameters, and the very high-power proton decoupling is not required. However, it is required in order to limit signal loss during mixing in other recoupling experiments. The parameter fitting is rather simple and the accuracy is increased.

4.8. Rotary resonance recoupling (R3)

Rotary resonance recoupling (R3) was used to measure chemical shift tensors,[153] and the relative orientation of the shift and the dipolar tensors.[154] It can also be used to conduct a 3D chemical shift correlation experiment to investigate molecular rearrangement.[155] Another interesting application of the rotary resonance is to obtain an NMR spectrum with peaks at the principal values of the chemical shift tensor.[156] The principle is that the spins in principal-value orientations experience an effective field of zero magnitude at the rotary resonance, hence their magnetization vectors do not 'oscillate' while spins at other orientations may be dephased.

4.9. Dipolar recoupling with a windowless sequence (DRAWS)

Another offset-insensitive scheme, named DRAWS (dipolar recoupling with a windowless sequence), was proposed by Gregory *et al.*[157] It can be regarded as the windowless version of DRAMA, and it has the same DQ efficiency. Using the DQ build-up curves, the internuclear distance can be measured.

4.10. Modulation of RF field amplitude, frequency, phase, and sample spinning rate

The multiple-pulse-based recoupling schemes are simple in practice and sufficiently powerful in most applications, but they do not necessarily offer the best performance in terms of coherence selection efficiency, independence of certain interactions and fulfilment of special requirements. Several recoupling schemes involving more sophisticated techniques have been invented in recent years. Fu *et al.*[158] used simultaneous modulation of frequency and amplitude (SFAM) to recover heteronuclear dipolar interaction at high spinning rate with little effect of finite pulse widths. Verel *et al.*[159] used adiabatic passage through rotational resonance (APRR) by continuously changing the spinning rate around the resonance condition. APRR was found to have high transfer efficiency and to be more broadbanded. Amplitude modulation-induced adiabatic passage,[160] termed DREAM (dipolar recoupling enhancement through amplitude modulation), to select spin pairs is found to be very useful for fast MAS experiments because the recoupling efficiency increases with spinning speed. Ishiii and Terao[161] analysed the recoupling schemes with phase/frequency/amplitude modulation and found it particularly useful for recovering powder lineshape at high spinning rates.

We point out that here these recoupling schemes follow the same principle as the techniques used for improving cross-polarization (in rotating tilted frame) at high spinning speeds by adiabatic passing of the Hartman–Hahn matching condition ('rotational resonance condition in TR') through properly modulating amplitudes[162–164] and frequencies.[165] Because of its simplicity and robustness, ramped amplitude cross-polarization[166–168] has become a routine in the experiment that uses cross-polarization.

4.11. Dipolar exchange-assisted recoupling (DEAR)

As generally understood, recoupling should be realized by coherent manipulation as shown by the aforementioned methods. However, in the sense of average Hamiltonian theory, recoupling is based on dephasing. As a result, any mechanism that effects dephasing can, at least in principle, be used to design recoupling schemes. This has been demonstrated by Sachleben *et al.*[169] In this

dipolar exchanged-assisted recoupling (DEAR), after the spin to be observed is excited by a 90° pulse and has evolved for a certain period of time, a second 90° pulse is applied and the magnetization is stored in the z-direction. During the storage period, the other spin relaxes considerably and therefore the dipolar coupling is not refocused after a third 90° pulse along with an equal evolution time. Hence, recoupling occurs. The advantage of this method is that only one of the coupled spins needs to be irradiated. However, the difference between the longitudinal relaxation times of the two spins must be sufficiently large.

5. CORRELATION AND SEPARATION

5.1. Chemical shift correlation

Measurement of chemical shift based on the magic-angle turning (MAT) experiment[170–173] has been extended in several directions. The 5-π pulse MAT experiment[174] was improved to overcome the resolution limitations in the evolution dimension,[175] by incorporating Gan's pseudo-2D sideband suppression technique.[176] Furthermore, by using a new multidimensional data-processing procedure called TIGER (technique for importing greater evolution resolution),[177] the sensitivity and resolution can be increased considerably. The 5-π experiment was given the new acronym FIRE-MAT (five π replicated magic angle turning).[174,175] Gan and Ernst[178] proposed an improved pulse sequence MAT$^{\pm}$, for 2D MAT experiments. The hypercomplex 2D data can be obtained with two separate experiments: the first uses the original MAT sequence (or MAT^{-}) while the second uses MAT^{+}, which differs from MAT^{-} only by a delay of the last pulse by $t_1/2$. MAT$^{\pm}$ (Fig. 6 top) yields pure-phase absorptive spectra free of sidebands at any spinning rate and has higher sensitivity than PHORMAT.

MAT$^{\pm}$ also allows the use of rotational echoes to extend the time-domain data in the evolution dimension, which reduces the data acquisition time or improves the digital resolution along the evolution dimension. An example of chemical shift correlation spectrum using MAT$^{\pm}$ is shown in Fig. 6. By using multipulse homonuclear decoupling applied to abundant nuclei such as ^{1}H, ^{31}P and ^{19}F, Hughes *et al.*[179] showed that MAT can also be used to measure the chemical shift tensors for those nuclear species. A 3D version of PHORMAT was proposed to measure the isotropic chemical shifts, anisotropies and heteronuclear dipolar coupling.[180] It can be regarded as an alternative to the PISEMA described by Rammamoorthy *et al.*[77]

By incorporating MELODRAMA[181] (Fig. 7), which restores ^{13}C–^{13}C dipolar coupling under high-speed magic-angle spinning, Sun *et al.*[182] proposed a 3D ^{15}N–^{13}C–^{13}C chemical shift correlation method. This is useful for dispersing overlapping spectra of biological macromolecules as shown in Fig. 8.

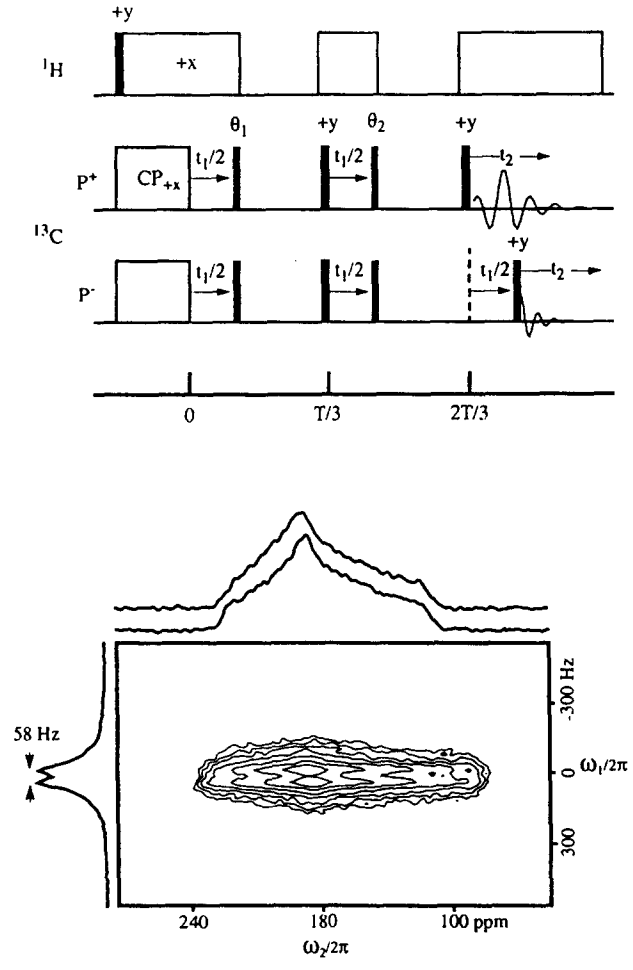

Fig. 6. *Top*: 2D MAT$^{\pm}$ sequence for correlating isotopic chemical shift and CSA with two separate experiments P$^+$ and P$^-$. All pulses following CP are 90°. A four-step phase cycling is used with $\theta_1 = -y, x, -y, x.$ and $\theta_2 = -y, x, x, -y$. The receiver phases are $x, -x, -y^*, -y^*$ for the P$^+$ pulse sequence and $x, -x, y^*, y^*$ for the P$^-$ pulse sequence. (The sign of receiver phases with an asterisk depends on the relation between the pulse phase and the receiver phase of the particular spectrometer in use. These receiver phases must be changed in sign when the quadrature phase cycle $(x, y, -x, -y)$ of the excitation pulse and the receiver phase in a single-pulse test experiment result in a null signal.) Phase alternation of the first ^{1}H 90° pulse and quadrature phase cycling of the last ^{13}C 90° pulse can be added to the above phase cycle. The time period T can be any multiple of a rotor period except for multiples of 3. *Bottom*: 2D isotropic chemical shift versus CSA spectrum of calcium formate powder with a three-fold MAT echo extension. (Taken from Gan and Ernst[178] with permission.)

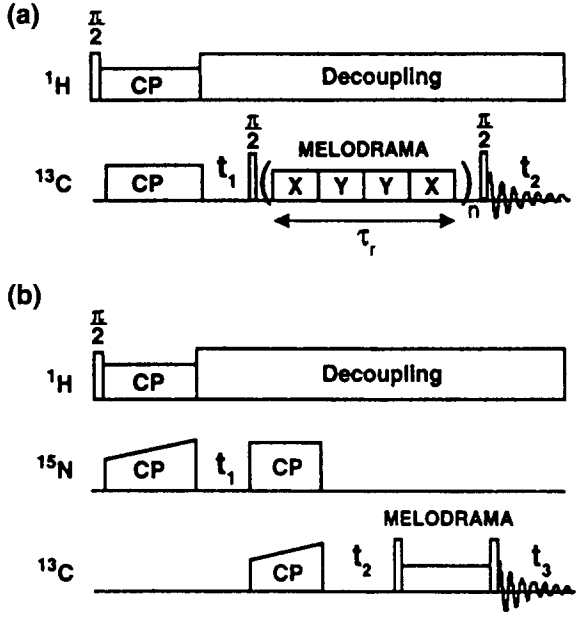

Fig. 7. (a) 2D MELODRAMA sequence for homonuclear ($^{13}C-^{13}C$) dipolar recoupling. The ^{13}C RF fields are adjusted to match the condition $\omega_{RF} = N\omega_r$, typically with $N = 4$ or 5. (b) 3D pulse sequence for $^{15}N-^{13}C-^{13}C$ chemical shift correlation spectroscopy. The proton to ^{15}N to ^{13}C transfers associated with the t_1 and t_2 periods are accomplished by RFDRCP or APHH-CP. $^{13}C-^{13}C$ recoupling is accomplished by the MELODRAMA sequence illustrated in (a). Pulse phase detection in all dimensions is accomplished by standard phase cycling procedures. High-power on-resonance CW decoupling is used during mixing periods, and TPPM decoupling during acquisition. (Adapted, with permission, from Sun *et al.*[182].)

5.2. Separation of local fields (SLF)

Using cross-polarization to establish correlation, and high spinning speed and/or FS-LG to decouple the dipolar interactions, SLF can be used to measure the proton/carbon chemical shifts.[183,184] By exploiting the differences in the lineshapes of different groups CH_n ($n = 0, 1, 2, 3$), a simple MAS-SLF scheme[185] was found to be useful for spectral assignment and to offer interesting information on local dipolar interactions. However, as with other simple MAS-SLF experiments,[186] the distance information from this method may not be accurate because it is difficult to take account precisely of the effects of the homonuclear dipolar interaction among the protons as well as the dynamical details of the lineshapes. The SLF experiment has also been implemented in 3D[74,75,78–81] and 4D[76] as well as for triple-channel probes.[81,187] An example of a 3D correlation spectrum is demonstrated in Fig. 9. SLF that

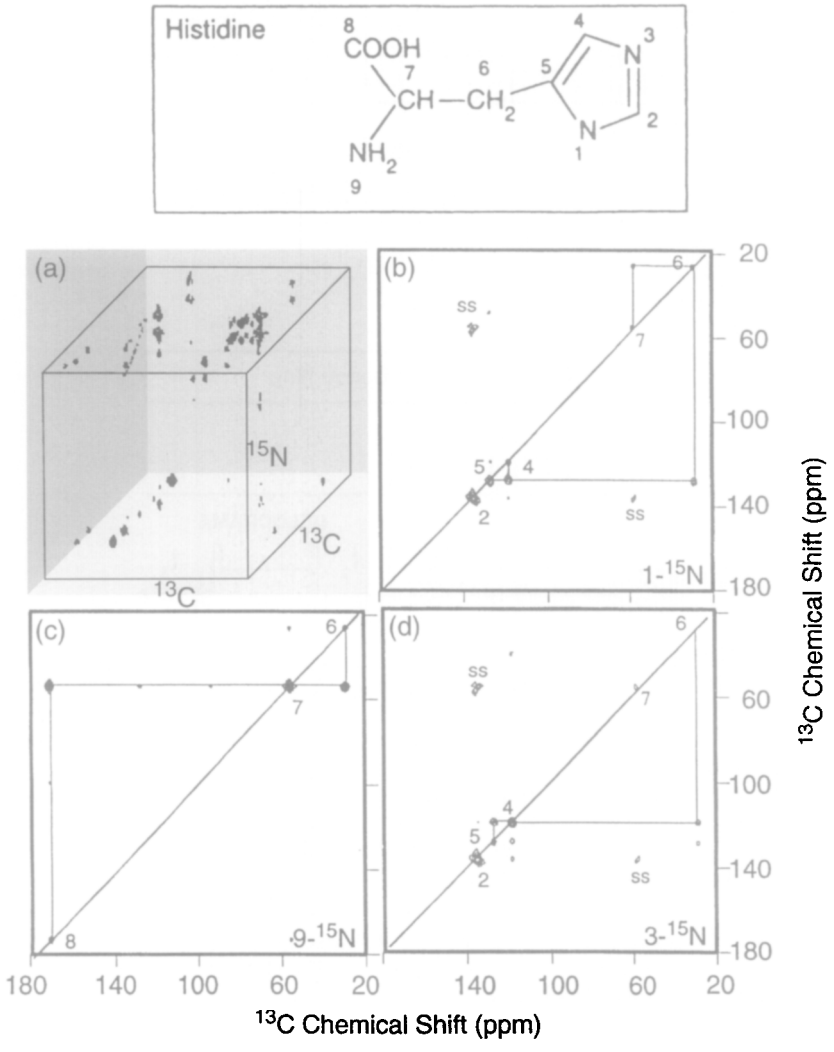

Fig. 8. (a) 3D $^{15}N-^{13}C-^{13}C$ chemical shift correlation spectrum of [U–^{13}C, ^{15}N]histidine (shown on top), showing the vertical and horizontal $^{13}C-^{13}C$ planes. (b, c, d) Slices corresponding to the three different ^{15}N nuclei in the molecule (positions 1, 3 and 9). Note that the ^{15}N slices show strong cross-peaks to the directly bonded ^{13}Cs and weaker cross-peaks to next-nearest neighbours generated by MELODRAMA recoupling. N1 shows strong diagonal connectivity to C2 and C5, and weaker diagonal peaks corresponding to C4 and C6. Negative absorption cross-peaks, indicating next-nearest neighbour bonding, are visible between C5 and C4, C5 and C6, and C6 and C7. A weak cross-peak between C2 and C4 is also visible. N3 shows strong diagonal connectivities to C2 and C4 and weak diagonal peak corresponding to C5. Negative and positive cross-peaks between C4 and C5 and between C4 and C6 correspond to nearest and next-nearest neighbour dipolar coupling, respectively. N9 shows a strong diagonal connectivity to C7 and weaker diagonal peaks corresponding to C6 and C8. (Adapted, with permission, from Sun *et al.*[182])

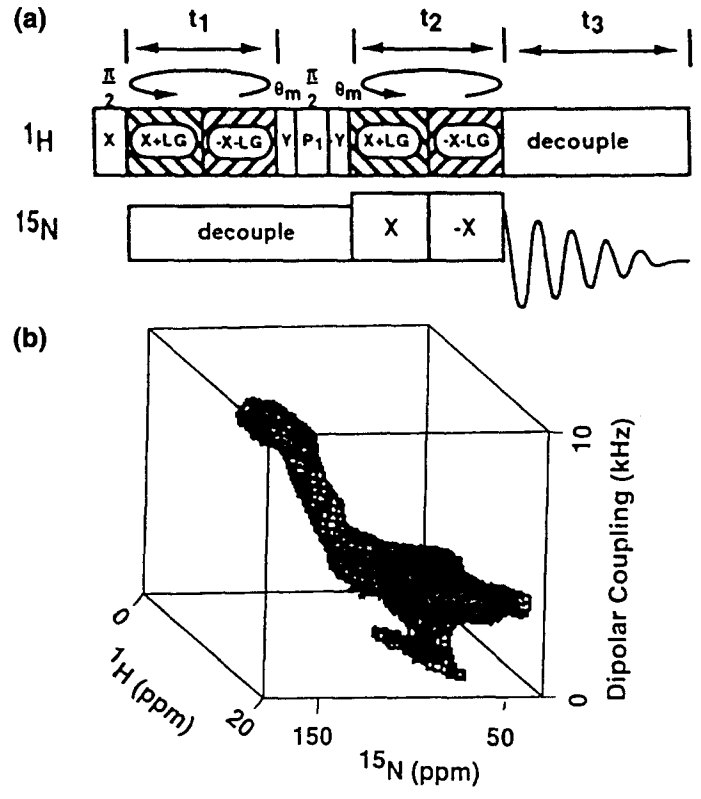

Fig. 9. (a) Pulse sequence for 3D experiment that correlates the chemical shifts of I and S nuclei and the I–S coupling. Homonuclear I–I couplings are suppressed during t_1 and t_2 by the off-resonance flip-flop LG pulse sequence. Heteronuclear decoupling is accomplished with the continuous irradiation of S and I spins during t_1 and t_3 respectively. In the t_2 period, I spin magnetization is selectively transferred to S via the I–S dipolar coupling. θ_m is a 54.7° pulse. Phase cycling is implemented for spin-temperature alternation and t_1 quadrature detection. (b) 3D ^{1}H shift/^{1}H–^{15}N coupling/^{15}N shift spectrum of a $^{15}N_{\epsilon 1}$-tryptophan powder sample. (Reproduced from Rammamoorthy *et al.*[80] with permission.)

correlates double-quantum coherence (rather than single-quantum coherence in usual SLF experiments) and chemical shift was proposed by Schmidt-Rohr[188] and was found to be useful for determining the (range of) torsion angles.

Although the SLF experiments described are still widely used when recoupling schemes are not necessary, more attention has been paid recently to those cases where high-spinning-speed MAS is used. Various kinds of recoupling schemes summarized in Section 4 are employed to recover heteronuclear dipolar information. For instance, REDOR dephasing schemes were used in dipolar-shift correlation experiments by Hong *et al.*[111,112,189] to determine torsion angle

and spectral assignment.[190] Dusald *et al.*[191] used '$n = 0$ rotational resonance' in their 1D MAS and 2D SLF experiments to determine the principal elements as well as the relative orientations of the chemical shift, dipolar and *J*-coupling tensors. Fujiwara *et al.*[192] used USEME (unified spin echo and magic echo) to assign ^{13}C and ^{15}N signals and also used it in their heteronuclear dipolar correlation experiments.[193] The principal values of both the dipolar and chemical shift tensors can be determined and the range of the dihedral angles (related to the relative orientation of the two tensors) can be delimited. C7 for filtering DQC was used to determine H–C–C–H torsion angle with good precision (20° for *cis* and 10° for *trans* geometry, respectively),[194,195] as demonstrated in Fig. 10. C7 has also been used to investigate the connectivity through dipolar coupling-mediated INADEQUATE experiments.[130] DQ-SLF experiments using other double-quantum filtering pulse sequences were also employed, such as DRAWS[196,197] and MELODRAMA.[198]

5.3. Chemical shift–quadrupolar correlation

There have been a number of publications on correlation or separation experiments involving quadrupolar nuclei. Using switching angle spinning (SAS), the correlation of quadrupolar and chemical shift interactions between the two spinning axes can be established to extract the quadrupolar and chemical shift tensors as well as their relative orientations.[199]

With multiple-quantum coherence MAS, it was found that this correlation can be implemented without using SAS.[200] High-resolution heteronuclear correlation spectra between spin-$\frac{1}{2}$ and quadrupolar spins can be realized with the SAS method[201] where the evolution is under dynamic-angle spinning (DAS) conditions so that the second-order interaction is averaged out; the correlation is through cross-polarization between the quadrupolar spin and spin-$\frac{1}{2}$ while the spinning axis is flipped to 0°. During the detection period, the sample is spun at the magic angle.

3D dynamic-angle correlation spectroscopy (DACSY) (Fig. 11) was proposed by Medek *et al.*,[202] which enables one to obtain the correlation of the Hamiltonians of various ranks. Clearly, this method offers more information than most conventional correlation spectra, so more precise determination of the interaction tensors and their relative orientations can be achieved.

5.4. *J*-coupling

J-coupling in solids is usually small in comparison with other interactions and it has played a much less important role in the studies of solid NMR. The pulse sequences widely employed in liquid NMR, such as INEPT and INAD-

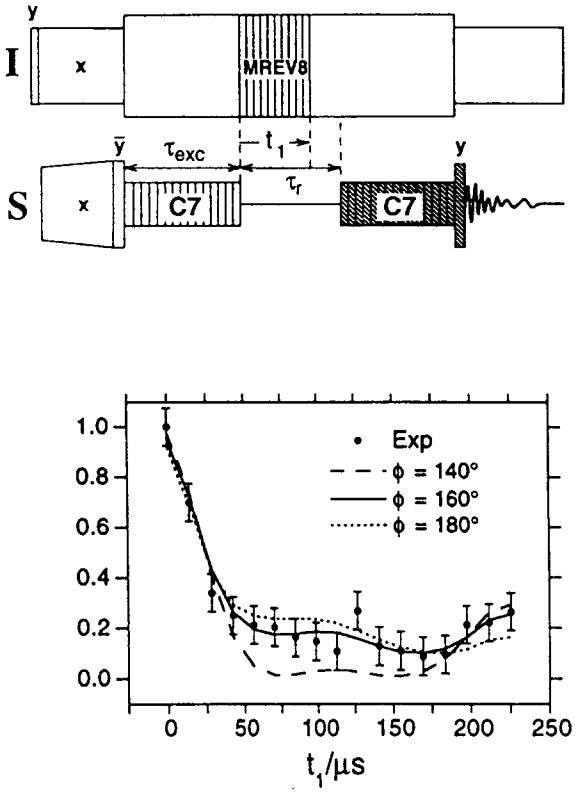

Fig. 10. (a) Pulse sequence for determination of H—C—C—H torsional angles under magic-angle spinning conditions, through heteronuclear dipolar modulation of the double-quantum coherences. The pulse sequence requires that the RF carrier is set to the mean of the ^{13}C isotropic shift frequencies. C7 is used for homonuclear recoupling. (b) Signal amplitudes for [10, 11-$^{13}C_2$]-rhodopsin in a double-quantum heteronuclear local field experiment. Filled circles are experimental integrated amplitudes as a function of the evolution interval t_1. The error bars indicate the standard deviation of the noise. Solid line is the simulation for a H—C—C—H torsional angle of $|\phi| = 160°$ and damping rate constant $\lambda = 5820\ s^{-1}$. Broken lines are best-fit simulations for H—C—C—H torsional angles of $|\phi| = 180°$ and $|\phi| = 140°$. The damping rate constants are $\lambda = 7680\ s^{-1}$ and $\lambda = 5340\ s^{-1}$, respectively. (From Feng *et al.*[195] with permission.)

EQUATE, can be used in special solid samples, for example where *J*-coupling is large or other interactions are negligibly weak.[203] However, with the recent developments in solid-state NMR, especially very high spinning speed and the invention of powerful decoupling techniques as described in earlier sections, the gap between solid and liquid NMR is decreasing.

A number of pulse sequences that usually apply to liquid NMR have now been realized in solid NMR. Lesage *et al.*[204] showed that the INADEQUATE

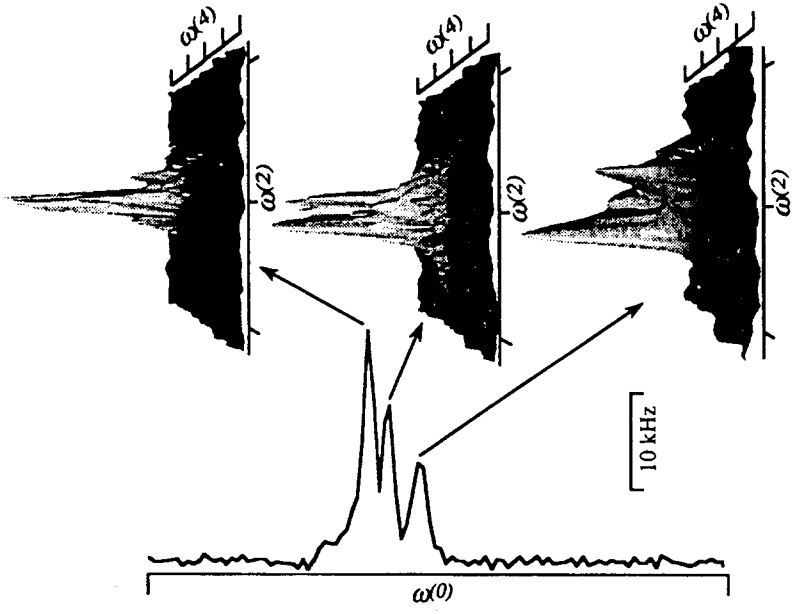
ω(4)
ω(2)
10 kHz
ω(0)

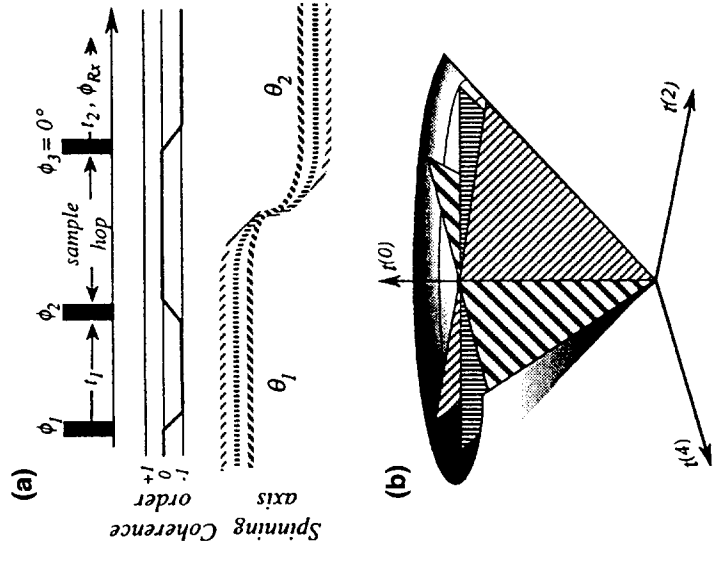
(a)
Coherence order
Spinning axis
ϕ_1
ϕ_2
$\phi_3 = 0°$
t_1
t_2, ϕ_{Rx}
sample hop
θ_1
θ_2
(b)
f(0)
f(2)
f(4)

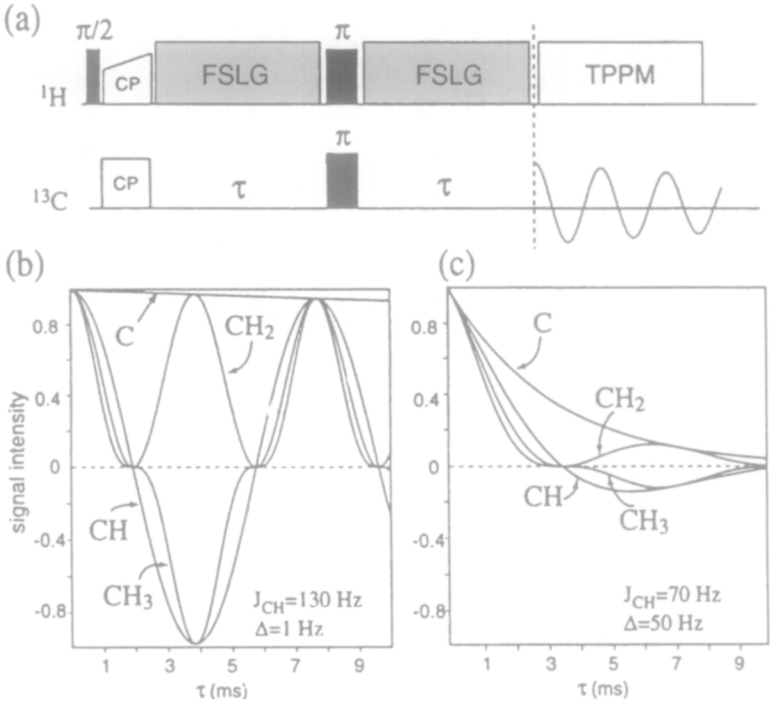

Fig. 12. (a) The pulse sequence suitable for the solid-state attached proton test (SS-APT). The theoretical evolution of carbon signal intensity is shown in (b) and (c) as a function of the delay τ. For each CH_n group ($n = 0, 1, 2, 3$) the curves were obtained with the expression $I = I_0 \cos^n(2\pi J_{CH}\tau)e^{-2\tau/T_2}$ where I_0 is the intensity after CP and T_2 the transverse relaxation time during the period 2τ (equal to $1/\pi\Delta$). The calculations are shown for two different values of linewidth Δ and J_{CH} coupling (1 and 130 Hz respectively for panel (b), and 50 and 70 Hz respectively for panel (c)) corresponding to the 'ideal liquid state' case and to the equivalent solid-state case. FSGL scaling was used. (Taken from Lesage *et al.*[207] with permission.)

Fig. 11. *Left*: Experimental schemes for the acquisition of 3D DACSY spectra on quadrupolar spins. The pulse sequence ((a) top) is analogous to the one used in 2D DAS experiment: it contains three 90° pulses with relative phase cycled so as to select anti-echo coherence transfer pathways, and initial and final sample spinning angles chosen so as to average out second and fourth rank anisotropies. (b) Sequence of t-space cross-sections that can be sampled by carrying out a series of 2D DAS acquisitions employing different pairs of complementary (θ_1, θ_2) spinning angles. $t^{(0)}$, $t^{(2)}$, $t^{(4)}$ are the integration of zeroth-, second- and fourth-order Legendre polynomials over the evolution time. *Right*: Schematic representation of the 3D DACSY NMR results obtained on a $RbNO_3$ sample at 4.7 T. The vertical trace corresponds to the projection of the 3D frequency data onto the isotropic $\omega^{(0)}$ axis; the 2D anisotropic lineshapes on the right correspond to the second/fourth-rank correlation distributions extracted at the isotropic frequencies indicated by the arrows. (Adapted from Medek *et al.*[202] with permission.)

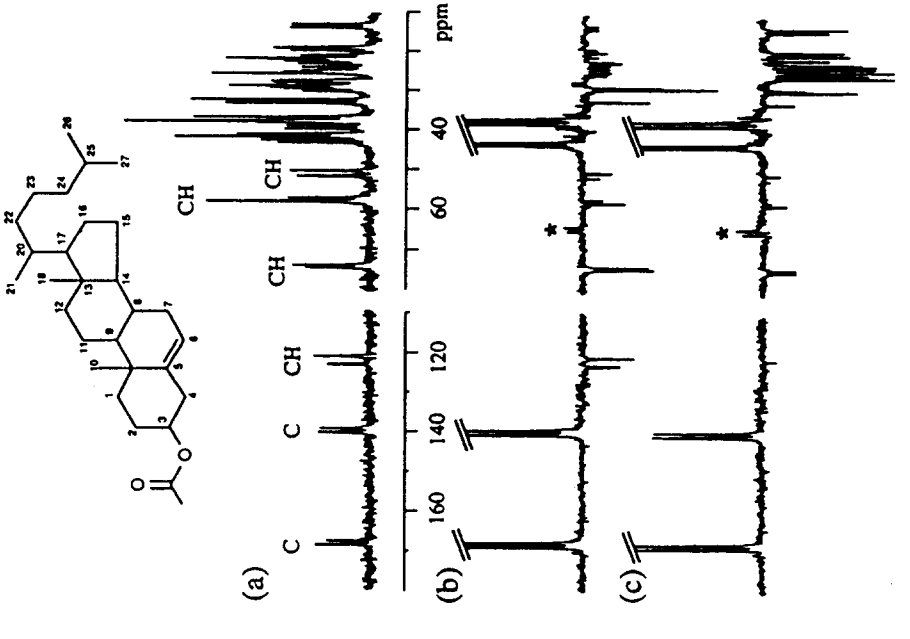
(a)
(b)
(c)
C
CH
CH
CH
160
140
120
60
40
ppm
*
O
O

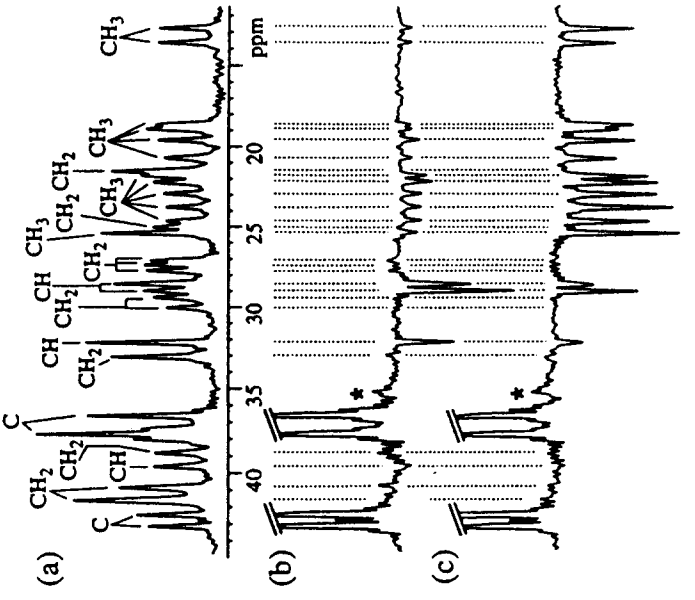
(a)
(b)
(c)
C
CH
CH2
CH
CH2
CH2
CH
CH2
CH3
CH3
CH2
CH2
CH3
CH3
40
35
30
25
20
ppm
*

experiment can be performed for solids of small molecules under conventional conditions. With high-power decoupling and RIL-ZQT sequence, Baldus *et al.*[205,206] realized total through-bond correlation spectroscopy (TOBSY) in solids. Using fast sample spinning and FS-LG, it is shown by Lesage *et al.*[207] that *J*-coupling can be well resolved and useful for spectral editing. The basic principle of using proton–carbon *J*-coupling to assign spectral peaks is explained in the caption of Fig. 12. The effectiveness of this method has been tested with complicated spin systems as shown in Fig. 13.

5.5. Multiquantum magic-angle spinning (MQMAS)

One of the most noticeable areas of progress in solid-state NMR in recent years is undoubtedly the introduction of the multiquantum magic-angle spinning (MQMAS) method proposed by Frydman and Harwood[208,209] that yields the high-resolution spectrum of the central transition of odd half-integer quadrupolar spins without using dynamic-angle spinning (DAS) or double rotation (DOR). Because of its simplicity, acquiring the high-resolution spectra of quadrupolar spin systems has become a routine experiment in solid state NMR studies. The original MQMAS correlation pulse sequence[208] used three pulses, the first two of which were used to excite MQCs. On the other hand, the two-pulse version of MQMAS (Fig. 14(a)), which is experimentally simpler, was subsequently found to produce higher sensitivities in addition to yielding better spectral lineshapes (pure absorptive).[209–217]

Extensive studies involving numerical analysis and experimental verification have been devoted to optimizing the pulse sequences,[210,211,216] by using QCPMG[218,219] or double frequency sweeping (DSF)[220] to achieve better sensitivities. Although the techniques used to obtain pure absorptive lineshapes, such as TPPI, and the hypercomplex method or gradient selection of coherences,[221] have been applied in MQMAS studies, it has been the case that dispersion was frequently found still to be serious, especially for high coherence ($|p| > 3$) cases, because of the asymmetry of the coherence transfers $0 \rightarrow \pm p$ for quadrupolar nuclear spin systems under RF pulse irradiation. This situation can be improved by application of the *z*-filtering method, which ensures the symmetry of the intensities of the coherences before

---

Fig. 13. *Left*: (a) 1D CP spectrum; (b) SS-APT spectrum with $\tau = 4.5$ ms and (c) SS-APT spectrum with $\tau = 6$ ms of cholesteryl acetate. *Right*: Expansion of the spectra shown on the left between 12 and 45 ppm. The assignments are indicated above the peaks: CH and CH_3 groups can be distinguished by the fact that the CH resonances give intense negative peaks for $\tau = 4.5$ ms, that diminish in intensity for $\tau = 6$ ms, whereas the opposite effect is observed for CH_3 resonances; the CH_2 groups give peaks that are weakly positive (like those around 27 ppm) or even null (like those around 30 ppm), whereas the quarternary carbons give intense positive resonances. (Taken from Lesage *et al.*[207] with permission.)

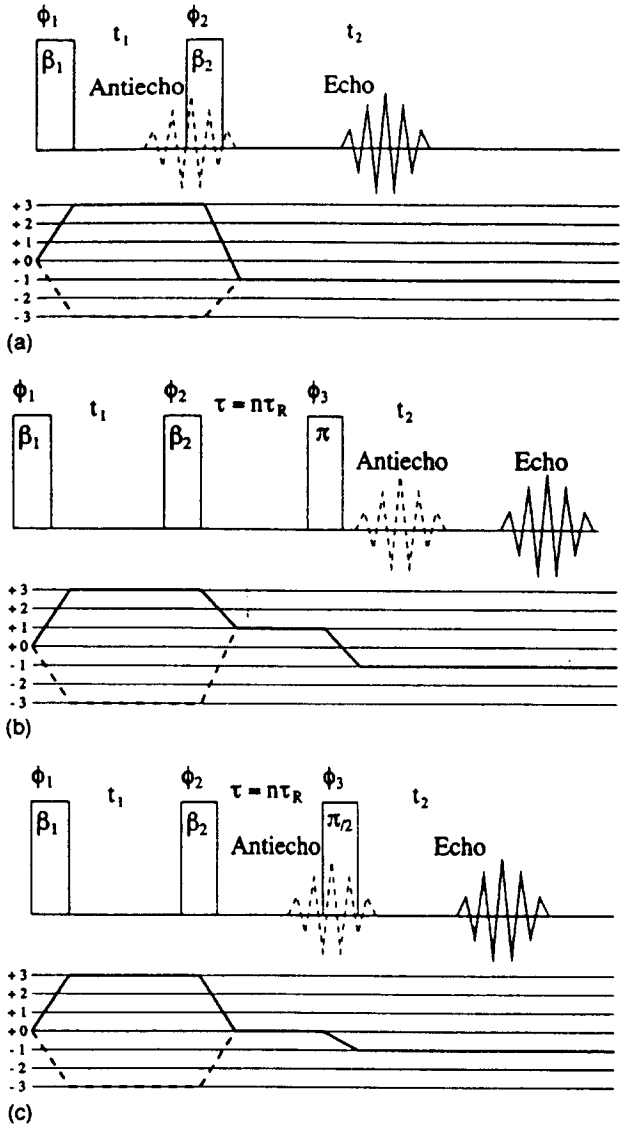

Fig. 14. (a) The two-pulse MQMAS sequence. The refocusing echo occurs at $t_2 = kt_1$ (solid line) and the anti-echo at $t_2 = -kt_1$ (dashed line). (b) The shifted-echo MQMAS sequence. An intermediate storage of the p-multiquantum coherence in the (+1) quantum coherence leads to a shift of the echo to $t_2 = kt_1 + n\tau_R$. Fourier transformation of the whole echo gives a pure-absorption multiquantum spectrum. (c) z-Filter MQMAS sequence. Symmetrical pathways make the anti-echo and echo intensities equal. It allows a pure p-multiquantum spectrum. (Adapted from Charpentier *et al.*[23] with permission.)

detection. The three-pulse version of the *z*-filtering method[217] (see Fig. 14(c)) is a simpler alternative to its four-pulse counterpart[222] because the former yields higher spectral sensitivities and is more easily optimized. Further improvement of the spectral lineshapes can be achieved by synchronizing the sample spinning with the pulse lengths.[216,223] The presence of the spinning sidebands in the first dimension was detected and satisfactorily explained.[224,225]

Systematic comparisons have been made recently between MQMAS NMR and VAS (variable-angle spinning), DAS and DOR NMR techniques in the study of quadrupolar nuclear spin systems.[226,227] Moreover, a comprehensive investigation was made of the MQMAS experiments performed in various magnetic fields from 400 to 800 MHz, with spinning rates from 10 to 35 kHz, as well as with different RF fields, etc.[228] Although the MQMAS method has rapidly become a favourite experimental choice, VAS, DAS and DOR are complementary techniques for some systems and can be incorporated with MQMAS.[216,227,229] A time-split method[222,230] was proposed to avoid the shearing transformation of the spectral data that is usually needed as a post-data-processing procedure to enhance the resolution in the first dimension of the 2D MQMAS NMR spectra. This renders data-processing easier, but the pure absorptivities of the resulting lineshapes are generally not as good those obtained by the two-pulse-plus-*z*-filtering method.[217]

The incorporation of MQMAS with cross-polarization,[231–234] heteronuclear correlation[235,236] and REDOR,[237,238] has been demonstrated to be useful in certain situations. Because of its experimental convenience, MQMAS has found many applications in studies of a wide range of practical chemical systems with different complexities, from simple inorganic compounds to catalysts and molecular sieves.[209,227–245] The high resolution achieved makes it easy to detect weak interactions involving quadrupole spins, e.g. *J*-coupling between spin-$\frac{1}{2}$ and spin-$\frac{3}{2}$ nuclei.[246] The advantages of MQMAS spectra over static and MAS spectra are shown diagrammatically in Fig. 15.

Based on the results of the investigations mentioned above, MQMAS can presently be regarded as an important new 'routine' experimental method in solid-state NMR. However, site quantification of nuclei portrayed in the spectra acquired by the MQMAS NMR technique is often found not to be wholly satisfactory, especially when the magnitudes of the quadrupolar coupling constants (QCCs) of the nuclei at different crystal lattice sites in the system under investigation vary in a wide range. The common situation is that the intensities of the signals from lattice sites occupied by those nuclei with large values of QCCs are reduced in magnitude. The quantification can be improved by the use of optimized pulse sequences[209,212,217] and synchronized data acquisition.[213,220]

Recently, a method exploiting the nutation characteristics of the coherences of quadrupolar spins in rotating solids under RF irradiation, named RIACT[247] (rotation induced adiabatic coherence transfer), was proposed to yield better site-quantitative MQMAS NMR spectra by carefully setting the pulse lengths according to the sample spinning speed. Because the adiabatic condition for coherence transfer is better satisfied at higher spinning rates for those nuclei

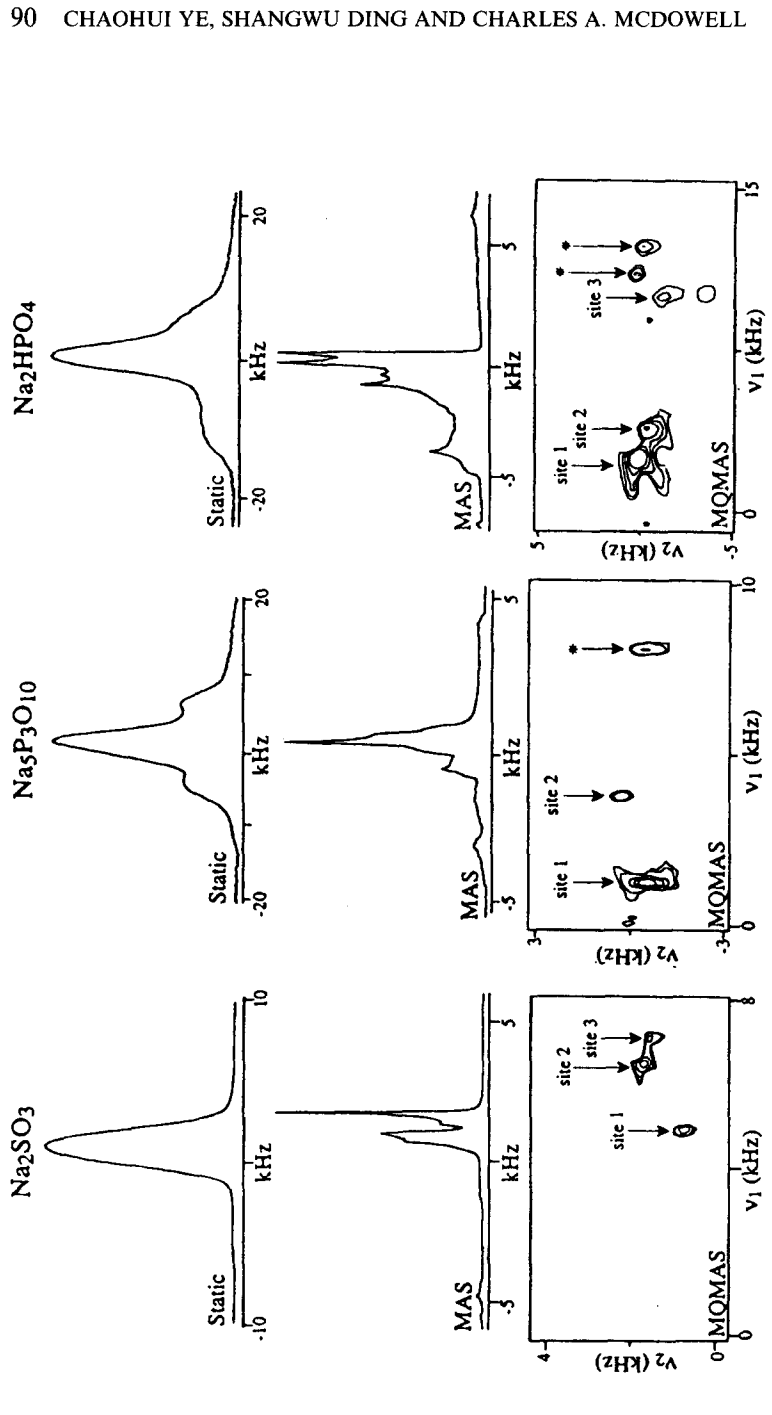

Fig. 15. Comparison between the static, MAS and MQMAS ^{23}Na NMR spectra of multisite sodium salts. Contour levels in the 2D plots were taken at 70%, 35%, 16%, 8%, and 4% of the maximum spectral intensities; asterisks indicate the spinning sidebands. (Reproduced, with permission, from Medek *et al.*[209])

with larger QCCs (i.e. the difference between the effective quadrupolar frequencies is decreased by sample spinning), the intensities of the signals for sites occupied by those nuclei with large values of QCCs can be relatively enhanced by using the RIACT method, hence yielding better site quantification of the MQMAS NMR spectra.

Two other solutions to achieving quantitative MQMAS spectra have been proposed.[248–250] One is hardware-oriented and uses pulse shaping[248,249] or composite pulses.[250] It was found that by using properly shaped pulses for excitation or conversion, MQMAS spectra with better quantification than that of RIACT can be achieved. The resultant spectra, however, usually remain highly nonquantitative even with the best use of these remedial measures. This is because the main reasons for the MQMAS spectra being nonquantitative all depend on the EFG and/or chemical shift tensors, and the deficiencies cannot be fully compensated in a unified way. Because of this, the second method, which involves theoretical simulations, was proposed.[251] The main reasoning behind this method is that the major sources that produce nonquantitative MQMAS spectra can be identified as follows: (1) the quadrupolar coupling constant (QCC)-dependent multiquantum excitation (0QCs $\rightarrow p$QCs, $p \geqslant 3$) and conversion (pQCs $\rightarrow$ 1QCs) efficiencies;[208–212,247–249] (2) the presence of rotational sidebands in the first dimension even at high spinning speeds;[224] (3) the RF offset effects;[246–250] (4) the QCC-dependent transverse relaxation times; and (5) the inhomogeneity of the static and RF magnetic fields, the instability of the rotor revolution and other experimental imperfections.

It is noted that, although the causes of nonquantification are multifactorial, the effects of sources (1)–(3) are totally computable from the nonquantitative MQMAS spectrum, from which the isotropic chemical shifts, δ_0, quadrupolar coupling constants (QCCs), $C_Q = e^2qQ/\hbar$, and asymmetry parameters, η_Q, of the EFG tensors can be evaluated. The effect of source (5) is assumed to be negligible if the experiments are carefully executed. The influence of source (4) is not easy to calculate exactly, but its effect can be included by assuming a certain relaxation model and experimental relaxation times for each site (for which interactions may often be orientation dependent). Good quantification has been obtained for a series of compounds.[251] We therefore believe that the MQMAS method can be enhanced with this quantification procedure and will find many interesting applications, particularly if it is implemented with the time-saving simulation schemes proposed by Charpentier *et al.*[252,253] It is also believed that MQMAS may be incorporated with solid NMR imaging and offers better resolution of images for quadrupole spin systems.

5.6. Orientation–orientation correlation (DECODER)

The properties of many materials such as polymers are affected by the anisotropic orientation distribution. The orientation distribution can be altered by various

processing techniques such as use of pressure, heating, electric field, ionizing irradiation, etc. Generally, the orientation distribution information cannot be extracted from the 1D NMR spectrum. This is because 1D NMR experiments are axially symmetric around the direction of the static magnetic field. Therefore, only the uniaxial average of the orientation distribution can be extracted.

By flipping the sample between the evolution and detection periods (so that the axial symmetry is broken), the correlation spectrum of two sample orientations can be established, as shown in the early single-crystal experiment by Carter *et al.*[254,255] This technique was employed by Henrichs[256] to propose a unique type of correlation spectrum in solid-state NMR by which the orientation correlation is established and the orientation distribution of ordered samples can be determined.

This technique was extended by Schmidt-Rohr *et al.*[257] and was given the acronym DECODER (direction exchange with correlation for orientation-distribution evaluation and reconstruction). The pulse sequence of the 2D version of this method, which is shown in Fig. 16(a), is basically a typical 2D exchange experiment except that the sample is reoriented during the mixing time. Consequently, the correlation of, for example, the chemical shift interaction at two different sample orientations is obtained.

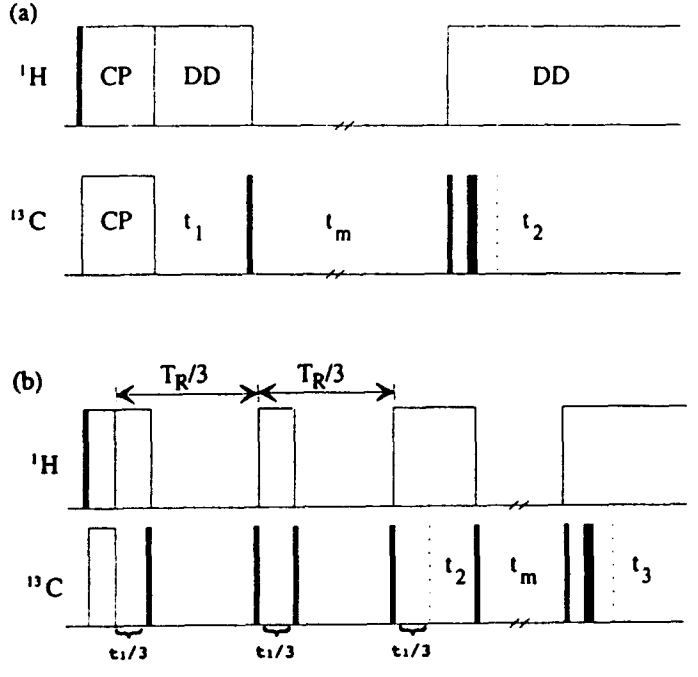

Fig. 16. Pulse sequence used in slow-spinning version of DECODER experiment. Each of the solid rectangles represents a 90° pulse. Standard CYCLOPS and spin-temperature alternation were used for phase cycling. (b) Pulse sequence used in the 3D experiment; the phase cycling for the t_1 part was similar to Grans[170]. (Adapted from Lewis *et al.*[260] with permission.)

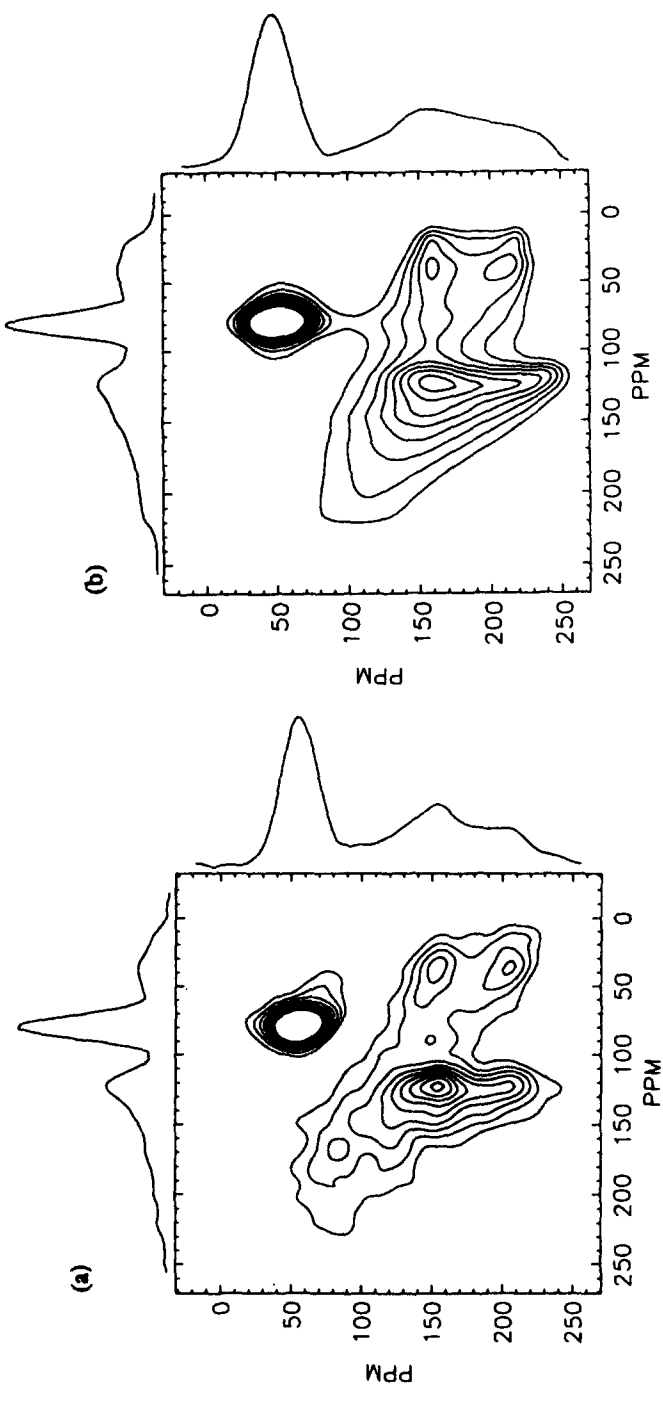

Fig. 17. (a) 2D CSA-DECODER spectrum of polyethyleneterephthalate fibres oriented perpendicular to the rotor axis with a mixing time of 9.6 ms equivalent to a rotation of 125° (b) Simulation of the experimental data using a uniaxial distribution with FWHM = 25°. (Adapted from Lewis *et al.*[260] with permission.)

Recently, Lewis *et al.*[260] simplified the experiment by incorporating slow magic-angle spinning (or magic-angle turning, MAT) to replace the sample flipping. With this technique, they proposed a general 3D version of the DECODER experiment (Fig. 16(b)) that can be used to reduce the overlapping and thereby make it possible to determine the distribution functions of individual sites. By theoretical simulation, the orientation distribution function can be calculated from the correlation spectrum, one example of which is shown in Fig.17. It correlates chemical shift interaction and can appropriately be called CSA-DECODER.[257,258] Other interactions can also be used and the

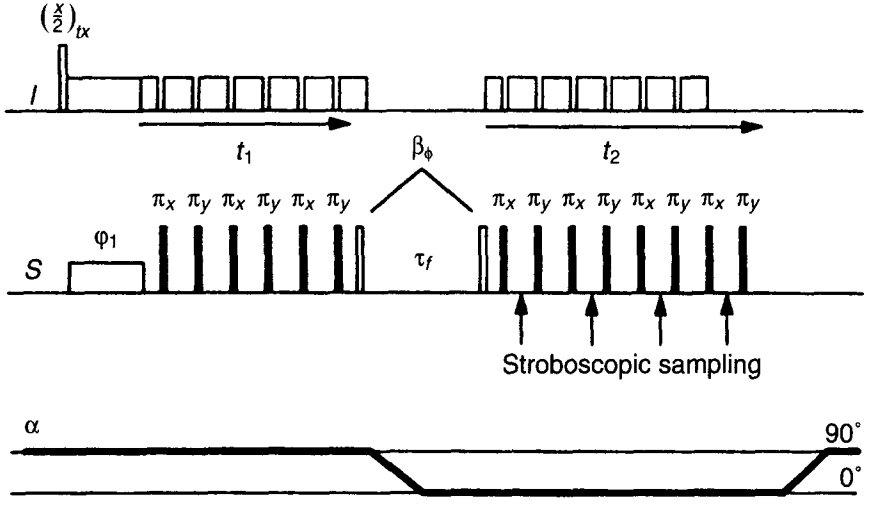

Fig. 18. Dipolar DECODER pulse sequence. The chemical shift term is suppressed during both the evolution and the detection periods by an xy–4 sequence. During the time delay τ_f, the orientation of the sample is changed and the magnetization is stored with a pair of pulses β_ϕ. (Reproduced from Utz *et al.*[259] with permission.)

Fig. 19. (a) Sketch of the channel-die apparatus used for the deformation experiment. Dimensions are in millimetres. The compression stamp is moved along the deformation direction D. The flow of the sample is constrained by the rigid walls of the die in the direction C, and free flow is possible in the direction F. (b) Stress (σ)–strain(ε) diagram resulting from channel-die extrusion of bisphenol-A polycarbonate at 300 K and a strain rate of $\dot{\varepsilon} = 0.01\ s^{-1}$. (c, d) Dipolar DECODER spectra of ^{13}C-labelled bisphenol-A polycarbonate before and after deformation. The spectra exhibit a characteristic star-like ridge pattern. Each of three types of corners (C, D, F) in the pattern corresponds to vectors oriented along a particular direction in the channel-die used for the experiment. (e, f) The anisotropy caused by the deformation becomes readily visible in the difference spectrum (deformed minus undeformed). For clarity, the negative (f) and positive contours (e) have been drawn separately. (Reproduced from Utz *et al.*[259] with permission.)

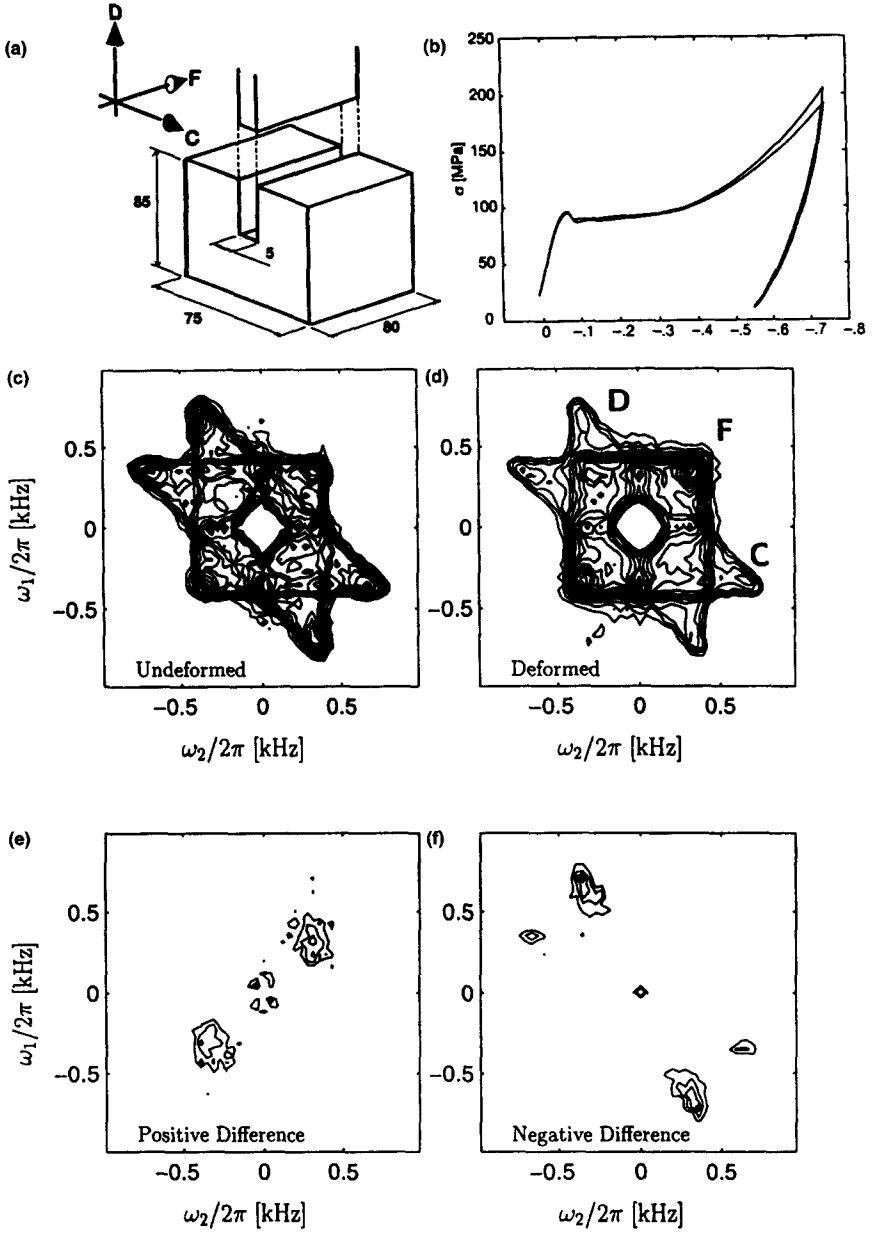
(a)
D
F
C
85
5
75
80
(b)
σ [MPa]
250
200
150
100
50
0
0 −.1 −.2 −.3 −.4 −.5 −.6 −.7 −.8
(c)
Undeformed
(d)
D
F
C
Deformed
0.5
0
−0.5
ω1/2π [kHz]
ω2/2π [kHz]
(e)
Positive Difference
(f)
Negative Difference

quadrupolar-DECODER[257] and dipolar-DECODER[259] (Fig. 18) were demonstrated using quadrupolar and dipolar interactions, respectively.

Because dipolar interaction is related to the internuclear vector, which is the direct description of the molecular framework, the relation between the orientation distribution function obtained from a dipolar-DECODER spectrum and the molecular frame distribution is simpler than that from CSA-DECODER and quadrupolar-DECODER spectrum. One example of the 2D dipolar-DECODER experimental spectrum is shown in Fig. 19. The change of the orientation distribution caused by the deformation can be measured by the difference of the spectra before and after deformation. Of course, since the dipolar interaction tensor is always axially symmetric, the information content of a dipolar-DECODER spectrum is decreased.

Song *et al.*[261] showed that rotor-synchronized 2D PASS experiment can also be used to find the orientation distribution function of chemical shift tensors. Because it permits the use of MAS, the sensitivity is higher than when static or slow-turning samples are used.

6. CROSS-POLARIZATION (CP) AND SPIN EXCHANGE/DIFFUSION (SE/SD)

In terms of physical mechanism, cross-polarization and spin diffusion are just two special cases of zero-quantum coherence (ZQC) transfer, one being heteronuclear ZQC transfer and the other homonuclear ZQC transfer. However, these two processes hold seemingly disproportionately important places in solid-state NMR, not only for historical reasons but also because they (particularly CP) are simple to implement and yet powerful in application. Moreover, most of the works reviewed in the previous sections focus on coherent characteristics of the process and hence on structural information rather than dynamic information. Both the coherent and incoherent steps during CP and SD/SE can easily be demonstrated and offer understanding of the dynamic processes. Because CP involves ZQC transfer in a tilted rotating frame while SD/SE takes place in the laboratory frame, RF fields are needed for CP experiments but RF is normally unnecessary for SD/SE unless high spinning speed is used and recoupling techniques must be used.

6.1. Cross-polarization

Although CPMAS is the most popular procedure in solid-state NMR, the physics of this phenomenon still requires more investigation. Using Floquet theory, a theoretical model for the description of CP experiments was proposed by Marks and Vega[262] for spin-$\frac{1}{2}$ systems and for CP between spin-$\frac{1}{2}$ and spin-1

systems.[263] Both the static and spinning sample cases were treated. At short time (much shorter than cross-relaxation time and $T_{1\rho}$ of the abundant spin), the process is basically coherent so that the evolution can be 'reversed'. This has been demonstrated with the observation of CP echoes.[264,265] Similar coherent behaviour was also observed for SD.[266]

Under high-speed MAS, CP might become inefficient because of weaker dipolar interaction results. Numerous solutions have been proposed in order to improve the CP efficiency, including phase inversion, amplitude modulation and frequency/amplitude modulation.[1,267–274] The simplest technique is RAMP-CP,[272–274] which is now widely adopted in practice.

Cross-polarization in tilted frame has been proposed.[275] In this scheme, the two effective fields matching the Hartmann–Hahn condition have a large offset comparable to two RF fields. This method was named SPECIFIC CP (spectrally induced filtering in combination with cross-polarization; Fig. 20) because the matching depends on the resonance offset of the involved nuclei. This method is clearly useful for spectral simplification, as demonstrated in Fig. 21. Under fast spinning conditions, *J*-coupling-mediated CP can be observed as shown by Verhoeven *et al.*[276]

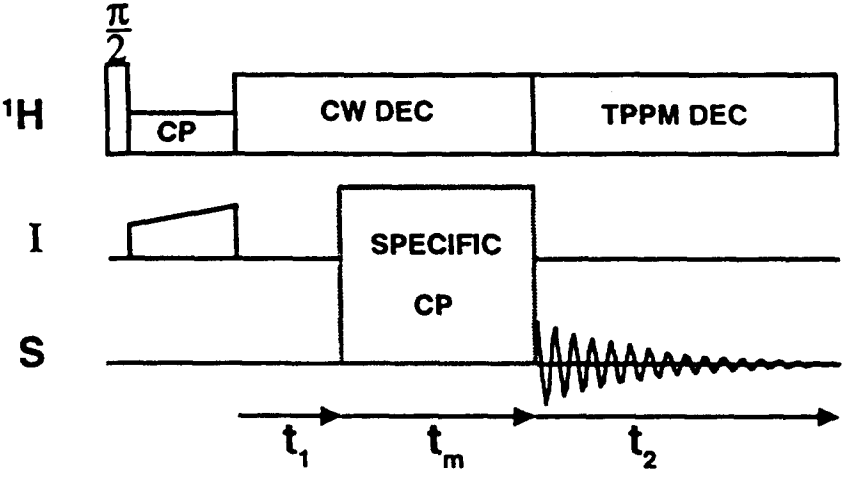

Fig. 20. Experimental setup for applications of the SPECIFIC CP experiment in the context of triple-resonance solid-state NMR experiments. After an initial broadband adiabatic CP step from protons to the *I* nuclei, SPECIFIC transfer to the observed *S* nucleus occurs during the mixing time t_m. The resulting signal represents a dipolar and chemical shift-filtered spectrum and can be controlled by variation of the carrier frequencies and the radiofrequency during the SPECIFIC transfer. A conventional HETCOR experiment is obtained by the introduction of an evolution time t_1. (Adapted from Baldus *et al.*[275] with permission.)

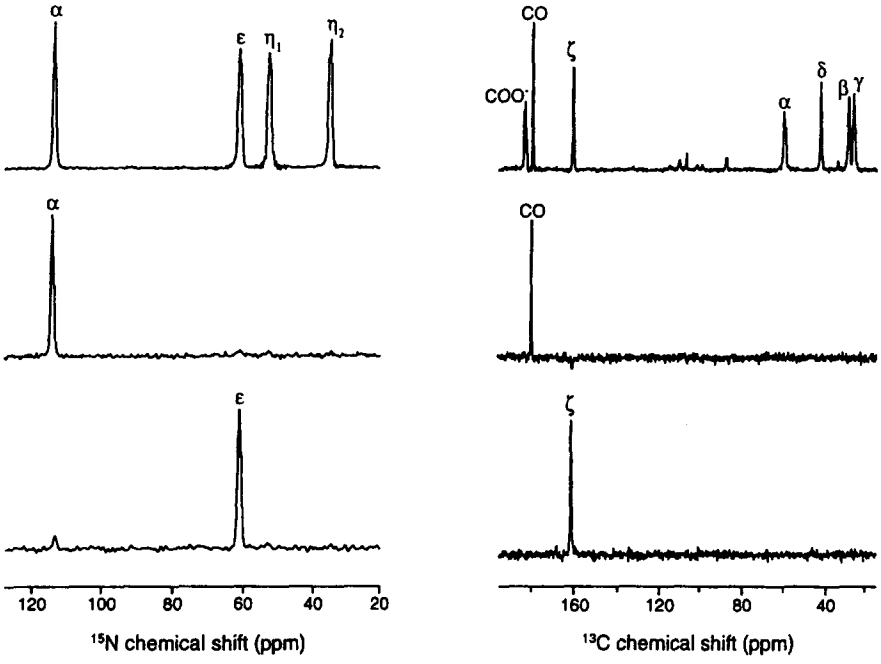

Fig. 21. ^{15}N (*left*) and ^{13}C (*right*) spectra of *N*-[1-^{13}C]acetyl-[U-^{13}C, ^{15}N]arginine dihydrate. *Left*: Direct proton-to-nitrogen CP (top) and carbon-to-nitrogen SPECIFIC CP with experimental parameters $\omega_{1C} = 17.0$ kHz, $\Omega_{CO} = 17.8$ kHz, $\omega_{1N} = 14.0$ kHz, $\Omega_{N_\alpha} = -1.4$ kHz (middle), and $\omega_{1C} = 17.0$ kHz, $\Omega_{C_\delta} = 9.1$ kHz, $\omega_{1N} = 14.0$ kHz, $\Omega_{N_\varepsilon} = 0.2$ kHz (bottom). *Right*: Direct proton-to-carbon CP (top) and nitrogen-to-carbon SPECIFIC CP with experimental parameters $\omega_{1N} = 4.0$ kHz, $\Omega_{N_\alpha} = 5.7$ kHz, $\omega_{1C} = 1.6$ kHz, $\Omega_{CO} = 0.4$ kHz (middle), and $\omega_{1N} = 4.0$ kHz, $\Omega_{N_\varepsilon} = 5.4$ kHz, $\omega_{1C} = 1.6$ kHz, $\Omega_{C_\zeta} = -0.2$ kHz (bottom). In both experiments, $\omega_R = 5.6$ kHz and a proton frequency of 317 MHz was used. (Adapted from Baldus *et al.*[275] with permission.)

6.2. Spin exchange/diffusion

Although the two processes, spin diffusion and spin exchange, are quite different in their physics, the experimental techniques used for them in NMR are the same. The experimental aspects of multidimensional exchange spectra in static solids were fully analysed by Schaefer *et al.*[277] In particular, the phase cycles for various types of experiments were tabulated. A comprehensive theoretical and experimental analysis of the rotor-synchronized 2D exchange spectroscopy with magic-angle spinning was given by Tycko *et al.*[278] The theoretical procedure was presented for calculating the amplitudes of the spinning sideband cross-peaks, which contain structural information (such as relative orientation of two isotopically labelled chemical groups within a

molecule in an unoriented sample). A sensitivity-enhancing method called orientationally weighted 2D MAS exchange spectroscopy was introduced by Tycko *et al.*[279] (see Fig. 22). Examples of the usefulness of this method in the determination of peptide conformation[280] and conformation distribution in helical peptides[281] were reported (Fig. 23).

For slow MAS experiments, it was found[282] that pure-phase spectra without unwanted cross-peaks can be obtained simply by combining rotor-synchronization with whole-echo acquisition (by placing a 180° pulse after the conversion pulse). This would make data acquisition and processing simpler, saving experimental time and permitting use of well-defined mixing times of an integer multiple of the rotation period.

Similarly to EIS (exchange-induced sidebands), the sideband intensities are altered during the mixing time.[283] Other 1D exchange experiments were proposed, including ODESSA[284] (one-dimensional exchange spectroscopy by sideband alteration) and time-reversed ODESSA.[285] ODESSA is suitable for samples with magnetically equivalent nuclei only, whereas time-reversed ODESSA can be used for multisite exchange experiments. In certain cases, these 1D experiments can be complementary to 2D MAS exchange experiments.[286]

The temperature dependence of the spectral spin diffusion and cross-relaxation was examined by Mueller *et al.*[287,288] with spin-$\frac{1}{2}$ and spin-1 systems. They showed that the diffusion rate can be strongly temperature dependent if it is motionally driven. It is therefore, unreliable to discriminate spin diffusion and chemical exchange by variable-temperature measurement of 2D exchange spectra. Mueller *et al.* suggested that the dependence of the polarization transfer rate on the spectral difference of the relevant resonances should be measured in a single crystal to safely distinguish the two different polarization transfer processes (see also ref. 289). They also explained satisfactorily why the relaxation of the quadrupolar order is much faster than the Zeeman order. This

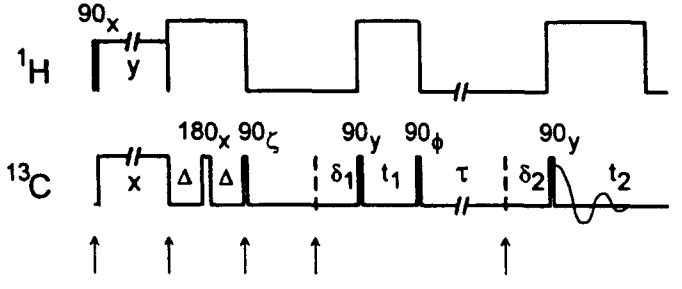

Fig. 22. Pulse sequence used to obtain orientationally weighted 2D MAS exchange spectra, with $\zeta = \pm y$ or $\pm x$ and alternate addition and subtraction of signals. Unweighted spectra are obtained by setting Δ to a value close to zero and $\zeta = \pm y$. The arrows indicate rotor cycles. (Reproduced from Tycko *et al.*[278] with permission.)

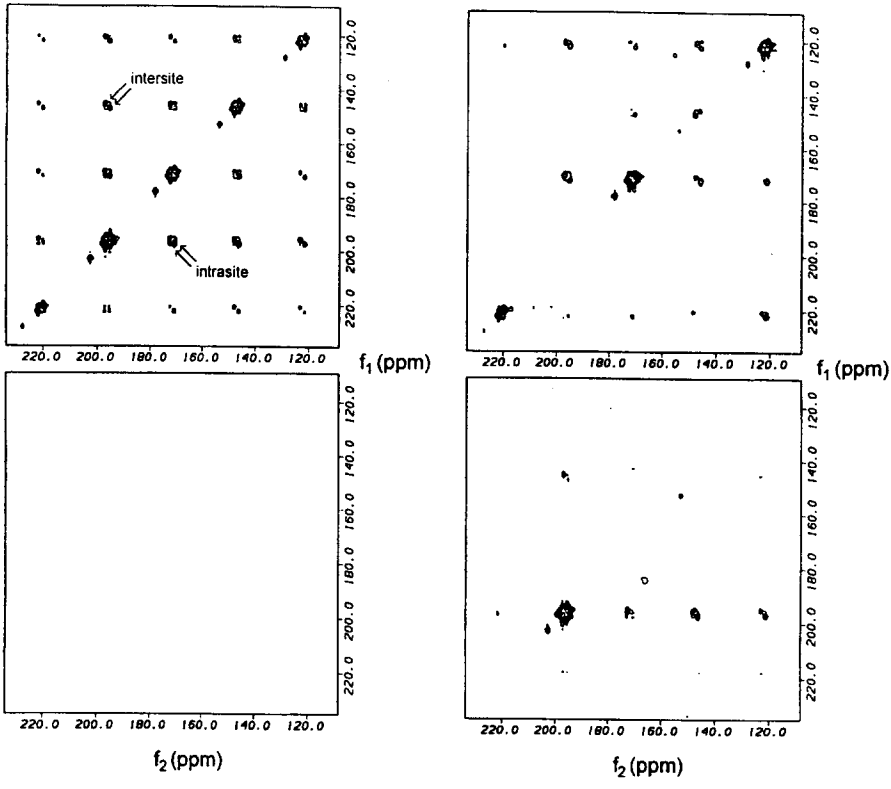

Fig. 23. *Left*: Unweighted 2D MAS exchange spectrum of L-alanylglycylglycine showing positive (top) and negative (bottom) contours at equal and opposite levels. Only the region containing carbonyl sidebands from −2 to +2 is shown. Examples of intersite and intrasite cross-peaks are indicated. *Right*: Orientationally weighted 2D MAS exchange spectrum of L-alanylglycylglycine obtained with the pulse sequence in Fig. 16 with $\zeta = \pm y$, showing positive (top) and negative (bottom) contours. (Reproduced from Tycko *et al.*[278] with permission.)

phenomenon is attributed to a result of the degeneration of spin diffusion into cross-relaxation.[290]

A 2D exchange experiment with temperature jump was employed by Fu *et al.*[291] to investigate the phase transition in solids. It was shown that this technique may offer significant new insights into the understanding of phase transitions in molecular solids.

A 2D CPMAS exchange experiment in which through-space (site) correlation is established via proton spin diffusion was proposed by Wilhelm *et al.*[292] for probing the isotropic chemical shift correlations. This technique has a number of advantages, including site selectivity, multiple correlations and broad spatial correlation range (1–200 nm). It was shown that this technique

can be used to characterize quantitatively domain sizes and proximities of a spatially heterogeneous material.

7. IMAGING

The methodological development and applications of solid-state NMR imaging have been progressing steadily, although a substantial gap between liquid and solid imaging remains owing to the intrinsic difficulties involved with solids. There are a number of excellent reviews[293–295] in this area covering the literature published prior to 1995.

New pulse sequences for solid imaging continue to emerge. Some of them focus on removing the limitations in the existing schemes, others on relieving certain demanding experimental requirements. Matsui *et al.*[296] showed that gradient decoupling[297] may be not necessary if a sinusoidal gradient field synchronized with the RF sequence is used or if the gradient is inverted in the middle of the RF irradiation (Fig. 24 top). They found as long as the RF field is at least 10 times larger than the resonance offset induced by the gradient, the spatial resolution is not significantly degraded by the line narrowing deterioration due to the gradient applied during the on-resonance RF pulsing (Fig. 24 bottom).

Mastui *et al.*[298] proposed a new version of the magic echo (ME) sequence, called tetrahedral magic echo (TME), which uses the so-called tetrahedral angle $\theta = 109.5°$ instead of 90° in the ME or modified ME (MME). This is substantially superior to ME or MME line narrowing for solids where heteronuclear dipolar interaction between protons and the other nuclear species is comparable to the homonuclear proton–proton interaction.

MAS imaging has been extended to spatially resolved spectroscopy.[299] Many NMR parameters such as chemical shift, dipolar interactions and relaxation times have been used as contrast parameters; many others remain to be investigated. As an exploration of the new contrast parameters in solid imaging, Matsui *et al.*[300] studied the possibility of imaging the second moment. Both conventional and fast (like EPI in liquids) imaging methods were proposed and may find applications in the study of the mobility of certain materials such as polymers because the second moment reflects the degree of molecular motion. There is one piece of work concerning the use of second-order quadrupolar broadening as the contrast parameter.[301] This showed that it can be useful for intermediate cases ($\nu_Q/\nu_{\text{Zeeman}} \approx 1$) but may not be useful for larger ratios, for which NQR imaging may be more appropriate.[302–317].

Because the stray field offers large static magnetic field gradients that usually cannot easily be achieved otherwise, the STRAFI (stray-field imaging) method remains a useful imaging technique, particularly where a large static gradient field is needed. A comprehensive review on STRAFI was given by McDonald.[318] A new method for calibrating the pulse length in high field

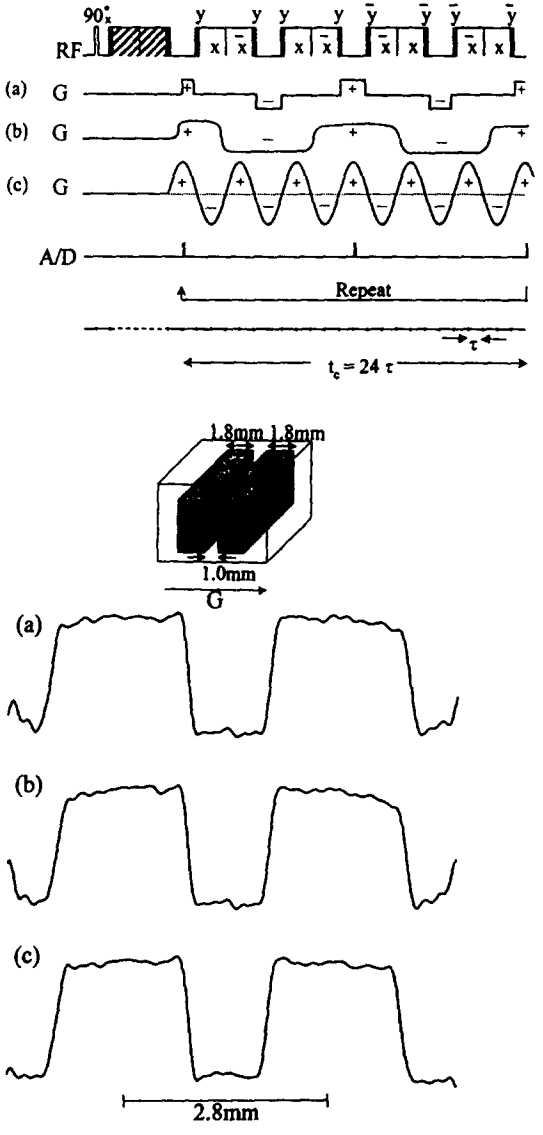

Fig. 24. *Top*: Magic-echo sequence, TREV-16TS, for solid-state imaging with: (a) ideally pulsed; (b) nonideally pulsed and (c) sinusoidal field gradients. On-resonance RF irradiations along x and $-x$ are sandwiched by 90°_y pulses (magic sandwich). The hatched magic sandwich consists of four magic sandwiches. *Bottom*: Projections of the one-dimensional test sample (admantane powder) obtained with the TREV-16TS sequence ($\tau = 30\ \mu s$) and the field gradients shown in Fig. 18. The RF field was set at 100 kHz. (Adapted from Matsui *et al.*[296] with permission.)

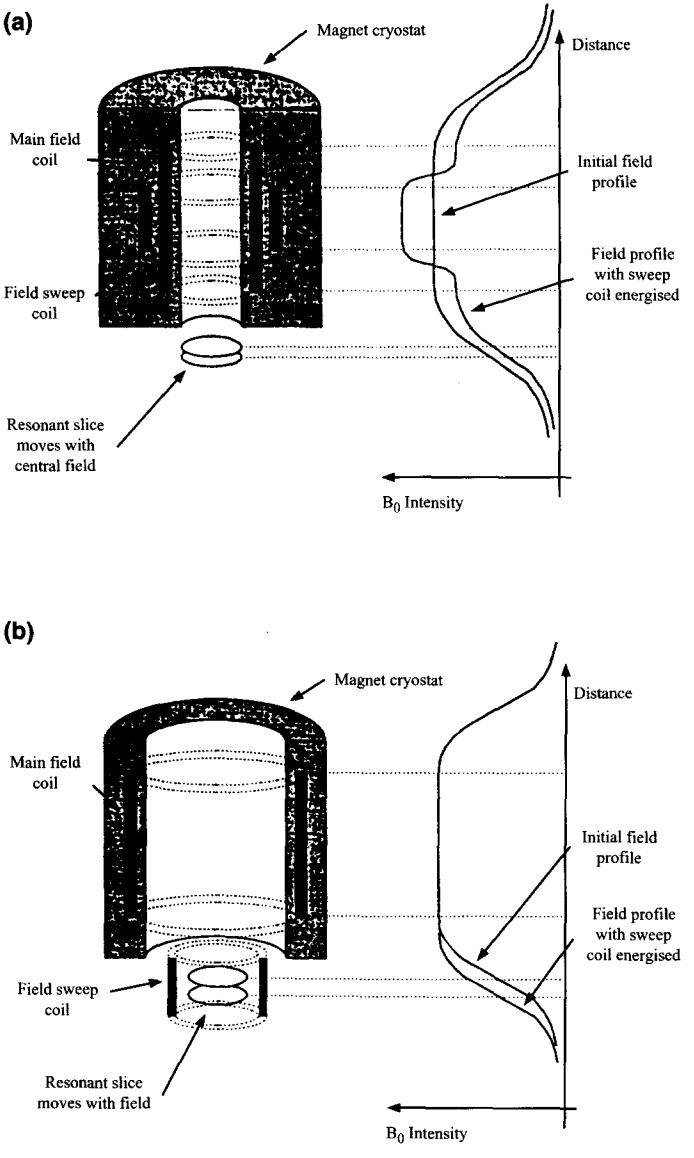

Fig. 25. Field sweep STRAFI. In a conventional STRAFI experiment the sample is moved through sensitive slice, whereas in this method the resonance condition is moved through the sample by varying the central magnetic field through its interaction with the sweep coil. (a) fs-STRAFI with an internal superconducting sweep coil. (b) The field sweep coil is offset from centre of the magnet and is loosely coupled to the main coil. The resonance position can be moved by energizing the sweep coil. The loose coupling between the coils allows the magnetic field to be modified locally to the sample without gross changes of the central field strength. (Reproduced from Mallet *et al.*[322] with permission.)

gradients was presented by Randall.[319] This method uses a pulse sequence $\alpha_x - \tau - (\alpha_x - \tau - \text{echo} - \tau)_n$ and enables one to estimate the pulse angle rapidly. With a stray field gradient of around 58 T m^{-1}, STRAFI has been demonstrated to be applicable to paramagnetic compounds with magnetic moments as high as 10 Bohr magnetons.[320] Not surprisingly, it was also found that STRAFI can be used to image half-integer quadrupolar spin systems using the central transition, since the first-order quadrupolar interaction does not affect that transition.[321]

A variant of STRAFI, called fs-STRAFI (field sweep STRAFI), was recently proposed using an additional magnetic field sweep coil so that the sample is kept static throughout the experiment.[322] The sweep coil can be an internal superconducting coil or it can be placed outside the magnet (Fig. 25). Because there is no physical movement of the sample to be studied, this fs-STRAFI method has advantages that there are no problems associated with position reproducibility, backlash, or misalignment in the sample travel. It is particularly suitable to those experiments where it is impractical to move the sample during the time scale of the experiment and/or where the region of interest is of the order of a few millimetres or less, such as with thin films, surface effects or boundary layers. The resolution of fs-STRAFI has been shown to be acceptable.[322] Alternatively, STRAFI has been found to be useful for films[323] owing to the use of a surface coil.

It was shown by Balcom *et al.*[324] that the disadvantages of time-inefficiency and possibly dangerous gradient vibration of the single point imaging (SPI) method[325–328] can be overcome using a ramped field gradient. The new version, termed SPRITE (single point ramped imaging with T_1 enhancement), can greatly reduce experimental times, minimize gradient vibration and enable the introduction of quantitative T_1 contrast or suppression into a variety of images.[329] This method can also be extended to the multiple point imaging case where a number of data points rather than only one (as in the original version) are sampled after the narrow excitation pulse.[330]

8. MISCELLANEOUS

Before closing, we summarize some less active but promising areas of research in or related to solid-state NMR. Some of them certainly point to the path leading to new regions of solid state NMR. Here we cite only important references during the reviewed period (1995–1999) in these fledgling areas, which include magnetic force imaging,[331–334] SQUID,[335] noise excitation,[336–339] DNP (dynamic nuclear polarization),[340,341] DNP imaging,[342] optically detected NMR,[343–352] wavelet transform NMR,[353] high-pressure MAS NMR,[354] laser-irradiated temperature-jump experiments,[355] MAS-assisted peptide synthesis,[356] and resolution enhancement of MAS spectra of paramagnetic compounds using zero-quantum coherence.[357]

Although most solid NMR experiments use powder samples, single-crystal experiments remain useful and new techniques continue to appear.[358,359]

As has been shown in an ever increasing number of practical systems, particularly polymers and biological macromolecular systems, solid state NMR/I is not only useful for 'real' solids but also very important and perhaps indispensible for 'neither-solid-nor-liquid' samples or 'both-solid-and-liquid' samples, which are nowadays called 'soft materials'. Hence, there is no definite boundary between solid state and liquid state NMR/I.

Finally, due to constraints of space, we have not been able to discuss here the wide range of applications for solid state NMR. We recognise that, due to the rapid progress in solid state NMR research, we may not have been able to cover all the new developments.

ACKNOWLEDGEMENTS

The authors thank the relevant publishers as well as the cited authors for kindly permitting us to reproduce their figures in this review. C.Y. appreciates the financial support from the Natural National Science Foundation of China and the Chinese Academy of Sciences. S.D. and C.A.McD. acknowledge the research grant from the National Science and Research Council of Canada.

REFERENCES

1. C. Ye, S. Ding and J. Zhou, *Annu. Rep. NMR Spectrosc.*, 1997, **33**, 37.
2. V. Soghomonian, M. Cotten, R. Rosanske and T. A. Corss, *J. Magn. Reson.*, 1997, **125**, 212.
3. J.-P. Amoureux, M. Priski, D. P. Lang and C. Fernanndez, *J. Magn. Reson.*, 1998, **131**, 170.
4. F. Wang and G. P. Grey, *J. Am. Chem. Soc.*, 1998, **120**, 970.
5. I. Schnell, A. Lupulescu, S. Hafner, D. E. Demco and H. W. Spiess, *J. Magn. Reson.*, 1998, **133**, 61.
6. S. Hafner and H. W. Spiess, *Con. Magn. Reson.*, 1998, **10**, 99.
7. I. Schnell, *Solid State NMR*, 1998, **12**, 9.
8. H. Kraus, M. Mueller, R. Prins and A. P. M. Kentgens, *J. Phys. Chem., 1998*, **B102**, 3862.
9. U. Scheler, *Solid State NMR*, 1998, **12**, 9.
10. F. Tauelle, A. Samoson, T. Loiseau and G. Ferey, *J. Phys. Chem.*, 1998, **B102**, 8588.
11. W. Zhang and D. G. Cory, *Phys. Rev. Lett.*, 1998, **80**, 1324.
12. W. Zhang and D. G. Cory, *J. Magn. Reson.*, 1998, **132**, 144.
13. S. Ray, V. Ladizhansky and S. Vega, *J. Magn. Reson.*, 1998, **135**, 427.
14. O. Weintraub and S. Vega, *Solid State NMR*, 1995, **4**, 341.
15. S. Ding and C. A. McDowell, *Mol. Phys.*, 1998, **95**, 841.
16. T. Nakai and C. A. McDowell, *J. Chem. Phys.*, 1992, **96**, 3452.
17. T. Nakai and C. A. McDowell, *Mol. Phys.*, 1996, **88**, 1263.
18. E. Kundla, I. Heinmaa, H. Kooskora and E. Lippmaa, *J. Magn. Reson.*, 1997, **129**, 53.
19. S. Ding and C. A. McDowell, *Chem. Phys. Lett.*, 1998, **288**, 230.
20. G. J. Boender, S. Vega and H. J. M. de Groot, *Mol. Phys.*, 1998, **95**, 921.
21. M. Eden, Y. K. Lee and M. H. Levitt, *J. Magn. Reson.*, 1996, **A120**, 56.

22. T. Charpentier, C. Fermon and J. Virlet, *J. Magn. Reson.*, 1998, **132**, 181.
23. T. Charpentier, C. Fermon and J. Virlet, *J. Chem. Phys.*, 1998, **109**, 3116.
24. M. Hohwy, H. Bildsoe, H. J. Jakobsen and N. C. Nielsen, *J. Magn. Reson.*, 1998, **136**, 6.
25. M. H. Levitt and M. Eden, *Mol. Phys.*, 1998, **95**, 879.
26. R. Bruschweiler and R. R. Ernst, *J. Magn. Reson.*, 1997, **124**, 122.
27. S. Ding and C. A. McDowell, *J. Chem. Phys.*, 1997, **107**, 7762.
28. S. Ding and C. A. McDowell, *J. Phys. Cond. Matter.*, 1999, **11**, L199.
29. J. H. Kristensen, H. Bildsoe, H. J. Jakobsen and N. C. Nielsen, *Prog. NMR Spctrosc.* 1999, **34**, 1.
30. J. G.Pearson, H. Le, L. K. Sanders, N. Godbout, R. H. Havlin and E. Oldfield, *J. Am. Chem. Soc.*, 1997, **119**, 11941.
31. R. H. Havlin, H. Le, D. D. Laws, A. C. deDios and E. Oldfield, *J. Am. Chem. Soc.*, 1997, **119**, 11951.
32. R. H. Havlin, N. Godbout, R. Salzmann, *et al.*, *J. Am. Chem. Soc.*, 1998, **120**, 3144.
33. M. T. MacMahon, A. C. deDios, N. Godbout, *et al.*, *J. Am. Chem. Soc.*, 1998, **120**, 4784.
34. R. Salzmann, C. J. Ziegler, N. Godbout, M. T. MacMahon, K. S. Suslick and E. Oldfield, *J. Am. Chem. Soc.*, 1998, **120**, 11323.
35. R. Salzmann, M. T. MacMahon, N. Godbout, L. K. Sanders, M. Wojdelski and E. Oldfield, *J. Am. Chem. Soc.*, 1999, **121**, 3818.
36. N. Godbout, L. K. Sanders, R. Salzmann, R. H. Havlin, M. Wojdelski and E. Oldfield, *J. Am. Chem. Soc.*, 1999, **121**, 3829.
37. B. Tesche and U. Haeberlen, *J. Magn. Reson.*, 1995, **A117**, 186.
38. F. Mauri, B. Pfrommer and S. G. Louie, *Phys. Rev. Lett.*, 1996, **77**, 5300.
39. F. Mauri and S. G. Louie, *Phys. Rev. Lett.*, 1996, **77**, 4246.
40. F. Mauri, B. Pfrommer and S. G. Louie, *Phys. Rev. Lett.*, 1997, **79**, 2340.
41. Y. G. Yoon, B. Pfrommer, F. Mauri and S. G. Louie, *Phys. Rev. Lett.*, 1997, **80**, 3388.
42. R. Bruschweiler and R. R. Ernst, *Chem. Phys. Lett.*, 1997, **264**, 393.
43. R. Bruschweiler, *Chem. Phys. Lett.*, 1997, **270**, 217.
44. N. R. Skrynnikov and R. Bruschweiler, *Chem. Phys. Lett.*, 1997, **281**, 239.
45. J. S. Waugh, *Mol. Phys.*, 1998, **95**, 731.
46. J. A. Jones and A. Pines, *Chem. Phys. Lett.*, 1995, **247**, 215.
47. J. A. Jones and A. Pines, *J. Chem. Phys.*, 1996, **107**, 3007.
48. A. S. Pikovsky, M. A. Zaks, and J. Kurths, *J. Phys. A: Math. Gen.*, 1996, **29**, 296.
49. L. L. Buishivlli, N. P. Giorgadze and R. R. Khomeriki, *J. Magn. Reson.*, 1998, **130**, 82.
50. D. Canet, J. Brondeau and C. Roumestand, *J. Magn. Reson.*, 1995, **A117**, 103.
51. M. Goldman, V. Fleury and M. Gueron, *J. Magn. Reson.*, 1996, **A118**, 11.
52. R. Tycko, *Phys. Rev. Lett.*, 1987, **58**, 2281.
53. M. Bak and N. C. Nielsen, *J. Magn. Reson.*, 1997, **125**, 132.
54. M. Eden and M. H. Levitt, *J. Magn. Reson.*, 1998, **132**, 220.
55. Y. Y. Lin, P. Hodgkinson, M. Ernst and A. Pines, *J. Magn. Reson.*, 1997, **128**, 30,
56. R. Prigl and U. Haeberlen, *Adv. Magn. Reson.*, 1996, **19**, 1.
57. I. Chang, G. Hinze, G. Diezemann, F. Fujara and H. Silescu, *Phys. Rev. Lett.*, 1996, **76**, 2523.
58. I. Chang, G. Diezemann, G. Hinze, R. Bohmer and H. Silescu, *J. Magn. Reson.*, 1997, **124**, 165.
59. H. Cho, *J. Magn. Reson.*, 1996, **A121**, 8.
60. F. H. Larsen, H. J. Jakobsen, P. D. Ellis and N. C. Nielsen, *J. Magn. Reson.*, 1998, **131**, 144.
61. F. H. Larsen, H. J. Jakobsen, P. D. Ellis and N. C. Nielsen, *Mol. Phys.*, 1998, **95**, 1185.
62. F. H. Larsen, A. S. Lipton, H. J. Jakobsen, N. C. Nielsen and P. D. Ellis, *J. Am. Chem. Soc.*, 1999, **121**, 3783.
63. K. Schmidt-Rohr, *J. Magn. Reson.*, 1998, **131**, 209.
64. S. Hafner and H. W. Spiess, *J. Magn. Reson.*, 1996, **A121**, 160.
65. S. Hafner and H. W. Spiess, *Solid State NMR*, 1997, **8**, 17.

66. E. Demco, S. Hafner and H. W. Spiess, *J. Magn. Reson.*, 1995, **A121**, 160.
67. M. Hohwy and N. C. Nielsen, *J. Chem. Phys.*, 1997, **106**, 7571.
68. M. Hohwy, P. V. Bower, H. J. Jakobsen and N. C. Nielsen, *Chem. Phys. Lett.*, 1997, **273**, 297.
69. M. Hohwy, J. T. Rasmussen, P. V. Bower, H. J. Jakobsen and N. C. Nielsen, *J. Magn. Reson.*, 1998, **133**, 374.
70. M. Lee and W. I. Goldburg, *Phys. Rev.*, 1965, **A140**, 1261.
71. A. Bielecki, A. C. Kolbert and M. H. Levitt, *Chem. Phys. Lett.*, 1989, **155**, 341.
72. M. H. Levitt, A. C. Kolbert, A. Bielecki and D. J. Ruben, *Solid State NMR*, 1993, **2**, 151.
73. C. H. Wu, A. Rammamoorthy and S. J. Opella, *J. Magn. Reson.*, 1994, **A109**, 270.
74. A. Rammamoorthy, C. H. Wu and S. J. Opella, *J. Magn. Reson.*, 1995, **B107**, 88.
75. A. Rammamoorthy and S. J. Opella, *Solid State NMR*, 1995, **4**, 387.
76. A. Rammamoorthy, L. M. Gierasch and S. J. Opella, *J. Magn. Reson.*, 1995, **B109**, 112.
77. A. Rammamoorthy, L. M. Gierasch and S. J. Opella, *J. Magn. Reson.*, 1996, **B110**, 102.
78. R. Jelinek, A. Rammamoorthy and S. J. Opella, *J. Am. Chem. Soc.*, 1995, **117**, 12348.
79. A. Rammamoorthy, L. M. Gierasch and S. J. Opella, *J. Magn. Reson.*, 1996, **B111**, 81.
80. A. Rammamoorthy, C. H. Wu and S. J. Opella, *J. Am. Chem. Soc.*, 1997, **119**, 10479.
81. Z. Gu and S. J. Opella, *J. Magn. Reson.*, 1999, **138**, 193.
82. J. D. Gross, P. R. Costa and R. G.Griffin, *J. Chem. Phys.*, 1998, **108**, 7286.
83. K. Takegoshi and T. Terao, *Solid State NMR*, 1999, **13**, 203.
84. A. E. Bennett, C. M. Rienstra, M. Auger, K. V. Lakshmi and R. G. Griffin, *J. Chem. Phys.*, 1995, **103**, 6951.
85. Z. Gan and R. R. Ernst, *Solid State NMR*, 1997, **5**, 153.
86. M. Eden and M. H. Levitt, *J. Chem. Phys.*, 1999, **111**, 1511.
87. P. Tekeley, P. Palmas and D. Canet, *J. Magn. Reson.*, 1994, **A107**, 129.
88. M. Ernst, A. Verhoeven and B. H. Meier, *J. Magn. Reson.*, 1998, **130**, 176.
89. D. L. Vanderhart and G. C. Campbell, *J. Magn. Reson.*, 1998, **134**, 88.
90. U. Schwerk, D. Michel and M. Pruski, *J. Magn. Reson.*, 1996, **A119**, 157.
91. M. Ernst, S. Bush, A. C. Kolbert and A. Pines, *J. Chem. Phys.*, 1996, **105**, 3387.
92. M. Ernst, A. C. Kolbert, K. Schmidt-Rohr and A. Pines, *J. Chem. Phys.*, 1996, **104**, 8258.
93. R. Fu, S. Caldarelli, V. Ermakov and G. Bodenhausen, *Solid State NMR*, 1996, **5**, 273.
94. R. Fu, V. L. Ermakov and G. Bodenhausen, *Solid State NMR*, 1996, **7**, 1.
95. D. R. Studelska, C. A. Klug, D. D. Beusen, L. M. McDowell and J. Schaefer, *J. Am. Chem. Soc.*, 1996, **118**, 5476.
96. M. E. Meritt, S. Th. Sigurdsson and G. P. Drobny, *J. Am. Chem. Soc.*, 1999, **121**, 6070.
97. A. K. Mehta, B. A. Tounge, S. T. Burns, X. Wu and K. W. Zilm, *39th Rocky Mountain Conference on Analytical Chemistry*, Denver, 1997.
98. X. Feng, M. Eden, A. Brinkman, *et al.*, *J. Am. Chem. Soc.*, 1997, **119**, 12006.
99. J. Schaefer, *J. Magn. Reson.*, 1999, **137**, 272.
100. J. M. Goetz and J. Schaefer, *J. Magn. Reson.*, 1997, **129**, 222.
101. J. M. Goetz and J. Schaefer, *J. Magn. Reson.*, 1997, **127**, 147.
102. T. Gullion, *J. Magn. Reson.*, 1993, **A101**, 320.
103. T. I. Igumenova, D. J. Mitchell and J. N. S. Evans, *J. Magn. Reson.*, 1997, **127**, 144.
104. T. S. Cull, J. M. Joers, T. Gullion, R. E. Norberg and M. S. Conradi, *J. Magn. Reson.*, 1998, **133**, 352.
105. C. A. Klug and J. Schaefer, *J. Magn. Reson.*, 1996, **A123**, 251.
106. K. T. Mueller, *J. Magn. Reson.*, 1995, **A113**, 81.
107. K. T. Mueller, T. P. Jarvie, D. J. Aurentz and B. W. Roberts, *Chem. Phys. Lett.*, 1995, **242**, 535.
108. T. P. Jarvie, G. T. Went and K. T. Mueller, *J. Am. Chem. Soc.*, 1996, **118**, 5330.
109. J-B. d. de la Cailerie and C. Fretigny, *J. Magn. Reson.*, 1998, **133**, 273.
110. F. G. Vogt, D. J. Aurentz and K. T. Mueller, *Mol. Phys.*, 1998, **95**, 907.

111. M. Hong, J. D. Gross, C. M. Rienstra, R. G. Griffin, K. K. Kumashiro and K. Schmidt-Rohr, *J. Magn. Reson.*, 1997, **129**, 85.
112. M. Hong, J. D. Gross, W. Hu and R. G. Griffin, *J. Magn. Reson.*, 1998, **135**, 169.
113. C. A. Fyfe, K. T. Mueller, H. Grondey and K. C. Wong-Moon, *Chem. Phys. Lett.*, 1992, **199**, 198.
114. C. A. Fyfe, K. C. Wong-Moon, Y. Huang, H. Grondey and K. T. Mueller, *J. Phys. Chem.*, 1995, **99**, 8707.
115. T. Gullion, *J. Magn. Reson.*, 1995, **A117**, 326.
116. C. P. Grey and A. J. Vega, *J. Am. Chem. Soc.*, 1995, **117**, 8232.
117. Y. Ba, H. M. Gao, G. P. Grey and T. Gullion, *J. Magn. Reson.*, 1998, **133**, 104.
118. T. Gullion, *Chem. Phys. Lett.*, 1995, **246**, 235.
119. A. E. Bennett, C. M. Rienstra, P. T. Lansbury Jr and R. G. Griffin, *J. Chem. Phys.*, 1996, **105**, 10289.
120. A. E. Bennett, C. M. Rienstra, J. M. Griffiths, W. Zhen, P. T. Lansbury Jr. and R. G. Griffin, *J. Chem. Phys.*, 1998, **108**, 9463.
121. A. E. Bennett, D. P. Weliky and R. Tycko, *J. Am. Chem. Soc.*, 1998, **120**, 4897.
122. G. J. Boender and S. Vega, *J. Magn. Reson.*, 1998, **133**, 281.
123. E. Zaborowski, H. Zimmermann and S. Vega, *J. Magn. Reson.*, 1999, **136**, 47.
124. Y. K. Lee, N. D. Kurur, M. Helmle, O. G. Jonannessen, N. C. Nielsen and M. H. Levitt, *Chem. Phys. Lett.*, 1995, **242**, 304.
125. M. Eden and M. H. Levitt, *Chem. Phys. Lett.*, 1998, **293**, 173.
126. H. Geen, J. Gottwald, R. Graf, I. Schnell, H. W. Spiess and J. I. Titman, *J. Magn. Reson.*, 1996, **125**, 224.
127. X. Feng, Y. K. Lee, D. Sandstrom, *et al.*, *Chem. Phys. Lett.*, 1996, **257**, 314.
128. X. Feng, M. Eden, A. Brinkman, *et al.*, *J. Am. Chem. Soc.*, 1997, **119**, 12006.
129. X. Feng, P. J. E. Verdegem, Y. K. Lee, *et al.*, *J. Am. Chem. Soc.*, 1997, **119**, 6853.
130. M. Hong, *J. Magn. Reson.*, 1999, **136**, 86.
131. T. Karlsson, A. Brinkmann, P. J. E. Verdegem, J. Lugtenburg and M. H. Levitt, *Solid State NMR*, 1999, **14**, 43.
132. H. Geen, R. Graf, A. S. D. Henrichs, *et al.*, *J. Magn. Reson.*, 1999, **138**, 167.
133. M. Hohwy, H. J. Jakobsen, M. Eden, M. H. Levitt and N. C. Nielsen, *J. Chem. Phys.*, 1998, **108**, 2686.
134. C. M. Rienstra, M. E. Hatcher, L. J. Mueller, B. Sun, S. W. Fesik and R. G. Griffin, *J. Am. Chem. Soc.*, 1998, **120**, 10602.
135. C. M. Rienstra, M. E. Hatcher, L. J. Mueller, B. Sun, S. W. Fesik and R. G. Griffin, *J. Am. Chem. Soc.*, 1998, **120**, 10602.
136. J. D. Gross, P. R. Costa and R. G. Griffin, *J. Chem. Phys.*, 1998, **108**, 7286.
137. M. Feike, D. E. Demco, R. Graf, J. Gottwarld, S. Hafner and H. W. Spiess, *J. Magn. Reson.*, 1996, **A122**, 214.
138. R. Graf, D. E. Demco, J. Gowttwald, S. Hafner and H. W. Spiess, *J. Chem. Phys.*, 1997, **106**, 885.
139. U. Friedrich, I. Schnell, D. E. Demco and H. W. Spiess, *Chem. Phys. Lett.*, 1998, **285**, 49.
140. I. Schnell, A. Luplescu, S. Hafner, D. E. Demco and W. Spiess, *J. Magn. Reson.*, 1998, **133**, 61.
141. U. Friedrich, I. Schnell, S. P. Brown, A. Lupusescu, D. E. Demco and H. W. Spiess, *Mol. Phys.*, 1998, **95**, 1209.
142. M. Baldus and B. H. Meier, *J. Magn. Reson.*, 1997, **128**, 172.
143. T. Fijiwara, A. Ramamoorthy, K. Nagayama, K. Hoika and T. Fujito, *Chem. Phys. Lett.*, 1993, **212**, 81.
144. M. Baldus, M. Tomaselli, B. H. Meier and R. R. Ernst, *Chem. Phys. Lett.*, 1994, **230**, 329.
145. K. Takegoshi and T. Terao, *Solid State NMR*, 1999, **13**, 203.
146. P. R. Costa, D. A. Kocisko, B. Q. Sun, P. T. Lansbury and R. G. Griffin, *J. Am. Chem. Soc.*, 1997, **119**, 10487.

147. J. Heller, R. Larsen, M. Ernst, *et al.*, *Chem. Phys. Lett.*, 1996, **251**, 223.
148. J. M. Koons, G. E. Pavlovskaya, A. A. Jones and P. T. Ingelfield, *J. Magn. Reson.*, 1997, **124**, 499.
149. K. Takegoshi, K. Nomura and T. Terao, *Chem. Phys. Lett.*, 1995, **232**, 424.
150. K. Takegoshi, K. Nomura and T. Terao, *J. Magn. Reson.*, 1997, **127**, 206.
151. K. Nomura, K. Takegoshi, T. Terao, K. Uchida and M. Kainosho, *J. Am. Chem. Soc.*, 1999, **121**, 4064.
152. P. R. Costa, B. Sun and R. G. Griffin, *J. Am. Chem. Soc.*, 1997, **119**, 10821.
153. Z. Gan, D. M. Grant and R. R. Ernst, *Chem. Phys. Lett.*, 1997, **254**, 349,
154. M. Bak and N. C. Nielsen, *J. Chem. Phys.*, 1997, **106**, 7578.
155. Z. Gan and R. R. Ernst, *J. Chem. Phys.*, 1998, **108**, 9444.
156. T. M. de Swiet, M. Tomaselli and A. Pines, *Chem. Phys. Lett.*, 1998, **285**, 59.
157. D. M. Gregory, G. M. Wolfe, T. P. Jarvie, J. C. Sheils and G. P. Drobny, *Mol. Phys.*, 1996, **89**, 1835.
158. R. Fu, S. A. Smith and G. Bodenhausen, *Chem. Phys. Lett.*, 1997, **272**, 361.
159. R. Verel, M. Baldus, M. Nijman, J. W. M. van Os and B. H. Meier, *Chem. Phys. Lett.*, 1997, **280**, 31.
160. R. Verel, M.Baldus, M. Ernst and B. H. Meier, *Chem. Phys. Lett.*, 1998, **287**, 421.
161. Y. Ishii and T. Terao, *J. Chem. Phys.*, 1998, **109**, 1366.
162. M. Baldus, D. G. Geurts, S. Hediger and B. H. Meier, *J. Magn. Reson.*, 1996, **118**, 140.
163. S. Hediger, P. Singner, M. Tomaselli, R. R. Ernst and B. H. Meier, *J. Magn. Reson.*, 1997, **125**, 291.
164. J. Raya and J. Hirchinger, *J. Magn. Reson.*, 1998, **133**, 341.
165. R. Fu, P. Pelupessy and G. Bodenhausen, *Chem. Phys. Lett.*, 1997, **264**, 63.
166. O. B. Peerson, X. Wu, I. Kustanovich and S. O. Smith, *J. Magn. Reson.*, 1993, **A104**, 334.
167. O. B. Peerson, X. Wu and S. O. Smith, *J. Magn. Reson.*, 1994, **A106**, 127.
168. G. Metz, X. Wu and S. O. Smith, *J. Magn. Reson.*, 1994, **A110**, 219.
169. J. Sachleben, V. Frydman and L. Frydman, *J. Am. Chem. Soc.*, 1996, **118**, 9786.
170. Z. Gan, *J. Am. Chem. Soc.*, 1992, **114**, 8307.
171. J. Hu, D. W. Alderman, C. Ye, R. J. Pugmire and D. M. Grant, *J. Magn. Reson.*, 1993, **A105**, 82.
172. J. Hu, A. M. Orendt, D. W. Alderman, R. J. Pugmire, C. Ye and D. M. Grant, *Solid State NMR*, 1994, **3**, 181.
173. J. Hu, W. Wang, F. Liu, *et al.*, *J. Magn. Reson.*, 1995, **A113**, 210.
174. J. Hu, D. W. Alderman, C. Ye, R. J. Pugmire and D. M. Grant, *J. Magn. Reson.*, 1993, **A105**, 82.
175. D. W. Alderman, G. McGeorge, J. Hu, R. J. Pugmire and D. M. Grant, *Mol. Phys.*, 1998, **95**, 1113.
176. Z. Gan, *J. Magn. Reson.*, 1994, **109**, 253.
177. G. McGeorge, J. Hu, C. L. Mayne, D. W. Alderman, R. J. Pugmire and D. M. Grant, *J. Magn. Reson.*, 1997, **129**, 134.
178. Z. Gan and R. R. Ernst, *J. Magn. Reson.*, 1996, **A123**, 140.
179. E. Hughes, E. B. Brouwer and R. K. Harris, *J. Magn. Reson.*, 1999, **138**, 256.
180. J. Hu, D. W. Alderman, R. J. Pugmire and D. M. Grant, *J. Magn. Reson.*, 1997, **126**, 120.
181. B. Q. Sun, P. R. Costa, D. Kosciko, P. T. Landsbury Jr, and R. G. Griffin, *J. Chem. Phys.*, 1995, **102**, 702.
182. B. Q. Sun, C. M. Rienstra, P. R. Costa, J. R. Williamson and R. G. Griffin, *J. Am. Chem. Soc.*, 1997, **119**, 8540.
183. B. J. van Rossum, G. J. Boender and H. J. M. de Groot, *J. Magn. Reson.*, 1996, **A120**, 274.
184. B. J. van Rossum, H. Forster and H. J. M. de Groot, *J. Magn. Reson.*, 1997, **124**, 516.
185. H. Pan, *J. Magn. Reson.*, 1997, **124**, 1.
186. P. Palmas, P. Tekely and D. Canet, *Solid State NMR*, 1995, **4**, 105.

187. J. C. Cheeryman and R. K. Harris, *J. Magn. Reson.*, 1997, **128**, 21.
188. K. Schmidt-Rohr, *J. Am. Chem. Soc.*, 1996, **118**, 7601.
189. M. Hong and R. G. Griffin, *J. Phys. Chem. B*, 1997, **101**, 5689.
190. M. Hong and R. G. Griffin, *J. Am. Chem. Soc.*, 1998, **120**, 7113.
191. S. Dusold, E. Klaus, A. Sebald, M. Bak and N. C. Nielsen, *J. Am. Chem. Soc.*, 1997, **119**, 7121.
192. T. Fujiwara, K. Sugase, M. Kainosho, A. Ono, A. Mei-Ono and H. Akutsu, *J. Am. Chem. Soc.*, 1995, **117**, 11351.
193. T. Fujiwara, T. Shimomura and H. Akutsu, *J. Magn. Reson.*, 1997, **124**, 147.
194. X. Feng, Y. K. Lee, D. Sanstrom, *et al.*, *Chem. Phys. Lett.*, 1996, **257**, 314.
195. X. Feng, P. J. E. Verdegem, Y. K. Lee, *et al.*, *Am. Chem. Soc.*, 1997, **119**, 6853.
196. D. M. Gregory, M. A. Mehta, J. C. Sheils and G. P. Drobny, *J. Chem. Phys.*, 1997, **107**, 28.
197. S. R. Kiihne, K. B. Geahigan, N. A. Oyler, H. Zebroski, M. A. Mehta and G. P. Drobny, *J. Phys. Chem. A*, 1999, **103**, 3890.
198. P. R. Costa, J. D. Gross, M. Hong and R. G. Griffin, *Chem. Phys. Lett.*, 1997, **280**, 95.
199. J. S. Shore, S. H. Wang, R. E. Taylor, A. T. Bell and A. Pines, *J. Chem. Phys.*, 1996, **105**, 9412.
200. A. Medek and L. Frydman, *J. Magn. Reson.*, 1999, **138**, 298.
201. T. P. Jarvie, R. M. Wenslow and K. T. Mueller, *J. Am. Chem. Soc.*, 1995, **117**, 570.
202. A. Medek, J. R. Sachleben, P. Beverwyk and L. Frydman, *J. Chem. Phys.*, 1996, **104**, 5374.
203. C. A. Fyfe, K. C. Wong-Moon, Y. Huang and H. Grondey, *J. Chem. Soc.*, 1995, **117**, 10397.
204. A. Lesage, C. Auger, S. Caldarelli and L. Emsley, *J. Am. Chem. Soc.*, 1997, **119**, 7867.
205. M. Baldus and M. H. Meier, *J. Magn. Reson.*, 1996, **A121**, 65.
206. M. Baldus, R. J. Iuliucci and B. H. Meier, *J. Am. Chem. Soc.*, 1997, **119**, 1121.
207. A. Lesage, S. Steuernagel and L. Emsley, *J. Am. Chem. Soc.*, 1998, **120**, 7095.
208. L. Frydman and J. S. Harwood, *J. Am. Chem. Soc.*, 1995, **117**, 5367.
209. A. Medek, J. S. Harwood and L. Frydman, *J. Am. Chem. Soc.*, 1995, **117**, 12779.
210. C. Fernandez and J. P. Amoureux, *Chem. Phys. Lett.*, 1995, **242**, 449.
211. C. Fernandez and J. P. Amoureux, *J. Magn. Reson.*, 1996, **5**, 315.
212. G. Wu, D. Rovnyak, B. Q. Sun and R. G. Griffin, *Chem. Phys. Lett.*, 1996, **249**, 210.
213. D. Massiot, B. Touzo, D. Trumeau, *et al.*, *Solid State NMR*, 1996, **6**, 73.
214. J. P. Amoureux, C. Fernandez and L. Frydman, *Chem. Phys. Lett.*, 1996, **259**, 347.
215. C. Fernandez and J. P. Amoureux, *Chem. Phys. Lett.*, 1995, **242**, 449.
216. J. P. Amoureux, C. Fernandez and S. Steuernagel, *J. Magn. Reson.*, 1996, **A123**, 116.
217. J. P. Amoureux and C. Fernandez, *Solid State NMR*, 1998, **10**, 211.
218. S. Steuernagel, *Solid State NMR*, 1998, **11**, 197.
219. T. Vosegaard, F. H. Larsen, H. J. Jakobsen, P. D. Ellis and N. C. Nielsen, *J. Am. Chem. Soc.*, 1997, **119**, 9055.
220. A. P. M. Kentgens and R. Verhagen, *Chem. Phys. Lett.*, 1999, **300**, 435.
221. C. A. Fyfe, J. Skibsted, H. Grondey and H. Meyer zu Altenschildesche, *Chem. Phys. Lett.*, 1997, **281**, 44.
222. S. P. Brown, S. J. Heyes and S. Wimperis, *J. Magn. Reson.*, 1996, **A119**, 280.
223. D. Massiot, *J. Magn. Reson.*, 1996, **A122**, 240.
224. L. Marinelli and L. Frydman, *Chem. Phys. Lett.*, 1997, **275**, 188.
225. J. P. Amoureux, D. P. Lang, M. Pruski and C. Fernandez, *J. Magn. Reson.*, 1998, **131**, 170.
226. R. E. Youngman, U. Werner-Zwanziger and J. W. Zwanziger, *Z. Naturforsch.*, 1996, **51a**, 321.
227. S. H. Wang, Z. Xu, J. H. Baltisberger, L. M. Bull, J. F. Stebbins and A. Pines, *Solid State NMR*, 1997, **8**, 1.
228. L. B. Alemany, S. Steuernagel, J. P. Amoureux, R. L. Callender and A. R. Barron, *Solid State NMR*, 1999, **14**, 1.
229. A. Samoson, *J. Magn. Reson.*, 1996, **A121**, 209.
230. S. P. Brown and S. Wimperis, *J. Magn. Reson.*, 1997, **124**, 279.

231. M. Pruski, D. P. Lang, C. Fernandez and J. P. Amoureux, *Solid State NMR*, 1997, **7**, 327.
232. C. Fernandez, L. Delevoye, J. P. Amoureux, D. P. Lang and M. Pruski, *J. Am. Chem. Soc.*, 1997, **119**, 6858.
233. P. K. Mudhu, A. Goldbourt, L. Frydman and S. Vega, *Chem. Phys. Lett.*, 1999, **307**, 41.
234. S. E. Ashbrook, S. P. Brown and S. Wimperis, *Solid State NMR*, 1998, **288**, 509.
235. S. H. Wang, S. M. De Paul and L. M. Bull, *J. Magn. Reson.*, 1997, **124**, 364.
236. J. V. Hanna, M. E. Smith and H. J. Whitefield, *J. Am. Chem. Soc.*, 1996, **118**, 5772.
237. C. Fernandez, D. P. Lang, J. P. Amoureux and M. Pruski, *J. Am. Chem. Soc.*, 1998, **120**, 2672.
238. M. Pruski, A. Bailly, D. P. Lang, J. P. Amoureux and C. Fernandez, *Chem. Phys. Lett.*, 1999, **307**, 35.
239. J. H. Baltisberger, Z. Xu, J. F. Stebbins, S. H. Wang and A. Pines, *J. Am. Chem. Soc.*, 1996, **118**, 7209.
240. P. J. Dirken, S. C. Kohn, M. E. Smith and E. R. H. van Eck, *Chem. Phys. Lett.*, 1996, **266**, 568.
241. C. Fernandez, J. P. Amoureux, J. M. Chezeau, L. Delmotte and H. Kessler, *Micropor. Mater.*, 1996, **6**, 331.
242. P. Sarv, C. Fernandez, J. P. Amoureux and H. Kessler, *J. Phys. Chem.*, 1996, **100**, 19223.
243. S. J. Hwang, C. Fernandez, J. P. Amoureux, J. Cho, S. W. Martin and M. Pruski, *Solid State NMR*, 1997, **8**, 109.
244. L. Delevoye, S. X. Liu, M. D. Welch, C. Fernandez, J. P. Amoureux and J. Klinowski, *J. Chem Soc., Farad. Trans.*, 1997, **93**, 2591.
245. G. Wu, D. Rovnyak, P. C. Huang and R. G. Griffin, *Chem. Phys. Lett.*, 1997, **277**, 79.
246. G. Wu, S. Kroeker, R. E. Wasylishen and R. G. Griffin, *J. Magn. Reson.*, 1997, **124**, 237.
247. G. Wu, D. Rovnyak and R. G. Griffin, *J. Am. Chem. Soc.*, 1996, **118**, 9326.
248. S. Ding and C. A. McDowell, *Chem. Phys. Lett.*, 1997, **270**, 81.
249. S. Ding and C. A. McDowell, *J. Magn. Reson.*, 1998, **135**, 61.
250. L. Marinelli, A. Medek and L. Frydman, *J. Magn. Reson.*, 1998, **132**, 88.
251. S. Ding and C. A. McDowell, *Chem. Phys. Lett.*, 1999, **307**, 215.
252. T. Charpentier, C. Fermon and J. Virlet, *J. Magn. Reson.*, 1998, **132**, 181.
253. T. Charpentier, C. Fermon and J. Virlet, *J. Chem. Phys.*, 1998, **109**, 3116.
254. C. M. Carter, D. W. Alderman and D. M. Grant, *J. Magn. Reson.*, 1985, **65**, 183.
255. C. M. Carter, D. W. Alderman and D. M. Grant, *J. Magn. Reson.*, 1987, **73**, 114.
256. P. M. Henrichs, *Macromol.*, 1987, **20**, 2099.
257. K. Schmidt-Rohr, M. Hehn, D. Schaefer and H. W. Spiess, *J. Chem. Phys.*, 1992, **97**, 2247.
258. B. F. Chemlka, K. Schmidt-Rohr and H. W. Spiess, *Macromolecules*, 1993, **26**, 2282.
259. M. Utz, J. Eisenegger, U. M. Suter and R. R. Ernst, *J. Magn. Reson.*, 1997, **128**, 217.
260. R. H. Lewis, H. W. Long, K. Schmidt-Rohr and H. W. Spiess, *J. Magn. Reson.*, 1995, **A115**, 26.
261. Z. Song, O. N. Antzutkin, A. Rupprecht and M. H. Levitt, *Chem. Phys. Lett.*, 1996, **253**, 349.
262. D. Marks and S. Vega, *J. Magn. Reson.*, 1996, **A118**, 157.
263. D. Marks, N. Zumbulyadis and S. Vega, *J. Magn. Reson.*, 1996, **A122**, 16.
264. M. Ernst, B. H. Meier, M. Tomaselli and A. Pines, *J. Chem. Phys.*, 1998, **108**, 9611.
265. M. Ernst, B. H. Meier, M. Tomaselli and A. Pines, *Mol. Phys.*, 1998, **95**, 849.
266. S. M. De Paul, M. Tomaselli, A. Pines, M. Ernst and B. H. Meier, *J. Chem. Phys.*, 1998, **108**, 826.
267. B. Q. Sun, P. R. Costa and R. G. Griffin, *J. Magn. Reson.*, 1995, **A112**, 191.
268. A. C. Kolbert and A. Bielecki, *J. Magn. Reson.*, 1995, **A116**, 29.
269. M. Baldus, D. G. Geurts, S. Hediger and B. H. Meier, *J. Magn. Reson.*, 1996, **118**, 140.
270. S. Hediger, P. Singer, M. Tomaelli, R. R. Ernst and B. H. Meier, *J. Magn. Reson.*, 1997, **125**, 291.
271. J. Raya and J. Hirchinger, *J. Magn. Reson.*, 1998, **133**, 341.
272. O. B. Peerson, X. Wu, I. Kustanovich and S. O. Smith, *J. Magn. Reson.*, 1993, **A104**, 334.

273. O. B. Peerson, X. Wu and S. O. Smith, *J. Magn. Reson.*, 1994, **A106**, 127.
274. G. Metz, X. Wu and S. O. Smith, *J. Magn. Reson.*, 1994, **A110**, 219.
275. M. Baldus, A. T. Petkova, J. Herzfeld and R. G. Griffin, *Mol. Phys.*, 1998, **95**, 1197.
276. A. Verhoeven, R. Verel and B. H. Meier, *Chem. Phys. Lett.*, 1997, **266**, 465.
277. D. Schaefer, J. Leisen and H. W. Spiess, *J. Magn. Reson.*, 1995, **A115**, 60.
278. R. Tycko, D. P. Weliky and A. E. Berger, *J. Chem. Phys.*, 1996, **105**, 7915.
279. R. Tycko, D. P. Weliky and A. E. Berger, *J. Chem. Phys.*, 1996, **105**, 7915.
280. D. P. Weliky and R. Tycko, *J. Am. Chem. Soc.*, 1996, **118**, 8487.
281. H. W. Long and R. Tycko, *J. Am. Chem. Soc.*, 1998, **120**, 7039.
282. M. Ernst, A. P. M. Kentgens and B. H. Meier, *J. Magn. Reson.*, 1999, **138**, 66.
283. Y. Yang, M. Schuster, B. Bluemich and H. W. Spiess, *Chem. Phys. Lett.*, 1987, **139**, 239.
284. V. Gerady-Montouillout, C. Malveau, P. Tekely, Z. Olender and Z. Luz, *J. Magn. Reson.*, 1996, **A123**, 7.
285. D. Reichert, H. Zimmermann, P. Tekely, R. Poupko and Z. Luz, *J. Magn. Reson.*, 1997, **125**, 245.
286. D. E. Favre, D. J. Schaefer and B. F. Chmelka, *J. Magn. Reson.*, 1998, **134**, 261.
287. A. Mueller and U. Haeberlen, *Chem. Phys. Lett.*, 1996, **248**, 249.
288. A. Mueller, H. Zimmermann and U. Haeberlen, *J. Magn. Reson.*, 1997, **126**, 66.
289. P. Speier, A. Mueller, C. Meinel and U. Haeberlen, *Mol. Phys.*, 1998, **95**, 859.
290. A. Mueller, H. Zimmermann and U. Haeberlen, *J. Magn. Reson.*, 1997, **126**, 66.
291. R. Fu, A. N. Klymachyov, G. Bodenhausen and N. S. Dalal, *J. Phys. Chem. B*, 1998, **102**, 8732.
292. M. Wilhelm, H. Feng, U. Tracht and H. W. Spiess, *J. Magn. Reson.*, 1998, **134**, 255.
293. D. G. Cory, *Annu. Rep. NMR Spectrosc.* 1992, **24**, 87.
294. P. Blumler and B. Blumich, *NMR: Basic Principles and Progress*, 1994, **30**, 211.
295. S. Hafner, D. E. Demco and R. Kimich, *Solid State NMR*, 1996, **6**, 275.
296. S. Matsui, M. Nonaka and T. Inouye, *J. Magn. Reson.*, 1999, **138**, 220.
297. D. G. Cory, *Solid State NMR*, 1997, **6**, 347.
298. S. Matsui, A. Uraoka and T. Inouye, *J. Magn. Reson.*, 1996, **A120**, 11.
299. U. Scheler, G. Schauss, B. Blumich and H. W. Spiess, *Solid State NMR*, 1997, **6**, 375.
300. S. Matsui, M. Nonaka, T. Nakai and T. Inouye, *Solid State NMR*, 1997, **10**, 39.
301. V. S. Swaminathan and B. H. Suits, *J. Magn. Reson.*, 1998, **132**, 274.
302. S. Matsui, K. Kose and T. Inouye, *J. Magn. Reson.*, 1990, **88**, 186.
303. E. Rommel, P. Nickel, R. Kimmich and D. Pusiol, *J. Magn. Reson.*, 1991, **91**, 630.
304. P. Nickel, E. Rommel, R. Kimmich and D. Pusiol, *Chem. Phys. Lett.*, 1991, **183**, 183.
305. E. Rommel, D. Pusiol, P. Nickel and R. Kimmich, *Meas. Sci. Tech.*, 1991, **2**, 866.
306. V. L. Ermakov, R. H. Kurbanov, D. Ya. Osokin and V. A. Shaganov, *Appl. Magn. Reson.*, 1992, **3**, 975.
307. E. Rommel, R. Kimmich, H. Robert and D. Pusiol, *Meas. Sci. Tech.*, 1992, **3**, 446.
308. Y. Lee, D. C. Michaels and L. G. Butler, *Chem. Phys. Lett.*, 1993, **206**, 464.
309. H. Robert, D. Pusiol, E. Rommel and R. Kimmich, *Z. Naturforsch.*, 1994, **49a**, 35.
310. P. Nickel, H. Robert, R. Kimmich and D. Pusiol, *J. Magn. Reson.*, 1994, **A111**, 191.
311. B. H. Suits and G. Y. Plude, *J. Magn. Reson.*, 1995, **A117**, 84.
312. R. Kimmich, *Z. Naturforsch.*, 1996, **51a**, 330.
313. H. Robert and D. Pusiol, *Z. Naturforsch.*, 1996, **51a**, 353.
314. H. Robert, A. Minuzzi and D. Pusiol, *J. Magn. Reson.*, 1996, **A118**, 189.
315. H. Robert and D. Pusiol, *J. Magn. Reson.*, 1996, **A118**, 279.
316. H. Robert and D. Pusiol, *J. Magn. Reson.*, 1997, **127**, 109.
317. V. S. Swaminathan and B. H. Suits, *J. Magn. Reson.*, 1999, **138**, 123.
318. P. J. MacDonald, *Prog. Nucl. Magn. Reson. Spectrosc.*, 1997, **30**, 69.
319. E. W. Randall, *Solid State NMR*, 1997, **8**, 179.
320. E. W. Randall, *Solid State NMR*, 1997, **8**, 173.

321. P. Bodart, T. Nunes and E. W. Randall, *Solid State NMR*, 1997, **8**, 257.
322. M. J. D. Mallet, M. R. Halse and J. H. Strange, *J. Magn. Reson.*, 1998, **132**, 172.
323. P. M. Glover, P. J. McDonald and B. Newling, *J. Magn. Reson.*, 1997, **126**, 207.
324. B. J. Balcom, R. P. MacGregor, S. D. Beyea, D. P. Green, R. L. Armstrong and T. W. Bremner, *J. Magn. Reson.*, 1996, **A123**, 131.
325. S. Emid and J. H. N. Greyghton, *Physica B*, 1985, **128**, 81.
326. P. J. McDonald, J. J. Attard and D. J. Taylor, *J. Magn. Reson.*, 1987, **72**, 224.
327. P. Bendel, M. Davis, E. Berman and G. W. Kabalka, *J. Magn. Reson.*, 1990, **88**, 369.
328. S. Gravina and D. G. Cory, *J. Magn. Reson.*, 1994, **B104**, 53.
329. B. J. Balcom, R. P. MacGregor, S. D. Beyea, D. P. Green, R. L. Armstrong and T. W. Bremner, *J. Magn. Reson.*, 1996, **A123**, 131.
330. P. J. Prado, B. J. Balcom, S. D. Beyea, R. L. Armstrong and T. W. Bremner, *Solid State NMR*, 1997, **10**, 1.
331. J. A. Sadles, J. L. Garbini, K. J. Bruland, *et al.*, *Rev. Mod. Phys.*, 1995, **67**, 249.
332. K. Wago, O. Zuger, R. Kendrick, C. S. Yannoni and D. Rugar, *J. Vac. Sci. Tech.*, 1996, **B14**, 1197.
333. O. Zuger, S. Hoen, C. S. Yannoni and D. Rugar, *J. Appl. Phys.*, 1996, **79**, 1881.
334. A. Schaff and W. S. Veeman, *J. Magn. Reson.*, 1997, **126**, 200.
335. D. M. TonThat, M. Ziegeweid, Y. Q. Song, *et al.*, *Chem. Phys. Lett.*, 1997, **272**, 245.
336. M. Y. Liao and D. B. Zax, *J. Phys. Chem.*, 1996, **100**, 1483.
337. B. G. M. Chew, M. L. Liao and D. B. Zax, *J. Magn. Reson.*, 1995, **A116**, 277.
338. D. K. Yang and D. B. Zax, *J. Magn. Reson.*, 1998, **135**, 267.
339. D. K. Yang, J. E. Atkins, C. C. Lester, and D. B. Zax, *Mol. Phys.*, 1998, **95**, 747.
340. A. O. Salman, M. M. Sunnetcioglu, R. Sungur and G. Bingol, *J. Magn. Reson.*, 1998, **134**, 1.
341. M. Alecci and D. L. Lurie, *J. Magn. Reson.*, 1999, **138**, 313.
342. T. Guiberteau and D. Grucker, *J. Magn. Reson.*, 1997, **124**, 263.
343. T. Pietrass, H. C. Gaede, A. Bifone, A. Pines and J. A. Ripmeester, *J. Am. Chem. Soc.*, 1995, **117**, 7520.
344. R. Tycko and J. A. Reimer, *J. Phys. Chem.*, 1996, **100**, 13240.
345. M. P. Augustine and K. W. Zilm, *J. Chem. Phys.*, 1996, **105**, 2998.
346. T. Pietrass, A. Bilfone, J. Kruger and J. A. Reimer, Phys. Rev. B, 1997, **55**, 4050.
347. M. P. Augustine and K. W. Zilm, *Chem. Phys. Lett.*, 1997, **280**, 24.
348. M. Shreiner, H. Hochstetter, H. Pascher and S. A. Studenikin, *J. Magn. Reson.*, 1997, **124**, 80.
349. T. Pietrass, R. Seydouxx and A. Pines, *J. Magn. Reson.*, 1998, **133**, 299.
350. E. Brunner, R. Seydouxx, M. Haake, A. Pines and J. A. Reimer, *J. Magn. Reson.*, 1998, **130**, 145.
351. R. Tycko, *Mol. Phys.*, 1998, **95**, 1169.
352. C. A. Michal and R. Tycko, *Phys. Rev. Lett.*, 1998, **81**, 3988.
353. G. Neue, *Solid State NMR*, 1997, **5**, 305.
354. T. Miyoshi, K. Takegoshi and T. Terao, *J. Magn. Reson.*, 1997, **125**, 383.
355. T. Mildner, H. Ernst, D. Freude and W. F. Holderich, *J. Am. Chem. Soc.*, 1997, **119**, 4258.
356. C. Dalluin, C. Boutillon, A. Tartar and G. Lippens, *J. Am. Chem. Soc.*, 1997, **119**, 10494.
357. T. P. Spaniol, A. Kubo and T. Terao, *Mol. Phys.*, 1999, **96**, 827.
358. R. J. Iuliucci and D. M. Grant, *Solid State NMR*, 1996, **6**, 55.
359. T. Vosegaard, E. Hald, V. Langer, *et al.*, *J. Magn. Reson.*, 1998, **135**, 126.

Pharmaceutical Applications of NMR

DAVID J. CRAIK and MARTIN J. SCANLON

Centre for Drug Design and Development, The University of Queensland, Brisbane, QLD 4072, Australia

1. INTRODUCTION

NMR continues to be a crucial technology within the pharmaceutical industry, with applications ranging from routine identification of newly synthesized molecules to fundamental drug design or discovery applications. This review updates an earlier one in *Annual Reports on NMR Spectroscopy* published in 1996[1] and focuses on developments since that time. We illustrate the various developments with selected examples from the literature and from our own work. No attempt has been made to provide an exhaustive coverage of all applications of NMR in drug design; rather, selected examples from key areas are described. Other recent reviews have focused on particular aspects, including structure-based design,[2] combinatorial chemistry[3,4] and analytical applications.[5,6]

2. OVERVIEW OF DRUG DESIGN AND DEVELOPMENT

The general scheme involved in the drug development process is illustrated in Fig. 1. This process begins with the design or discovery of a lead compound

ANNUAL REPORTS ON NMR SPECTROSCOPY
VOLUME 42 ISBN 0-12-505342-8

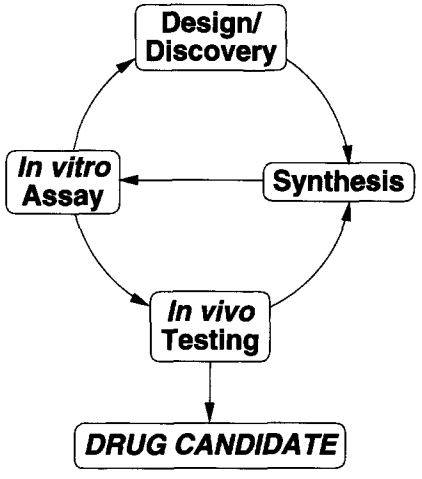

Fig. 1. Overview of the process of drug development.

possessing a desired bioactivity. *Design* implies a rational approach to obtaining the lead compound. This may be based on the structure of a known drug or bioactive molecule, in a process categorized as 'ligand-based' design. Alternatively, in 'receptor-based' design the synthesis of lead compounds is directed by knowledge of the structure of a biological target. *Discovery* refers to the identification of a lead compound either by screening or by chance observation. A wide range of sophisticated screening techniques has been developed over recent years and NMR promises to play a significant role in some of these.

Whether it has been designed or discovered, the next stage in the development process of a lead molecule is optimization to improve its affinity and/or specificity. This may require several rounds of design, synthesis and assay before a suitable candidate is identified and taken forward for more extensive testing. Once *in vivo* studies commence, further chemical modification may be required to produce desirable pharmacokinetic properties or to protect the compound from enzymatic breakdown and metabolism, before a suitable drug candidate emerges.

3. ROLE OF NMR IN DRUG DEVELOPMENT

NMR spectroscopy has been applied at various stages of the drug development process.[7] These applications can be broadly categorized as analytical NMR (identification and characterization of molecules of less than a few thousand daltons in mass); NMR-based screening (the measurement of NMR parameters, for a ligand, for mixtures of ligands, or for a macromolecular

target, to identify potential lead molecules); NMR structure-based design (elucidation of high-resolution structures of macromolecular targets and target–ligand complexes); and *in vivo* NMR (studies of isolated organs or whole animals).

Analytical NMR has been used in the pharmaceutical industry primarily as a tool for verification of the structures of synthesized molecules. However, analytical NMR methods have more widespread applications, for example in quantitative analysis of impurity profiles, in characterizing the composition of drug products and in investigating the metabolites of drugs in body fluids. These applications are the subject of a recent review.[8] Many new analytical NMR applications have resulted from recent developments in the pharmaceutical industry that have changed the types of samples that require analysis. For example, there has been an increasing reliance on high-throughput screening of combinatorial libraries for the identification of lead compounds. Such libraries typically contain large numbers of compounds, often present in small amounts and/or in mixtures and sometimes attached to a solid-phase support. The requirement for analysis of these libraries has led to the development of novel NMR instrumentation and methodologies.

In addition to extending the utility of analytical NMR, these developments have had a direct impact on screening methodologies, where NMR spectroscopy may now be used directly as a rapid and sensitive method for the characterization of binding affinities of mixtures of compounds in combinatorial libraries.[3,9–11] A powerful screening method based on observation of NMR signals from a protein target has been developed by researchers at Abbott laboratories.[12] Termed SAR (structure-activity relationship) by NMR, this technique has proved to be extremely valuable for the identification of novel lead compounds.

Structure-based design relies on the techniques of macromolecular NMR spectroscopy, and has had its major impact in the determination of the three-dimensional solution structures of protein targets. However, with the numerous Genome Projects producing new sequences and potential targets at a prodigious rate, there has been great pressure to develop faster and more effective ways of determining protein structures. Higher-field instruments are leading to increased resolution and sensitivity, while novel methods offer the potential to extend the utility of NMR to far larger biological systems. For example, the study of drugs and ligands bound to membrane-bound receptors is the subject of a recent review.[13] In addition, methods for the study of molecular motion at the binding site of drug–receptor complexes are contributing to an understanding of the dynamics of these interactions (reviewed by Roberts[14]).

Finally, *in vivo* NMR methods have been used to investigate the effects of drugs in target organs. These applications will not be discussed further here but are the subject of a recent review.[15] The remainder of this chapter will cover in more detail the recent developments in pharmaceutical applications of NMR,

with particular focus on analytical, structure–based and screening applications, followed by a few selected examples.

3.1. Analytical NMR

The largest single use of NMR in the pharmaceutical industry continues to be the identification of molecules synthesized as part of drug discovery and development programmes. To a large extent, this application may be regarded as of a routine nature based on analysis of well-established NMR parameters such as chemical shifts, coupling constants and nuclear Overhauser effects (NOEs). The principles of such analyses are well known and need not be reviewed here. Instead, we focus on developments in NMR spectroscopy that have extended the range of analytical applications to different types of samples that are now routinely produced in the pharmaceutical industry. For example, developments in combinatorial chemistry, which allow for the simultaneous or parallel synthesis of libraries of compounds, often on solid-phase supports, have provided a significant challenge for NMR. Conventional high-resolution NMR requires the use of homogeneous samples in solution in relatively large sample sizes (typically hundreds of microlitres) to achieve acceptable lineshapes. Until recently, these requirements have prevented the use of NMR for the characterization of compounds while they remain bound to a solid phase support. However, recent developments allow for the analysis of complex mixtures, combinatorial libraries, bound drugs and small or heterogeneous samples.

3.1.1. Applications of NMR in solid-phase synthesis

Solid-phase synthesis (SPS) is now a widely used technique in the production of large numbers of diverse compounds or libraries that are utilized in the process of drug discovery. The widespread use of this technology has driven the development of techniques for the analysis of materials while they are still attached to the solid-phase support.[4,5,16] Cleaving the product from the resin prior to analysis has a number of drawbacks: the cleavage process has the potential to alter the product, it necessarily results in a lowering of the yield, it is time-consuming, and the requirement for cleavage before analysis presents difficulties for monitoring a reaction in progress. Two distinct methods are now available for analysing the products of SPS reactions while they remain attached to the solid-phase support. These methods are termed gel-phase and magic-angle spinning (MAS) NMR.

(i) Gel-phase NMR. Gel-phase NMR involves recording spectra on the SPS resin in a standard NMR tube. As the compounds of interest remain bound to the solid support, their motion is restricted, which results in a broadening of the

NMR signals. To alleviate this problem to some degree, the SPS resins are swollen as much as possible before the spectra are acquired. The resulting slurries are neither fully solid nor fully liquid, hence the term gel-phase NMR used to describe the technique. Even in this gel-phase state, the SPS resin slurry contains regions of differing magnetic susceptibility, which cause local variation in the magnetic field and result in line broadening. For this reason, gel-phase NMR is generally limited to the observation of heteronuclei, whose lower frequencies lessen the effects of the magnetic susceptibility line broadenings. The most commonly observed nucleus in gel-phase NMR is ^{13}C and, although the technique of ^{13}C gel-phase NMR is not a new one, it has recently been used to monitor the synthesis of both peptides[17] and organic compounds[18,19] on solid-phase supports (Fig. 2).

The major drawback of the ^{13}C gel-phase NMR is lack of sensitivity, which makes it impractical for fast reaction monitoring as thousands of transients must be acquired to obtain a sufficient signal-to-noise ratio. Another approach involves the incorporation of ^{13}C labels near the reaction site of interest,[20] which compensates for the lack of sensitivity. This 'fast ^{13}C gel-phase NMR' allows data to be acquired in ~15 min and has proved useful in monitoring the progress of reactions.[21,22] Gel-phase NMR has also been reported using nuclei other than ^{13}C. ^{19}F NMR has the advantage that its inherent sensitivity is very high and most solid supports do not contain fluorine; a number of recent examples have described the use of ^{19}F gel-phase NMR in reaction monitoring.[23–26] ^{31}P gel-phase NMR has also been used for reaction monitoring.[26] Although gel-phase NMR has found a number of applications in SPS, its utility is limited in that the ^{1}H spectra it generates contain very broad lines that prevent determination of structures via the acquisition of high-resolution ^{1}H NMR spectra.

(ii) High-resolution magic-angle spinning NMR. It is well established that magic-angle spinning (MAS) has the ability to reduce the line broadening caused by residual dipolar interactions and magnetic susceptibility differences in heterogeneous samples.[27,28] However, it required the development of specialized magnetic susceptibility-matched MAS probes before the first truly high-resolution (HR) spectra of organic compounds bound to SPS resins were reported.[29] The basic principles behind the technique have been described[30] and its development continues.[6,16]

With an increasing interest in peptides as potential lead compounds in drug design, the technique has become particularly important in the pharmaceutical industry. The utility of HR-MAS NMR for the characterization of peptides attached to solid-phase supports has been demonstrated by Jelinek *et al.*[31] The improved resolution afforded by MAS is clearly demonstrated in Fig. 3. In fact, the quality of the spectra is such that resonance assignments and structure determination of the peptide were accomplished with the peptide still attached to the solid-phase support. Similarly, Dhalluin *et al.*[32] used HR-MAS NMR to monitor the progress of a reaction on a solid-phase support.

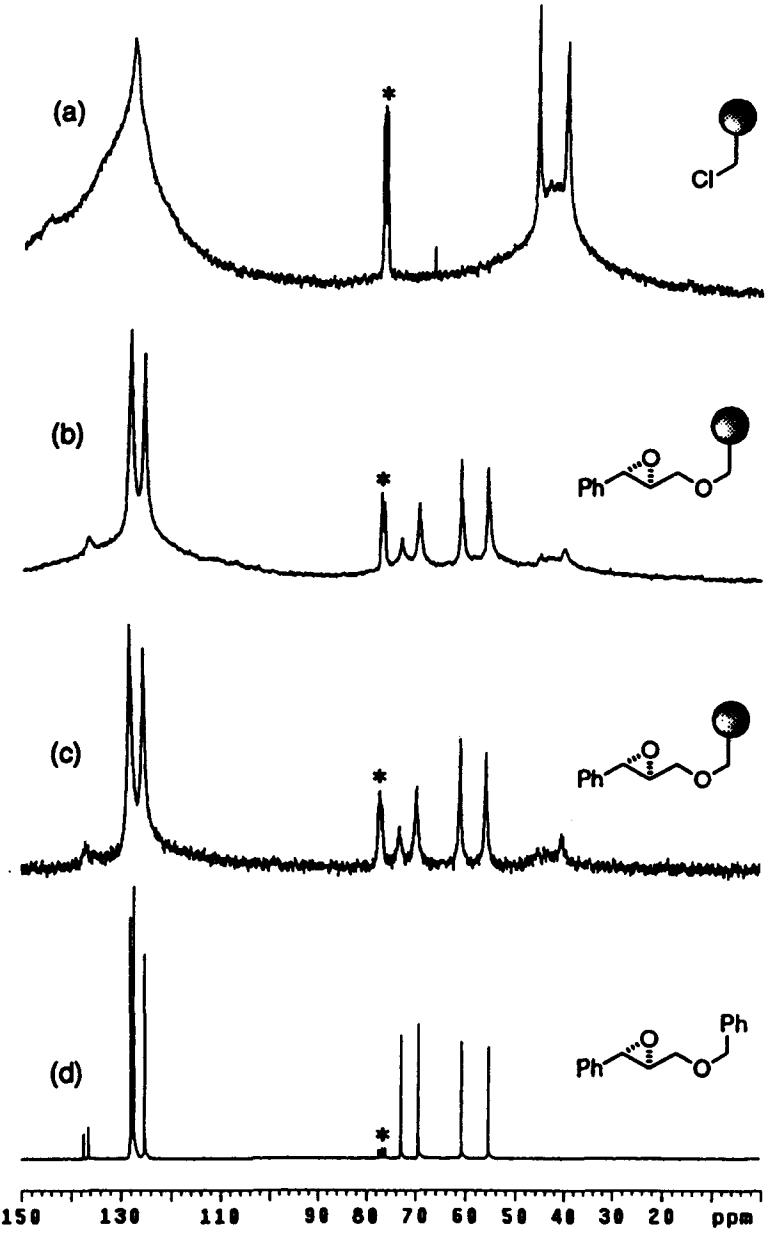

Fig. 2. ^{13}C Gel-phase NMR spectra of modified polystyrene–2%-co-DVB in $CDCl_3$ at 75 MHz. (a) Merrifield resin; (b) epoxy alcohol bound polymer at room temperature; (c) epoxy alcohol bound polymer at 50°C; (d) model compound in solution. The solvent resonance is marked with an asterisk. (Reproduced from Shapiro and Gounarides[4] with permission.)

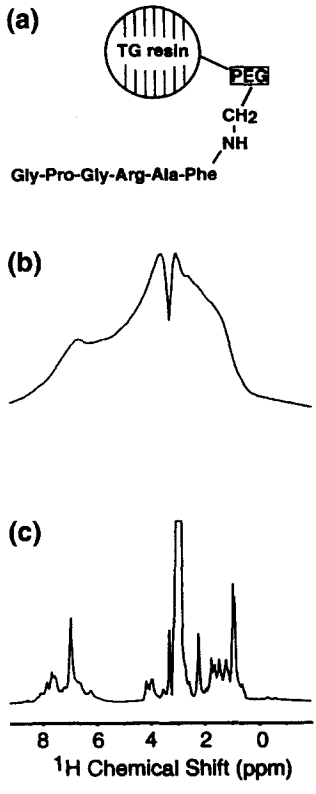

Fig. 3. ^{1}H NMR spectra of a hexapeptide bound to tentagel resin. (a) Schematic diagram of the peptide–resin complex; (b) stationary sample of the complex swollen in DMSO-d_6; (c) the same sample recorded with magic-angle spinning at 5 kHz. (Reproduced from Jelinek *et al.*[31] with permission.)

The sensitivity requirements of HR-MAS NMR are determined to a certain extent by the chemistry used to produce a combinatorial library. In the most extreme case, each compound in the library is present only on a single bead of the solid-phase support and therefore it is necessary to obtain spectra from a single bead. Despite the practical difficulties associated with both the handling and data acquisition of single-bead spectra, it has been shown to be a suitable technique, both for analysis[33] and reaction monitoring.[34]

The development of HR-MAS probes has resulted in several technical developments extending beyond the analysis of SPS products. HR-MAS NMR has also been used for structure determination of very small samples containing submicrogram quantities of biological molecules;[35] it has been used for the biochemical characterization of tissue samples in normal and disease states;[36] and more recently it has been used in a screening role to identify substances with binding activity from a mixture of compounds,[37] as described later in this review.

3.1.2. High-throughput and LC-NMR

Another major challenge for NMR spectroscopy has been the increased use of high-throughput screening in the drug discovery process. Although HR-MAS NMR has provided a method for analysing the progress of SPS reactions, the majority of bioassays are conducted on compounds in solution. Consequently, it is also desirable to analyse the structure of the compounds being assayed using solution-phase NMR methods. This involves analysis of a large number of samples, which often need to be transferred from a microtitre plate to the NMR probe and are generally present in small volumes, and usually in aqueous solutions. Another problem is posed by the analysis of mixtures of compounds. It is very difficult to perform detailed structural analysis of individual components in a mixture. Therefore, it is preferable to separate the mixture prior to NMR analysis

Several recent developments in liquid chromatography (LC)-NMR (reviewed in refs[6,38,39]) have enabled direct flow applications of pharmaceutical mixtures through the NMR probe so that on-line analysis can be carried out. Sensitivity problems have been addressed through the use of higher-field magnets, improved probe technology and the development of small-volume probes. The problem of solvent suppression is twofold: first there is a requirement to suppress the large solvent signals arising from the mobile phase; second, changes in the composition of the mobile phase result in significant variation in the chemical shifts of the solvent resonances. Automated solvent suppression schemes have been developed that provide an effective solution to these problems.[40,41]

LC-NMR data may be acquired in either onflow or stopped-flow modes. In the onflow mode, effluent flows directly from the column through the probe, where spectra are collected at fixed time intervals. Figure 4 shows a typical onflow LC-NMR spectrum.[6] In the stopped-flow mode, several fractions are collected and analysed individually at a later time. Although mass spectrometry continues to be the favoured technique for the analysis of combinatorial libraries, the value of LC-NMR was demonstrated in a study by Chin *et al.*[42] in a stopped-flow study of four positional isomers of dimethoxybenzoylglycine. Iso-molecular-weight mixtures such as this can be problematic to analyse using mass spectrometry; however, in this case assignment of the compounds was readily accomplished from the LC-NMR data (Fig. 5).

The use of LC-NMR as an analytical tool in combinatorial chemistry remains limited. Its major application within the pharmaceutical industry is in the identification of drug metabolites.[38] For this purpose LC-NMR has been further coupled to a mass spectrometer to generate an LC-NMR-MS system.[43] The combination of the three techniques provides a powerful tool for structural characterization.

An alternative approach for the analysis of combinatorial libraries has been to remove the chromatographic column from the LC-NMR system to generate

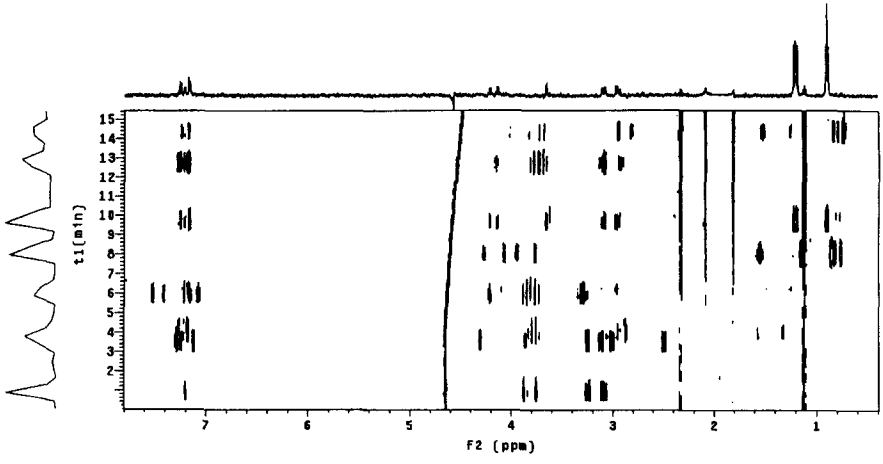

Fig. 4. An onflow gradient LC-NMR spectrum of a mixture of peptides separated using a CH_3CN/D_2O solvent gradient. (Reproduced from Keifer[6] with permission.)

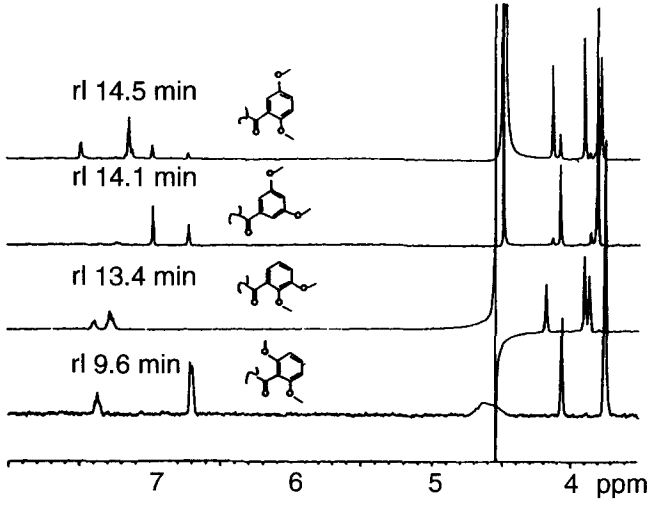

Fig. 5. A stacked plot of the stopped-flow HPLC NMR data of the four positional isomers shown. (Reproduced from Chin *et al.*[42] with permission. Copyright (1998) American Chemical Society.)

a 'columnless' LC-NMR that can be used for high-throughput NMR.[5,6] Such systems incorporate an autosampler, which is used to inject samples either into a conventional LC port, termed flow injection analysis (FIA)-NMR, or directly into the probe for direct-injection (DI)-NMR. These flow injection systems are capable of generating high-resolution ^1H NMR spectra of 1 mg ml^{-1} samples

with turnaround times of ~2 min. The results of such an analysis for a series of compounds taken from a 96-well microtitre plate are shown in Fig. 6.

The major bottleneck created by these high-throughput NMR techniques is in the analysis of the vast amount of data that is generated. A number of commercial packages are now available that use chemical shift/structure databases to aid in the interpretation of the spectra. However, fully automated spectral analysis systems are still under development.

3.1.3. Summary

It is apparent from the above discussion that the major innovations in analytical applications of NMR over recent years have involved overcoming the challenges associated with new types of samples, which have been driven by

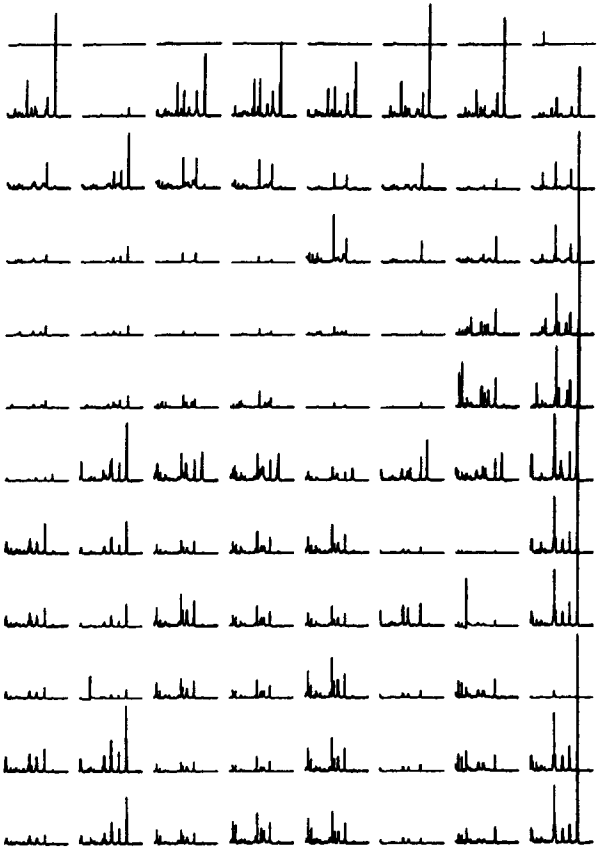

Fig. 6. ^{1}H NMR spectra of a library of compounds from a 96-well microtitre plate acquired by direct-injection NMR. (Reproduced from Keifer[6] with permission.)

combinatorial chemistry and high-throughput screening. The importance of this analytical 'support' role of NMR should not be underestimated, but the remainder of this article will focus on those areas where NMR has played a more central role in the drug discovery or development process. These include the use of NMR to design or discover new compounds using either structure-based or screening approaches.

3.2. Structure-based design

The use of NMR in structure-based design has increased substantially over recent years, reflecting continuing improvement in NMR technologies, the increasing availability of suitably labelled target macromolecules, and pressures from within the pharmaceutical industry for faster methods of drug discovery.

Drug–receptor interactions involve two components – a ligand (the drug) and a macromolecular target (the receptor). Structure-based design requires a knowledge of one or both of these components: preferably both, and preferably in complex with each other. However, in some cases structural information is accessible only for one of the components, usually the ligand, and hence it is necessary to consider two structure-based approaches to drug design: 'ligand-based' drug design, and 'receptor-based' drug design.

In ligand-based design the structure of a naturally occurring hormone, neurotransmitter or other small molecule is determined by NMR and is used as a basis for the design of analogues. Usually the intention is to design antagonists of the naturally occurring ligand, although in some cases agonists may be useful. Provided an assay is available to test the activity of the newly designed molecules, this approach may be conducted in complete ignorance of the structure of the receptor. If a range of different ligands is available or can be synthesized, then it may be possible to use the family of structures to develop a pharmacophore model of the receptor site and use this in the design of novel ligands, although this is not essential in all ligand-based design approaches.

In receptor-based design, the structure of the biological target site is used to design ligands that will interact with and, usually, block that site. Since NMR methods are currently limited to the study of proteins with mass <35 kDa, receptor-based design requires x-ray crystallographic information for larger proteins. Whatever the source of the structural information on the receptor, the completely *de novo* design of ligands based on a target protein structure has so far proved an elusive goal.[44] In most examples of receptor-based design it has proved easier to generate lead ligands by screening computer databases of ligand structures for those that fit the receptor site. This has the advantage over the completely *de novo* design of a ligand from atomic building blocks that at least the selected compound is known to be synthetically accessible. More successful still has been the use of ligand–macromolecule complexes to guide

the design of ligands with improved binding. Knowledge of how a known ligand fits into the receptor site is significantly more valuable than just the shape of the unbound receptor site itself. Thus, in the current review, receptor-based design will relate largely to the use of NMR for understanding the mode of interaction of a ligand with a receptor and the use of the information for fine-tuning such interactions in new and improved ligands.

There are many specific types of information that are useful in ligand-based or receptor-based drug design and there are a variety of NMR techniques that can be used to deduce them. These are summarized in Table 1. There is clearly overlap in the NMR methods that may be used in structure-based design but they are grouped for convenience under the headings of the ligand, the macromolecule and the complex. Within each category, the information types are listed in order of increasing complexity and, potentially, increasing value in the drug design process. For example, in ligand-based design, the simplest experiment to perform is to determine the solution conformation of a target ligand. Information that adds value to this includes knowledge of charge/tautomeric states, and ligand dynamics. Further added value comes from a determination of the bound conformation and deduction of a pharmacophore model for the receptor based on information from many ligands.

Table 1. Information on ligands, macromolecules and their complexes sought in structure-based design and relevant NMR technologies used to derive this information

Target	Information	NMR Technology
Ligand	Solution conformation	1D/2D NMR
	Charge/tautomeric state	Chemical shift
	Solution dynamics	Line shape/relaxation analysis
	Bound conformation	TrNOE
	Pharmacophore models	All of the above, including 1D/2D of multiple ligands
Macromolecule	3D structure	2D/3D/4D NMR
	Macromolecular dynamics	Relaxation time measurements
	Structure of articulated macromolecules (e.g. multimeric or membrane-bound receptors)	TROSY
Ligand–macromolecule complex	Stoichiometry of complex	Chemical shift titration
	Kinetics of binding	Line width, titration analysis
	Location of interacting sites	HSQC, isotope editing
	Orientation of bound ligand	NOE docking
	Structure of complex	3D/4D NMR
	Dynamics of complex	Relaxation time measurements

The summary in Table 1 is the basis for the following more detailed discussion on each of the listed types of information, including specific examples of their application.

3.2.1. Solution conformation of ligands

Usually only 1D or 2D NMR methods are required to determine the solution conformation of bioactive ligands. Useful tools include analysis of chemical shifts, coupling constants, and NOEs, and the relevant methods are well described in standard NMR texts. An assumption inherent in such studies is that the solution conformation will be maintained on binding to the receptor. This is justified in the case of relatively rigid ligands, but for potentially flexible ligands the possibility of changes in conformation on binding must be considered. It is convenient to illustrate this principle, and indeed that of ligand-based design in general, using a discussion of endothelin analogues.

Endothelin (ET) was discovered in 1985 as a peptide-based endothelial-derived constricting factor and has since gained prominence as a pharmacological target, with more than 2500 papers published describing various aspects of its biochemistry, pharmacology and physiology. Interest in the peptide arises because of its potent renal, pulmonary and neuroendocrine activities. Endothelin and its isoforms have been implicated in a wide variety of disease states including ischaemia, cerebral vasospasm, stroke, renal failure, hypertension and heart failure.[45] Endothelin exerts its pharmacological effect by acting on specific G-protein-coupled receptors. In mammalian species, two receptors (ET_A and ET_B) have been cloned. Both receptors are widely distributed in human tissue and are distinguished by different responses to the various ET isoforms, ET-1, ET-2 and ET-3 (Fig. 7).

The 3D structure of this 21-amino-acid peptide consists of several distinct regions, including a random coil N-terminus, a β-turn over residues 5–8, followed by a short helical region and then a flexible C-terminal tail.[1] The presence of the flexible tail in solution is not surprising, as may be imagined from the sequence shown in Fig. 7.

While solution structures of endothelin and its analogues[46–60] have been valuable in defining the gross conformation of these molecules, the flexibility of the tail in solution makes it difficult to extrapolate to the bound state. Indeed, an x-ray structure of ET-1 has a quite different structure for the C-terminal tail from that of the random coil arrangement in solution.[60] The bound conformation may be different again. There is clearly an advantage to having lead molecules with reduced flexibility. Indeed, small cyclic molecules that are more rigid have provided more valuable leads to the development of potent endothelin antagonists. Early small cyclic peptide inhibitors included BQ123 and BE18257B (Fig. 8) which are ET_A selective antagonists. ET_B selective cyclic peptides have also been described (for a review see ref. 1). The discovery and applications of these molecules illustrate the principle that cyclic peptides are

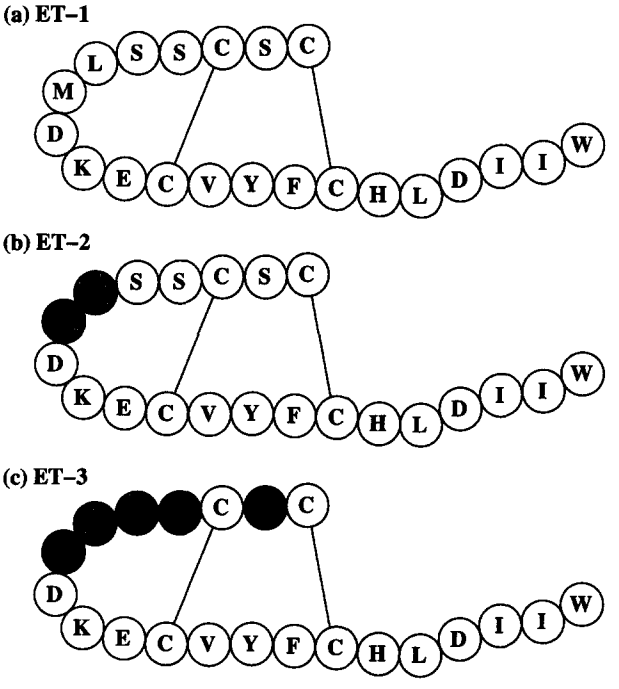

Fig. 7. Primary sequences and disulfide bond connectivities of endothelin isoforms ET-1, ET-2 and ET-3. Shading is used to indicate regions of sequence variability relative to ET-1.

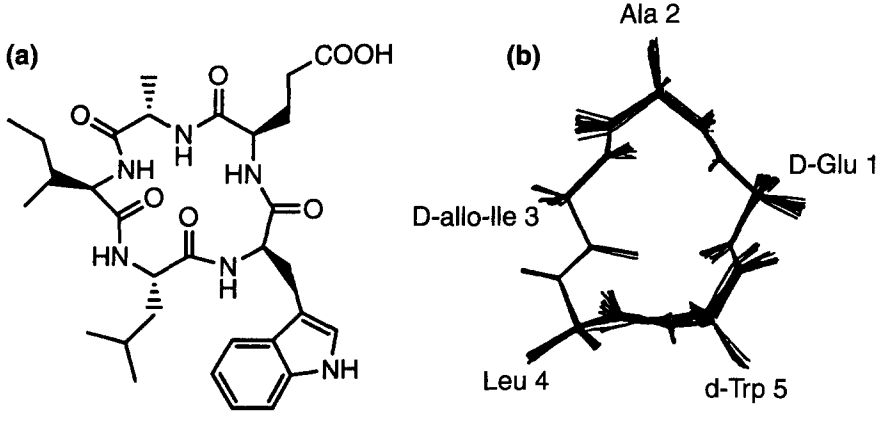

Fig. 8. (a) Primary structure of the cyclic endothelin antagonist BE18257B and (b) a family of 36 NMR structures which demonstrates the well-defined nature of the cyclic peptide backbone. (Reprinted with permission from Coles *et al.*[148] Copyright (1993) American Chemical Society.)

often more suitable as lead ligands in drug design compared to acyclic derivatives. In addition to their generally improved bioavailability and resistance to protease attack, they also tend to have better defined and less flexible conformations than linear counterparts, and hence determination of their structures in solution potentially yields information that may be quite similar to that for the bound conformation.

The rather well-defined solution conformation of BE18257B shown in Fig. 8 contrasts with the flexibility of the tail region of endothelin, which this peptide is thought to mimic. We shall return to endothelin as a target in drug design in the following section, in that case in relation to a nonpeptidic antagonist. The underlying theme we have attempted to illustrate is that ligand-based design often proceeds from initial studies of flexible endogenous molecules (particularly peptides) to constrained mimics and often culminates in the development of nonpeptidic drug leads.

3.2.2. Charge state of ionisable groups/tautomeric equilibria

One of the major advantages of NMR over other structural techniques such as x-ray crystallography is that it has the potential to provide information not only on structure but also on the electronic properties of molecules. Many potential drug leads contain ionizable groups and a determination of their charge state in solution and/or at the bound site or, if relevant, their tautomeric form, can be important in the design of analogues.

Such electronic effects are readily deduced from chemical shifts. A recent example from our laboratory concerns the antimicrobial peptide drosocin.[61] This 19-amino-acid peptide is secreted by *Drosophila* species in response to septic injury and is a potent antibacterial. The sequence of the peptide (shown below using the one-letter amino acid code) contains a glycosylated threonine at a mid-chain position that appears to be important in enhancing antimicrobial activity.

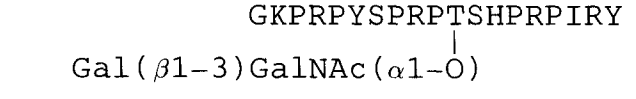

A structure determination of the peptide[61] showed that it was largely disordered in solution, but there were a significant number of NOE contacts between the sugar residues and the peptide backbone (Fig. 9). This suggested the possibility that the His residue at position 13 might be potentially masked by the sugar residue, perhaps modifying its pK_a and possibly accounting for a change in activity between glycosylated and nonglycosylated peptides. However, a simple NMR titration in which chemical shifts of the His H4 proton were monitored as a function of pH for both glycosylated and nonglycosylated peptides (Fig. 10) showed no difference in pK_a between the two. This simple NMR titration experiment thus allowed one possible contributing factor to be eliminated from

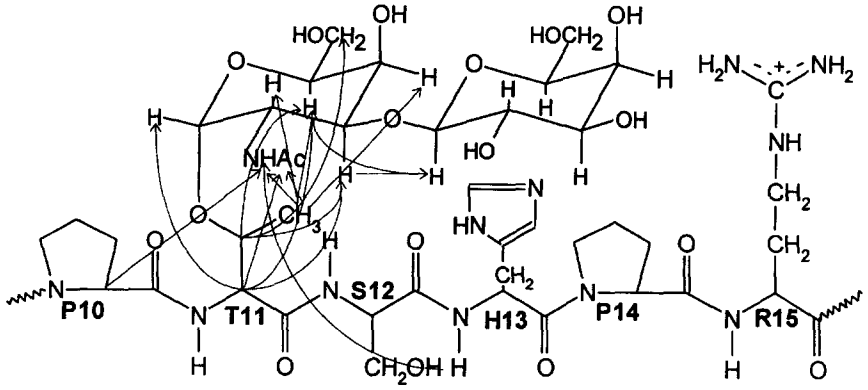

Fig. 9. Schematic representation of NOEs between the peptide backbone and the sugar moiety of the antimicrobial peptide drosocin. (Reproduced from McManus *et al.*[61] with permission. Copyright (1999) American Chemical Society.)

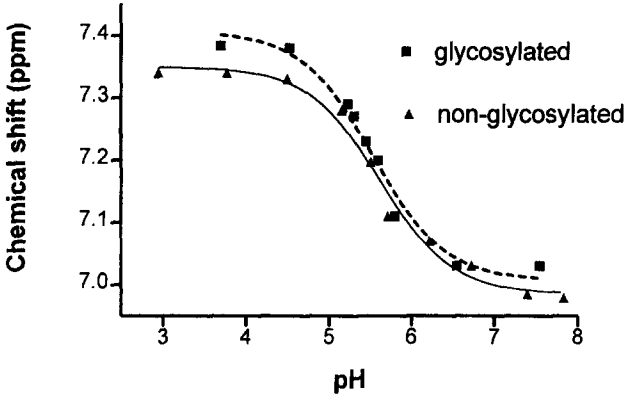

Fig. 10. Chemical shift changes for the H4 proton of His13 in drosocin and its nonglycosylated derivative as a function of pH, shown to illustrate the principles of pK_a determination using NMR. Fitting the curves to the Henderson–Hassellbach equation yields pK_a values of 5.5 and 5.6 for the glycosylated and nonglycosylated derivatives respectively. (Reproduced from McManus *et al.*[61] with permission. Copyright (1999) American Chemical Society.)

consideration and focused efforts to explain differences in bioactivity onto other factors.

Tautomerization is a relatively common feature of drug molecules that is equally amenable to simple analysis using chemical shifts or coupling constants as probes. This was recently demonstrated in a study of some nonpeptide endothelin analogues.[45]

Starting from the modestly active compound **1** (Table 2), derived by screening a compound library for ET_A antagonists, the nanomolar inhibitor **2**

Table 2. Substitution pattern and receptor binding affinity of nonpeptidic endothelin antagonists[a]

Compound	R^1	R^2	IC_{50} (nmol l^{-1})	
			ET_A	ET_B
(**1**) PD012527	Cl	H	430	27000
(**2**) PD155080	OCH_3	H	>0.4	4550
(**3**) PD156707	OCH_3	3,4,5-OCH_3	0.3	780
(**4**)	OCH_3	3,5-OCH_3-4-$O(CH_2)_3SO_3Na$	0.38	1600

[a] from refs 45, 62.

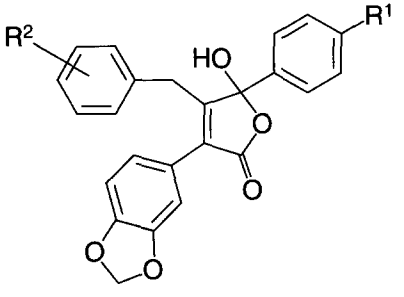

was developed. Further optimization via examination of electronic and structural requirements led to the subnanomolar inhibitor **3**, which was subsequently put forward for evaluation in a number of preclinical disease models for stroke.

These molecules display keto–enol tautomerization as illustrated in Fig. 11. The open-form keto-acid salts and the closed-form butenolides exist in a pH-dependent equilibrium in solution, and at physiological pH both forms exists. In principle, the biological activity could reside in either or both forms.

The extent of tautomerization was established by evaluation of NMR spectra as a function of pH (from 2.65 to 9.05).[45] At acidic pH, compound **2** exists essentially completely in the closed butenolide form. As the pH is slowly raised by addition of NaOD, the spectrum begins to exhibit properties

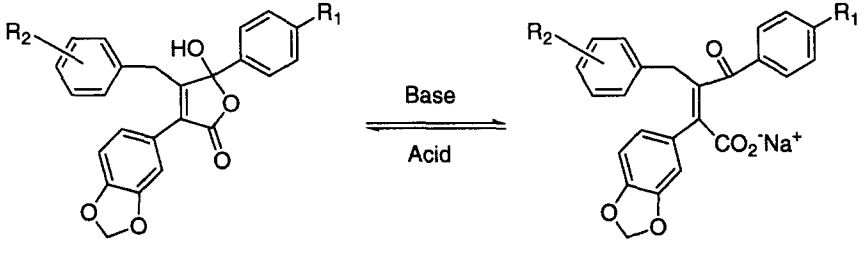

Fig. 11. Tautomeric equilibrium in butenolide-based endothelin antagonists.

associated with the open-form keto-acid, and at basic pH the compound is essentially all in the open form. The coupling pattern shown by the benzylic protons is a particular characteristic marker of the tautomeric process. At acidic pH, the benzylic protons exhibit an AB quartet pattern consistent with the ring-closed structure. As the pH is raised, this pattern coalesces to a singlet, broad at neutral pH and sharp at basic pH as would be expected with the open form keto-acid structure. After the pH was basic, addition of DCl to acidify the solution caused the spectrum to return to its original appearance, consistent with a reversible tautomerization process. Identical biological results were obtained with the salt and parent in all pharmacological assays, reflecting equilibration at physiological pH, thus making it difficult to identify the biologically active form.

Methylation of the OH group in compounds **1**–**3** results in a loss of activity. As these analogues cannot tautomerize to form open keto-acids, it seems likely that the open form is responsible for activity, although the other possibility (i.e. that the closed form is active and that there may be hydrogen-bonding interactions with the OH that are lost on methylation) also needs to be considered.

In addition to its impact on the biologically active form, the tautomeric process has profound implications for formulation of drug candidates, as illustrated in some recent further development work on compound **3**.[62] While it is easy to synthesize and isolate water-soluble salts of the keto-acids, once they are placed in aqueous solution the tautomeric equilibrium determines how much of each form is present. Indeed, if the closed butenolide tautomer is sufficiently water insoluble, it can precipitate out of solution and the equilibrium can drive the complete precipitation of the compound. While **3** has good oral activity, its intravenous use is limited by the insolubility of the closed-form butenolide tautomer without the use of a specific and complex buffered formulation. Thus, in recent work Patt *et al.*[62] developed a series of water-soluble butenolides to overcome this limitation for parenteral uses. This culminated in the development of **4** (Table 2), currently in preclinical evaluation.

This description of the development of **4** provides a good illustration of the fact that the availability of an active molecule is not the end of the drug development pathway, and that formulation considerations can be critical. In this case NMR played a significant role in understanding tautomeric processes that had a direct bearing on solubility and hence on formulation.

3.2.3. Ligand dynamics – Lineshape and relaxation data

Although solution dynamics of drug molecules is not generally the most critical factor to consider in drug design, dynamics certainly does have the potential to affect binding via entropic contributions to the free energy of binding. In general, the more flexible a ligand is, the more unfavourable will be the loss in entropy on binding, assuming a relatively rigid bound state of the ligand. However, in some cases flexibility of a ligand may be a positive factor. This

applies, for example, if a degree of flexibility is required to allow a ligand access to a buried active site, or if activation of a receptor requires a conformational change mediated by ligand binding. Therefore, a knowledge of the flexibility of lead molecules is an important supplement to the structural and electronic information available from NMR.

The two major NMR methods for obtaining information on ligand flexibility are lineshape analysis and relaxation measurements (usually ^{13}C or ^{15}N T_1, T_2 or heteronuclear NOE measurements). In general terms, the former is sensitive to motions on the milli- to microsecond time scale and the latter to nanosecond time scales. To some extent, structure calculations on peptide-based lead molecules can also give an indication of regions of flexibility from an examination of local regions of disorder among a family of calculated structures. Caution must be exercised in making the connection between disorder and flexibility as other factors can contribute to disorder, but in many cases the correlation is observed. A recent example concerns the solution structure of three isomers of the α-conotoxin GI[63] described in Section 4.1. In that case attempts to increase structural diversity via the engineering of non-native disulfide bonds showed that non-native isomers were not only different in conformation but were considerably more flexible than the native isomer.

In an example that illustrates the application of NMR relaxation measurements for studying ligand flexibility, Kessler and colleagues[64] investigated the role of disulfide bonds in the α-amylase inhibitor, tendamistat. This small protein contains two disulfide bonds, Cys11–Cys27 and Cys45–Cys73, and opening of the latter is known to reduce the melting temperature of the protein, i.e. To reduce its stability, but not to affect its α-amylase inhibitor function. The latter observation suggests that this disulfide bond may not affect either the structure or the dynamics of the molecule. To investigate this, perhaps surprising, possibility, heteronuclear NOE measurements were used to determine the effect of the selective removal of the single disulfide bond on the dynamics of the molecule. This was done by comparing various NMR parameters for the single disulfide-deficient variant Cys45Ala/Cys73Ala and the wild-type protein. To assess structural changes, chemical shift differences, intrastrand NOE effects and protected amide protons were used to compare the connectivity of the secondary structure elements of variant and wild-type proteins. Removal of the Cys45–Cys73 bond by the Cys45Ala/Cys73Ala mutation was found to have no influence upon the β-barrel structure of tendamistat, apart from very local changes at the mutation sites. Dynamic properties of the wild-type protein were studied by natural-abundance $^{13}C_\alpha$ heteronuclear NOE experiments. ^{15}N isotope labelling was necessary to obtain the relaxation parameters of the variant, because of sample degradation during the long data acquisition time required for ^{13}C measurements.

The relaxation data in Fig. 12 show that the only region of significant internal mobility in either the wild-type or variant protein is at the N-terminus. Note the sign difference for the different heteronuclear X-{^1H} NOEs, with an increased mobility leading to an increase in NOE for ^{13}C and a decrease for ^{15}N

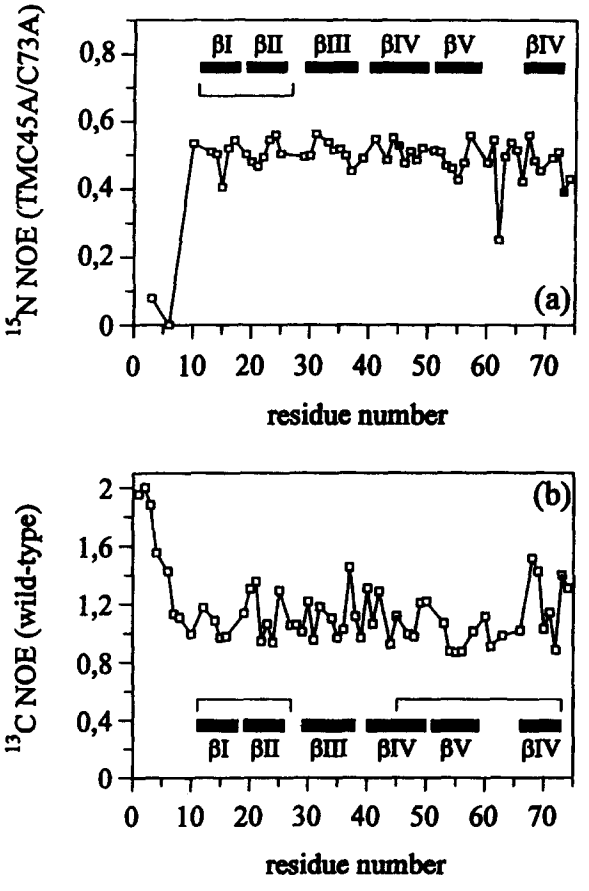

Fig. 12. Heteronuclear NOE factors for (a) ^{15}N backbone nuclei of tendamistat C45A/C73A and (b) $^{13}C_{\alpha}$ nuclei of the wild-type protein. Solid bars indicate the β-strands and solid squares positions 45 and 73 in the variant. Disulfide bridges are marked by thin lines. (Reproduced from Balbach *et al.*[64] with permission. Copyright (1998) Wiley-Liss Inc., a subsidiary of John Wiley & Sons Inc.)

due to the opposite signs of the gyromagnetic ratios of the two nuclei. The NOE measurements show that there is little difference in internal flexibility between the two proteins, consistent with their similar α-amylase inhibitory activity. In this case it appears that the role of the Cys45/Cys73 disulfide bond is more related to thermodynamic stability and the secretion efficiency of the protein rather than to limiting its flexibility.

The thyroid hormones, exemplified by thyroxine, provide another case where NMR relaxation time measurements give an insight into internal flexibility, and perhaps mode of action, of pharmaceutically important molecules. Synthetic thyroxine, **5**, is widely used for the treatment of thyroid disorders, and indeed was the second most widely prescribed drug in the United States in 1998.

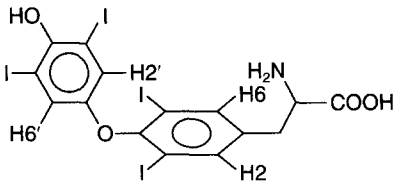

[5] (Thyroxine)

The thyroid hormones act by binding to a nuclear receptor and appear to control receptor function by inducing a conformational change that directs the alignment of secondary structure elements of the receptor critical for function.[65] We have used both relaxation time measurements and dynamic NMR lineshape analysis as tools to define conformational flexibility of the hormones.[66–68] Table 3 shows experimental ^{13}C T_1 and NOE data for thyroxine together with best-fit theoretical values for these parameters based on two different models for the motion of thyroxine in solution. The simple isotropic model in which the drug is regarded as a rigid body tumbling in solution is clearly unable to simultaneously fit the T_1 and NOE data, while the two-state jump model, which incorporates a degree of internal mobility based on rapid flipping between conformational states, is better able to account for the experimental data. Although it is difficult to define precisely the nature of the internal motion, it is clear that rapid (nanosecond) internal motion is present and this appears to involve small-amplitude (±50°) torsions about the aromatic ring axes. The correlation time for overall tumbling of thyroxine was deduced to be approximately 0.35 ns, with the internal motion approximately 30-fold faster.[67]

Previous studies of the ^1H NMR spectrum of thyroxine as a function of temperature had demonstrated the presence of additional larger-amplitude, but slower ring flips also.[69] At low temperature two signals are seen for the H2′ and

Table 3. ^{13}C NMR chemical shift and relaxation data for thyroxine

		Experimental[a]		Theoretical[b]			
				Isotropic motion		Two-state internal motion	
Position	Chemical shift (ppm)	T_1 (s)	NOE	T_1 (s)	NOE	T_1 (s)	NOE
C2′,6′	127.3	0.63	2.53	0.63	2.96	0.63	2.53
C2,6	142.6	0.63	2.63	0.63	2.96	0.63	2.58
Cα	57.1	0.51	2.37	0.51	2.94	0.51	2.57
Cβ	36.4	0.64	2.29	0.64	2.96	0.64	2.51

[a] Measured relaxation data at 75 MHz and 305 K.[67]
[b] Theoretical best-fit values based on the indicated models for molecular motion.

H6′ protons. These signals broaden with increasing temperature, then coalesce and sharpen as the temperature is further increased. This is due to exchange of the environments of the two protons brought about by 180° rotation of the 'outer' ring of thyroxine, possibly combined with concerted motion of the 'inner' ring. Substitution of the observed coalescence temperature (T_c) and the shift difference of the two signals at low temperature ($\delta\nu$) allowed the free energy of activation for this slow ring-flip process to be established from Eq. (1).[68,69]

$$\Delta G^{\neq} = 19.14\ T_c[9.97 + \log(T_c/\delta\nu)] \quad (1)$$

The derived barriers for several thyroid hormones are in the range 36–38 kJ mol^{-1}, which corresponds to large-amplitude ring flips on the milli- to microsecond time scale. From a combination of the relaxation data and the dynamic lineshape analysis data, it was possible to propose a unified model that accounts for both the fast and slow internal motions, as summarized in Fig. 13.

In this model, both aromatic rings of the thyroid hormones jump rapidly between two energetically equivalent conformations on a nanosecond time scale ((a) ↔ (b) and (c) ↔ (d) in Fig. 13). The half-angle of the jump varies between 27° and 55°, depending on the solvent, corresponding to an average displacement of about 90° between the two extreme jump positions. These separate states are not detectable on the chemical shift time scale but lead to an average proximal environment for H_a and an average distal environment for H_b (due to rapid interchange between (a) and (b) in Fig. 13), which are seen in the low-temperature spectra. However, these fast motions are detected by relaxation studies. While the rate of this motion is rapid, its amplitude is not sufficient to average the environment of proximal and distal protons. Occasionally (about once every 1000 jumps), the outer ring jumps farther than the nominal 90° range, exchanging the environments of the proximal and distal protons ((a) ↔ (c) and (b) ↔ (d) in Fig. 13). While the actual rate of an individual ring flip is rapid, the effective rate of the process is on the microsecond time scale because, on average, a large number of small-amplitude jumps occur for every large-amplitude ring flip. It is the exchanging of proximal and distal protons on the microsecond time scale that is detected by the variable-temperature lineshape studies.

The fact that thyroxine is apparently able to move so freely over a moderately large region of conformational space has implications for receptor binding. The crystal structure of the thyroid receptor ligand-binding domain complexed with the thyroid agonist 3, 5-dimethyl-3′-isopropylthyronine[65] shows that the thyroid hormones bind at the centre of the hydrophobic core of the ligand-binding domain and may play a structural role in the conformational changes that activate the receptor. The structures of the retinoid-X receptor ligand-binding domain[70] and the retinoic acid-retinoic acid–receptor ligand-binding domain complex[71] indicate that significant conformational changes accompany ligand

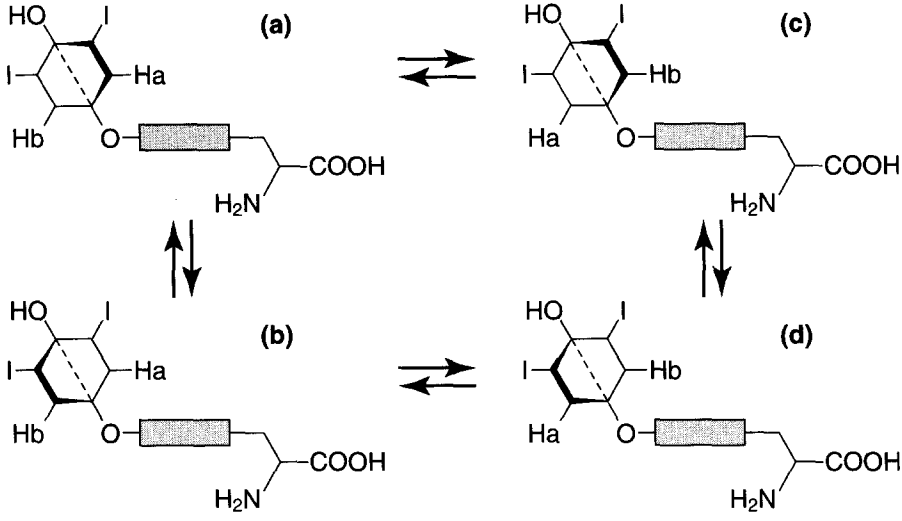

Fig. 13. Schematic illustrations of motions of the outer ring of thyroxine. The dotted line through the outer ring shows the jump axis about which the ring rotates. (a) H_a is shown in the proximal position and is closer to the viewer than H_b owing to the torsion angle ϕ being greater than 0°. This conformation corresponds to one of the two states of the two-state jump model and agrees with the 'twist' of the outer ring observed in the crystal structure. (b) Rotation about the dotted line through the centre of the outer ring moves H_a away from the viewer and brings H_b toward the viewer. This corresponds to the second state of the outer ring in the two-state jump model. (c) H_b is now in the proximal position and closer to the viewer than H_a. (d) H_b is in the proximal position and is now farther from the viewer than H_a. Transition from (a) to (b) and from (c) to (d) involves small-amplitude jumps on the nanosecond time scale and is detected by NMR relaxation measurements. Although not illustrated in the figure, the inner ring also exhibits this type of motion. Transitions (a) to (c) and (b) to (d) result in a 180° flips of the outer ring and exchange of the environments of H_a and H_b. This ring flip occurs on a microsecond time scale and is detected by variable-temperature lineshape studies. (Reproduced from Duggan and Craik[67] with permission. Copyright (1996) American Chemical Society.)

binding. The conformational flexibility shown by the thyroid hormones may also be required for binding. It has been suggested that the rapid 'wiggling' of the aromatic rings could enable the hormone to work its way to the centre of the ligand binding domain as the protein reorders itself about the ligand and may in fact trigger receptor conformational changes.[67]

Another example of the application of lineshape analysis to ligand dynamics is described in Section 4.3 for the drug trimetrexate, which binds to dihydrofolate reductase (DHFR). From that example it is clear that the techniques described above can equally be applied to ligands when bound to their receptors. In some cases significant but highly specific mobility appears to be present at the bound site.

3.2.4. Conformation of bound ligands – Transferred NOEs

In ligand-based drug design it is not necessary to have knowledge of the structure of the receptor, or even of the location of the binding site, but the conformation of the ligand bound to the receptor is crucial. It is clearly better if this can be measured directly rather then be inferred from the conformation of the free ligand. In certain circumstances this information on the bound conformation can be obtained from the transferred NOE (TrNOE) technique.[72,73] This method takes advantage of the fact that NOEs build up more rapidly in a ligand–macromolecule complex than they do in free ligand and, given appropriate exchange conditions for a mixture of ligand and macromolecule (typically satisfied for $K \geqslant 10^{-1}\,\mathrm{l\,mol^{-1}}$ for the equilibrium represented by Eq. (2), signals from a free ligand may be used to determine the bound conformation.

$$L + M \rightleftharpoons L \cdot M \tag{2}$$

The theory of the technique has been reviewed previously[74] and developments that minimize potential artefacts from spin diffusion have been described.[14] Since it is not necessary to monitor signals from the macromolecule in this technique, it is usually present in substoichiometric amounts, thus requiring only minimal amounts of what is usually the more expensive component of ligand–macromolecule complexes. In addition, the molecular weight restrictions inherent in full 3D structure determinations of complexes are ameliorated and the conformations of ligands bound to very large macromolecules may be determined. For example, the technique was recently used to determine the structure of an antibiotic bound to the ribosome.[75] A range of other applications including enzyme–substrate, protein–carbohydrate and protein–peptide interactions have recently been summarized.[14]

In addition to its application as a tool for determining bound conformations of ligands, this method has also been used recently as a screening aid for the identification from mixtures of ligands that bind to a protein of interest. This application is addressed in more detail in Section 3.3.

3.2.5. Pharmacophore modelling – Conformations of many ligands

Determination of the conformations of a range of ligands that all act at the same receptor site can provide significantly more information than just a single ligand structure. With a sufficiently broad range of ligands it is often possible to generate a pharmacophore model of the receptor site, deduced on the basis of conserved structural features and conformations of binding ligands. A recent example from our laboratory concerns the ω-conotoxins – small peptide ligands that bond to voltage-sensitive calcium channels and are potential drug leads for conditions including pain and stroke. From structural studies of a range of these ω-conotoxins and from literature data on various mutants with

altered binding affinities, it was possible to determine that only a localized region of the surface of these molecules was involved in receptor binding.[76] This allowed a pharmacophore model of putative receptor binding pockets to be developed.

The advantage of such a pharmacophore model in this case is that smaller, nonpeptide molecules that might have improved stability and bioavailability over their peptidic counterparts can, in principle, be designed. The NMR approach used in such pharmacophore modelling often involves a combination of many of the techniques already described above. Thus, by determining information about structure and electronic properties for a range of different ligands, all acting at the same receptor site, it is often possible to infer information about the binding site even if direct structural studies of this site are not possible. The conotoxins are discussed in more detail in Section 4.1.

3.2.6. 3D studies of protein targets – 2D, 3D and 4D multinuclear NMR

We now move from studies on ligands, in some cases used to infer information about receptors, to direct studies of the receptors themselves. NMR methods of determining the structures of proteins of up to 35 kDa have been reviewed extensively.[77–79] It suffices to say that for smaller proteins ($\leqslant$7 kDa) it is usually possible to determine the structures, mainly using 2D NMR, without the need for isotopic labelling. For proteins in the range 7–14 kDa, ^{15}N labelling and a combination of 2D/3D NMR experiments is usually sufficient, while for larger proteins, $^{13}C/^{15}N$ labelling and 3D or 4D NMR is more or less mandatory. For proteins at the top end of the currently accessible range (25–35 kDa), there are additional advantages associated with partial deuteration of the protein.

A number of recently developed methods offer the potential for improving the quality of NMR structures and for increasing the size of proteins that will be examined. In particular, the use of residual dipolar couplings and of anisotropic contributions to relaxation provide new kinds of restraints that promise to lead to more accurate NMR structures.[78,80] The recently developed TROSY (transverse relaxation optimized spectroscopy) method[81] exploits relaxation phenomena to produce spectra with narrow lines, and promises to significantly expand the size of protein targets that can be examined by NMR from the current limit of ~35 kDa to perhaps ~150 kDa.

Most of the discussion on receptors has focused on proteins. DNA represents another valuable target in drug design. Most studies in which DNA is the target are done using short model oligonucleotides to mimic the binding region of DNA. The regular repeating nature of DNA structures makes this a more successful approach then similar attempts to dissect out binding regions of receptor proteins, when often the whole protein must be present to maintain a viable binding site. The principles involved in structure determination of nucleic acid targets are similar to those for proteins, but in practice nucleic acid structures are somewhat more difficult to solve.

In general, most of the macromolecular structures solved to date by NMR have been <25 kDa in size. While this is smaller than that achievable by x-ray methods, the quality of NMR structures is generally similar to that obtained by x-ray methods. For either NMR or x-ray methods, however, the structural data merely provides the background information with which a receptor-based drug design programme may begin. As already mentioned, the *de novo* design of ligands based on a receptor structure is a very difficult task but one that is likely to become more common in the future as computer-based approaches to molecular design improve.[44]

3.2.7. Dynamics of proteins

Proteins exhibit a range of internal motions from the millisecond to the nanosecond time scale and a full understanding of how small drugs might interact with such a 'moving target' requires more than just the time-averaged macromolecular structure. Thus, over recent years much effort has been directed towards defining motions within proteins.

The most commonly applied approach has been to use ^{13}C or ^{15}N relaxation parameters such as T_1, T_2 and the heteronuclear NOE to derive correlation times for overall motion, together with rates and amplitudes of internal motions.[82] While the precise interpretation of the NMR relaxation data in terms of motional parameters remains dependent on the appropriateness of the motional model chosen, the results from many studies on the dynamics of proteins are sufficiently clear to confirm that nanosecond time scale motions in proteins are common. Although the existence of such motion is beyond doubt, it is probably fair to say that the results of dynamics studies published to date have, in general, been more reassuring than informative; that is, in most cases extra internal motions are associated with protein termini or in loops, a conclusion that could probably have been deduced from inspection of structures alone. The functional significance of motions on the nanosecond time scale remains unclear and so far there have been few cases where significant differences in motions on this time scale between ligand-free and ligand-bound forms of proteins have been measured. It will be interesting to assess the functional significance of such motions as more data become available. Slower motions have, however, been correlated with function in a number of proteins, with a good example being HIV protease, described in more detail in Section 4.2.

As mentioned earlier, regions of disorder in the spatial ensemble of calculated NMR structures can, in principle, be due to internal motions but can also reflect a relative lack of NOEs in such regions. A recent analysis[83] suggests that ill-defined regions in structural ensembles often do reflect slow, large-amplitude motions, and so it is not always necessary to resort to relaxation time measurements if only a general idea of molecular motions is required for a particular protein. Even if relaxation measurements are done, it is often not necessary to undertake and extensive analysis to derive correlation

times, as trends are often apparent from the raw experimental data. For example, in the case of tendamistat described above (Fig. 12), it is clear directly from the heteronuclear NOE data that significant internal mobility is present at the N-terminus.

3.2.8. Membrane bound receptors

The majority of targets for currently known drugs are membrane-bound receptors, yet this represents the class of proteins for which we know least about structures. Membrane proteins are notoriously difficult to characterize at a structural level because they are difficult to crystallize, thus inhibiting x-ray crystallographic studies, and are both too large and too difficult to reconstitute in suitable media for NMR studies. Nevertheless, solid-state NMR methods are beginning to show great promise that eventually such targets may be structurally characterized.[84] A recent review[13] summarized, for example, the significant advances that have been made using rotational resonance solid-state NMR measurements to determine precise distances in membrane-bound proteins.

3.2.9. Stoichiometry of complex/kinetics of binding

The information sought and techniques described so far have related either to the ligand or to the macromolecule. In this and the following sections, we focus on complexes between the two. One of the most basic pieces of information about any complex is its stoichiometry. In many cases the stoichiometry of a drug–receptor complex is 1 : 1, but variations in either direction are possible: for example, many cytokine ligands involve dimerization of receptors, while some receptors have multiple binding sites for ligands. While stoichiometry is often best determined from other biophysical or binding studies, NMR does provide ways of determining this information if required. This is most often done by monitoring the appearance of signals in a titration of ligand versus macromolecule. The NMR techniques used in such studies have been reviewed previously in *Annual Reports*[74] in an article focusing on macromolecule–ligand interactions.

The kinetics of binding events play a crucial role in determining the appearance of NMR spectra of such ligand–macromolecule mixtures, and in particular the conditions of fast exchange or slow exchange are crucial in determining the types of spectra encountered. In the slow-exchange limit, separate signals for free and bound species are observed during the titration. This applies for tight-binding complexes and is the situation in which the most useful information can be extracted from NMR spectra. Since separate signals for the bound state of the ligand and/or macromolecule can be observed, much useful information on the nature of the bound state can be derived. In the case of fast exchange, corresponding to weaker complexes, only an average signal

corresponding to the weighted average of bound and free states is observed. In this case chemical shifts and other NMR parameters vary with the mole ratio of ligand to macromolecule. While direct information on the complex is more difficult to obtain in this case, analysis of the chemical shift titration and linewidth trends allows information on stoichiometry and kinetics to be obtained.[74] Analysis of 2D HSQC (heteronuclear single-quantum coherence) spectra of weakly binding complexes also allows binding sites to be localized and has formed the basis for a new lead discovery technique referred to as SAR by NMR. This is described in more detail in Section 3.3.

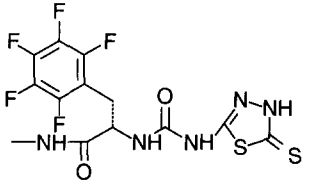

[6] (PNU-142373)

An example of a slow-exchange situation may be seen for the binding of the inhibitor PNU-142373, **6**, to the enzyme stromelysin. The ^{19}F spectrum in Fig. 14 illustrates several general principles. First, note that the use of a rare probe nucleus such as ^{19}F produces spectra of elegant simplicity. As there is no naturally occurring ^{19}F in the macromolecule, there are no interfering signals from it. Second, the offset in chemical shift between bound and free signals reflects the different environment of the bound and free states. Third, signals from bound ligand are broader than those from free ligand owing to the higher molecular weight of the complex. This is best illustrated by the free and bound signals from the *para* fluorine of **6**. The bound signals from the *ortho* fluorines

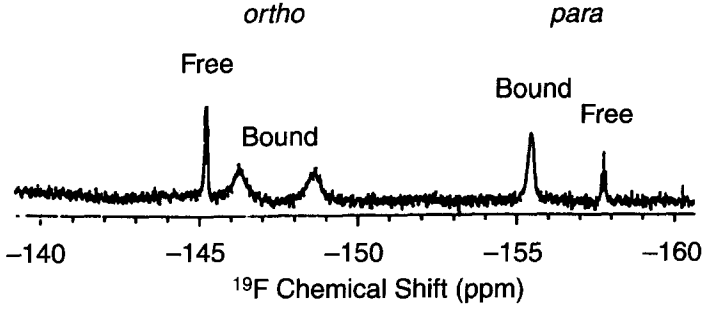

Fig. 14. Region of the 1D^{19}F NMR spectrum of the stromelysin/PNU-142372 complex. Signals from the free (sharp) and bound (broad) PNU-142372 (structure **6**) are observed. (Reproduced from Stockman[2] with permission.)

are broader still, and are separated from one another in the bound state but degenerate in the free ligand. The additional broadening reflects the fact that the fluorinated aromatic ring, while held sufficiently rigidly in the complex to yield separate environments on different sides of the ring, is still undergoing a degree of flipping, which manifests itself as exchange broadening of the two *ortho* signals. A ring-flip rate of 100 s^{-1} was estimated from the difference in linewidth for the bound *para* and *ortho* signals.[85]

3.2.10. Location of interacting sites

Once the stoichiometry and kinetics of binding have been established, the next piece of useful information in defining a complex is an indication of which parts of the ligand interact with which parts of the macromolecule. Simple HSQC-type experiments or isotope editing/filtering methods are often used for such studies.[86–88] In these experiments, either the ligand or the macromolecule is labelled with ^{15}N and/or ^{13}C. Titration with the unlabelled interacting species perturbs the spectrum of the labelled species (either by causing chemical shift changes if the complex is in fast exchange, or resulting in the addition of new signals from bound species if the complex is in slow exchange). Since the interaction between ligand and macromolecule usually involves only one face of a ligand and one small region of the macromolecule, much of the spectrum of each remains unperturbed. The perturbed regions are those involved in the interaction, and if assignments have been made then information about the interacting sites can readily be obtained from such studies.

3.2.11. Orientation of bound ligands

If some information on the location of the binding site is available from either NMR or other techniques, then the next level of information about the complex that can be useful in drug design is the orientation of the ligand at the binding site. In the absence of a full structure determination of the complex, it is sometimes possible to gain information on orientation from NOE docking experiments. The concept here is that a small number of NOEs between ligand and macromolecule that can be unambiguously identified may be valuable in orienting the ligand. Often such studies are contemplated when the structure of the macromolecule itself, or of a closely related macromolecule, is already known and information on the environment and conformation of a ligand is desired without the need for resorting to time-consuming full structure calculations on the complex.

Gradwell and Feeney[89] have analysed factors important in such NOE docking experiments. In their analysis, a high-resolution x-ray structure of a protein-ligand complex was used to simulate loose distance restraints of varying degrees of quality that might typically be estimated from experimental NOE intensities. These simulated data were used to examine the effect of the

number, distribution and representation of the experimental constraints on the precision and accuracy of the calculated structures. A standard simulated annealing protocol was used, as well as a more novel method based on rigid-body dynamics. The results showed some parallels with those from similar studies on complete protein NMR structure determinations, but it was found that more constraints per torsion angle were required to define docked structures of similar quality. This is because the conformation and orientation of the ligand are only defined by NOEs and not by covalent attachment as is the case for amino acid side-chains in a protein structure. The effectiveness of different NOE-constraint averaging methods was explored and the benefits of using 'R^{-6} averaging' rather than 'centre averaging' with small sets of NOE constraints were demonstrated. With these consideration in mind, it appears that NOE docking can be a very cost-efficient procedure for defining the environment, orientation and conformation of ligands.

3.2.12. Structures/dynamics of macromolecule–ligand complexes

The techniques used to determine the structures of macromolecule–ligand complexes are similar to those used to determine the structure of uncomplexed macromolecules. While there are some disadvantages relative to determining structures of the uncomplexed macromolecule, including the higher molecular weight of the complex, and complications associated with exchange, the fact that two species are involved can be used to advantage. For example, by selectively labelling either the ligand or the macromolecule and using various isotope editing/filtering techniques,[90,91] it is possible to simplify the spectra of the complex by viewing only one component at a time.

We will defer describing an example of an NMR determination of a macromolecule–ligand complex until Section 4.3, as part of a more general overview of DHFR–ligand complexes, but it suffices to say that there are now many examples in the literature of macromolecule–ligand complexes and some of these have recently been reviewed.[2]

Similarly, the techniques already described for determining the dynamics of ligands or macromolecules are also directly applicable to complexes. Again, specific examples are given in Section 4, including the use of relaxation data to study dynamics in HIV protease/inhibitor complexes and the use of dynamic lineshape studies for studying correlated ligand–protein dynamics in DHFR complexes.

3.2.13. Overview of structure-based design

From the preceding discussion it can be seen that NMR can provide a vast range of information on ligands, macromolecules and their complexes. However, within the pharmaceutical industry the value of a particular piece of information must be assessed against the cost of obtaining it. As might be

Table 4. Resource requirements for NMR technologies in structure-based design

Information	Ligand-based design			Receptor-based design		
	Ligand conformation	Pharmocophore model	Bound ligand conformation	Binding site/ orientation	3D structures	Dynamics
NMR method	1D/2D of multiple ligands		TrNOE	NOE-docking	NOE-restrained simulated annealing	Relaxation time measurements/line shape analysis
Ligand (mg)	1	12	1	1	1	1
Protein (mg)	0	0	1	10	>10	>10
Spectrometer time (days)	0.5	$n \times 0.5^a$	1	2	4	10
Approximate cost	\$500	n\$500	\$1500	\$1500	\$2000–5000	\$10 000

[a] n is the number of ligands studied to develop the pharmacophore model.

expected, the information that is easiest to obtain usually corresponds to that which is least expensive, in terms of materials costs, personnel and spectrometer time. Table 4 summarizes resource requirements for various NMR techniques. It is stressed that the cost and time estimates are highly variable and the figures are presented as rough guidelines only. For example, in cases where expression of a particular protein may be difficult, or where a protein is unstable and multiple samples are required, the costs could be significantly greater. However, the general trend apparent from the table is that the closer one gets to a full characterization of a complex, the more expensive in both materials costs and spectrometer time the task becomes.

3.3. Screening

As is clear from the previous section, many of the applications of NMR in the drug discovery process have involved obtaining structural information on drug targets or complexes of drug and target. More recently, it has been shown that NMR may be used to discover compounds that bind to protein targets. This represents a shift away from the more traditional use of NMR as a tool for structure characterization and towards a screening role in the generation of lead compounds for drug discovery. The general strategy used in the screening process is to monitor NMR signals in order to identify small molecules that bind weakly to a target protein. This binding information may then be used to design tighter-binding compounds, which serve as drug leads.

The methods that have been developed may be classified into two categories: those that monitor NMR signals from the protein target,[12] and those that monitor NMR signals from the small-molecule ligand.[11] The strategy for monitoring protein signals, which was first described by the group of Fesik at Abbott Laboratories, is widely referred to as SAR by NMR and is described in the following section. This is followed by a discussion of several screening strategies that involve monitoring ligand signals.

3.3.1. SAR by NMR

In this approach to drug discovery, ^{15}N HSQC spectra of a target protein are recorded before and after addition of pools of small molecules. If one of the ligands within the pool binds to the protein, perturbations to the HSQC spectrum are observed. The location of the binding site may be deduced by noting which signals are specifically perturbed, as illustrated in Fig. 15. The affinity of ligands discovered in this way is often rather modest (in the millimolar range), but after optimization by synthesis and screening of analogues of the initial hit, improvement to micromolar affinity may readily be achieved. A second, unrelated ligand that binds at an adjacent site is then identified and optimized in a similar way. A closer analysis of the ternary complex formed by

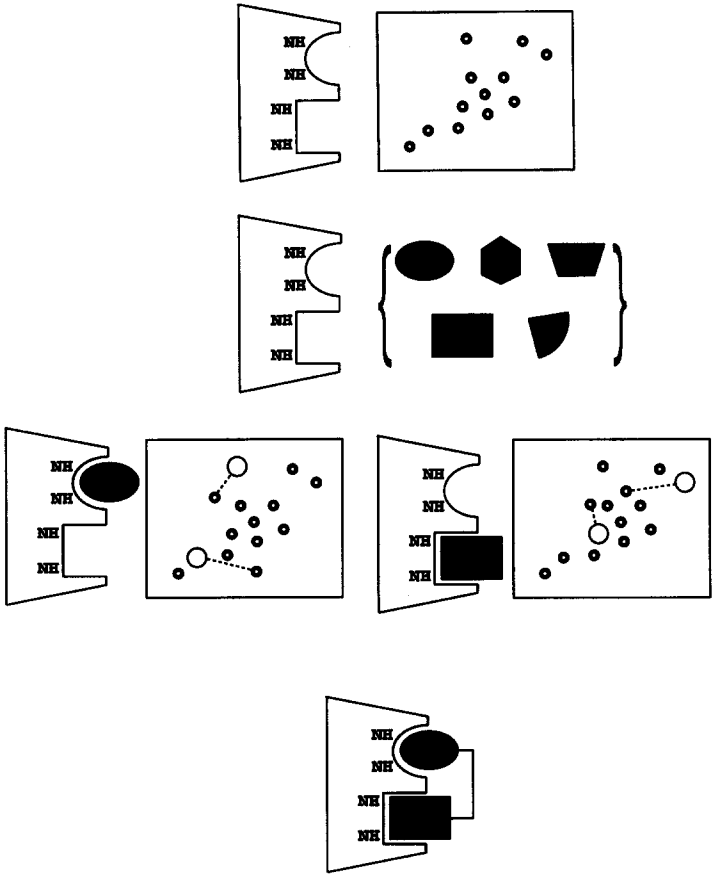

Fig. 15. Schematic illustration of the design of SAR by NMR. The HSQC spectra yield a single peak for each backbone amide proton in the target protein. Ligands that bind to the protein perturb the chemical shifts of localized regions of the protein, thus identifying the binding site. When two proximate binding ligands are identified, they are chemically linked to produce a tight-binding lead molecule.

the two ligands is then used to identity sites at which the two ligands might be joined. Synthesis of new bifunctional ligands using a library of linkers is then used to identify a compound with high affinity for the target protein.

The use of pools of ligands in the initial screens and the high sensitivity of HSQC spectra allow large numbers of small molecules (~1000/day) to be screened. The method is very cost-efficient, and only small numbers of linked molecules need be synthesized because selection of linkers can be made on the basis of structural information about the complexes. In the first exemplification of the technique, a molecule that binds tightly (K_d = 19 nmol l^{-1}) to the FK506 binding protein was discovered by linking two quite weakly binding molecules

(K_d = 2 μmol l^{-1} and 100 μmol l^{-1}), as illustrated in Fig. 16. The technique has since been used to successfully produce novel high-affinity ligands for a range of other important drug targets including stromelysin[92] and human papillomavirus E2 protein.[93] It appears that this method will become widely used within the pharmaceutical industry and many examples of its application are anticipated.

3.3.2. Monitoring of ligand signals

Several alternative strategies have been described for the screening of small molecules binding to a target protein. These techniques all involve the measurement of NMR parameters that exhibit marked dependence on the molecular mass, including transferred NOEs, line broadening and diffusion measurements. There are certain advantages to the observation of ligand rather than protein signals. First, it is possible to identify easily all of the signals from a mixture of several small components simultaneously. Therefore, identification of the binding component(s) is straightforward. Second, observation of ligand signals removes the need for isotope labelling and allows for the screening of targets that cannot be assigned by current NMR methods and are therefore not amenable to SAR by NMR.

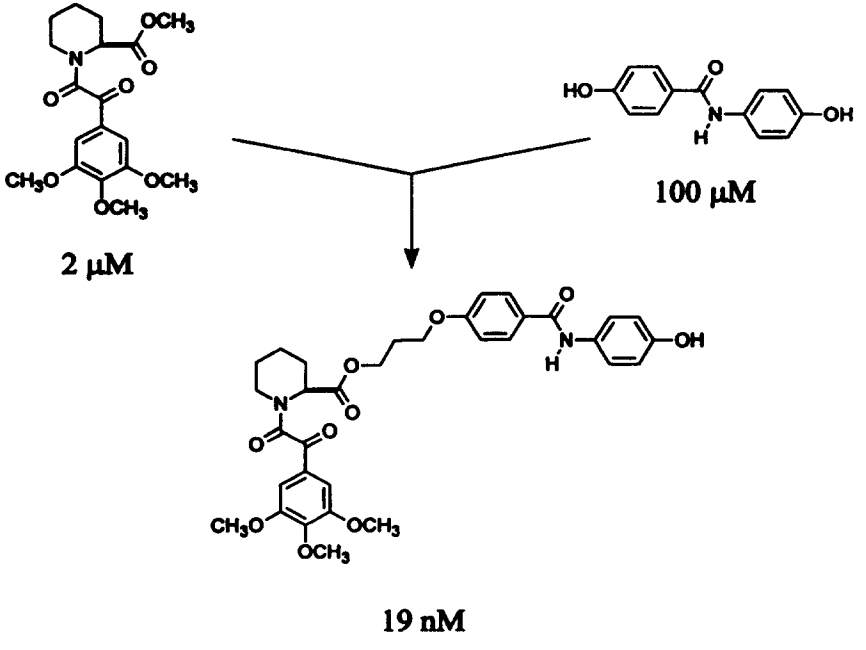

Fig. 16. Development of a nanomolar inhibitor for FK506 binding protein from two micromolar inhibitors using SAR by NMR. (Reproduced from Stockman[2] with permission.)

(i) Transferred NOEs in screening. As noted in Section 3.2 the transferred NOE technique has been widely used to determine the bound conformation of ligands that are in fast exchange on the relaxation time scale. The theory of this technique has been described previously[72,73] and pharmaceutical applications have been reviewed.[1] The method makes use of the fact that when a small ligand binds to a large target molecule, the sign and build-up rate of the NOEs are changed. Although this method has most often been used to derive information about the bound conformation of a single ligand, it is ideally suited to the task of screening, as it provides a sensitive and reliable indication of binding.

The application of TRNOE to identification of a binding component from a mixture, which has been termed 'bioaffinity NMR spectroscopy', was demonstrated by Meyer *et al.*,[10] who identified a single component in a mixture of oligosaccharides that bound to *Aleuria aurantia* agglutinin. Libraries consisting of 6 and 15 polysaccharides, respectively, were screened and in each case a single binding component was identified. More recently, the same technique has been used to identify an antagonist of E-selectin from a mixture of polysaccharides.[94] In this case a single binding component was identified from a mixture of 11 components. One of the strengths of this approach is highlighted in this study, where the E-selectin target had a molecular mass of approximately 220 kDa, which is well beyond the accessible range for HSQC spectroscopy and, therefore, beyond the scope of SAR by NMR.

(ii) Relaxation methods. Like the NOE, the transverse relaxation time (T_2) exhibits a marked dependence on molecular mass and is therefore a suitable parameter for the screening of mixtures. When a small ligand binds to a large protein target, there is a marked reduction in the ligand T_2 value that results in a broadening of the NMR signals. Binding components in a mixture can be identified, as only the NMR signal of the components in the mixture that bind to the macromolecular target are broadened. The extent of broadening is related to the affinity of the ligand and may be measured by comparing spectra of the ligand in the absence and presence of the protein target. Fejzo *et al.*[95] have reported the use of differential line broadening and transferred NOE spectroscopy to study the quaternary complex of the immunosuppressant FK506 with the immunophilin FKBP-12 and a recombinant fragment of the calcineurin receptor. Differential line-broadening effects and transferred NOEs were observed for FK506 in the quaternary complex relative to the binary complex of FK506/FKBP-12. The line broadening results were compared to and found to be consistent with the contacts observed in the x-ray structure of the quaternary complex. This study highlighted the utility of differential line broadening measurements for the identification and characterization of protein–ligand interactions in higher-molecular-weight systems.

The application of relaxation-edited detection of ligand binding to screening mixtures of ligands has been elegantly demonstrated by Hajduk *et al.*,[9] also using FKBP. A mixture of nine compounds was prepared containing

2-phenylimidazole, **7** (Fig. 17), which binds to FKBP with an affinity of 200 μmoll^{-1}, and eight compounds that do not bind. The approach exploits the differences in transverse relaxation times of the free and bound ligand. A suitable CPMG spin lock time is chosen that maximizes the difference between the signals of bound and unbound species. In order to detect ligand binding, several relaxation edited spectra were recorded as shown in Fig. 17.

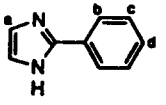

[7]

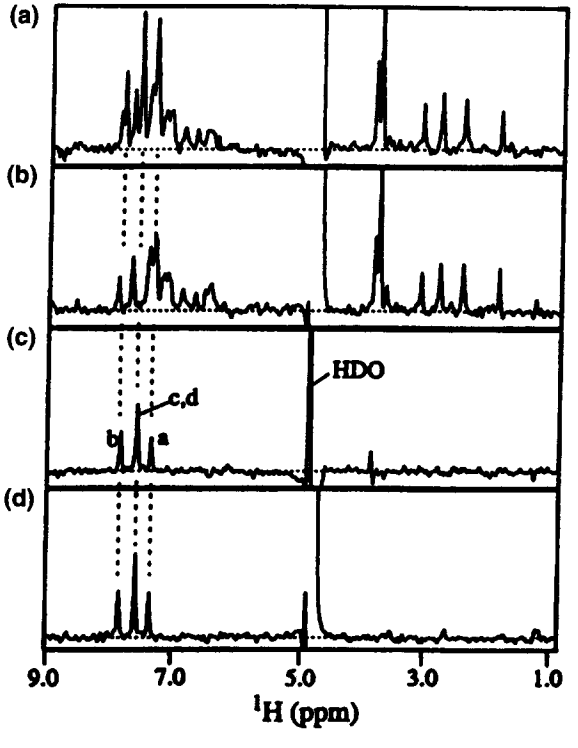

Fig. 17. Analysis of ligand binding to FKBP using the relaxation-edited approach: (a) Relaxation-edited spectrum of a mixture of compounds in the absence of FKBP. (b) Relaxation-edited spectrum of the same mixture in the presence of FKBP after correcting for residual protein signals by subtracting a spectrum of FKBP alone. (c) The difference spectrum obtained by subtracting (b) from (a). (d) A reference spectrum of **7** alone. (Reproduced from Hajduk *et al.*[9] with permission.)

The relaxation-edited approach is applicable to ligands with a wide range of affinities for their target protein. In order to optimize the approach it is necessary to know approximate transverse relaxation rates for the ligands and the macromolecular target. Short spin locking times preferentially detect high-affinity ligands, while longer spin locking times allow the identification of more weakly binding species.

(iii) Diffusion editing. A similar approach has been described that utilizes the difference in diffusion coefficients between a small ligand and a macromolecule–ligand complex. A small molecule diffuses several orders of magnitude faster than a large macromolecule in solution. If a small molecule binds to a macromolecular target, then its diffusion coefficient will be reduced by an amount depending upon the affinity of the small molecule for the target. This technique has been described as 'affinity NMR'. The utility of this approach has been described by Hajduk *et al.*,[9] who have used diffusion editing to identify small molecules that interact with the catalytic domain of the matrix metalloproteinase stromelysin. A mixture of nine compounds was prepared containing 4-cyano-4′-hydroxybiphyenyl, **8** (Fig. 18), and eight compounds that do not bind to the protein. In the presence of acetohydroxamic acid, **8** binds to stromelysin with a dissociation constant of $\sim 20\ \mu mol\,l^{-1}$. The diffusion-based experiments employed a pulsed field gradient stimulated echo (PFG-STE). At low gradient strengths signals are observed for both the protein and the unbound signals, whereas at higher gradient strengths only the protein signals are observed. Difference spectra recorded at low gradient strength in the absence and presence of protein reveal only signals from the compound that binds to stromelysin (Fig. 18).

An extension to this approach has been used by Gonnella *et al.*[96] that uses a combination of diffusion editing and isotope filtering. Spectra were recorded using a $^{15}N/^{13}C$-labelled sample of the catalytic domain from stromelysin with a mixture of two low-molecular-weight compounds, only one of which binds to the protein. A diffusion-edited experiment was recorded at high gradient strength to select for the signals from the protein–ligand complex. Isotope filtering was then used to remove the protein signals, leaving only signals from the bound inhibitor. While this approach has the advantage that it does not rely on obtaining difference spectra, the requirement for labelled protein is likely to limit its utility as a general screening strategy.

(iv) The SHAPES strategy. A combined approach to screening by monitoring the ligand signals to identify components in a mixture that bind to a macromolecular target has recently been described by Moore.[11] The strategy uses line broadening and transferred NOE measurements to identify weakly binding components in a mixture. The library of small molecules in the mixture were selected from the scaffolds or 'shapes' most commonly found in known therapeutics.[97] The strategy is used only as a means of identifying weakly

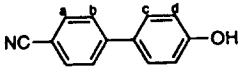

[8]

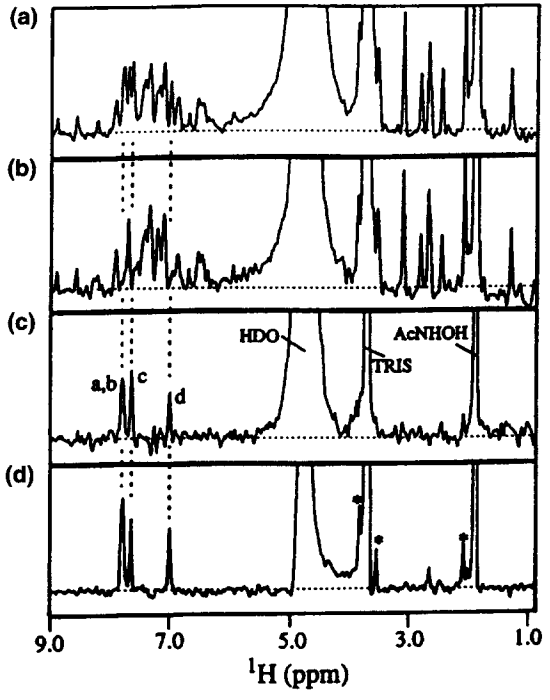

Fig. 18. Analysis of ligand binding to the catalytic domain of stromelysin using the diffusion-edited approach. (a) PFG-STE spectrum of a mixture of compounds in the absence of stromelysin using low gradient strength. (b) PFG-STE spectrum of the same mixture in the presence of stromelysin with the use of low gradient strength, after correcting for residual protein signals by subtracting a PFG-STE spectrum of the same sample recorded with high gradient strength. (c) The difference spectrum obtained by subtracting (b) from (a). (d) A reference spectrum of **8** alone Signals arising from impurities are marked with an asterisk (*). (Reproduced from Hajduk *et al.*[9] with permission. Copyright (1997) American Chemical Society.)

binding lead compounds to guide the subsequent high-throughput screening efforts.

3.3.3. Summary

The preceding discussion highlights several areas in which NMR screening has been applied to the drug discovery process. Although the NMR techniques

utilized in these approaches are not new, the approaches themselves have provided novel methods for the identification of lead compounds. These methods continue to be developed to allow for high-throughput screening of large compound libraries. SAR by NMR appears to be the method of choice, although its application is currently limited to moderately small targets of < 40 kDa. For larger targets, a more suitable approach involves monitoring signals from the ligands. These NMR-based approaches provide simple and robust assays for the discovery of high-affinity ligands for a range of potential targets. It is likely that the availability of these high-throughput NMR-based screening techniques will greatly facilitate the process of drug discovery.

4. SELECTED EXAMPLES

4.1. Conotoxins

In this section we will focus on some of the applications for structure-based drug design undertaken in our laboratory, in particular, making use of small disulfide-rich toxins as initial drug leads. We have been particularly interested in a family of molecules known as the conotoxins, small peptide-based toxins of 13–30 amino acids from cone snails of the genus *Conus*. These molecules are ideal for study by NMR because they are small, they contain multiple disulfide bonds and possess a well-defined three-dimensional structure with good dispersion of signals, and in general they are relatively rigid molecules. Their therapeutic importance arises because they bind specifically to different ion-channels as indicated in Table 5.

Ion channels are regarded as of great importance within the pharmaceutical industry as an important class of pharmaceutical targets. Currently, about 100 ion channels have been identified. Database searching of new genomes is revealing the existence of many more ion channels and it is likely that there are more than 1000 that will ultimately be identified. Consequently, ligands that target these channels selectively are important, both for deducing the physiological roles of different subtypes of ion channel and in determining structural requirements for selective modulation of the channel activity.

The conotoxins are divided into several classes depending on their biological activity and the number of cystine residues and their connections within the sequence, as shown in Table 5. Classes include the α-conotoxins (which target the nicotinic acetylcholine receptor), μ-conotoxins (which target sodium channels), ω-conotoxins (which target voltage-sensitive calcium channels) and κ-conotoxins (which target potassium channels). In most cases these families, as well as being distinguished on the basis of biological activity, are also distinguished by common structural features. In particular, the Cys residues are highly conserved and the pattern of their spacing in the sequence defines several different frameworks. These are often specified according to the

Table 5. Amino acid sequences of major classes of conotoxins

α-Conotoxins (2-loop framework peptides that inhibit nicotinic acetylcholine receptors)	
GI	ECCN-PACGRHYS--C*
GIA	ECCN-PACGRHYS--CGK*
GII	ECCH-PACGKHFS--C*
MI	GRCCH-PACGKNYS-C*
SI	ICCN-PACGPKYS--C*
SIA	YCCH-PACGKNFD--C*
SII	GCCCNOACGPBYG--CGTSCS
PnIA	GCCSLPPCAANNPDYC*
PnIB	GCCSLPPCALSNPDYC*
ImI	GCCSDPRCAWR----C*
EI	RDOCCYHPTCNMSNPQIC*
MII	GCCSNPVCHLEHSNLC*
EpI	GCCSDPRCNMNNPDY(SO4)C*
AuIB	GCCSYPPCFATNPD-C
μ-Conotoxins (3-loop framework that block sodium channels)	
GIIIA	RDCCTOOKKCKDRQCKOQRCCA*
GIIIB	RDCCTOORKCKDRRCKOMKCCA*
GIIIC	RDCCTOOKKCKDRRCKOLKCCA*
PIIIA	RLCCGFOKSCRSRQCKOHRCC*
ω-Conotoxins (4-loop framework peptides that block calcium channels)	
GVIA	CKSOGSSCSOTSYNCC-RSCNOYTKRCY
GVIB	CKSOGSSCSOTSYNCC-RSCNOYTKRCYG*
GVIC	CKSOGSSCSOTSYNCC-RSCNOYTKRC*
SVIA	CRSSGSOCGVTSI-CCGR-C--YRGKCT*
SVIB	CKLKGQSCRKTSYDCCSGSCGRS-GKC*
GVIIA	CKSOGTOCSRGMRDCC--SCLLYSNKCRRY*
GVIIB	CKSOGTOCSRGMRDCCT-SCLSYSNKCRRY*
MVIIA	CKGKGAKCSRLMYDCCTGSCRS--GKC*
MVIIB	CKGKGASCHRTSYDCCTGSCNR--GKC*
MVIIC	CKGKGAPCRKTMYDCCSGSCGRR-GKC*
MVIID	CQGRGASCRKTMYNCCSGSCNR--GRC*
TVIA	CLSOGSSCSOTSYNCC-RSCNOYSRKCY*
δ-Conotoxins (4 loop framework peptides that delay inactivation of sodium channels)	
TxVIA	WCKQSGEMCNLLDQNCCDGY-CIVLVCT
TxVIB	WCKQSGEMCNLLDQNCCDGY-CIVFVCT
GmVIA	VKPCRKEGQLCDPIFQNCCRGWNC-VLFCV
NgVIA	SKCFSOGTFCGIKOGLCCSVR-CFSLFCISFE
PVIA	EACYAPGTFCGIKOGLCCSEF-CLPGVCFG*
κ-Conotoxins (4 loop framework peptides that block potassium channels)	
PVIIA	CRIONQKCFQHLDDCCRKKCNNRFNKCV
Other (4 loop framework peptides that block sodium channels	
GS	ACSGRGSRCOOQCCMGLRCGRGNPQKCIGAHZDV

Amino acid sequences shown with cysteines (**bold**) aligned within each structural framework.
*Processed carboxyl terminal. O = hydroxyproline residue. Z = γ-carboxyglutamic acid residue.

number of loops in the peptide backbone between Cys residues, as indicated in Fig. 19. The structures of a large number of conotoxins have been determined by NMR over the last few years and the findings are now illustrated with selected examples from these different frameworks.

4.1.1. α-Conotoxins

The α-conotoxins target the nicotinic acetylcholine receptor (nAChR), which is responsible for a wide range of physiological functions as well being implicated in neuronal growth and development. They are valuable ligands for probing structure–function relationships of various nAChR subtypes as they are potent antagonists and exhibit marked selectivity between the peripheral and neuronal forms of the receptor. Typically, the α-conotoxins are 12–19 residues in length and are characterized by two conserved disulfide bonds and two loops in the peptide backbone between the cysteines (Fig. 19). The number of amino acids in these two intracysteine loops varies, giving rise to the α3/5, α4/3, α4/6 and α4/7 subclasses of α-conotoxins. Although we have determined structures from all of these subclasses,[63,98–101] we will focus here on two examples: ImI, a member of the α-conotoxin family with selectivity for neuronal nAChRs,[102] and the muscle-specific α-conotoxin GI, which was the first and one of the smallest α-conotoxins to be discovered.

α-Conotoxin ImI is derived from the venom of the vermivorous snail *Conus imperialis* and is the first peptide ligand that binds selectively to the neuronal α_7 homopentameric subtype of the nAChR. This receptor has emerged as an important target in several disease states and the potential therapeutic value of a highly specific agonist is evident from findings that high doses of nicotine are beneficial to sufferers from cognitive and attention deficits, Parkinson's disease, Tourette's syndrome, ulcerative colitis and schizophrenia. However,

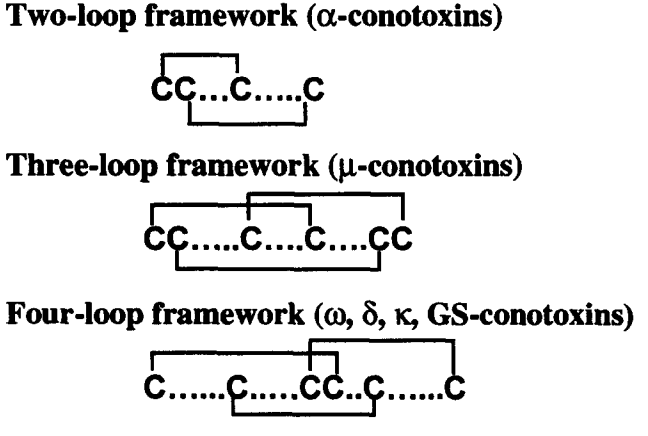

Fig. 19. Cys spacing of common conotoxin frameworks.

side-effects arising from high doses of nicotine are often more detrimental than the disease state, and alternative specific ligands are of much interest. Mutational analyses[103] have identified four residues (Asp5, Pro6, Arg6, and Trp10) in ImI that are crucial for activity. Recent structural studies[99,104–106] show that the functional residues are clustered on one face of the molecule, providing clues as to possible binding modes of this valuable lead molecule, as shown in Fig. 20.

To further probe the structural requirements for activity within the α-conotoxin family, a series of non-natural disulfide bond mutants of conotoxin GI was recently examined.[63] The interest in GI is focused on its use as a model to explore conformational diversity resulting from disulfide bond engineering. As already noted, conotoxins are characterized by their particularly high content of cysteine, with the cysteine residues almost invariably connected in pairs to form disulfide bonds. In peptide toxins, even more than in larger proteins, these disulfide bonds have a crucial bearing on three-dimensional structure and function. As the number of cysteine residues in a peptide increases, the number of ways of connecting them in disulfide bonds increases dramatically, leading to a large number of potential isomers. It is interesting and significant that invariably only one of the possible isomers occurs naturally – venoms do not normally contain different isomers of the same conotoxin with different connections of the disulfide bonds. However, using solid-phase chemical methods it is possible to selectively produce each of the individual disulfide bond isomers. We have used this approach to synthesize all three possible disulfide bond isomers of the α-conotoxin GI and have determined their structures.[63] The three isomers are referred to as GI(2–7;3–13), GI(2–13;3–7), and GI(2–3;7–13), reflecting the respective disulfide bond connectivities between cysteine residues at positions 2, 3, 7 and 13 in the GI sequence (Fig. 21). The structural findings may be summarized by noting that the native

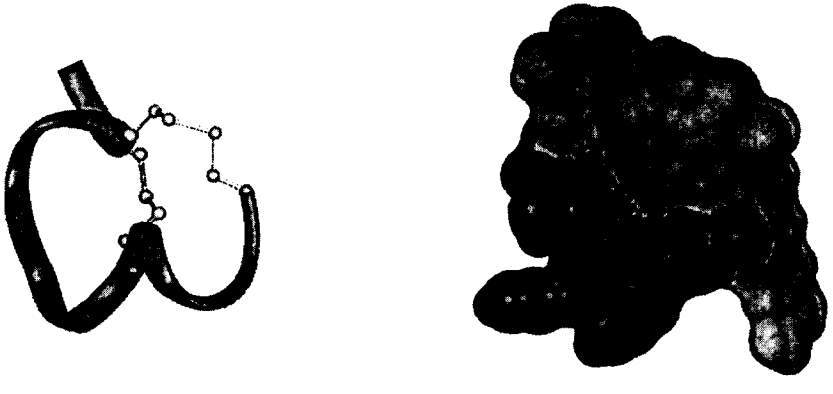

Fig. 20. Ribbon and surface representations of the structure of ImI. Functionally important residues (dark shading) are clustered close together.

connectivity of the four constituent cysteine residues produces a significantly more stable and well-defined structure than either of the two alternative arrangements of the disulfide bonds.[63] A single solution conformation was detected for the native isomer, GI(2–7;3–13), which consists primarily of a distorted 3_{10}-helix from residues 5 to 11. The two non-native forms exhibited multiple conformations in solution, with the major populated forms being quite different in structure both from each other and from the native form. Thus the disulfide bonds in GI play a major role in determining both the structure and stability of the peptide. A trend for increased conformational flexibility was observed in the order GI(2–7; 3–13) < GI(2–13; 3–7) < GI(2–3; 7–13).

Interest in making non-native isomers arises because peptide analogues are widely regarded as valuable drug leads and in recent years there has been much effort directed towards the development of peptide libraries. It has been of particular interest to develop methods to increase the surface variability of peptides because the diversity of peptide libraries is, to some extent, limited by the use of the 20 natural amino acids. The study described above shows that the use of alternative disulfide bond connectivities provides another way of altering molecular conformations without modifying the sequence.

4.1.2. Sodium channel-binding toxins

The α-conotoxins exemplify a case where toxins of similar structure display differences in specificity towards different receptor subtypes. However, there are also situations in which toxins with completely different structures compete for binding at the same ion-channel subtypes, as illustrated by recent structural

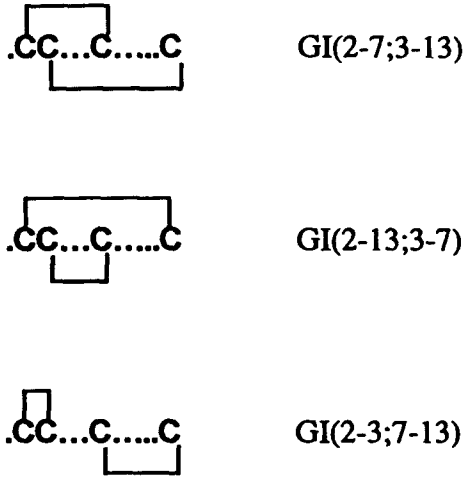

Fig. 21. Disulfide isomers of conotoxin GI.

findings on two sodium channel-binding peptides.[107,108] The piscivorous cone snail *Conus geographus* produces polypeptide neurotoxins that specifically inhibit skeletal muscle and eel electroplax sodium channels. These toxins, the μ-conotoxins and conotoxin GS, are attractive probes of sodium channel structure because of their high binding affinity and ability to discriminate between the skeletal muscle and the neuronal and cardiac channel isoforms.[109,110] It is remarkable that, while these peptides belong to the same pharmacological class, they have different structural frameworks, as illustrated in Fig. 19. The μ-conotoxins, a family of highly basic 22-residue polypeptides (GIIIA, GIIIB and GIIIC), contain six cysteine residues that are paired in a 1–4, 2–5, 3–6 pattern to form three intramolecular disulfide bonds and a three-loop framework. By contrast, conotoxin GS has a strikingly different sequence and is 50% larger than the μ-conotoxins. This polypeptide contains six cysteine residues arranged in a similar 1–4, 2–5, 3–6 pattern; however, differences in the spacings between cysteine residues results in a four-loop framework rather than a three-loop framework. Despite the low sequence identity, conotoxin GS binds competitively with the μ-conotoxins, suggesting overlapping binding sites on the extracellular surface of skeletal muscle and eel electroplax sodium channel.[110]

We recently showed that the three-dimensional structure of GIIIB consists of a distorted 3_{10}-helix, a small β-hairpin, a *cis*-hydroxyproline and several turns.[107] The molecule is stabilized by three disulfide bonds, two of which connect the helix and the β-hairpin, forming a structural core with similarities to the CS$\alpha\beta$ motif.[111] This motif is common to several families of small proteins including scorpion toxins and insect defensins. Other structural features include multiple arginine and lysine side-chains that project into the solvent in a radial orientation relative to the core of the molecule. Conotoxin GS adopts a structure that consists of a compact, disulfide-bonded core from which project several loops and the C-terminus.[108] The main element of secondary structure is a double-stranded antiparallel β-sheet comprising residues 17–20 and 26–29 connected by a turn involving residues 21–25 to give a β-hairpin structure. A further peripheral β-strand involving residues 7–9 is almost perpendicular to the β-hairpin, with Ser7 hydrogen-bonded to the central β-strand forming an isolated β-bridge. The differences between the two types of sodium channel blocking peptide are illustrated in Fig. 22.

The availability of solution structures for several μ-conotoxins and conotoxin GS forms the basis for the design of analogues that may be used to define the binding surface and to undertake complementary mutagenesis on the sodium channel to identify the interacting residues.

4.1.3. ω-Conotoxins

The ω-conotoxins, which bind to voltage-sensitive calcium channel, are perhaps the most extensively studied members of the conotoxin family and comprise a six-cysteine/four-loop framework. They are exemplified in Fig. 23 by our

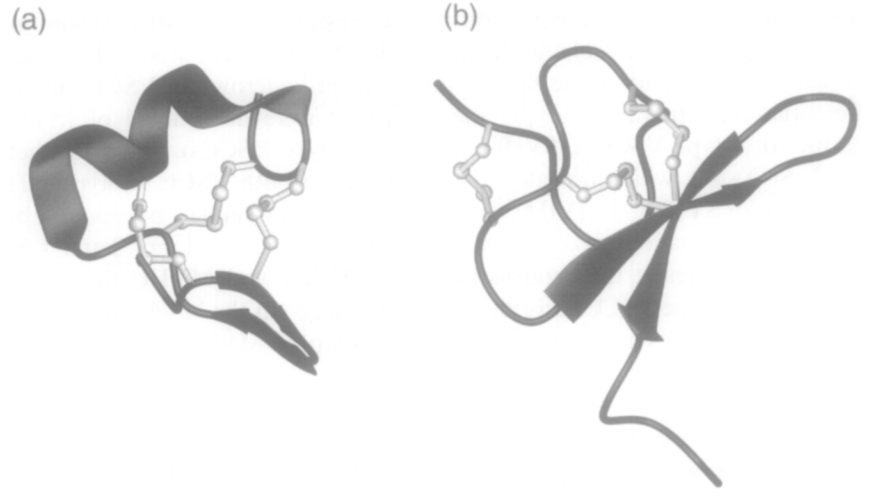

Fig. 22. Ribbon diagrams of the structures of (a) conotoxin μ-GIIIB and (b) GS.

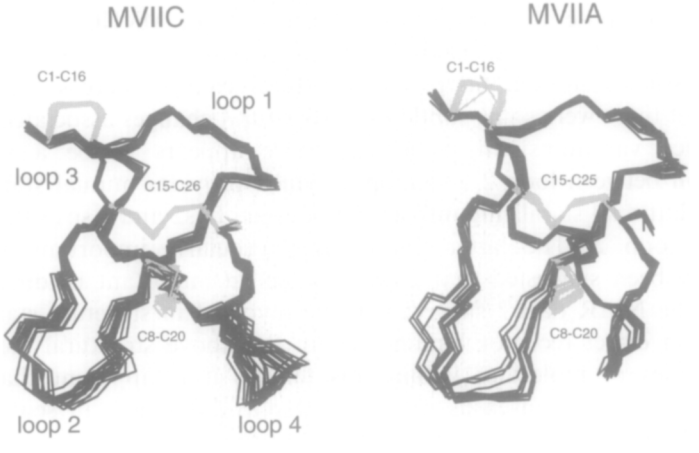

Fig. 23. ω-conotoxins MVIIA and MVIIC. The three disulfide bonds that make up the cystine-knot motif are indicated, as are the four loops in the peptide backbone. Note the small difference in the orientation of loops 2 and 4 between the two molecules.

recent structure of MVIIA,[76,112,113] which incorporates a triple-stranded β-sheet and several turns. A remarkable feature of the six-cysteine/four-loop framework is the presence of a cystine knot within the structures. This motif consists of an embedded ring formed by two of the disulfide bonds and their connecting backbone segments, which is penetrated by the third disulfide bond.[114] Four backbone loops protrude from this core.

Different ω-conotoxins have a wide range of specificities for different subtypes of the voltage-sensitive calcium channels (VSCC) and recent studies have been directed at understanding the factors important in determining VSCC subtype differentiation.[76] In one study,[112] the structures were determined of MVIIA (specific to N-type VSCCs), SVIB (specific to P-type VSCCs), and a synthetic hybrid, SNX-202, which has altered specificities to both VSCC subtypes. The global folds of SVIB and MVIIA were found to be quite similar, but some subtle differences were manifest as orientational differences between loops 2 and 4. We found a similar result in a comparison[76] of MVIIA and MVIIC (like SVIB, specific to P/Q-type VSCCs), as illustrated in Fig. 23. In the latter study a series of chimeric molecules in which each of the four loops in MVIIA and MVIIC was substituted for the corresponding loop in the other molecule was synthesized, producing a suite of 16 hybrid peptides, i.e. MVIIA, MVIIC and 14 chimeras corresponding to all possible loop splice variants. A wide range of different N versus P/Q type selectivity was observed for the chimeric molecules, but the data can be summarized by noting that homogeneous combinations of loop 2 and loop 4 are required simultaneously for specificity to a particular channel subtype, i.e. chimeras having loop 2 from MVIIA and loop 4 from MVIIC or vice versa were nonselective, while those with both loops 2 and 4 from MVIIA were N-type selective, and those with both loops 2 and 4 from MVIIC were P/Q-type selective, irrespective of the combinations of loops 1 and 3.

NMR studies showed no global structural changes across the chimeric family, but there were some subtle local structural changes associated with the loop splice variations. In particular, there appears to be a significant interaction between loop 2 and loop 4, which provides mutual stabilization, and an additional stabilizing interaction between Lys2 and Asp14 that further stabilizes loop 2. The latter finding is particularly important as it had previously been suggested that Lys2 may be an important binding residue, whereas the NMR data[76] suggest it to be involved in structure stabilization rather than direct receptor binding. From the above structural studies and other studies of molecules within this family, it is apparent that the ω-conotoxins form a consensus structure despite differences in sequence and VSCC subtype specificity. This indicates that the ω-conotoxin macrosites for the N/P/Q-subfamily of VSCCs are related, with specificity for receptor targets being conferred by the positions of functional side-chains on the surface of the peptides, particularly in loops 2 and 4.

The ω-conotoxins have attracted much recent interest owing to their potential application in the treatment of chronic pain, exemplified by the success of ω-conotoxin MVIIA (Ziconotide) in phase III clinical trials initiated by the US pharmaceutical company Neurex. Ziconotide also has potential applications in other conditions associated with regulation of calcium channels. As with all peptides, though, bioavailability considerations and possible side-effects mean that the mode of delivery needs careful consideration. In the current pain trials, an infusion pump is used for delivery of peptide direct into

the spinal cord. Second-generation Ziconotide products are likely to involve smaller molecules designed on the basis of structures of MVIIA-like peptides. The findings from NMR that all of the important binding residues are in loops 2 and 4 and that these are all located close together in space at least suggests the possibility that small molecules that mimic these regions may be designed.

4.2. HIV protease

The human immunodeficiency virus (HIV) was identified as the causative agent of acquired immune deficiency syndrome (AIDS) in 1983.[115] Since that time, intensive research efforts have focused on the life cycle of the virus with a view to identifying potential targets for the development of drugs for the treatment of AIDS. The HIV genome contains three major genes (*gag*, *pol* and *env*)[116] that encode a total of three structural proteins, two envelope proteins three enzymes and six accessory proteins. High-resolution structures have now been solved for all of the viral enzymes, structural proteins and envelope proteins as well as three of the accessory proteins (Fig. 24).[117] The *gag* and *pol* gene products are expressed as polyproteins that are processed by a protease enzyme to produce essential structural proteins. The HIV-1 protease was first identified as a putative aspartic acid protease encoded within the *pol* gene.[118,119] In fact, the protease is translated as a *gag-pol* fusion product[120] and released by autocatalysis.[121,122] Inactivation of the enzyme by either site-directed mutagenesis or chemical inhibition produces a noninfective virus.[123] Because of this essential role in the HIV life cycle, HIV protease has become a major target for structure-based drug design.

The first structures of the HIV protease were modelled on eukaryotic aspartic proteases.[119,124] Homology modelling to the structure of a protease from Rous sarcoma virus (RSV)[125] refined the initial models. However, more detailed structural information became available when the crystal structures of native HIV protease were reported by several laboratories.[126–129] There are now well over 100 structures of HIV protease and protease inhibitor complexes in the HIV-protease structure database.[130,131] The availability of this wealth of high-resolution structural information has been the driving force behind numerous structure-based design programmes.[130–132] The majority of the high-resolution structural information on HIV-protease has been obtained from x-ray crystallography data.[131] Although there are relatively few examples in the structure database of HIV-protease/inhibitor complexes that have been determined using NMR spectroscopy, the NMR data, taken together with the structural data from x-ray experiments, have contributed to an understanding of protease-inhibitor recognition and dynamics. Indeed, studies of HIV-protease/inhibitor complexes are a powerful example of the way in which complementary information obtained from x-ray crystallography and NMR spectroscopy can be utilized to facilitate structure-based drug design.

HIV-protease/inhibitor complexes have a molecular weight of approximately 22 kDa. Although NMR spectroscopy is well suited to determination of the structure of molecules in this size range, efforts to determine the solution structure of the complex were hampered by the fact that the protease undergoes rapid autocatalysis in solution. It required the development of potent inhibitors before NMR studies of the complex became feasible. The first solution structure of HIV-protease bound to the cyclic urea inhibitor DMP-323 (Fig. 25) was reported by Yamazaki in 1996.[133] The protease exists as a homodimer. Each 99-residue monomer contains ten β-strands and the dimer is stabilized by a four-stranded antiparallel β-sheet formed by the N- and C-terminal strands of each monomer. The active site of the enzyme is formed at the interface, where each monomer contributes a catalytic triad (Asp25-Thr26-Gly27) that is

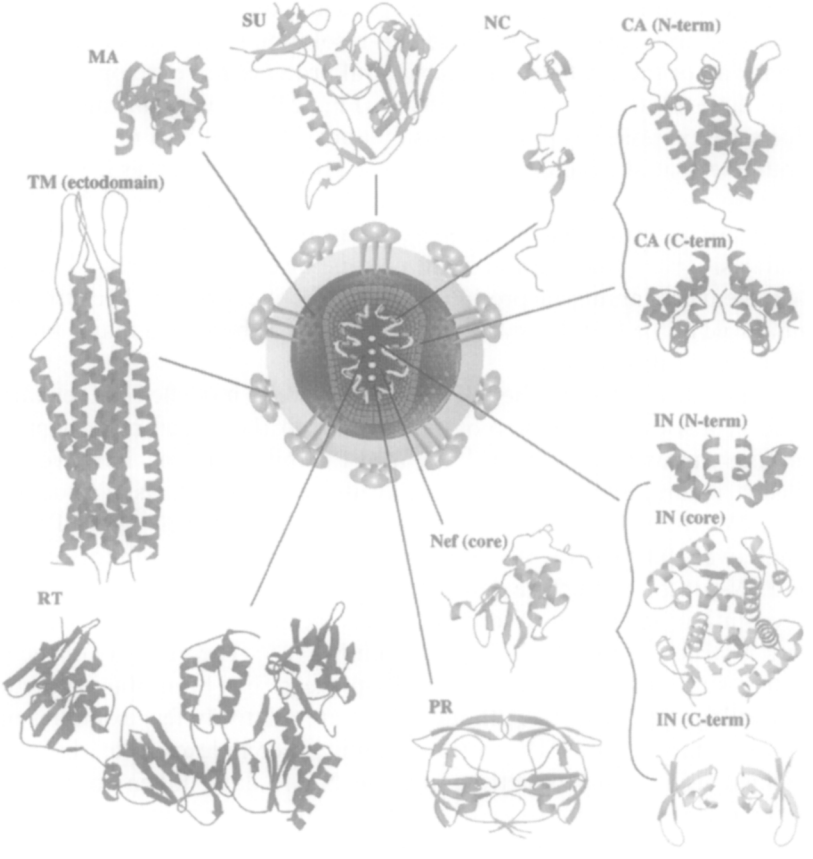

Fig. 24. Schematic drawing of a mature HIV virion surrounded by ribbon diagrams of the structurally characterized proteins and protein fragments. (Reproduced from Turner and Summers[117] with permission.)

responsible for cleavage of the protease substrates. The 'flap region' is located above the reactive site and is formed by a hairpin from each monomer of two antiparallel β-strands joined by a β-turn. There is little difference between the solution and crystal structures of protease-inhibitor complexes, except in those regions where the polypeptide chain is disordered. However, experiments in solution have allowed access to parameters that are not directly accessible from crystal data. These parameters, such as the amplitude and frequency of backbone dynamics, the protonation states of the catalytic aspartate residues and the rate of monomer interchange, are essential in understanding the interaction of HIV-protease with potent inhibitors.

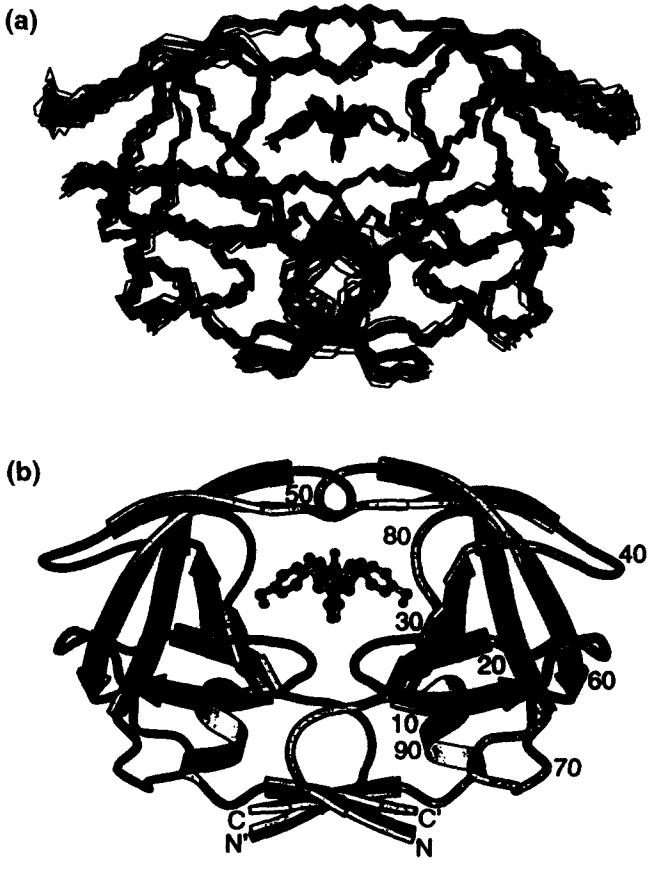

Fig. 25. (a) View of the superimposed heavy atom (N, Cα, C) of the ensemble of structures of the HIV-1 protease/DMP323 complex. (b) Ribbon diagram of the minimized average structure of the complex. (Reproduced from Yamazaki *et al.*[133] with permission. Copyright (1996) The Protein Society, Cambridge University Press.)

The cyclic urea inhibitor DMP-323 was designed by analysis of crystal structures of HIV protease-inhibitor complexes. A feature common to many of the complexes of HIV protease is a buried water molecule that bridges the inhibitor and Ile50 and Ile150 in the flaps. Interactions with this water molecule are thought to induce the fit of the flaps over the inhibitor.[134] In contrast, mammalian aspartic-protease/inhibitor complexes are unable to accommodate an equivalent water molecule[130]. This observation led to the design of a series of cyclic urea-based inhibitors that are capable of displacing the buried water molecule.[134] As well as improving the specificity of inhibitors to the viral protease, displacement of the water molecule was expected to increase the entropic contribution to inhibitor binding and thus enhance the affinity of complex formation. The cyclic urea inhibitors have been shown to be highly potent and specific inhibitors of HIV-protease.[134] For DMP-323 it has been shown in both the crystal structure[134] and in solution[135] that the urea moiety does indeed replace the buried water molecule.

Although DMP-323 replaces one buried water molecule, several others are observed in the crystal structure of the complex. A more recent NMR study investigated the role of these water molecules to determine whether any had a structural role in the formation of the HIV-protease/DMP-323 complex.[136] In favourable cases, NMR can be used to estimate the residence times of hydration water molecules,[137] thus providing information about the time scale of the interaction of buried water with the bulk solvent. This analysis led to the identification of a symmetry-related pair of water molecules that may have a structural role in formation of the complex. Such information may prove useful in the design of future cyclic urea inhibitors. An interesting finding in this study was the fact that each of the hydroxyl protons of DMP-323 is in rapid exchange with solvent. This is a surprising result since two of these hydroxyl protons are completely buried and form a network of hydrogen bonds with the catalytic Asp25/Asp125 side-chains.[138] Furthermore, the dissociation rate of DMP-323 is less than $1\ s^{-1}$ under the conditions of the experiment, which is too small to average the chemical shifts of the hydroxyl protons and the bulk water. The observation is ascribed to local fluctuations in the complex that allow solvent molecules to penetrate into the binding site. This conclusion is supported by the observation that the catalytic protons of the Asp25/Asp125 side chains in the protease-DMP-323 complex undergo H–D exchange with solvent even though they are buried and hydrogen-bonded to the inhibitor.[138] These studies highlight that even well-ordered structures such as the protease/DMP-323 complex may be flexible on the millisecond to microsecond time scale.

Interestingly, in the DMP-323 complex, both of the catalytic Asp25/Asp125 side-chains are protonated over the pH range 2–7.[138] The protonated Asp25/Asp125 residues form a network of hydrogen bonds with the hydroxyl groups of DMP-323. In contrast, it has been shown that in the complex with the asymmetric inhibitor KNI-272, the side-chain of Asp25 is protonated, while that of Asp125 is not. A suggested explanation for this is that both oxygens of

the Asp125 side-chain are deprotonated in order to accept two hydrogen bonds, one from a bound water molecule and one from the inhibitor. In contrast, the side-chain of Asp25 is protonated so that it can donate a hydrogen bond to the inhibitor.[139] Consequently, the protonation state of the enzyme is influenced strongly by interaction with specific inhibitors, and this knowledge is essential for a detailed understanding of the protease–drug interactions.

NMR has also been used to study the relationship between flexibility and enzymatic function for HIV-protease. For the protease/DMP-323 complex, ^{15}N spin-relaxation studies determined that residues that are flexible correlate well with residues that are disordered in the NMR structure of the complex.[140] For example, residues in poorly defined loops were found to undergo large-amplitude internal motions on the nanosecond to picosecond time scale. In contrast, two regions of the molecule were found to execute motions on the millisecond to microsecond time scale. The first of these is at the N-terminus of the protein around Thr4-Leu5. This is adjacent to the major site of autolysis of the protease and it has been suggested that the rate of cleavage may regulate HIV-protease activity *in vivo*.[141] Consequently, the observed flexibility may be important for regulation of protein function. The second region found to be undergoing millisecond–microsecond motion was the tips of the flaps around Ile50-Gly51. In crystal structures, this region of the protease is well ordered and not involved in crystal contacts; however, its conformation varies from structure to structure. This motion is interpreted as a dynamic conformational exchange process, which is fast relative to the chemical shift time scale. Thus, when the protease is bound to a symmetric inhibitor in solution, this conformational exchange results in the chemical shifts of the flap residues in the two monomers being identical.[133,140] In contrast, when the protease is bound to an asymmetric inhibitor, such as KNI-272, crystal structures show that each monomer interacts with the inhibitor in a different way.[139] This is reflected in the fact that the chemical shifts of the monomers are different when asymmetric inhibitors are bound.[136,142] Analysis of spectra from such an asymmetric complex has revealed that the inhibitor is capable of 'flipping' its orientation with respect to the two monomers without dissociating from the complex.[143] These data again highlight the importance of defining both the structural and dynamic aspects of binding in order to understand the requirements for potent interactions between HIV-protease and its inhibitors.

The development of inhibitors of HIV protease represents a major success for structure-based drug design. When HIV was first identified in the early 1980s, there were no known drugs effective for treatment of infection. A combination of x-ray crystallography, NMR spectroscopy, computer modelling and chemical synthesis has resulted in the development of several effective HIV-protease inhibitors. Five drugs are already approved by the US Food and Drug Administration, with several more in clinical trials. However, in common with other retroviruses, HIV has a high transcription error rate that results in a

rapid mutational rate. One of the results is the production of a divergent population of viruses in which the sequence of the HIV-protease produced may differ substantially.[144,145] As a consequence, drug-resistant strains of the virus emerge. Clearly, knowledge of the structural principles that govern inhibition of the protease and the mechanism by which the virus develops resistance will continue to be important in the development of effective new drugs.

4.3. Dihydrofolate reductase

Dihydrofolate reductase (DHFR) is an important intracellular enzyme that is the target of several clinically used antifolate drugs. These include methotrexate, **9**, an anticancer compound, and trimethoprim, **10**, an antibacterial, which act by inhibiting the enzyme in malignant cells or parasites, respectively. The small size of DHFR (18–20 kDa) makes it amenable to structural studies and there have been numerous complexes determined using both x-ray and NMR methods. Many of these studies have been reviewed extensively, so the focus here will be on a recent illustrative example on the structure of a new complex of DHFR with trimetrexate, **11**. Trimetrexate was initially investigated as an antimalarial agent but has subsequently been found to have antineoplastic activity against breast, neck and head cancers. It has also been used as an antibacterial for the treatment of *Pneumocystis carinii* pneumonia (PCP) in AIDS patients. Trimetrexate combines some of the features of trimethoprim and methotrexate, as seen from the structures illustrated.

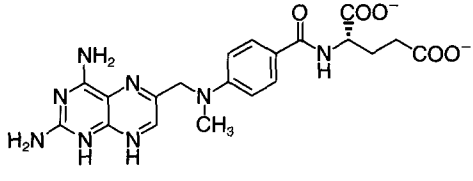

[9] Methotrexate

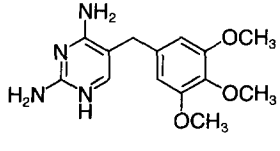

[10] Trimethoprim

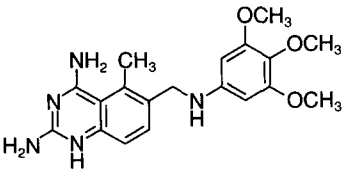

[11] Trimetrexate

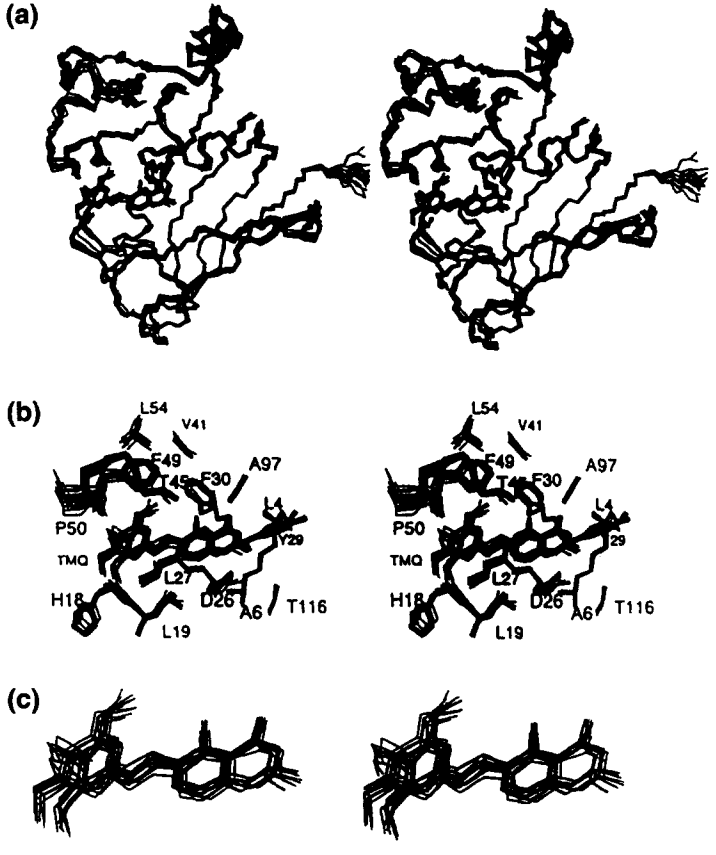

Fig. 26. Stereoview of a superposition over the backbone atoms (N, C_α and C) of residues 1–162 of the final 22 structures of the DHFR–trimetrexate complex. (a) View of the protein backbone and the trimetrexate heavy atoms. (b) View of trimetrexate in the binding site of enzyme. (c) Conformation of trimetrexate in the binding site of enzyme. The orientation of trimetrexate is identical for all three figures (a)–(c) and only its heavy atoms are shown. (Reproduced from Polshakov *et al.*[146] with permission. Copyright (1999) The Protein Society, Cambridge University Press.)

The three-dimensional structure of the complex of DHFR with trimetrexate was determined using about 2000 distance restraints, 300 angle restraints and 100 hydrogen-bonding restraints.[146] Simulated annealing calculations produced a family of 22 structures consistent with the constraints. Several intermolecular protein–ligand NOEs were obtained using a novel approach monitoring temperature effects of NOE signals resulting from dynamic processes in the bound ligand. At low temperature (5°C) the trimethoxy ring of bound trimetrexate flips sufficiently slowly to give narrow signals in slow exchange, which give good NOE cross-peaks. At higher temperature these broaden and their NOE cross-peaks disappear, thus allowing the signals in the lower-temperature spectrum to be identified as NOEs involving ligand protons. Figure 26 shows the structure of the complex, including the orientation of the ligand in the binding site.

The binding site for trimetrexate is well-defined and was compared with the binding sites in related complexes formed with methotrexate and trimethoprim. No major conformational differences were detected between the different complexes. The 2,4-diaminopyrimidine-containing moieties in the three drugs bind essentially in the same binding pocket and the remaining parts of their molecules adapt their conformations such that they can make effective van der Waals interactions with essentially the same set of hydrophobic amino acids, the side-chain orientations and local conformations of which are not greatly changed in the different complexes.

The ring flipping of the trimethoxy aromatic ring mentioned above is manifest in the spectra shown in Fig. 27. The presence of such dynamic processes involving the ligand appear to be not uncommon in macromolecule–ligand complexes and the ability of NMR methods to detect such phenomena

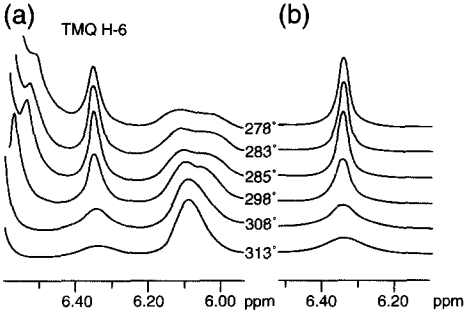

Fig. 27. (a) ^1H spectra at 600 MHz of the DHFR-trimetrexate complex (3 mmol l^{-1}; D_2O buffer) recorded at different temperatures and showing the H6′ signal of trimetrexate involved in slow exchange with the H2′ proton due to ring flipping. (b) Calculated line shapes for the H6′ signal. This signal is in a noncrowded region of the observed spectrum, which facilitates the lineshape analysis. (Reproduced from Polshakov *et al.*[146] with permission. Copyright (1999) The Protein Society, Cambridge University Press.)

represents one distinct advantage of NMR over x-ray methods of structure determination. Relaxation measurements were also used to probe the dynamics of the protein and no large-amplitude motions were found, apart from at the C-terminus.[146]

The power of NMR methods for studying dynamics of complexes is beautifully illustrated by an earlier study of the complex of DHFR with methotrexate.[147] In this case a correlated dynamic rotation of a carboxylate group on the ligand and Arg57 of the protein was detected as illustrated in Fig. 28.

5. FUTURE PROSPECTS

NMR has a bright future ahead for continuing contributions to pharmaceutical research. The information available from genomics projects will

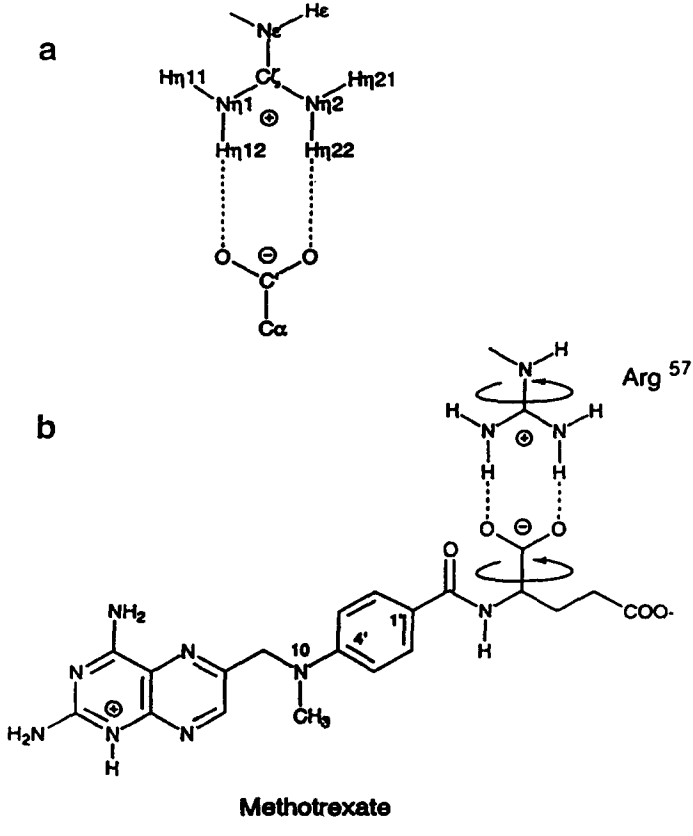

Fig. 28. Correlated motions of a carboxylate group from methotrexate and Arg57 of DHFR detected by NMR. (Reproduced from Nieto *et al.*[147] with permission.)

tremendously increase the number of new targets identified and NMR methods for assessing these targets will be required. While the rate at which new macromolecular targets are being discovered is exceeding dramatically the rate at which their structures can be solved, it is not always necessary to determine the full 3D structure to obtain information that is useful to drug design. The power of NMR spectroscopy will continue to be in the diversity of information it can provide about ligands, macromolecules and their interactions.

ACKNOWLEDGEMENTS

D.J.C. is an Australian Research Council Professorial Fellow and M.J.S. is an ARC Australian Research Fellow. Work in our laboratory is supported by grants from the Australian Research Council and the National Health and Medical Research Council.

REFERENCES

1. D. J. Craik, K. J. Nielsen and K. A. Higgins, *Annu Rep. NMR Spectrosc.*, 1995, **32**, 143.
2. B. J. Stockman, *Prog. Nucl. Magn. Reson. Spectrosc.*, 1998, **33**, 109.
3. M. J. Shapiro and J. R. Wareing, *Curr. Opin. Chem. Biol.*, 1998, **2**, 372.
4. M. J. Shapiro and J. S. Gounarides, *Prog. Nucl. Magn. Reson. Spectrosc.*, 1999, **35**, 153.
5. P. A. Keifer, *Drug Discovery Today*, 1997, **2**, 468.
6. P. A. Keifer, *Curr. Opin. Biotechnol.*, 1999, **10**, 34.
7. D. J. Craik (ed.), *NMR in Drug Design*, CRC Press, Boca Raton, 1996.
8. U. Holzgrabe, B. W. Diehl and I. Wawer, *J. Pharm. Biomed. Anal.*, 1998, **17**, 557.
9. P. J. Hajduk, E. T. Olejniczak and S. W. Fesik, *J. Am. Chem. Soc.*, 1997, **119**, 12257.
10. B. Meyer, T. Weimar and T. Peters, *Eur. J. Biochem.*, 1997, **246**, 705.
11. J. M. Moore, *Curr. Opin. Biotechnol.*, 1999, **10**, 54.
12. S. B. Shuker, P. J. Hajduk, R. P. Meadows and S. W. Fesik, *Science*, 1996, **274**, 1531.
13. A. Watts, *Curr. Opin. Biotechnol.*, 1999, **10**, 48.
14. G. C. Roberts, *Curr. Opin. Biotechnol.*, 1999, **10**, 42.
15. M. Rudin, N. Beckmann, R. Porszasz, T. Reese, D. Bochelen and A. Sauter, *NMR Biomed.*, 1999, **12**, 69.
16. P. A. Keifer, *Drugs of the Future*, 1998, **23**, 301.
17. H. B. Lee and S. Balasubramanian, *J. Org. Chem.*, 1999, **64**, 3454.
18. D. R. Barn, J. R. Morphy and D. C. Rees, *Tetrahedron Lett.*, 1996, **37**, 3213.
19. A. Vidal-Ferran, N. Bampos, A. Moyano, M. A. Pericas, A. Riera and J. K. M. Sanders, *J. Org. Chem.*, 1998, **63**, 6309–6318.
20. G. C. Look, M. M. Murphy, D. A. Campbell and M. A. Gallop, *Tetrahedron Lett.*, 1995, **36**, 2937.
21. M. F. Gordeev, E. M. Gordon and D. V. Patel, *J. Org. Chem.*, 1997, **62**, 8177.
22. E. M. Gordon, M. A. Gallop and D. V. Patel, *Acc. Chem Res.*, 1996, **29**, 144.
23. M. J. Shapiro, G. Kumaravel, R. C. Petter and R. Beveridge, *Tetrahedron Lett.*, 1996, **37**, 4671.
24. A. Svensson, T. Fex and J. Kihlberg, *Tetrahedron Lett.*, 1996, **37**, 7649.
25. A. Svensson, K. E. Bergquist, T. Fex and J. Kihlberg, *Tetrahedron Lett.*, 1998, **39**, 7193.

26. D. Stones, D. J. Miller, M. W. Beaton, T. J. Rutherford and D. Gani, *Tetrahedron Lett.*, 1998, **39**, 4875.
27. L. E. Drain, *Proc. Phys. Soc.*, 1962, **80**, 1380.
28. D. Doskocilova and B. Schnieder, *Chem. Phys. Lett.*, 1970, **6**.
29. W. L. Fitch, G. Detre, C. P. Holmes, J. N. Shoolery and P. A. Keifer, *J. Org. Chem.*, 1984, **59**, 7955.
30. P. A. Keifer, L. Baltusis, D. M. Rice, A. A. Tymiak and J. N. Shoolery, *J. Magn. Reson. Ser. A*, 1996, **119**, 65.
31. R. Jelinek, A. P. Valente, K. G. Valentine and S. J. Opella, *J. Magn. Reson.*, 1997, **125**, 185.
32. C. Dhalluin, C. Boutillon, A. Tamar and G. Lippens, *J. Am. Chem. Soc.*, 1997, **119**, 10494.
33. S. K. Sarkar, R. S. Garigipati, J. L. Adams and P. A. Keifer, *J. Am. Chem. Soc.*, 1996, **118**, 2305.
34. M. Pursch, G. Schlotterbock, L.-H. Tseng, K. Albert and W. Rapp, *Angew. Chem. Int. Ed. Engl.*, 1996, **35**, 2867.
35. M. Delepierre, A. Prochnicka-Chalufour and L. D. Possani, *Biochemistry*, 1997, **36**, 2649.
36. D. Moka, R. Vorreuther, H. Schicha, *et al.*, *J. Pharm. Biomed. Anal.*, 1998, **17**, 125.
37. J. Klein, R. Meinecke, M. Mayer and B. Mayer, *J. Am. Chem. Soc.*, 1999, **121**, 5336.
38. J. C. Lindon, J. K. Nicholson, U. G. Sidelmann and I. D. Wilson, *Drug Metab. Rev.*, 1997, **29**, 705.
39. J. C. Lindon, J. K. Nicholson and I. D. Wilson, *Adv. Chromatogr.*, 1996, **36**, 315.
40. S. H. Smallcombe, S. L. Patt and P. A. Keifer, *J. Magn. Reson. Ser. A*, 1995, **117**, 295.
41. C. Dalvit and J. M. Bohlen, *Magn. Reson. Chem.*, 1996, **34**, 829.
42. J. Chin, J. B. Fell, M. Jarosinski, M. J. Shapiro and J. R. Wareing, *J. Org. Chem.*, 1998, **63**, 386.
43. F. S. Pullen, A. G. Swanson, M. J. Newman and D. S. Richards, *Rapid Commun. Mass. Spectrom*, 1995, **9**, 1003.
44. R. E. Hubbard, *Curr. Opin. Biotechnol.*, 1997, **8**, 696.
45. W. C. Patt, J. J. Edmunds, J. T. Repine, *et al.*, *J. Med. Chem.*, 1997, **40**, 1063.
46. S. R. Krystek Jr., D. A. Bassolino, J. Novotny, C. Chen, T. M. Marschner and N. H. Andersen, *FEBS Lett.*, 1991, **281**, 212.
47. N. H. Andersen, C. P. Chen, T. M. Marschner, S. R. Krystek Jr. and D. A. Bassolino, *Biochemistry*, 1992, **31**, 1280.
48. V. Saudek, J. Hoflack and J. T. Pelton, *FEBS Lett.*, 1989, **257**, 145.
49. S. Endo, H. Inooka, Y. Ishibashi, C. Kitada, E. Mizuta and M. Fujino, *FEBS Lett.*, 1989, **257**, 149.
50. R. G. Mills, S. I. O'Donoghue, R. Smith and G. F. King, *Biochemistry*, 1992, **31**, 5640.
51. S. Munro, D. Craik, C. McConville, *et al.*, *FEBS Lett.*, 1991, **278**, 9.
52. M. D. Reily and J. B. Dunbar Jr., *Biochem. Biophys. Res. Commun.*, 1991, **178**, 570.
53. H. Tamaoki, Y. Kobayashi, S. Nishimura, *et al.*, *Protein Eng.*, 1991, **4**, 509.
54. A. Aumelas, L. Chiche, E. Mahe, *et al.*, *Int. J. Peptide Protein Res.*, 1991, **37**, 315.
55. D. C. Dalgarno, L. Slater, S. Chackalamannil and M. M. Senior, *Int. J. Peptide Protein Res.*, 1992, **40**, 515.
56. Y. Boulanger, E. Biron, A. Khiat and A. Fournier, *J. Peptide Res.*, 1999, **53**, 214.
57. K. Arvidsson, T. Nemoto, Y. Mitsui, S. Ohashi and H. Nakanishi, *Eur. J. Biochem.*, 1998, **257**, 380.
58. C. M. Hewage, L. Jiang, J. A. Parkinson, R. Ramage and I. H. Sadler, *J. Peptide Sci.*, 1997, **3**, 415.
59. A. Aumelas, L. Chiche, S. Kubo, N. Chino, H. Tamaoki and Y. Kobayashi, *Biochemistry*, 1995, **34**, 4546.
60. B. A. Wallace, R. W. Janes, D. A. Bassolino and S. R. Krystek Jr., *Protein Sci.*, 1995, **4**, 75.
61. A. M. McManus, L. Otvos Jr., R. Hoffmann and D. J. Craik, *Biochemistry*, 1999, **38**, 705.
62. W. C. Patt, X. M. Cheng, J. T. Repine, *et al.*, *J. Med. Chem.*, 1999, **42**, 2162.

63. J. Gehrmann, P. F. Alewood and D. J. Craik, *J. Mol. Biol.*, 1998, **278**, 401.
64. J. Balbach, S. Seip, H. Kessler, M. Scharf, N. Kashani-Poor and J. W. Engels, *Proteins*, 1998, **33**, 285.
65. R. L. Wagner, J. W. Apriletti, M. E. McGrath, B. L. West, J. D. Baxter and R. J. Fletterick, *Nature*, 1995, **378**, 690.
66. D. J. Craik, B. M. Duggan and S. L. A. Munro, in *Biological Inhibitors* (ed. M. I. Choudary), p. 255, Harwood Academic Publishers, Amsterdam, 1996.
67. B. M. Duggan and D. J. Craik, *J. Med. Chem.*, 1996, **39**, 4007.
68. B. M. Duggan and D. J. Craik, *J. Med. Chem.*, 1997, **40**, 2259.
69. D. J. Gale, D. J. Craik and R. T. C. Brownlee, *Magn. Reson. Chem.*, 1988, **26**, 275.
70. W. Bourguet, M. Ruff, P. Chambon, H. Gronemeyer and D. Moras, *Nature*, 1995, **375**, 377.
71. J. P. Renaud, N. Rochel, M. Ruff, *et al.*, *Nature*, 1995, **378**, 681.
72. A. P. Campbell and B. D. Sykes, *Annu. Rev. Biophys. Biomol. Struct.*, 1993, **22**, 99.
73. B. D. Sykes, *Curr. Opin. Biotechnol.*, 1993, **4**, 392.
74. D. J. Craik and K. A. Higgins, *Annu. Rep. NMR Spectrosc.*, 1990, **22**, 61.
75. G. Bertho, J. Gharbi-Benarous, M. Delaforge and J.P. Girault, *Bioorg. Med. Chem.*, 1998, **6**, 209.
76. K. J. Nielsen, D. Adams, L. Thomas, *et al.*, *J. Mol. Biol.*, 1999, **289**, 1405.
77. G. M. Clore and A. M. Gronenborn, *Curr. Opin. Chem. Biol.*, 1998, **2**, 564.
78. N. Tjandra and A. Bax, *Science*, 1997, **278**, 1111.
79. G. F. King and J. P. Mackay, in *NMR in Drug Design*, (ed. D.J. Craik), p. 101, CRC Press, Boca Raton, 1996.
80. N. Tjandra, D. S. Garrett, A. M. Gronenborn, A. Bax and G. M. Clore, *Nat. Struct. Biol.*, 1997, **4**, 443.
81. K. Pervushin, R. Riek, G. Wider and K. Wuthrich, *Proc. Natl. Acad. Sci. USA*, 1997, **94**, 12366.
82. L. E. Kay, *Nat. Struct. Biol.*, 1998, **5**, 513.
83. R. Abseher, L. Horstink, C. W. Hilbers and M. Nilges, *Proteins*, 1998, **31**, 370.
84. F. M. Marassi and S. J. Opella, *Curr. Opin. Struct. Biol.*, 1998, **8**, 640.
85. B. J. Stockman, D. J. Waldon, J. A. Gates, *et al.*, *Protein Sci.*, 1998, **7**, 2281.
86. H. Ottleben, M. Haasemann, R. Ramachandran, M. Gorlach, W. Muller-Esterl and L.R. Brown, *Eur. J. Biochem.*, 1997, **244**, 471.
87. J. V. Hines, H. Chang, M. S. Gerdeman and D. E. Warn, *Bioorg. Med. Chem. Lett.*, 1999, **9**, 1255.
88. W. D. Morgan, B. Birdsall, P. M. Nieto, A. R. Gargaro and J. Feeney, *Biochemistry*, 1999, **38**, 2127.
89. M. J. Gradwell and J. Feeney, *J. Biomol. NMR*, 1996, **7**, 48.
90. A. M. Gronenborn and G. M. Clore, *Crit. Rev. Biochem. Mol. Biol.*, 1995, **30**, 351.
91. L. E. Kay, *Prog. Biophys. Mol. Biol.*, 1995, **63**, 277.
92. P. J. Hajduk, R. P. Meadows and S. W. Fesik, *Science*, 1997, **278**, 497.
93. P. J. Hajduk, J. Dinges, G. F. Miknis, *et al.*, *J. Med. Chem.*, 1997, **40**, 3144.
94. D. Henrichsen, B. Ernst, J. L. Magnani, W.-T. Wang, B. Meyer and T. Peters, *Angew. Chem. Int. Ed.*, 1999, **38**, 98.
95. J. Fejzo, C. A. Lepre, J. W. Peng, M. S. Su, J. A. Thomson and J. M. Moore, *Protein Sci.*, 1996, **5**, 1917.
96. N. Gonnella, M. Lin, M. J. Shapiro, J. R. Wareing and X. Zhang, *J. Magn. Reson.*, 1998, **131**, 336.
97. G. W. Bemis and M. A. Murcko, *J. Med. Chem.*, 1996, **39**, 2887.
98. J. M. Hill, C. J. Oomen, L. P. Miranda, J. P. Bingham, P. F. Alewood and D. J. Craik, *Biochemistry*, 1998, **37**, 15621.
99. J. Gehrmann, N. L. Daly, P. F. Alewood and D. J. Craik, *J. Med. Chem.*, 1999, **42**, 2364.

100. S. H. Hu, J. Gehrmann, P. F. Alewood, D. J. Craik and J. L. Martin, *Biochemistry*, 1997, **36**, 11323.
101. S. H. Hu, J. Gehrmann, L. W. Guddat, P. F. Alewood, D. J. Craik and J. L. Martin, *Structure*, 1996, **4**, 417.
102. J. M. McIntosh, D. Yoshikami, E. Mahe, *et al.*, *J. Biol. Chem.*, 1994, **269**, 16733.
103. P. A. Quiram and S. M. Sine, *J. Biol. Chem.*, 1998, **273**, 11007.
104. H. Gouda and S. Hirono, *Biochim. Biophys. Acta.*, 1999, **1431**. 384.
105. J. P. Rogers, P. Luginbuhl, G. S. Shen, R. T. McCabe, R. C. Stevens and D. E. Wemmer, *Biochemistry*, 1999, **38**, 3874.
106. I. V. Maslennikov, Z. O. Shenkarev, M. N. Zhmak, *et al.*, *FEBS Lett.*, 1999, **444**, 275.
107. J. M. Hill, P. F. Alewood and D. J. Craik, *Biochemistry*, 1996, **35**, 8824.
108. J. M. Hill, P. F. Alewood and D. J. Craik, *Structure*, 1997, **5**, 571.
109. E. Moczydlowski, B. M. Olivera, W. R. Gray and G. R. Strichartz, *Proc. Natl. Acad. Sci. USA*, 1986, **83**, 5321.
110. Y. Yanagawa, T. Abe, M. Satake, S. Odani, J. Suzuki and K. Ishikawa, *Biochemistry*, 1988, **27**, 6256.
111. B. Cornet, J. M. Bonmatin, C. Hetru, J. A. Hoffmann, M. Ptak and F. Vovelle, *Structure*, 1995, **3**, 435.
112. K. J. Nielsen, L. Thomas, R. J. Lewis, P. F. Alewood and D. J. Craik, *J. Mol. Biol.*, 1996, **263**, 297.
113. K. J. Nielsen, D. A. Adams, P. F. Alewood, *et al.*, *Biochemistry*, 1999, **38**, 6741.
114. P. K. Pallaghy, K. J. Nielsen, D. J. Craik and R. S. Norton, *Protein Sci.*, 1994, **3**, 1833.
115. F. Barre-Sinoussi, J. C. Chermann, F. Rey, *et al.*, *Science*, 1983, **220**, 868.
116. L. Ratner, W. Haseltine, R. Patarca, *et al.*, *Nature*, 1985, **313**, 277.
117. B. G. Turner and M. F. Summers, *J. Mol. Biol.*, 1999, **285**, 1.
118. L. H. Pearl and W. R. Taylor, *Nature*, 1987, **328**, 482.
119. L. H. Pearl and W. R. Taylor, *Nature*, 1987, **329**, 351.
120. T. Jacks, M. D. Power, F. R. Masiarz, P. A. Luciw, P. J. Barr and H. E. Varmus, *Nature*, 1988, **331**, 280.
121. C. Debouck, J. G. Gorniak, J. E. Strickler, T. D. Meek, B. W. Metcalf and M. Rosenberg, *Proc. Natl. Acad. Sci. USA*, 1987, **84**, 8903.
122. W. G. Farmerie, D. D. Loeb, N. C. Casavant, C. A. D. Hutchison, M. H. Edgell and R. Swanstrom, *Science*, 1987, **236**, 305.
123. N. E. Kohl, E. A. Emini, W. A. Schleif, *et al.*, *Proc. Natl. Acad. Sci., USA*, 1988, **85**, 4686.
124. I. V. Pechik, A. E. Gustchina, N. S. Andreeva and A. A. Fedorov, *FEBS Lett.*, 1989, **247**, 118.
125. I. T. Weber, M. Miller, M. Jaskolski, J. Leis, A. M. Skalka and A. Wlodawer, *Science*, 1989, **243**, 928.
126. R. Lapatto, T. Blundell, A. Hemmings, *et al.*, *Nature*, 1989, **342**, 299.
127. M. A. Navia, P. M. Fitzgerald, B. M. McKeever, *et al.*, *Nature*, 1989, **337**, 615.
128. S. Spinelli, Q. Z. Liu, P. M. Alzari, P. H. Hirel and R. J. Poljak, *Biochimie*, 1991, **73**, 1391.
129. A. Wlodawer, M. Miller, M. Jaskolski, *et al.*, *Science*, 1989, **245**, 616.
130. A. Wlodawer and J. W. Erickson, *Annu. Rev. Biochem.*, 1993, **62**, 543.
131. A. Wlodawer and J. Vondrasek, *Annu. Rev. Biophys. Biomolec. Struct.*, 1998, **27**, 249.
132. D. J. Kempf and H. L. Sham, *Curr. Pharm. Des.*, 1996, **2**, 225.
133. T. Yamazaki, A. P. Hinck, Y. X. Wang, *et al.*, *Protein Sci.*, 1996, **5**, 495.
134. P. Y. S. Lam, P. K. Jadhav, C. J. Eyermann, *et al.*, *Science*, 1994, **263**, 380.
135. S. Grzesiek, A. Bax, L. K. Nicholson, *et al.*, *J. Am. Chem. Soc.*, 1994, **116**, 1581.
136. Y. X. Wang, D. I. Freedberg, S. Grzesiek, *et al.*, *Biochemistry*, 1996, **35**, 12694.
137. G. Otting, E. Liepinsh and K. Wuthrich, *Science*, 1991, **254**, 974.
138. T. Yamazaki, L. K. Nicholson, D. A. Torchia, *et al.*, *J. Am. Chem. Soc.*, 1994, **116**, 10791.
139. E. T. Baldwin, T. N. Bhat, S. Gulnik, *et al.*, *Structure*, 1995, **3**, 581.
140. L. K. Nicholson, T. Yamazaki, D. A. Torchia, *et al.*, *Nat. Struct. Biol.*, 1995, **2**, 274.

141. J. R. Rose, R. Salto and C. S. Craik, *J. Biol. Chem.*, 1993, **268**, 11939.
142. D. I. Freedberg, Y.-Z. Wang, S. J. Stahl, *et al.*, *J. Am. Chem. Soc.*, 1998, **120**, 7916.
143. E. Katon, T. Yamazaki, Y. Kiso, *et al.*, *J. Am. Chem. Soc.*, 1999, **121**, 2607.
144. D. L. Winslow, S. Stack, R. King, H. Scarnati, A. Bincsik and M. J. Otto, *AIDS Res. Hum. Retroviruses*, 1995, **11**, 107.
145. J. H. Condra, W. A. Schleif, O. M. Blahy, *et al.*, *Nature*, 1995, **374**, 569.
146. V. I. Polshakov, B. Birdsall, T. A. Frenkiel, A. R. Gargaro and J. Feeney, *Protein Sci.*, 1999, **8**, 467.
147. P. M. Nieto, B. Birdsall, W. D. Morgan, T. A. Frenkiel, A. R. Gargaro and J. Feeney, *FEBS Lett.*, 1997, **405**, 16.
148. M. Coles, V. Sowemimo, D. Scanlon, S. L. Munro and D. J. Craik, *J. Med. Chem.*, 1993, **36**, 2658.

Index

Page numbers in *italics* refer to figures and tables.